Assessing adipose tissue depot differences in thermogenesis during early life in sheep and browning response in humans with pheochromocytoma

Graeme Davies BSc (Hons)

Thesis submitted to the University of Nottingham for
the degree of Doctor of Philosophy

August 2016

Declaration

The majority of this thesis was carried out at the Department of Child Health, Obstetrics and Gynaecology, Queens Medical Centre, University of Nottingham between October 2012 and August 2016. Some of the experimental work (Chapter 5) was conducted at the University of California, Los Angeles between September 2014 and July 2015.

This thesis illustrates my own work unless otherwise stated and was conducted under the supervision of Professor Michael Symonds and Professor Helen Budge at the University of Nottingham and Professor Harold Sacks and Dr Laurent Vergnes at the University of California, Los Angeles. This report is an accurate representation of the work performed and no other study reproducing this work, to my knowledge, has been carried out within the University of Nottingham.



Graeme Davies

August 2016

Abstract

Obesity and associated comorbidities such as diabetes are currently major global health problems. It has been shown that individual sites or depots of fat have different properties and effects on whole body physiology. Of particular interest are depots that display thermogenic characteristics, known as brown or beige adipose tissue, which may be able to increase energy expenditure and clear excess glucose and lipids from the circulation. The aim of this thesis was to compare adipose tissue depots in terms of their capacity for thermogenesis in early life using sheep as an animal model and browning response to chronic adrenergic stress in humans with pheochromocytoma.

Epicardial and paracardial adipose tissues were focused on in the sheep study as they have been described as thermogenic in some adult humans but these findings have been inconclusive. The characterisation of these depots and their capacity for thermogenesis in early life has not been established, especially in comparison to other known depots of white and brown adipose tissue. My results show that epicardial and paracardial adipose tissue have increased thermogenic gene expression and uncoupling protein 1 in comparison to omental white adipose tissue suggesting they may play a role in thermogenesis in early life. These depots undergo remodelling over the first 28 days changing from brown to white adipose tissue. In sheep, this adipose tissue transition occurs without evidence of apoptosis and which may suggest other cellular mechanisms are responsible for this process.

The browning capacity of different fat depots is important for targeting therapeutic interventions. As a model of catecholamine excess, samples of human

periadrenal and subcutaneous adipose tissue were collected from patients with pheochromocytoma as well as patients undergoing adrenalectomy for benign tumours (control group). The data suggests periadrenal adipose tissue can undergo browning in some patients with pheochromocytoma. These patients had the highest plasma catecholamine concentrations suggesting a possible threshold is required to elicit browning. Subcutaneous adipose tissue did not display signs of browning suggesting that this depot does not respond to chronic adrenergic stress. It may therefore have a lack of browning capacity compared to visceral depots. In conclusion, both studies suggest differences between adipose tissue depots in thermogenic capacity both in development in early life and capacity for browning in later life.

Acknowledgements

Firstly, I would like to thank the University of Nottingham and the Cardiometabolic research foundation, Los Angeles for providing funding which allowed me to complete this PhD. Thank you to the University of Nottingham Graduate School and the Biochemical Society for generously providing travel grants which allowed to me to present my work at international conferences.

Thanks to my project supervisors Professors Michael Symonds and Helen Budge for their support, encouragement, advice and guidance throughout my PhD. Thank you to Professor Harold Sacks for his informative comments on my work, hospitality, funding through the Cardiometabolic Research Foundation Los Angeles and initiating the collaborative human pheochromocytoma project at the University of California, Los Angeles (UCLA). I am very grateful to Professor Karen Reue for allowing me to spend a productive and enjoyable 10 months conducting research in her lab at UCLA and for providing insightful comments on the project. Thank you to Dr Laurent Vergnes for teaching me a great deal about molecular biology, cellular bioenergetics experiments and for his support, supervision and guidance during my time at UCLA.

I would like to thank all the staff and students at Child Health in Nottingham. Special thanks to Mr Mark Pope, Dr Ian Bloor, Mrs Victoria Wilson and Mrs Catherine Pincott-Allen for teaching me how to conduct the laboratory procedures, for providing technical support and a few laughs along the way. Thanks to friends and colleagues Miss Rachel Woods, Dr Ian Bloor, Dr Stuart Astbury, Dr Caz Henry, Dr Neele Dellschaft, Dr Lindsay Robinson and Dr Mark Birtwistle for their friendship, support and encouragement throughout this PhD. Thank you to Mr Peter Aldiss for allowing me to collaborate on writing a review article, informative discussions and sharing his infectious enthusiasm for science. Thank you to Dr Jenny Link and Mr Natee Link for their friendship and helping me to settle in Los Angeles.

Finally, I would like to thank my family for their love, support and encouragement (plus occasional proof reading). I dedicate this thesis to my grandparents Irene Davies and Stefan Lehky.

Contents

Abstract 3

Acknowledgements 5

Contents 6

List of figures 13

List of tables 18

Abbreviations 19

Chapter 1 Introduction 22

1.1 Obesity and diabetes 22

1.2 Adipose tissue 24

1.2.1 White adipose tissue 25

1.2.2 Brown Adipose Tissue 29

1.3 Adipose tissue 'browning' and beige adipocytes 44

1.4 Origins of brown, white and beige adipocytes 48

1.5 Beneficial roles of thermogenic adipose tissue in metabolism and energy balance – evidence from animal models 51

1.6 Human thermogenic adipose tissue 54

1.6.1 Human brown or beige adipocyte characterisation 57

1.6.2 Epicardial and Paracardial fat as brown/beige fat 58

1.6.3 The heart as an endocrine organ promoting adipose tissue browning 66

1.7 Clinical significance of human brown adipose tissue on energy balance and insulin sensitivity 70

1.8 Pheochromocytoma as a model of chronic adrenergic stress and adipose tissue browning 72
1.9 Age related BAT atrophy or adipose tissue 'whitening' 73
1.10 Sheep as an animal model of BAT development and whitening 75
1.11 Aims and Hypotheses 76
Chapter 2 Materials and methods 78
2.1 Sheep study 78
2.1.1 Experimental design and sampling 79
2.2 Laboratory procedures 82
2.2.1 Plasma BNP Analysis by Enzyme Immunoassay 82
2.2.2 RNA isolation 84
2.2.3 Reverse Transcription 86
2.2.4 End-point PCR 87
2.2.5 Primer design and testing 88
2.2.6 Gel electrophoresis of PCR products 92
2.2.6 Gel Extraction 92
2.2.7 Quantitative Reverse Transcription PCR (qPCR) 93
2.2.8 Mitochondrial DNA to nuclear DNA ratio 97
2.2.9 Mitochondrial Protein Extraction Procedure 98
2.2.10 Protein quantification by Bicinchoninic acid assay 99
2.2.11 Western Blotting 100
2.2.12 Histology 104
2.2.13 Immunohistochemistry 107

2.2.14 TUNEL assay 108

2.3 Human Pheochromocytoma study 111

2.3.1 Study subjects and adipose tissue sampling 111

2.3.2 Exclusion Criteria 112

2.4 Laboratory Procedures 112

2.4.1 Catecholamine Plasma analysis 112

2.4.2 Glucose Plasma analysis 113

2.4.3 Non-esterified Fatty Acid Plasma Analysis 114

2.4.4 FGF21 Plasma Analysis 114

2.4.5 ANP Plasma Analysis 115

2.4.6 BNP Plasma Analysis 116

2.4.7 Histology 117

2.4.8 Immunohistochemistry 117

2.4.9 Cellular bioenergetics analysis 118

2.4.10 RNA Extraction 126

2.4.11 cDNA synthesis 127

2.4.12 qPCR analysis 127

2.4.13 Mitochondrial DNA to genomic DNA ratio 131

2.4.14 UCP1 promoter SNP sequencing 131

2.4.15 Western Blotting 132

2.4.16 Cell culture 134

2.4.17 Outdoor temperature analyses 138

2.6 Statistical Analysis 139

Chapter 3 Characterisation of epicardial and paracardial compared to omental adipose tissue during early life in sheep 141

3.1 Introduction 141

3.1 Hypothesis 143

3.2 Methods 143

3.3 Results 144

3.4.1 The effect of age on lamb bodyweight 144

3.4.2 The effect of age on tissue weight of perirenal, paracardial and omental fat 145

3.4.3 Postnatal age and gene expression modification of paracardial, epicardial and omental adipose tissue depots 147

3.4.4 UCP1 Western blots 157

3.4.5 Correlation between UCP1 mRNA and protein 159

3.4.6 Mitochondrial abundance, gene and protein expression 160

3.4.7 Haematoxylin and Eosin stained tissue sections 164

3.4.8 UCP1 Immunohistochemistry 168

3.4.9 Assessment of apoptosis during brown to white adipose tissue transition 171

3.5 Discussion 174

3.5.1 Epicardial and paracardial adipose tissue express thermogenic genes, possess UCP1 and may be intermediate between known white and brown adipose tissue depots in thermogenic capacity 174

3.5.2 Beige adipocyte markers do not show a clear pattern of expression between adipose tissue depots or with age in sheep 181

3.5.3 Lipolysis gene expression does not follow thermogenic gene expression and is increased in perirenal adipose tissue compared to other visceral depots studied 183

3.5.4 RIP140, a UCP1 inhibitor is upregulated in omental compared to epicardial and paracardial adipose tissue 187

3.5.5 Other white adipocyte related genes did not show a clear pattern of expression 188

3.5.6 A brown to white adipose tissue transition occurs in perirenal and pericardial adipose tissue without evidence of apoptosis 190

3.5 Summary and conclusions 193

Chapter 4 Gene expression analysis of cardiac natriuretic peptide signalling in paracardial, epicardial and omental adipose tissue depots 195

4.1 Introduction 195

4.2 Hypothesis 196

4.3 Methods 196

4.4 Results 197

4.4.1 Plasma BNP concentrations in early life 197

4.4.2 Expression of cardiac peptide receptor mRNA 199

4.4.3 PRKGI gene expression 201

4.4.4 Western blots 203

4.5 Discussion 203

4.5.1 BNP plasma concentrations show a decrease between days 7 and 28 203

4.5.2 Cardiac natriuretic peptide signalling or sensitivity may be increased in omental adipose tissue compared to pericardial fat depots 205

4.6 Summary and conclusions 208

Chapter 5 Adipose tissue depot specific effects of chronic adrenergic stimulation in humans with pheochromocytoma 210

5.1 Introduction 210

5.2 Hypothesis 211

5.3 Methods 211

5.4 Results 212

5.4.1 Patient characteristics 212

5.4.2 Adipose tissue morphology and study groups 213

5.4.3 Study group characteristics 214

5.4.4 Plasma analyses 215

5.4.5. Thermogenic gene expression results 219

5.4.6 Tissue gene expression analysis of beige adipocyte markers 225

5.4.7 White adipocyte marker ASC-1 227

5.4.8 UCP1 Western Blot results 228

5.4.9 UCP1 IHC results 230

5.4.10 Mitochondrial gene expression and abundance 231

5.4.11 Cellular bioenergetics analyses 236

5.4.12 Frequency of-3286A/G UCP1 polymorphism 242

5.4.13 Outdoor temperature analysis 243

5.5 Discussion 245

5.5.1 Browning of pADR adipose tissue and augmented mitochondrial function occurs in a subset of pheo patients with highest plasma noradrenaline concentrations 245

5.5.2 SAT does not undergo browning in patients with pheochromocytoma 251

5.5.3 Beige adipocyte markers were not conclusive of increased beige adipocyte abundance in patients with adipose tissue browning 256

5.5.4 Summary and conclusions 258

Chapter 6 Conclusion 259

6.1 General aims 259

6.2 Summary of study findings 260

6.2.1 Sheep studies 260

6.2.2 Human pheochromocytoma study 261

6.3 Limitations of the studies 262

6.3.1 Sheep as an animal model of human adipose tissue development and thermogenesis 262

6.3.2 Technical limitations of the sheep studies 263

6.3.3 Human pheochromocytoma study 264

6.3.4 Technical limitations of the human pheochromocytoma study 265

6.4 Future work 266

6.4.1 Future work based on the findings of sheep studies 266

6.4.2 Future work based on human pheochromocytoma study 267

6.5 Final remarks 268

References 269

Appendices 299

Publications 299

Oral presentations 299

Poster presentations 300

Subject characteristics 301

List of figures

Figure 1.1 Light microscope image of human periadrenal white adipose tissue showing the characteristic unilocular lipid droplet of white adipocytes 26

Figure 1.2 Morphology of brown and white adipocytes. Adapted and redrawn from (Sell et al., 2004). 30

Figure 1.3 The structure of uncoupling protein 1 (UCP1) on the inner mitochondrial membrane of thermogenic adipocytes. 32

Figure 1.4 Role of uncoupling protein 1 (UCP1) in uncoupling oxidative phosphorylation. 34

Figure 1.5 Putative models of uncoupling protein 1 (UCP1) proton transport mechanism. 37

Figure 1.6 The molecular pathway of UCP1 upregulation and thermogenesis to cold exposure 42

Figure 1.7 Schematic diagram of adipocyte origins. 50

Figure 1.8 The major locations of BAT in human adults and infants. 56

Figure 1.9 The anatomy of human epicardial and paracardial adipose tissue in relation to the heart. 59

Figure 1.10 Effects of cardiac natriuretic peptides on adipose tissue thermogenesis. 69

Figure 2.1 Schematic diagram of overall study design and tissue sampling. 81

Figure 2.2 Schematic diagram of the principle of enzyme immunoassay 82

Figure 2.3 Standard curve of BNP EIA showing absorbance and concentration for extrapolation of unknown samples 84

Figure 2.4 Schematic diagram of the polymerase chain reaction. 88

Figure 2.5 qPCR standard curve and efficiency 94

Figure 2.6 Figure 2.6 Melt curve analysis of product (PGC1α) showing a single product is amplified by qPCR 95

Figure 2.7 Schematic diagram of the principal steps in western blotting. 101
Figure 2.8 Schematic diagram of TUNEL assay principle. 109
Figure 2.9 Setup of mitochondrial bioenergetics experiments using a Seahorse XF24 Extracellular Flux Analyzer. 124
Figure 2.10 Effect of compounds used in coupling and electron flow assays on complexes of the electron transport chain. 125
Figure 2.11 Summary of 3T3-L1 experimental design 136
Figure 3.1 Age group comparisons of lamb bodyweights in kilograms. 144
Figure 3.2 Age group comparisons of perirenal, paracardial and omental tissue weights in grams. 146
Figure 3.3 Age group comparisons of perirenal, paracardial and omental tissue weights in grams expressed relative to animal bodyweight in kilograms. 147
Figure 3.4 Thermogenic gene expression in paracardial, epicardial and omental adipose tissue. A: UCP1 B: DIO2 C: PGC1α D: ADRB3. 149
Figure 3.5 WAT related gene expression in paracardial, epicardial and omental adipose tissue. A: Leptin B: RIP140 C: TCF21 151
Figure 3.6 Beige adipocyte marker gene expression in paracardial, epicardial and omental adipose tissue. A: CD137 B: SHOX2 153
Figure 3.7 PPARγ gene expression in paracardial, epicardial and omental adipose tissue. 154
Figure 3.8 Lipolytic gene expression in paracardial, epicardial, omental and perirenal adipose tissue. A: ATGL B: HSL C: PLIN1 156
Figure 3.9 Representative image of a western blot for with primary antibodies for uncoupling protein 1 (UCP1, 32kDa) and cytochrome c (CYCS, 15kDa). 157
Figure 3.10 UCP1 densitometry in expressed as a percentage of a calibrator 7 day perirenal sample that was loaded on all gels (% calibrator) from Western blots in

perirenal (PR) at 7 days, paracardial (Para) epicardial (Epi) and omental adipose tissue at 7 and 28 days..... 158
Figure 3.11 Correlation between Log (2) transformed data of UCP1 mRNA and protein. 159
Figure 3.12 Representative images of mitochondrial pellets observed during mitochondrial isolation. 160
Figure 3.13 Cytochrome c gene expression in paracardial, epicardial and omental adipose tissue. 161
Figure 3.14 Cytochrome c protein abundance in perirenal, paracardial, epicardial and omental adipose tissues at 7 and 28 days. 162
Figure 3.15 Ratio of MTCO1 mitochondrial DNA (mtDNA) to 18S nuclear DNA (nDNA) abundance in perirenal, paracardial, epicardial and omental adipose tissue. 163
Figure 3.16 Correlation between log(2) transformed UCP1 mRNA and mtDNA/nDNA ratio. 164
Figure 3.17 Representative images of Haematoxylin and Eosin stained 5µm tissue sections. 167
Figure 3.18 Representative images of UCP1 stained 5µm tissue sections. 170
Figure 3.19 Assessment of apoptotic cells in adipose tissue through TUNEL assay. 173
Figure 3.20 Heatmap of thermogenic, mitochondrial, beige and white adipocyte markers. 175
Figure 4.1 Plasma BNP concentrations analysed by enzyme immunoassay (EIA). 198
Figure 4.2 NPRA gene expression in paracardial, epicardial and omental adipose tissue. 199
Figure 4.3 Natriuretic peptide receptor type C (NPRC) gene expression in paracardial, epicardial and omental adipose tissue..... 200
Figure 4.4 Ratio of NPRA:NPRC gene expression in Paracardial, epicardial and omental adipose tissue. 201

Figure 4.5 Protein kinase G I (PRKGI) gene expression in paracardial, epicardial and omental adipose tissue. 202
Figure 5.1 Representative images of Haematoxylin and Eosin stained 5μm tissue sections. 214
Figure 5.2 Comparison of plasma catecholamine concentrations of control, pheo unilocular and pheomultilocular patients. 218
Figure 5.3 Thermogenic gene expression UCP1, PGC1a, DIO2 & ADRB3. 221
Figure 5.4 UCP1 gene expression in 3T3-L1 adipocytes treated with human plasma. 222
Figure 5.5 Cellular bioenergetics analysis of immortalized brown adipocytes treated with human plasma. 225
Figure 5.6 Beige marker gene expression PAT2, MTUSvar3 and KCNK3 226
Figure 5.7 White adipocyte marker ASC-1 gene expression 227
Figure 5.8 Western blot images from A) pADR Control, Phei unilocular (PU) and Pheo Multilocular (PM), n=4 per group. B) SAT Control (n=3), Pheo unilocular (PU, n=2) and Pheo multilocular (PM, n=2). 229
Figure 5.9 Representative images of 5μm thick sections stained with UCP1 antibody. 230
Figure 5.10 Mitochondrial gene expression NDUFB9, SDHB, UQCRFS1 and COX7B 233
Figure 5.11 ACADM gene expression. 234
Figure 5.12 Mitochondrial abundance analyses. 235
Figure 5.13 Coupling assay: OCR measurements vs Time for paired pADR (red) and SAT (blue) samples from the same patient. 236
Figure 5.14 Coupling assay oxygen consumption rates (OCR) of isolated mitochondria. 238
Figure 5.15 Electron flow assay: Oxygen consumption rate (OCR) vs Time for pADR (red) and SAT (blue) samples from the same patient. 239
Figure 5.16 Electron flow assay oxygen consumption rates (OCR) of isolated mitochondria. 241

Figure 5.17 Sequencing reads for -3286A/G UCP1 polymorphisms A/A, A/G and G/G. SNP location in shown by an arrow. 242

Figure 5.18 Linear regression of ln transformed UCP1 mRNA and average outdoor temperature (^{o}F) in month of and month prior to surgery. 244

List of tables

Table 2.1 Primers used for ovine reference (ref) and target gene mRNA quantification. 91

Table 2.2 Protocol for haematoxylin and eosin staining of adipose tissue sections..... 107

Table 2.3 Primer sequences used for human reference (ref) and target gene mRNA quantification by qPCR..... 130

Table 5.1 Summary of patient characteristics for control and pheo patients. 212

Table 5.2 Summary of patient characteristics for study groups control, pheo unilocular (PU) and pheo multilocular (PM) based on pADR adipose tissue morphology. Data presented as means ± SEM. 215

Table 5.3 Plasma hormone and metabolite concentrations for study groups control, pheo unilocular (PU) and pheo multilocular (PM)..... 218

Table 5.4 Frequency table of genotypes of UCP1 SNP polymorphism 243

Abbreviations

Abbreviation	Meaning
ABC	ATP-binding cassette
ADP	Adenosine diphosphate
ADRB3	Adrenergic β3 receptor
ANGPTL4	Angiopoietin-like 4
ANP	Atrial natriuretic peptide
ApoA5	Apoliprotein A 5
APS	Ammonium persulphate
ATF2	Activated transcription factor 2
ATGL	Adipose triglyceride lipase
ATP	Adenosine triphosphate
BAT	Brown Adipose Tissue
BCA	Bicinchoninic acid
BMI	Body Mass Index
BNP	B-type natriuretic peptide
BRITE	Brown in white
cAMP	Cyclic adenosine monophosphate
cGMP	Cyclic guanosine monophosphate
CRE	Cyclic AMP response element
CREB	cAMP reponse element binding protein
CVD	Cardiovascular disease
DAB	Diaminobenzidine
DIO2	Type II deiodinases
EAT	Epicardial adipose tissue
EBF2	Early B-cell factor 2
EIA-BNP	BNP Enzyme Immunoassay kit
ELISA	Enzyme-linked Immunoassay
EPI	Epicardial
FCCP	Carbonyl cyanide-4-(trifluoromethoxy)phenylhydrazone
FFA	Free fatty acids

FGF21	Fibroblast growth factor 21
GDP	Guanosine diphosphate
GLUT4	Glucose transporter 4
HDL	High density lipoprotein
HOXC9	Homeobox C9
HSL	Hormone sensitive lipase
iBAT	Interscapular brown adipose tissue
IHC	Immunohistochemistry
IL-6	Interleukin-6
IRS	Insulin receptor substrate
KCNK3	Potassium channel subfamily K member 3
kDa	Kilodalton
LCFA	Long Chain Fatty Acids
LPL	Lipoprotein lipase
MAPK	Mitogen-activated protein kinase
Mhy11	Myosin heavy chain 11
mRNA	Messenger ribonucleic acid
mtDNA	Mitochondrial DNA
MTUS1	Microtubule tumour suppressor 1
Myf5	Myogenic factor 5
NA	Noradrenaline
nDNA	Nuclear DNA
NEFA	Non-esterified fatty acids
NP	Natriuretic peptide
NPRA	Natriuretic peptide receptor activated
NPRC	Natriuretic peptide receptor clearance
NRTC	Non-reverse transcriptase control
NST	Non-shivering thermogenesis
NTC	Non-template control
ob	Obese
P38 MAPK	p38 mitogen activated kinase
PARA	Paracardial
PAX7	Paired box 7

PCR	Polymerase chain reaction
PET	Positron emission tomography
PET-CT	PET followed by computerised tomography
PGC1a	Peroxisome proliferator-activated receptor gamma coactivator 1-alpha
PKA	Protein kinase A
PLIN1	Perilipin 1
PR	Perirenal
PRDM16	PRD1-BF1-RIZ1 homologous domain containing 16
PRKGI	Protein kinase G I
qPCR	Quantitative Reverse Transcription PCR
RCR	Respiratory control ratio
RIP140	Receptor-interacting protein 140
RNA	Ribonucleic acid
ROCK	Rho-associated kinase
SAT	Subcutaneous adipose tissue
SDS-PAGE	Sodium dodecyl sulphate -polyacrylamide gel electrophoresis
SHOX2	Short stature homeobox 2
SVF	Stromal vascular fraction
T3	Triiodothyronine
T4	Thyroxine
TAG	Triacylglycerol
TBS	Tris-buffered saline
TCF21	Transcription factor 21
TdT	Terminal deoxynucleotidyl transferase
TEMED	Tetramethlethylenediamine
TMPD	N,N,N′,N′-tetramethyl-p-phenylenediamine
TNFα	Tumour necrosis factor α
TRE	Thyroid hormone response element
TTBS	Tween 20 tris-buffered saline
TUNEL	Terminal deoxynucleotidyl transferase dUTP Nick-End Labeling
UCP1	Uncoupling protein 1
WAT	White adipose tissue
YWHAZ	14-3-3 protein zeta/delta

Chapter 1 Introduction

My thesis consists of studies focusing on differences in thermogenic capacity between adipose tissue depots. The first study, conducted at the University of Nottingham, examined the development and characteristics of epicardial and paracardial adipose tissues compared to known white and brown fat depots using sheep as an animal model. The second study, conducted at the University of California, Los Angeles, focused on differences in browning capacity between periadrenal (visceral) and subcutaneous adipose tissues in response to chronic adrenergic stress observed in human pheochromocytoma. This chapter summarises the current literature on aspects of brown adipose tissue thermogenesis, browning of white adipose tissues and their possible contributions to improving metabolic health with evidence from animal and human studies.

1.1 Obesity and diabetes

Obesity can be broadly defined as the excess accumulation of fat to such an extent that physiological function is impaired. Obese individuals are at an increased risk of type II diabetes mellitus, where pancreatic β-cells are dysfunctional and individuals are insulin resistant. The prevalence of obesity and diabetes represent major global health problems, with an estimated 600 million adults classified as obese (World Health Organization, 2014) and 422 million

adults living with diabetes, the majority have type II diabetes commonly linked with increased adiposity (NCD-RisC, 2016). More concerning still is the increasing prevalence of obesity in children, with an estimated 41 million children classed as overweight or obese worldwide in 2014 (World Health Organization, 2014). Although obesity is more common in developed countries such as the United States and the United Kingdom, developing nations are also affected by increasing incidence of overweight/obesity (Prentice, 2006; World Health Organization, 2014).

Obesity and overweight is associated with other co-morbidities including cardiovascular disease (CVD) (Hubert et al., 1983), fatty liver disease (Ludwig et al., 1980), reduced fertility (Leary et al., 2015) and several types of cancer (Renehan et al., 2008). The development of metabolic syndrome, a cluster of risk factors for increased CVD risk encompassing hypertension, decreased high density lipoprotein (HDL) concentrations and elevated serum triacylglycerol (TAG) (Cleeman et al., 2001), is associated with obesity – in particular, with the accumulation of lipid storage around internal organs (visceral adiposity) (Carr et al., 2004). Co-morbidities in children have also been observed, such as type II diabetes mellitus (Haines et al., 2007), non-alcoholic fatty liver disease (Alisi et al., 2009), CVD and premature death (Franks et al., 2010).

A simple and commonly used method for obesity assessment is the calculation of Body Mass Index (BMI), given by the formula: *BMI= Weight (kg)/ Height (m^2)*. Based on the World Health Organization classification system, a BMI ≥25 is classed as overweight and a BMI ≥30 as obese (Organization, 2006). However, a

major limitation of this is that BMI only considers body weight *per se* rather than the relative amounts of fat and fat-free mass contributing to total body mass (Gibney, 2002). Therefore, the use of waist circumference in adults may be a useful addition to BMI for an indication of central adiposity as the localisation of lipid storage in the body may determine future adverse effects on physiology (Klein et al., 2007). The use of BMI *per se* is also not suitable for use in children as changes in BMI with age follow a non-linear pattern (Power et al., 1997). Therefore, body mass index centiles which take into account natural BMI variation with age are preferred (Power et al., 1997).

The aetiology of obesity is complex and it is likely that a range of factors contribute to its development. Although various genetic and environmental factors are involved, the main determinant of body fat gain is an imbalance between energy intake and energy expenditure (Tremblay et al., 1992). The amount, type and location of adipose tissue accumulation within the body are likely to be crucial factors in the progression of obesity and the health of an individual.

1.2 Adipose tissue

Regarded as a specialised form of connective tissue, adipose tissue is an essential organ required for survival in humans and other mammals (Cinti, 2012). It is heterogeneous in nature, being composed of a variety of cells in addition to adipocytes, including stromavascular cells, immune cells and connective tissue matrix (Kershaw and Flier, 2004). Adipose tissue was classically considered to be

an inactive organ that stored calories when supply exceeded demand and provided thermal insulation (Wertheimer and Shapiro, 1948). In recent years, however, this prevailing view which regarded adipose tissue as an organ of limited functional capacity has been altered considerably. It is now known that different types of adipocyte exist which differ both in embryological origin and physiological function.

1.2.1 White adipose tissue

Obesity and related co-morbidities are caused by the excess accumulation of white adipose tissue (WAT), which stores energy in the form of triacylglycerol. White adipocytes, the principal components of white adipose tissue, display a characteristic unilocular lipid droplet composed of TAG and cholesterol ester, (Figure 1.1), which constitutes over 90% of the cytoplasmic volume (Smorlesi et al., 2012). Lipolysis of stored TAG can be stimulated upon fasting, resulting in the release of fatty acids for oxidation in muscle and other organs (Gordon, 1957; Gordon and Cherkes, 1956). The histological appearance of WAT is shown in Figure 1.1.

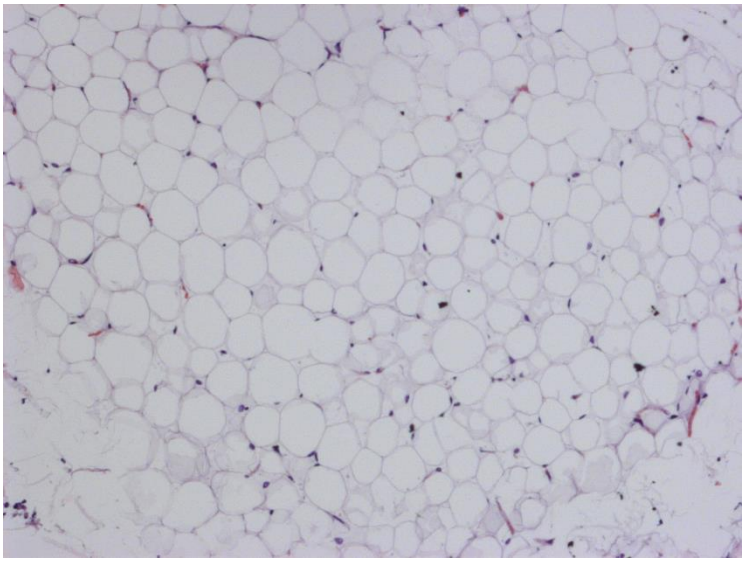


Figure 1.1 Light microscope image of human periadrenal white adipose tissue showing the characteristic unilocular lipid droplet of white adipocytes. Image taken at 10x magnification. (G Davies, unpublished data).

WAT is widely dispersed in humans and other mammals, although the locations in which the tissue accumulates can be divided anatomically into subcutaneous and visceral depots (Smorlesi et al., 2012). Subcutaneous adipose tissue is located underneath skin and can be further subdivided based on the anatomical relation to the *fascia superficialis* into superficial and deep depots (Kelley et al., 2000). Visceral adipose tissues are divided into several depots surrounding the major organs within the thoracic cavity (Kelley et al., 2000), of which, omental is one of the most widely studied depots.

It is well established that visceral and subcutaneous adipose depots have different properties and characteristics. The storage of excess visceral adipose tissue is associated with adverse metabolic outcomes such as insulin resistance whereas subcutaneous adipose tissue accumulation is associated with increased insulin sensitivity (McLaughlin et al., 2011). It has been suggested that visceral

adipose tissue accumulation may lead to insulin resistance through the release of fatty acids into the portal vein, which are then transported to the liver and affect hepatic metabolism known as the 'portal theory' (Bjorntorp, 1990). Some evidence suggests that this may be due to decreased insulin clearance by the liver (Mittelman et al., 2000) caused by a decrease in insulin receptor abundance (Kabir et al., 2005). A study in mice found that visceral adipose tissue transplantation into the mesenterium (drained by the portal vein) resulted in significantly increased insulin resistance compared to transplantation to the peritoneum (Rytka et al., 2011) suggesting the anatomical location of adipose tissue fat drainage is critical.

Despite these findings, a complete understanding of insulin resistance at the molecular level has not been achieved at present. One possible mechanism is excess circulating non-esterified fatty acids (NEFA) in the circulation, which are commonly seen in obese individuals (Arner and Ryden, 2015; Opie and Walfish, 1963). NEFA have been shown to compete with glucose as substrates for oxidation in skeletal muscle, a pathway known as the 'Randle cycle' (Randle et al., 1963). These high circulating NEFA concentrations may then prevent glucose utilisation leading to hyperglycaemia (Randle et al., 1963).

In normal insulin signalling, insulin binds to the insulin receptor which has tyrosine kinase activity (Gammeltoft and Van Obberghen, 1986), phosphorylating insulin receptor substrate (IRS) proteins (Sadoul et al., 1985). This in turn activates downstream Akt leading to glucose transporter 4 (GLUT4) translocation to the cell surface and the uptake of glucose (Kohn et al., 1996). It

has been found that in the skeletal muscle of insulin resistant or diabetic subjects, a reduction in phosphorylated IRS occurs (Goodyear et al., 1995) leading to reduced downstream signalling, GLUT4 and glucose uptake (Bjornholm et al., 1997). Free fatty acids have been shown to elicit this aberrant signalling (Griffin et al., 1999) possibly through increased lipid metabolites, leading to IRS serine phosphorylation instead of tyrosine which does not initiate the downstream signalling pathway (Yu et al., 2002). Further work will be needed to determine other factors involved as insulin resistance remains a key link to obesity and related co-morbidities.

1.2.1.1 White adipose tissue as an endocrine organ

In addition to energy storage, white adipose tissue serves a dual function as an endocrine organ (Poulos et al., 2010). Furthermore, it has been postulated that white adipose tissue may act as the largest endocrine organ in humans, especially in obese individuals (Hassan et al., 2012; Trayhurn, 2007). A range of endocrine factors are released from white adipocytes including a variety of cytokines (Adamczak and Wiecek, 2013) which have roles in inflammation and insulin resistance (Tack et al., 2012). Adipokines such leptin are also topics of intensive research due to effects on energy balance and regulation (Carbone et al., 2012).

In 1950 it was observed that a mutation in the obese (ob) gene caused severe obesity in rodents (Ingalls et al., 1950). More recent studies have also demonstrated mutations in this gene cause type II diabetes (Zhang et al., 1994). The gene in question codes for a 16-kilodalton protein found to circulate in

mouse and human plasma, referred to as leptin (Halaas et al., 1995). It is now known that leptin is a hormone which regulates a variety of physiological functions including satiety, energy expenditure and obesity progression (Coppari and Bjorboek, 2012). These effects are modulated by the binding of leptin to the leptin receptor, expressed in the hypothalamus and central nervous system (Friedman, 2009) and activates the JAK-STAT signalling pathway (Houseknecht et al., 1998). In animal models at least, leptin has downstream effects on feeding behaviour and energy balance (Jovanovic and Yeo, 2010). Leptin is produced primarily by white adipocytes (Ricci and Bevilacqua, 2012) and circulating plasma levels rise with increasing adiposity (Yeo and Heisler, 2012). Although leptin administration may be beneficial for rare cases of obese individuals deficient in leptin (Paz-Filho et al., 2011; Pelleymounter et al., 1995), it is worth noting that many obese individuals often demonstrate leptin resistance (Heymsfield et al., 1999), where high concentrations of circulating leptin are observed but do not strongly suppress appetite (Halaas et al., 1997). This presents a major limitation in the use of leptin as therapy for global obesity (Coppari and Bjorboek, 2012; Yeo and Heisler, 2012).

1.2.2 Brown Adipose Tissue

The presence of brown adipose tissue (BAT) has been known for many years: the earliest work was recorded in 1551 by Conrad Gessner, reporting the tissue in the interscapular region of the marmot, although the function remained unknown (Lee et al., 2013). Knowledge of the function of BAT was greatly

improved when heat generation from this organ was observed in rabbits (Hull and Segall, 1965) and human newborns (Dawkins and Scopes, 1965).

1.2.2.1 Function and characteristics of BAT

It is now known that BAT is able to generate heat across a wide range of eutherian mammals within the functional units of BAT, brown adipocytes. The morphological characteristics of brown adipocytes are easily distinguished from those of white adipocytes by small multilocular lipid droplets (see Figure 1.2) and highly abundant large mitochondria (Sell et al., 2004).

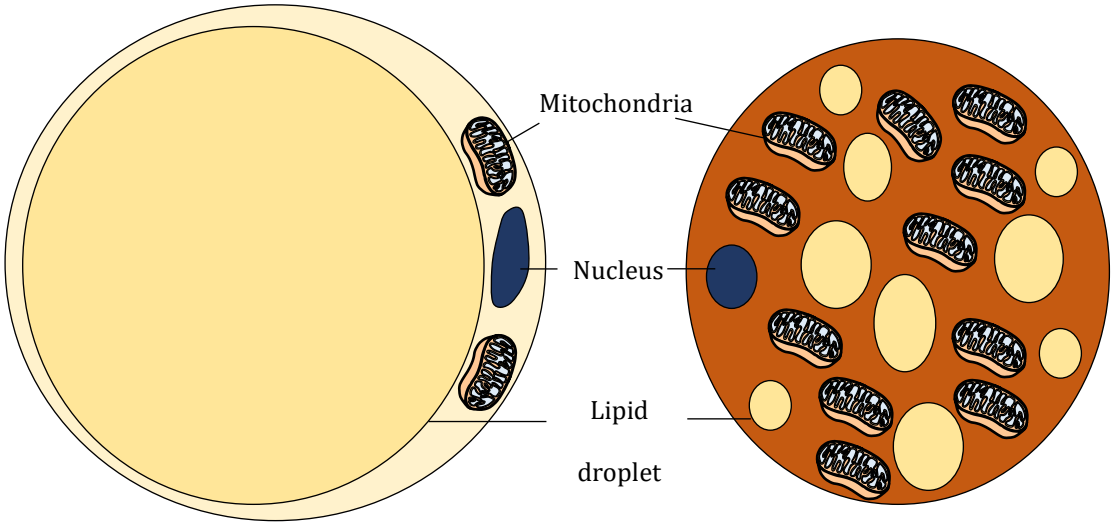


Figure 1.2 Morphology of brown and white adipocytes. Adapted and redrawn from (Sell et al., 2004).

Heat production by brown adipocytes is conferred by the presence of uncoupling protein 1 (UCP1), a 306 amino acid (32kDa) protein embedded in the inner mitochondrial membrane (Lin and Klingenberg, 1980). The structure of UCP1 is formed from 6 subunits forming a transmembrane spanning protein with the N (amino) group and the terminal C (carboxyl) end in the intermembrane space

(Miroux et al., 1993). It is often termed a 'tripartite' structure as 3 domains consisting of 2 hydrophobic α-helices are present. Of note, a nucleotide binding site is present on 3 of these domains (Klingenberg et al., 1999). A schematic diagram of the structure of UCP1 is shown in Figure 1.3.

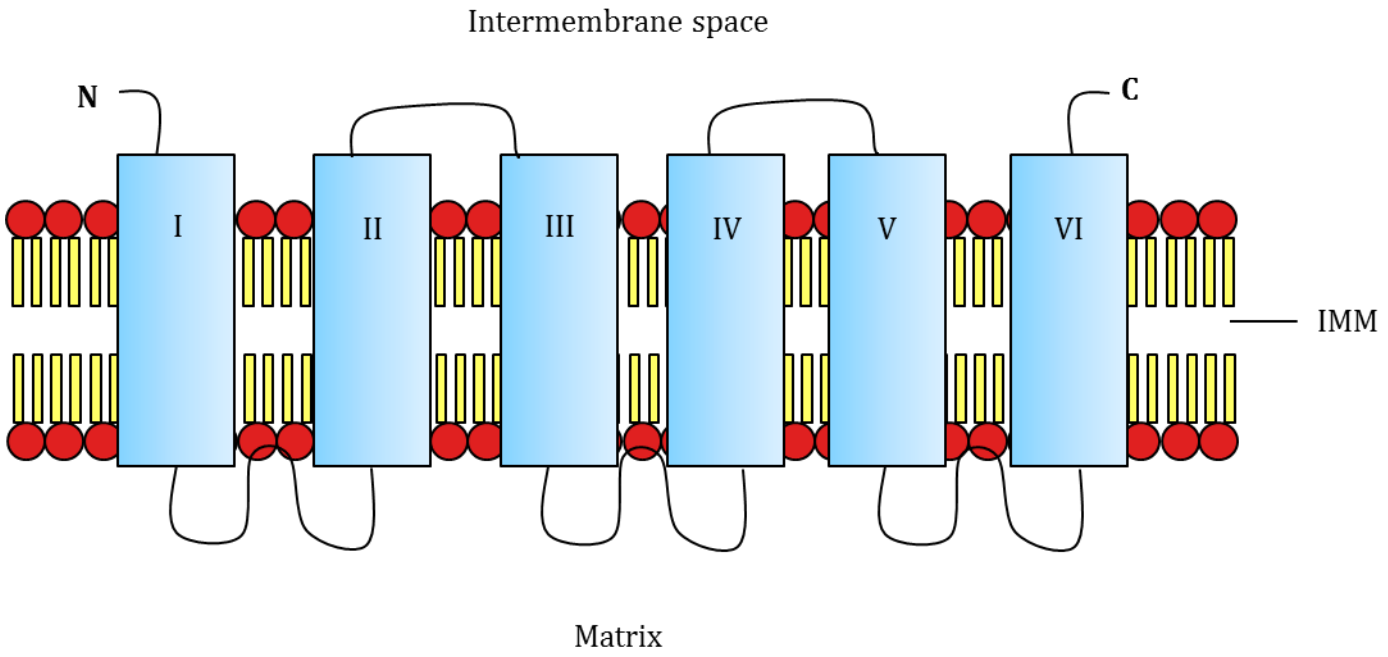


Figure 1.3 The structure of uncoupling protein 1 (UCP1) on the inner mitochondrial membrane (IMM) of thermogenic adipocytes.

It is composed of 6 subunits of 2 repeated domains hence the 'tripartite' structure. Subunits are linked by polypeptide chains. Simplified and adapted from Krauss et al (2005)

UCP1 expression was previously considered to be BAT–specific (Palou et al., 1998), although this may no longer be the case as discussed in section 1.3. UCP1 is responsible for heat dissipation through uncoupling oxidative phosphorylation (Heaton et al., 1978). In the mitochondria of most other cell types, the energy released during the transport of electrons through complex I-IV is used to establish a proton gradient leading to a high concentration of protons in the intermembrane space. Protons can be transported through adenosine triphosphate (ATP) synthase and the energy released is used to re-synthesise ATP from adenosine diphosphate (ADP) and inorganic phosphate (Berg, 2007). In contrast UCP1 allows the reflux of protons whilst bypassing ATP synthase (Nicholls and Locke, 1984) resulting in the release of heat without coupling to ATP synthesis. An overview of this process is shown in Figure 1.4.

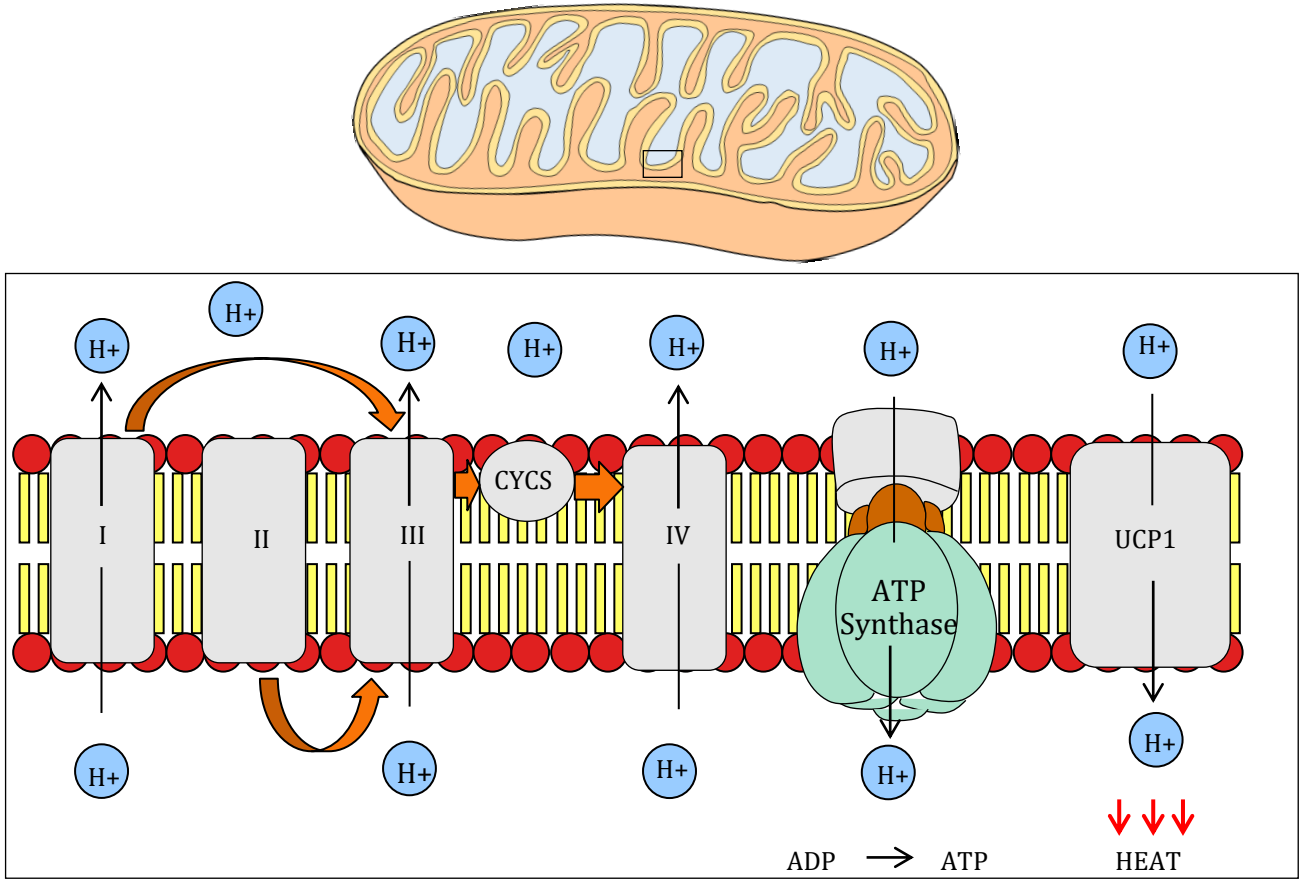


Figure 1.4 Role of uncoupling protein 1 (UCP1) in uncoupling oxidative phosphorylation.

The electron transport chain uses the energy of electron transfer to pump proton across the inner mitochondrial membrane generating a proton motive force (transport of electrons between complexes is shown by orange arrows). The energy released from the movement of protons back across the membrane is used to re-synthesise adenosine triphosphate (ATP) by ATP Synthase. UCP1 allows the movement of protons back across the membrane without ATP synthesis and the energy is released as heat.

A detailed understanding of proton transport by UCP1 at the molecular and biochemical level is currently lacking and studies have reported conflicting results. Several models have been proposed and, as full discussion of these is beyond the scope of this thesis, three main models including the most recent study will be discussed briefly. Two classical models for the action of UCP1 are the proton fatty acid buffering model (Fig 1.5 A) and the fatty acid cycling model (Fig 1.5 B). The 'proton buffering' model, postulates that UCP1 acts as a proton channel where the carboxyl group of long chain fatty acids (LCFA) and amino acid residues lining the UCP1 pore facilitate the transport of protons (Winkler and Klingenberg, 1994). The proton is then released into the mitochondrial matrix.

The fatty acid circuit model (Skulachev, 1991) suggests that protonated fatty acids can freely 'flip flop' across the inner mitochondrial membrane independently of UCP1. The fatty acid is then deprotonated and the proton is released into the mitochondrial matrix. UCP1 can then transport fatty acids to the intermembrane space to repeat the cycle. Several other studies have also provided evidence for this model (Garlid et al., 1996; Jezek et al., 1996; Kamp and Hamilton, 1992; Kamp et al., 1993).

The most recent model (Fedorenko et al., 2012) suggests protonated LCFA generated in the inner mitochondrial membrane bind to UCP1 itself and pass through the pore where the proton is released into the mitochondrial matrix. LCFA do not dissociate from UCP1 but can be transported to the other side of the pore in the absence of protons. Fatty acids were not found to be able to be

transported from the mitochondrial matrix through UCP1 however which would not support the previous fatty acid cycling model. A schematic diagram of this model is known in Figure 1.5 C. It should be noted that the evidence for these models comes from *in vitro* studies and may differ from the mechanism *in vivo* (Fedorenko et al., 2012). Given the conflicting evidence for a model of UCP1 action, further studies are needed to determine this.

Purine nucleotides, such as guanosine diphosphate (GDP) have been found to inhibit UCP1 by binding to a nucleotide binding site on the cytosolic side of the inner mitochondrial membrane (Nedergaard et al., 2001). However fatty acids can overcome purine nucleotide inhibition possibly through competitive binding with LCFA (Fedorenko et al., 2012). Fatty acid binding also causes a conformational change in UCP1 (Divakaruni et al., 2012) that may support a tight and loose binding hypothesis. Purine nucleotide binding causes a tight conformational state where proton conductivity is inhibited whereas the loose conformation retains proton transport capacity (Huang and Klingenberg, 1996). It is possible therefore, that fatty acids would promote the loose UCP1 complex. The physiological regulation of UCP1 inhibition by nucleotides is unknown, particularly if UCP1 inhibition by ADP and ATP occurs *in vivo*. It is has been reported that ATP synthase abundance is low in the brown adipocyte (Kramarova et al., 2008) which may ensure ATP concentrations do not inhibit UCP1 activity.

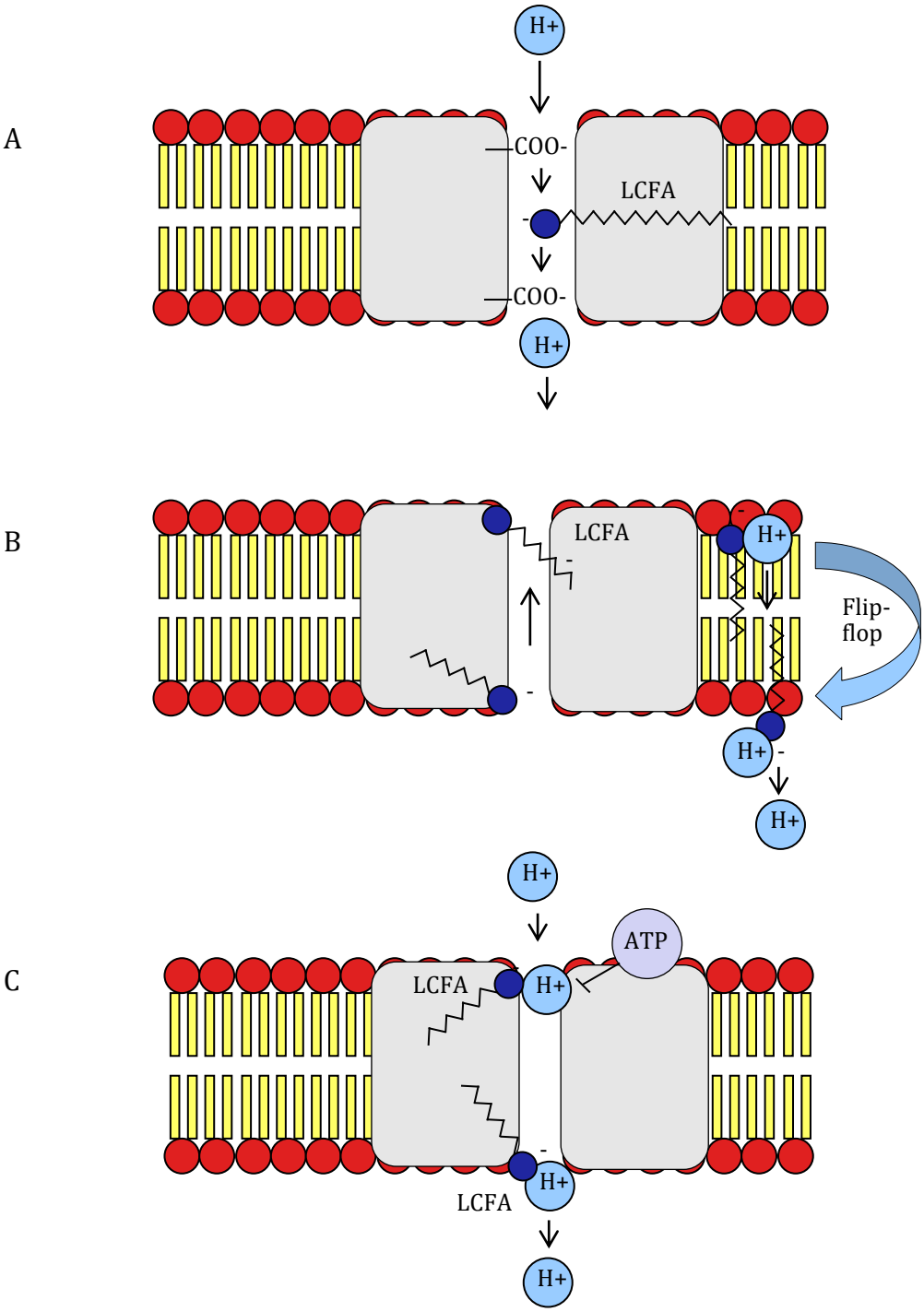


Figure 1.5 Putative models of uncoupling protein 1 (UCP1) proton transport mechanism. *A) Proton buffering model where UCP1 acts as a proton carrier facilitated by carboxyl groups of long chain fatty acids (LCFA) and amino acids within UCP1. B) Fatty acid cycling model where protonated fatty acids can freely flip flop across the inner mitochondrial membrane but UCP1 increases with proton flux by transporting fatty acids back into the intermembrane space. C) UCP1 is an anion carrier and protonated LCFA can be transported across the mitochondrial membrane. Adenosine triphosphate may inhibit this transport by competing for binding sites on UCP1*

1.2.2.2 UCP1 function from an evolutionary perspective

The purpose of UCP1 has often been postulated to be the maintenance of body temperature of the newborn to cold exposure in the extra-uterine environment. As a result of cold exposure, non-shivering thermogenesis (NST) occurs which can be defined as the production of heat without the contraction of skeletal muscle (Tews and Wabitsch, 2011). BAT has been identified as the primary effector of this process (Tews and Wabitsch, 2011) and rodents in particular, are reliant on BAT as the sole tissue responsible for NST (Nedergaard et al., 2001). Evidence for this comes from the use of UCP1 knockout ($^{-/-}$) mice which, when exposed to cold temperatures of 5°C, lose body heat more rapidly than wild type mice (Enerback et al., 1997) and also have decreased survival to long term cold exposure (Golozoubova et al., 2001). UCP1 has been found in a wide range of small and large eutherian mammals including hamsters (Trayhurn et al., 1989), sheep (Finn et al., 1998), reindeer (Soppela et al., 1992) and humans (Virtanen et al., 2009). Indeed, the presence of a protein with high homology to mouse UCP1 has been found in the Lesser hedgehog tenrec (*Echinops telfairi)*, from the ancient afrotherian clade of eutherians which displays poikilothermic and endothermic episodes. In this animal BAT appears to be most active in the poikilothermic to endothermic transition (Oelkrug et al., 2013). This gives evidence that the function of an uncoupling protein such as UCP1 is well conserved across mammals that are phylogenetically distinct and may have been advantageous to the evolution of the modern endothermic mammals. Interestingly, dolphins may also have UCP1 positive BAT interspersed with

blubber suggesting an importance in the thermal regulation of aquatic mammals (Hashimoto et al., 2015), again supporting the evolutionary importance of this protein.

There may however be some exceptions among endothermic mammals such as the pig which has a disrupted UCP1 gene (Berg et al., 2006). Although the protein has recently been shown by western blot (Mostyn et al., 2014), other studies have failed to show UCP1 positive porcine adipose tissue during early life (Trayhurn et al., 1989) and it has not yet been shown to be functional in uncoupling oxidative phosphorylation. If UCP1 is absent or dysfunctional in pigs it may be due to mammals of the *Suidae* family existing in tropical climates where non-shivering thermogenesis would not be required and shivering alone is sufficient for thermoregulation (Berg et al., 2006). It should be noted that although compensatory mechanisms such as shivering are also present in UCP1$^{-/-}$ mice, increased oxidative stress is observed in skeletal muscle (Stier et al., 2014) which may ultimately have detrimental effects on the lifespan of the animals (Golozoubova et al., 2001). Therefore non-shivering thermogenesis may be a metabolically beneficial process in thermoregulation.

1.2.2.3 Molecular pathway of non-shivering in cold exposure

Cold exposure activates sympathetic nerves releasing the neurotransmitter noradrenaline to innervated tissues (Dulloo et al., 1988) including BAT (Young et al., 1982). Plasma noradrenaline, but not adrenaline concentrations, typically increase in cold exposed animals (Barrand et al., 1981; Vollmer et al., 1992) as

noradrenaline is also released from the adrenal medulla (Barrand et al., 1981; Kvetnansky et al., 1971). Catecholamines appear to be essential in cold-induced thermogenesis, as mice unable to synthesise adrenaline and noradrenaline show reduced UCP1 mRNA and larger unilocular adipocytes within interscapular BAT after cold exposure (Thomas and Palmiter, 1997). Noradrenaline binds to adrenergic β-receptors; in particular, the β-3 receptor isoform predominates in brown adipocytes (Granneman et al., 1991). Noradrenaline binding causes downstream signalling initiated through cyclic adenosine monophosphate (cAMP) which activates Protein kinase A (Cao et al., 2001). Protein kinase A (PKA) activates p38 mitogen-activated protein kinase (MAPK) which phosphorylates activated transcription factor 2 (ATF2) and cAMP reponse element binding protein (CREB) and increases binding to the cyclic AMP response element (CRE) on the promoter of UCP1 causing an increase in transcription (Cao et al., 2001).

PKA also acts to increase lipolysis from stored intracellular triglyceride (Schimmel et al., 1980). PKA can phosphorylate adipose triglyceride lipase (ATGL) causing the initial breakdown of TAG to diacylglycerol (DAG) (Pagnon et al., 2012; Zimmermann et al., 2004). Hormone sensitive lipase (HSL) is also phosphorylated causing the catabolism of DAG to monoacylglcerol (Haemmerle et al., 2002). Perilipin (PLIN1), a lipid droplet associated protein, is also phosphorylated which facilitates the translocation of phosphorylated HSL to the lipid droplet for lipolysis (Miyoshi et al., 2006). This occurs in both WAT and BAT but lipolysis appears to be essential for non-shivering thermogenesis in BAT *in*

vivo (Souza et al., 2007). It is likely therefore that lipolysis releases fatty acids for UCP1 action as discussed in the models of UCP1 action previously.

In addition to intracellular lipids being used for thermogenesis (Fedorenko et al., 2012), it has been shown that lipids are channelled into BAT from the circulation (Bartelt et al., 2011; Dijk et al., 2015). The mechanism for this has recently been elucidated, revealing that lipoprotein lipase (LPL), responsible for the hydrolysis of circulating TAG in target tissues such as BAT during cold exposure, is inhibited by Angiopoietin-like 4 (ANGPTL4), (Dijk et al., 2015). ANGPTL4 is abundantly expressed in WAT and BAT (Dijk et al., 2015); however in sustained cold exposure, it is oppositely regulated between the two adipose tissues. Decreased ANGPTL4 mRNA is observed in BAT but is upregulated in WAT, resulting in a channelling of free fatty acids into BAT from the circulation (Dijk et al., 2015) through hydrolysis by LPL and fatty acid transport by CD36. A schematic diagram of this pathway is shown in Fig 1.6.

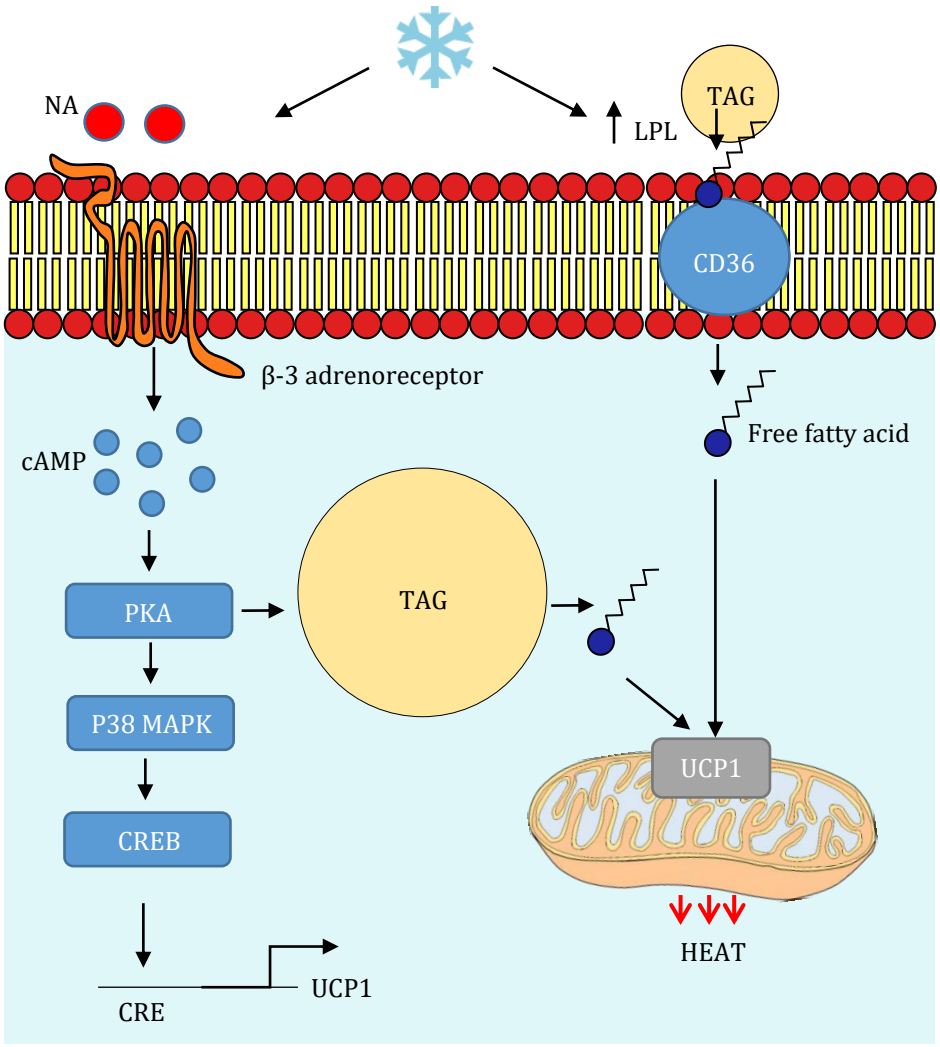


Figure 1.6 The molecular pathway of UCP1 upregulation and thermogenesis to cold exposure

Cold exposure causes the release of noradrenaline (NA) which binds to the β-3 adrenoceptor on the plasma membrane of brown adipocytes. This leads to increased second messenger cyclic adenosine monophosphate (cAMP) which activates protein kinase A (PKA). PKA phosphorylates p38 mitogen activated kinase (p38 MAPK) which can then phosphorylate cAMP response element binding protein (CREB), a transcription factor which binds to the cyclic AMP response element (CRE) on the promoter of uncoupling protein 1 (UCP1) to increase mRNA transcription. PKA can also activate lipolysis from intracellular lipid droplets of triacylglcerol (TAG) to provide free fatty acids for uncoupling protein 1 thermogenesis. Alternatively brown adipocytes can take up fatty acids from the circulation as lipoprotein lipase is more active in cold exposure, causing the influx of free fatty acids into the adipocyte through CD36 that can be used for thermogenesis.

1.2.2.4 Other endocrine stimuli of non-shivering thermogenesis

In addition to catecholamines, other hormones have been found to increase thermogenesis within adipose tissue. Thyroid hormones for example are also well established to upregulate UCP1. The biologically active form of the thyroid hormones is triiodothyronine (T3) although the prohormone thyroxine (T4) is more abundant in the circulation (Mondal et al., 2016). In BAT, T4 is converted to T3 by type II deiodinases (DIO2) (Silva and Larsen, 1985). DIO2 is upregulated during cold exposure (de Jesus et al., 2001) and is necessary for cold-induced thermogenesis (de Jesus et al., 2001). The action of thyroid hormones is synergistic with noradrenaline in upregulating UCP1 (Bianco et al., 1988). Conversely, hypothyroidism in rats also results in reduced capacity to respond to catecholamines (Bianco et al., 1988) and adenylyl cyclase activity is reduced (Carvalho et al., 1996). $DIO2^{-/-}$ mice are unable to upregulate UCP1 in response to noradrenaline infusion and defects in lipolysis and thermogenesis can be rescued by T3 infusion (de Jesus et al., 2001). The addition of T3 is also able to upregulate UCP1 in rat brown adipocytes (Guerra et al., 1996). Conversely, catecholamines stimulate T3 production and DIO2 activity (Silva and Larsen, 1983). The action of thyroid hormones on UCP1 occurs through the thyroid receptor β (Ribeiro et al., 2010), leading to increased transcription of UCP1 (de Jesus et al., 2001). This occurs as thyroid hormones translocate to the nucleus where they can bind to the thyroid hormone response element (TRE) on the enhancer of UCP1 and increase transcriptional activity to cAMP (Rabelo et al., 1995).

Fibroblast growth factor (FGF) 21 has also been found to increase non-shivering thermogenesis (Hondares et al., 2011). It can be induced by noradrenaline and β-adrenergic signalling (Chartoumpekis et al., 2011; Hondares et al., 2011). Although primarily produced by the liver (Markan et al., 2014) it is also synthesised within brown adipocytes (Hondares et al., 2011). FGF21 binds to the β-klotho receptor and FGF receptors 1c and 4 (Ogawa et al., 2007). Treatment of mice with FGF21 causes browning of inguinal and perirenal adipose tissue with upregulated UCP1 and DIO2 expression (Fisher et al., 2012). Indeed, $FGF21^{-/-}$ mice are cold sensitive and have reduced UCP1 mRNA compared to wild type mice (Fisher et al., 2012). A recent study has also suggested that FGF21 can increase plasma lipid clearance by BAT and WAT due to the upregulation of CD36 and LPL (Schlein et al., 2016).

1.3 Adipose tissue 'browning' and beige adipocytes

Brown adipocytes have been described as the only cells capable of thermogenesis through the action of UCP1. However, this definition may no longer be adequate to distinguish these cells from other adipocytes. After cold exposure, adipocytes with multilocular lipid droplet morphology have often been observed in previously white fat depots (Cousin et al., 1992; Guerra et al., 1998; Vitali et al., 2012), a process known as adipose tissue 'browning'. Certain adipose tissue depots seem to be more prone to browning, as in rodents, the inguinal subcutaneous depot displays striking increases in UCP1 gene expression in response to cold and other factors whereas epididymal (visceral) adipose tissue does not (Seale et al., 2011; Walden et al., 2012). It is clear that not all adipocytes

within the inguinal adipose tissue depot are capable of this browning however, suggesting a subpopulation of inducible cells exists within some depots of white adipose tissue (Himms-Hagen et al., 2000).

The proliferation of these induced UCP1 positive adipocytes has been noted during treatment with adrenergic β-3 receptor agonists (Cousin et al., 1992). These have often been termed 'Brown in white' (BRITE) cells (Petrovic et al., 2010) or beige adipocytes (Ishibashi and Seale, 2010). Beige adipocytes are so called as they appear to be intermediate between that of brown and white adipocytes. Under basal conditions, they display a low abundance of UCP1 (Wu et al., 2012) and are morphologically similar to white adipocytes with a large unilocular lipid droplet (Rosenwald et al., 2013). They have also been termed 'inducible adipocytes', as, under stimulation to cold, they have the capacity to upregulate UCP1 abundance comparable to classical brown adipocytes (Wu et al., 2012). The morphology of beige adipocytes also takes on characteristics of classical brown adipocytes including an increase in mitochondrial biogenesis and multilocular lipid droplets (Rosenwald et al., 2013). The abundance of UCP1 mRNA at the tissue level (for example in murine inguinal adipose tissue), however, remains below that of classical BAT, possibly due to the heterogeneity of the tissue depot (Walden et al., 2012).

There has been recent debate regarding the functional thermogenic capacity of UCP1 within beige adipocytes. Cellular bioenergetics experiments report a striking inhibition of mitochondrial respiration by GDP from the inguinal adipose tissue of cold acclimated mice (Shabalina et al., 2013). This effect was not

observed in mitochondria from the inguinal adipose tissue depot of UCP1 $^{-/-}$ mice, despite similar morphological changes in adipocytes with cold exposure (Shabalina et al., 2013). Conversely, cells isolated from the stromal vascular fraction of inguinal adipocytes and differentiated to UCP1 positive adipocytes did not display increased uncoupled respiration compared to cells differentiated to white adipocytes (Keipert and Jastroch, 2014). Discrepancies between the two studies may be accounted for by the use of isolated mitochondria by Shabalina et al whereas primary adipocytes were used by Keipert and Jastroch. It is possible that the primary adipocytes may not have retained the characteristics of the tissue from which they were derived, for example, CD137 is downregulated in inguinal adipose tissue in cold exposure but primary cells do not demonstrate this change when exposed to β-agonists (de Jong et al., 2015). Also Keipert and Jastroch exposed mice to 23°C compared to a more severe cold challenge of 4-6°C used by Shablina. It is possible therefore that UCP1 is active in beige adipocytes only in severe cold exposure, however this requires further investigation.

When induced by cold, beige adipocytes have been found to express certain genes to a greater extent that classical brown and white adipose tissues/adipocytes. These genes have been termed beige adipose tissue or adipocyte 'markers' but studies investigating these have reported conflicting results. The first report of a distinct molecular signature of browned inguinal adipose tissue was from Walden et al who found increased expression of homeobox C9 (HOXC9) and short stature homeobox 2 (SHOX2) compared to epididymal (white) and interscapular BAT (classical brown) (Walden et al., 2012). This has since been revised as HOXC9 does not appear to increase in

inguinal adipose tissue in cold exposure and primary cells do not show an increase in HOXC9 when treated with noradrenaline (de Jong et al., 2015). Other markers of beige adipocytes were also proposed including CD137 which was highly expressed in inguinal adipose tissue compared to interscapular BAT and epididymal fat depots (de Jong et al., 2015). Microtubule tumour suppressor 1 (MTUS1) variant 3 and potassium channel subfamily K member 3 (KCNK3) mRNA transcripts are enriched in inguinal adipose tissue of mice treated with β-agonists and have also been proposed as beige markers (Shinoda et al., 2015). Furthermore, RNA silencing of MTUS1 variant 3 and KCNK3 in primary cells from inguinal adipose tissue reduces UCP1 abundance and uncoupled respiration, suggesting the genes play a key role in beige adipocyte thermogenesis (Shinoda et al., 2015). The expression of these transcripts may therefore help to define the composition of beige adipocytes within adipose tissue.

Although beige adipocytes are classed as a separate type of adipocyte, it has recently been shown that this may be a functional adaptation to white adipocytes where the adipocytes can reversibly transdifferentiate. Using elegant labelling techniques, Rosenwald et al showed that UCP1 positive adipocytes induced during cold exposure are still present at rewarming but adopt a unilocular adipocyte morphology and are UCP1 negative (Rosenwald et al., 2013). Many of these same cells are able to be reactivated with subsequent cold exposure (Rosenwald et al., 2013). Although this clearly demonstrates that browning is a reversible process and that beige adipocytes can have both white adipocyte and thermogenic characteristics depending on environmental stimuli, the direct interconversion of white to beige appears inconclusive. For example, it is not

clear why only a subset of white or beige adipocytes are UCP1 positive after cold exposure as it may be expected that all adipocytes would undergo browning if they are a homogeneous cell population. It has been demonstrated that UCP1 positive adipocytes within inguinal adipose tissue are located near the vasculature (Barreau et al., 2016), so it is possible that certain factors from the circulation needed for browning are only provided in adequate amounts to adjacent adipocytes. However, further work is required to understand the mechanism behind the browning of some adipocytes and not others. To gain an understanding of the possible plasticity of adipocyte types it is important to consider their developmental origin.

1.4 Origins of brown, white and beige adipocytes

It had previously been thought that both white and brown adipocytes shared a common embryological origin (Kajimura et al., 2010). However, recent lineage tracing studies have revealed that at least some adipocytes may have separate and multiple origins. The majority of classical brown adipocytes derive from dermomyotomal precursors that express paired box 7 (Pax7) and myogenic factor 5 (Myf5) similar to skeletal muscle (Lepper and Fan, 2010). These precursor cells can then differentiate into either skeletal muscle or brown adipocytes and cell fate is controlled by PRD1-BF1-RIZ1 homologous domain containing 16 (PRDM16) (Seale et al., 2008). Expression of PRDM16 causes the development of brown adipocytes and, conversely, ablation of PRDM16 reduces brown adipocyte characteristics and gives rise to skeletal muscle (Seale et al.,

2008). However brown adipocytes within white fat depots can either be Myf5 positive or negative (Sanchez-Gurmaches and Guertin, 2013).

White and beige adipocytes have been suggested to develop from Myf5 negative precursors (Wu et al., 2012). Whether beige and white adipocytes have separate lineages is under debate given the possible transdifferentiation hypothesis described above. There is evidence to suggest that beige adipocytes may derive from smooth muscle precursor cells, however the smooth muscle marker myosin heavy chain 11 (Mhy11) only labelled ~ 9% of UCP1 positive adipocytes within the inguinal adipose tissue (Long et al., 2014) possibly suggesting that the majority of these cells derive from a separate lineage. *In vitro* experiments have shown that mature smooth muscle cells can acquire lipid droplets and express UCP1 similar to beige adipocytes (Long et al., 2014). It is unknown at present if this occurs under physiological conditions *in vivo*. The transcription factors PRDM16 (Seale et al., 2011) and early B-cell factor 2 (EBF2) (Stine et al., 2016) appear to be particularly important for beige adipocyte cell fate, as disruption or ablation of the gene causes a decrease in thermogenic adipocytes and overexpression promotes beige adipocyte appearance. PRDM16 in particular is abundantly expressed within inguinal adipose tissue compared to epididymal adipose tissue (Seale et al., 2011) and therefore may suggest a reason for the browning properties of inguinal adipose tissue in mice. A schematic diagram of possible adipocyte origins is shown in Figure 1.7.

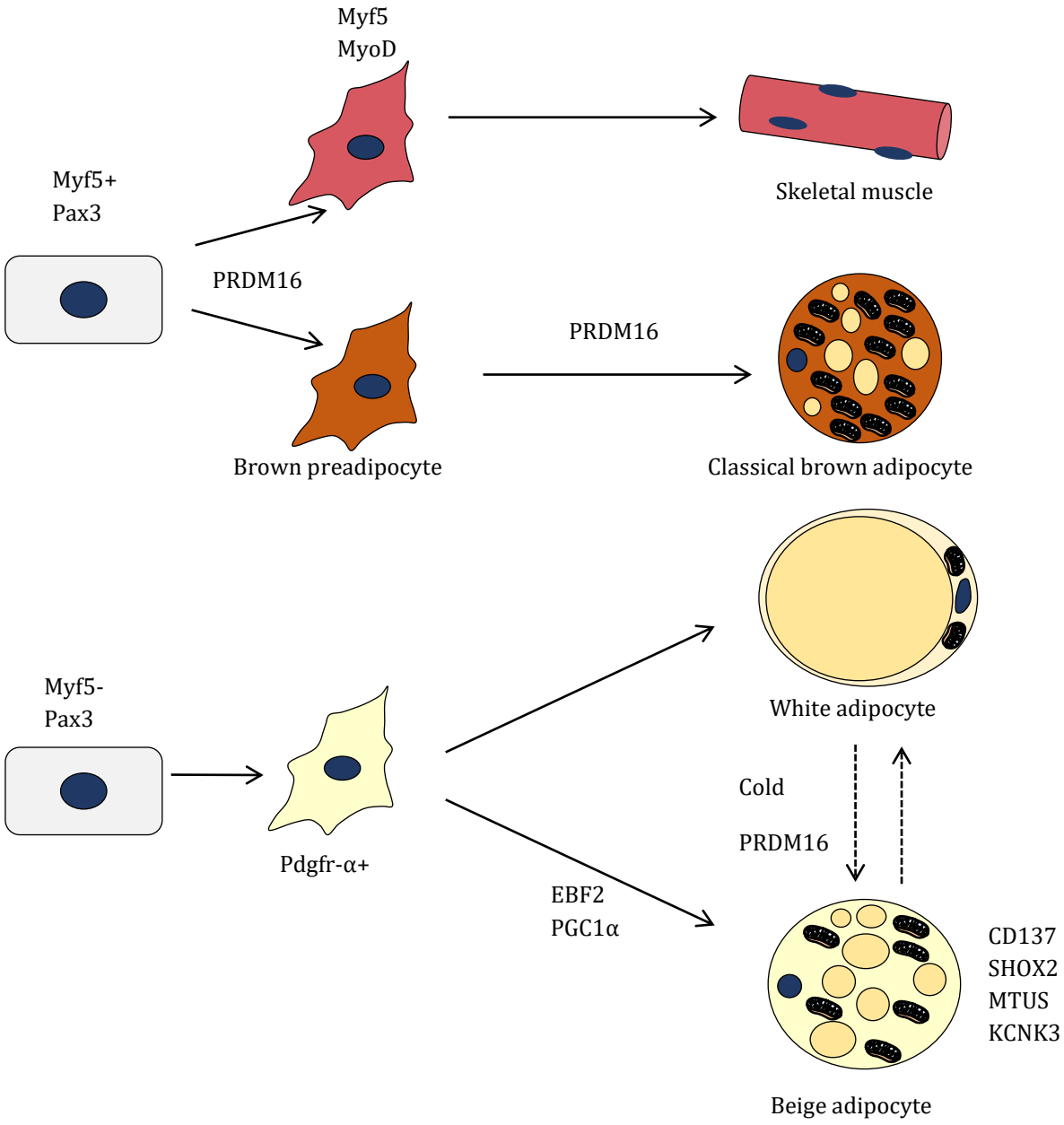


Figure 1.7 Schematic diagram of adipocyte origins.

Brown adipocytes generally develop from myogenic factor 5 (Myf5) and paired box 3 (Pax3) positive precursors and can develop into either skeletal muscle or classical brown adipocytes with cell fate determined by PRD1-BF1-RIZ1 homologous domain containing 16 (PRDM16) expression. White and beige adipocytes generally develop from Myf5- Pax3 positive precursors. Beige adipocytes may develop separately requiring early B-cell factor 2 (EBF2) and Peroxisome proliferator-activated receptor gamma coactivator 1-alpha (PGC1α) expression. Reversible transdifferentiation between white and beige adipocytes in response to stimuli such as cold or expression of PRDM16 may also be possible

1.5 Beneficial roles of thermogenic adipose tissue in metabolism and energy balance – evidence from animal models

Although a role of BAT in NST has been known for some time, it is only relatively recently that a possible role for BAT in energy balance and obesity prevention has become apparent (Farmer, 2009; Lee et al., 2013; Lichtenbelt, 2011). Animal studies have been pivotal in determining a role for BAT in energy balance and regulation. In particular, transgenic mice have aided research into the effects of uncoupling and thermogenesis on obesity development and metabolic health.

The deletion of a target gene or 'knockout' is particularly useful in elucidating the function of a gene (or the translated protein) in physiology and metabolism. Once a gene is deleted, the resulting effect on physiology can be assessed (Picotto and Wickman, 1998). This is often performed in rodents as the genome is well characterised and classical methods of generating knockout animals through homologous recombination (Tong et al., 2010; Zijlstra et al., 1989) can be achieved relatively quickly. It should be noted that modern CRISPR/Cas genetic engineering approaches allow for faster generation of knockout animals compared to traditional methods using homologous recombination (Yang et al., 2014). Knockouts can be compared to wild type animals (without the gene deletion) (Bordicchia et al., 2012), which allows for highly controlled studies on animals of the same genetic background to assess the function of a particular gene. As some gene deletions can result in embryonic lethality (Acharya et al., 2012), it is also possible to delete the gene in a specific tissue, known as a

'conditional' knockout (Gierut et al., 2014). This is achieved through a knock-in of Cre recombinase under the control of a tissue-specific promoter (Gierut et al., 2014), for example, aP2 in adipose tissue (Graves et al., 1992). When expressed, the Cre recombinase can inactivate target genes flanked by loxP sites (Gierut et al., 2014). This provides a powerful method to examine effects of a gene knockout in a particular tissue where normal function should be conserved in other tissues.

However a disadvantage of gene knockouts is that compensatory mechanisms may mask the effect of the deleted target gene. A compensatory mechanism was noted on UCP1 knockout ($^{-/-}$) mice for example, which prevented the role of UCP1 in bodyweight regulation to be observed in early studies. The first study of UCP $^{-/-}$ mice reported no effect on bodyweight or feeding behaviour compared to wild type mice (Enerback et al., 1997). However, both knockout and wild type mice in this study were housed at temperatures below thermoneutrality i.e. the temperature at which a stable core body temperature is achieved without shivering or evaporative water loss mechanisms such as sweating (Gordon, 2012). This may mask the effects of UCP1 ablation as the mice can compensate by increased shivering (Golozoubova et al., 2001), thereby increases in muscular activity prevent weight gain (Cannon and Nedergaard, 2010). The effect of UCP1 ablation on bodyweight in mice becomes apparent close to thermoneutrality (Cannon and Nedergaard, 2010). Indeed, UCP1 ablated mice show increased propensity to obesity when fed high fat, and to a lesser extent, standard chow diets at thermoneutrality (Feldmann et al., 2009). Surgical ablation of

interscapular brown fat, the main BAT depot in the mouse, also elicits profound increases in bodyweight (Connolly et al., 1982).

Conversely, increased uncoupling through ectopic expression of UCP1 can mediate weight loss (Kozak and Anunciado-Koza, 2008). Genetically obese mice with ectopic expression of UCP1 in white fat depots have significantly reduced body weights with decreased subcutaneous fat (Kopecky et al., 1995). In addition, the overexpression of PRDM16 in mice results in increased WAT browning and reduced weight gain to high fat diet (Seale et al., 2011). This suggests that BAT, or adipose tissue browning, has a crucial role in energy balance in some animal models and increased uncoupling may mediate bodyweight regulation.

Intriguingly, in addition to the effects of BAT on energy homeostasis, significant effects on glucose tolerance and insulin sensitivity have been noted. The Lou/C rat strain displays marked browning of inguinal adipose tissue compared to Wistar rats when treated with β-agonists and also has increased insulin sensitivity associated with browning (Poher et al., 2015). The insulin-stimulated glucose uptake was increased in inguinal and epididymal tissues (Poher et al., 2015) suggesting that beige adipocytes in these depots may clear glucose from the circulation. Transplantation of interscapular BAT into the visceral cavity of mice also significantly improves insulin sensitivity and glucose uptake into adipose tissues compared to sham-treated controls (Stanford et al., 2013). Obese mice with activated BAT from cold exposure also show amelioration of insulin

resistance (Bartelt et al., 2011). Therefore, activated BAT may be able to improve insulin sensitivity possibly through the clearance of glucose from the circulation.

BAT can also utilise significant lipid as well as glucose. Bartelt et al. demonstrated that in rodents, BAT is responsible for the clearance of triacyglycerol (TAG)-rich lipoproteins, a process dependant on the action of LPL and CD36 (Bartelt et al., 2011). These effects may be particularly promising in pathological states: hyperlipidaemic apoliprotein A 5 $(ApoA5)^{-/-}$ mice show significantly reduced plasma lipid after 4 and 24 hour cold exposure (Bartelt et al., 2011). Increased lipid uptake was observed in the interscapular BAT but not subcutaneous adipose tissue (Bartelt et al., 2011) possibly suggesting beige adipocytes did not contribute substantially to this effect.

1.6 Human thermogenic adipose tissue

Given the evolutionary role of BAT in maintaining temperature homeostasis during early life in eutherian mammals it is unsurprising that human newborns and infants also possess BAT. An accurate description of the organ in the interscapular region of human infants, together with noted similarities with other species, was provided by Hatai who referred to the organ as the 'hibernating gland' (Hatai, 1902). Further anatomical studies also described this same interscapular brown fat in newborn humans (Bonnot, 1908). Important work on the appearance and prevalence of BAT throughout the life span was conducted by Heaton et al from human cadaver specimens (Heaton, 1972). Multilocular adipocytes characteristic of brown adipocytes were noted in the

intrascapular region of children in the first decade of life (Heaton, 1972). In children and adults, multilocular adipose tissue was found in the neck and perirenal depots up to the third decade of life. In some depots such as aortic and mediastinal fat, multilocular adipocytes appeared to be conserved into the fourth and fifth decades of life (Heaton, 1972). This work was conducted prior to the discovery of UCP1 however, so the abundance of the protein in human adipose tissues was not reported.

These findings of possible BAT in humans were largely ignored for many years and it was considered to be present only in the newborn. It was not until a series of papers published in 2009 reignited interest in the topic by demonstrating observable amounts of brown fat in the supraclavicular region of human adults (Cypess et al., 2009; van Marken Lichtenbelt et al., 2009; Virtanen et al., 2009). These studies used positron emission tomography (PET) or PET followed by computerised tomography (PET-CT) scans to observe the uptake of a radioactive form of glucose, ^{18}F-FDG, into regions of supraclavicular BAT. Cypess et al. biopsied these regions showing high glucose uptake and demonstrated bonafide BAT through the expression of UCP1 (Cypess et al., 2009).

Other BAT depots present in adults include perirenal/adrenal, pericardial/mediastinal and perirenal (Enerback, 2010). A schematic diagram of the anatomical locations of BAT in the newborn and adult human is shown in Figure 1.8.

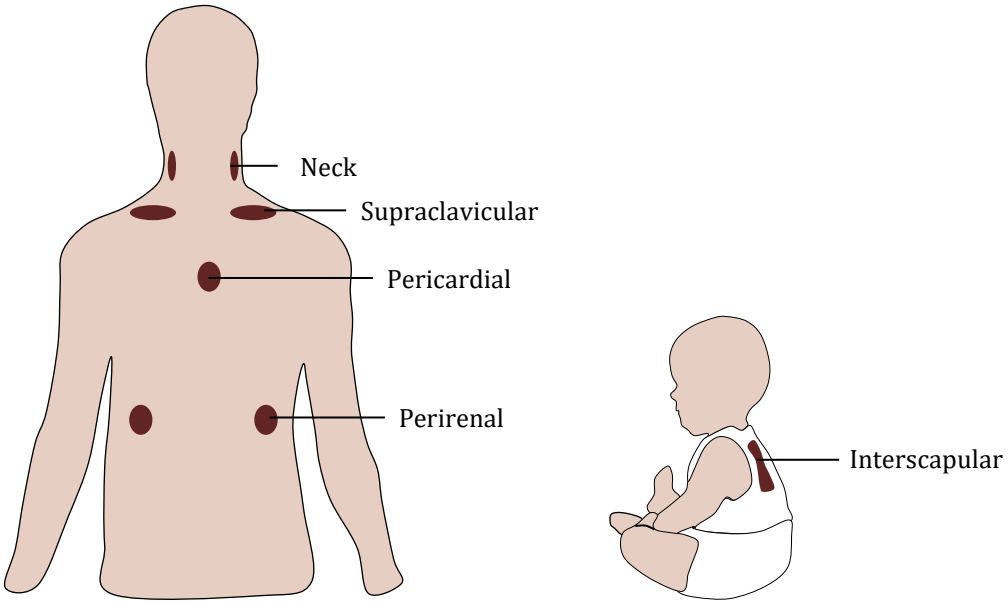


Figure 1.8 The major locations of BAT in human adults and infants.

Human adults typically possess BAT in the neck, supraclavicular, pericardial and perirenal adipose tissue depots (Left). Human newborns and infants possess interscapular BAT (right). Fat depot sizes are not to scale. Adapted and redrawn from (Enerback, 2010) and (Peirce et al., 2014).

Studies examining the prevalence of BAT in adult humans using ^{18}F-FDG PET-CT have produced variable results. Recent findings have suggested that BAT is present in 5-10% of the adult human population (Lee et al., 2011). A large study conducted by Cypess et al. reported detectable BAT in 76 of 1013 women (7.5%) and 30 of 959 men (3.1%) which the authors suggest demonstrates a ratio of greater than 2:1 females to males, and inverse correlations were noted for age (Cypess et al., 2009). A greater amount of BAT in female patients compared to males, as well as seasonal variation in BAT activity was also noted by Au-Yong et al., however the rate of detectable BAT was still low and only observed in 167 of 3614 patients (4.6%) (Au-Yong et al., 2009).

Although these results appear to cast doubt on the significance of brown fat in adult human physiology, many of these ^{18}F-FDG PET or PET-CT studies have been conducted at thermoneutrality (Au-Yong et al., 2009; Cypess et al., 2009) which decreases BAT detection rates compared to scans performed during cold exposure (Saito et al., 2009). It has also been found that supraclavicular tissue biopsies from PET-CT negative patients have shown characteristics of brown adipocytes, including multilocular lipid droplets and UCP1 positive staining by immunohistochemistry (Jespersen et al., 2013; Lee et al., 2011). In addition, scans repeated multiple times on the same patient do not show consistent positive or negative BAT detection (Lee et al., 2013; Rousseau et al., 2006) which may suggest limitations with the reproducibility of this technique. That ^{18}F-FDG PET uses radioactive glucose is also a limitation as the main substrate used for BAT thermogenesis is fatty acids (Bartelt et al., 2011). Taken together, it may be possible that PET/PET-CT may not be able to detect all active BAT and further work is needed using a range of imaging modalities to determine the prevalence in the adult population.

1.6.1 Human brown or beige adipocyte characterisation

Interscapular BAT from human infants has been reported as being composed of classical brown adipocytes due expression of ZIC1 mRNA (Lidell et al., 2013) which is selective for brown adipocytes (Petrovic et al., 2010). In adults however, the supraclavicular adipose tissue depot has been reported as having a molecular signature similar to murine beige (inguinal) adipose tissue rather than classical interscapular BAT (Sharp et al., 2012). Gene expression analyses revealed

markers HOXC8, HOXC9 and CITED1 in human areas of BAT similar to adipocytes isolated from the inguinal adipose tissue and stimulated with rosiglitazone, (a PPARγ agonist) suggestive of a beige adipocyte composition (Sharp et al., 2012). The detection of beige adipocytes within adipose tissues may depend on the anatomical depth in relation to the skin. Adipose tissue samples obtained from the neck region of individuals undergoing thyroidectomy showed a gradient of adipose tissue phenotype with possible differences in adipocyte type (Cypess et al., 2013). Superficial subcutaneous adipose tissue was comprised of white unilocular adipocytes whereas fat located deeper in the neck (carotid sheath) showed slight UCP1 staining. The deepest located fat (Longus colli) had abundant UCP1 and multilocular adipocytes (Cypess et al., 2013). Adipose tissue located around the Longus colli was composed of classical brown adipocytes due to the expression of ZIC1 whereas the intermediate adipose tissue located around the carotid sheath could not be categorised due to the lack of both brown and beige markers (Cypess et al., 2013). Taken together, it is likely that the adipocyte composition of human thermogenic adipose tissue depends on the anatomical location and possibly the age of the individual.

1.6.2 Epicardial and Paracardial fat as brown/beige fat

In addition to the classical locations of BAT such as neck, supraclavicular and perirenal fat, other fat depots have been found to possess UCP1 in humans and other mammals, such as epicardial (Sacks et al., 2009) and paracardial adipose tissue (Ojha et al., 2013). Both of these depots are located around the heart: epicardial adipose tissue is located between the visceral pericardium and outer

wall of the myocardium (Sacks et al., 2009) and paracardial fat (also known as mediastinal or intra-thoracic fat) is bound in front by the chest wall and behind by the external surface of the pericardium (Sacks and Fain, 2011). Pericardial adipose tissue refers to combined epicardial and paracardial fat depots (Wheeler et al., 2005). The anatomy of these adipose tissues in relation to the heart is demonstrated in Figure 1.9. A cross-section of paracardial adipose tissue is shown in Figure 1.9 for epicardial adipose tissue to be shown; however paracardial adipose tissue covers the entire pericardium around the heart.

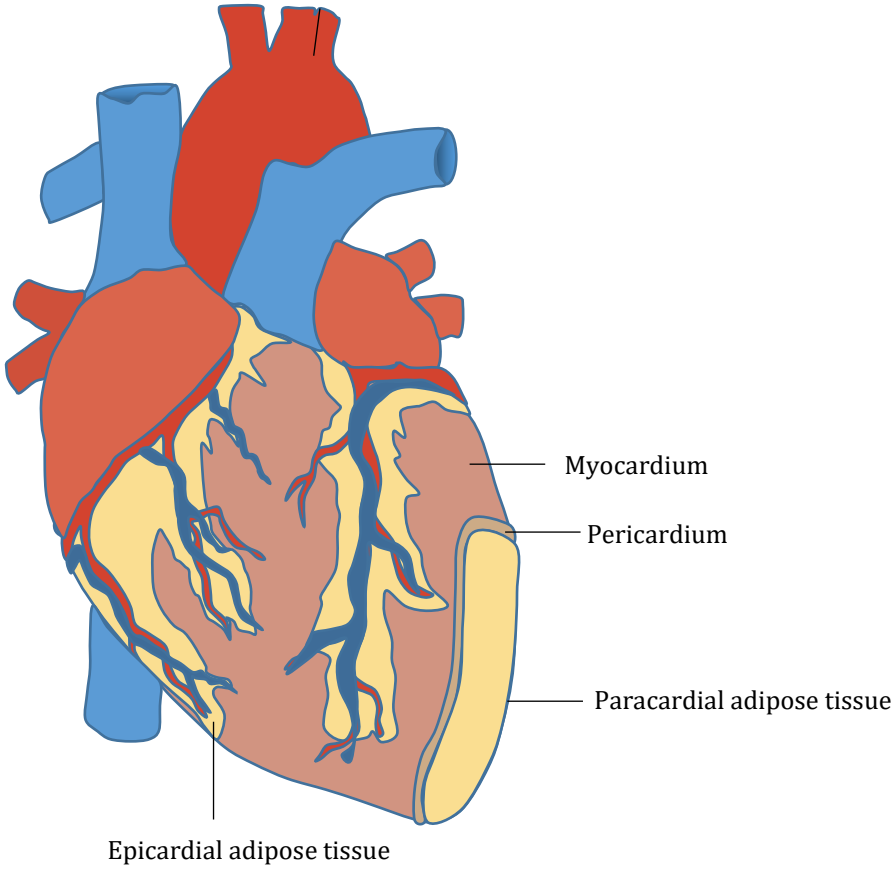


Figure 1.9 The anatomy of human epicardial and paracardial adipose tissue in relation to the heart.

1.6.2.1 Epicardial Fat

It has long been known that increased epicardial adipose tissue thickness or volume measured by echocardiography is associated with CVD and atherosclerosis in a number of studies in both obese adolescents (Akyol et al., 2013; Boyraz et al., 2013) and adult humans (Altin et al., 2016; Sengul et al., 2011). The contribution of epicardial adipose tissue to atherosclerosis in the underlying blood vessel has been shown causally in a pig model, where resection of epicardial adipose tissue on a small section of the left anterior descending coronary artery prevents atherosclerotic plaque development, but not in other parts of the vessel where epicardial adipose tissue remains intact (McKenney et al., 2014). Although the exact mechanism for this is not clear, it may be hypothesised that lipid spill over may occur into the coronary artery if excess lipid is stored in peri-coronary epicardial fat. Indeed, it has been found that the expression of genes involved in lipid transport such as ATP-binding cassette (ABC) transporters are upregulated in epicardial adipose tissue from the peri-coronary artery (Gaborit et al., 2015). Although not causal, it could be hypothesised therefore that lipids are transported from the epicardial adipose tissue into the coronary arteries by ABC transporters.

Epicardial adipose tissue has also been found to secrete pro-inflammatory cytokines such as tumour necrosis factor α (TNFα) and interleukin-6 (IL-6) (Mazurek et al., 2003). These may contribute to the progression of atherosclerosis in underlying vessels. Adiponectin, a hormone known to have anti-inflammatory and anti-atherosclerotic properties is secreted by epicardial

adipose tissue at a reduced rate in subjects with coronary artery disease (Iacobellis et al., 2005) which may also contribute to atherosclerosis. The secretion of adiponectin by epicardial adipose tissue may suggest that in healthy non-obese individuals, epicardial fat may also have cardio-protective effects. The hormone adrenomedullin has also shown to be protective against atherosclerosis in rodents (Pan et al., 2010). Adrenomedullin expression has also been detected in epicardial adipose tissue, and is reduced in patients with coronary artery disease (Iacobellis et al., 2009). Therefore both pro-atherosclerotic and cardio-protective adipokines are released from epicardial adipose tissue that could play a role in atherosclerosis of the underlying blood vessels. It should be noted that the characteristics of epicardial adipose tissue and cytokine profile may differ therefore depending on the adiposity of an individual as previously described in other depots (Hotamisligil et al., 1995). Also, as epicardial adipose tissue samples cannot be taken from healthy humans due to ethical considerations (Gaborit et al., 2015), a full understanding of epicardial adipose tissue function and characteristics in non-pathological physiology remains elusive.

To add to a possible beneficial role in metabolism, it is interesting that epicardial adipose tissue has recently been found to possess UCP1 and have BAT-like characteristics in some adult humans. Sacks et al. studied biopsies of epicardial fat and also analysed biopsies of subcutaneous fat from thoracic, abdominal and leg regions from different patients for comparison (Sacks et al., 2009). Epicardial adipose tissue had high expression of genes involved in committing adipocytes to the thermogenic programme, such as UCP1 and PRDM16 compared to subcutaneous depots (Sacks et al., 2009). Surprisingly, UCP1 mRNA in epicardial

adipose tissue was positively correlated to BMI (Sacks et al., 2009). It is not clear why this would be the case or if this difference was conserved at the protein level as this was not reported. A more recent study reported abundant UCP1 mRNA in human epicardial adipose tissue that interestingly, was correlated with plasma HDL (Chechi et al., 2013). The presence of UCP1 protein in human epicardial fat has been confirmed with Western blotting (Sacks et al., 2013). In contrast, mesenteric, omental and subcutaneous adipose tissue samples obtained from a different cohort of patients for comparison displayed a lack of UCP1 (Sacks et al., 2013). However UCP1 was not observed by immunohistochemistry despite the same UCP1 antibody successfully staining for UCP1 in human supraclavicular adipose samples (Sacks et al., 2013). Therefore, although epicardial adipose tissue may be a depot capable of thermogenesis, the results are not fully conclusive at present.

Epicardial fat has been suggested to be composed of adipocytes which display characteristics of beige cells rather than classical brown adipocytes (Sacks et al., 2013). This was due to the presence of markers recently suggested to be selective for beige adipocytes such as CD137 (Wu et al., 2012). The expression of other beige markers such as TMEM26 and TBX1 has also been observed in human epicardial fat (Chechi and Richard, 2015). Interestingly, the presence of beige adipocytes and thermogenic capacity may differ depending on the anatomical location of the epicardial adipose tissue on the heart. Gaborit et al compared epicardial adipose tissue resected from peri-atrial, peri-ventricular and peri-coronary locations (Gaborit et al., 2015). Peri-ventricular epicardial adipose tissue showed the most pronounced beige phenotype with the highest

UCP1 mRNA expression compared to peri-atrial epicardial fat (Gaborit et al., 2015). This suggests that thermogenic properties and adipocyte composition are not uniform across the entire epicardial adipose tissue depot. UCP1 protein expression and functional cellular bioenergetics were not compared between different anatomical locations of epicardial adipose tissue which would provide further information on differences between epicardial adipose tissue locations.

Given the association of epicardial adipose tissue with CVD but also the release of adiponectin and possible BAT-like properties into adulthood it raises several questions regarding its function, which is not known at present. One function may be to act as a store of free fatty acids for the myocardium as fat is the main substrate for myocardial contraction (Bing et al., 1954). It may also have a protective effect, preventing excess free fatty acids from entering the circulation (Marchington and Pond, 1990; Sacks and Fain, 2007). In guinea pigs, epicardial adipose tissue shows high rates of lipid turnover and lipolysis (Marchington et al., 1989) which could provide fatty acids either for the myocardium or for thermogenesis through UCP1. The presence of UCP1 in epicardial adipose tissue and the proximity of the depot to the heart may provide heat to the myocardium through uncoupling to prevent hypothermia (Iacobellis et al., 2011), in line with the evolutionary role of UCP1. That epicardial fat may function as a brown or thermogenic adipose tissue, may suggest that UCP1 is responsible for fatty acid clearance rather than storage of lipid which could reduce CVD risk. Interestingly, a recent study has reported decreased PGC1α and UCP1 mRNA abundance in epicardial adipose tissue from patients with type II diabetes and coronary artery disease compared to those with coronary artery disease but without diabetes

(Moreno-Santos et al., 2016). In addition, lower PGC1α gene expression was noted in patients with an increased number of injured coronary arteries (Moreno-Santos et al., 2016). These results suggest that mitochondrial biogenesis or thermogenesis within the epicardial adipose tissue depots may provide a protective effect on atherosclerosis development. Further evidence would need to be obtained in both healthy and pathophysiological states (using animal models) to determine the thermogenic function of epicardial adipose tissue.

1.6.2.2 Paracardial Fat

In comparison with epicardial adipose tissue, relatively little is known about the characteristics of paracardial adipose tissue. An association between paracardial adipose tissue volume or amount and CVD risk is less clear, as human studies have often failed to distinguish between epicardial and paracardial adipose tissue (Liu et al., 2010; Rosito et al., 2008). Paracardial adipose tissue volume was recently assessed by Lu et al and was found to be significantly greater in patients with high risk plaques (i.e. high density calcified plaques) compared to low risk plaques but was not significantly different after correcting for various risk factors (Lu et al., 2016). In a study of an Amish population, paracardial (referred to as pericardial) adipose tissue volume was not associated with coronary artery calcification but was correlated to total fat mass (Liu et al., 2014). Similarly, paracardial (referred to as intrathoracic) adipose tissue volume was not associated with CVD in patients from the Framingham Heart Study (Mahabadi et al., 2009).

Based on current studies, it is not clear why epicardial adipose tissue shows a greater association with CAD than paracardial adipose tissue. Gene expression studies on adipose tissue biopsies from patients with coronary artery disease have reported that epicardial and paracardial fat depots display similar molecular signatures (Guauque-Olarte et al., 2011). Paracardial adipose tissue also displays an inflammatory profile in patients with CVD (Atalar et al., 2013). It is possible, that the lack of contiguity between paracardial adipose tissue and the myocardium due to the interposing pericardium, limits the contribution of paracardial adipose tissue to atherosclerosis. Further studies are required to determine the contribution of paracardial adipose tissue to CVD risk.

Similar to epicardial adipose tissue, paracardial fat has also been shown to express UCP1 mRNA in a recent human study, although this mRNA abundance was lower than the expression of UCP1 in murine BAT and, more surprisingly, murine WAT (Cheung et al., 2013). Using gene expression analysis in comparison to subcutaneous fat depots, thermogenic markers of brown fat such as UCP1 and PGC1α were upregulated in the mediastinal (paracardial) depot (Cheung et al., 2013). A recent human study has suggested that UCP1 mRNA is down regulated in paracardial compared to epicardial fat and is similar to abdominal subcutaneous adipose tissue (Chechi et al., 2013). Western blotting performed by Cheung et al. did not demonstrate the presence of UCP1 protein within the paracardial depot (Cheung et al., 2013) in accordance with a study by Sacks et al which also did not show UCP1 protein in paracardial fat (Sacks et al., 2009). However, the presence of UCP1 was observed with UCP1 immunohistochemistry, albeit in only 2 out of 10 subjects (Cheung et al., 2013) suggesting that UCP1

positive adipocytes may not be common in paracardial adipose tissue in the adult population. The significance of these depots functioning as brown fat to whole body metabolism remains to be fully explored and compared to depots within the same organism thought to contain metabolically active BAT.

1.6.3 The heart as an endocrine organ promoting adipose tissue browning

As epicardial and paracardial adipose tissue depots have been shown to possess thermogenic characteristics at least in some human adults, it is interesting that the heart has been shown to release endocrine factors causing UCP1 upregulation and adipose tissue browning. Bordicchia et al. demonstrated that cardiac natriuretic peptides have a significant role in adipose tissue thermogenesis (Bordicchia et al., 2012). The heart releases atrial natriuretic peptide (ANP) from the atria (de Bold, 1985) and B-type natriuretic peptide (BNP) predominantly from the ventricles, although small amounts may also be synthesised by the atria (Mukoyama et al., 1991). ANP is released as an active hormone whereas BNP is released as a 108 amino acid prohormone and is cleaved into the 32 amino acid biologically active BNP in the circulation, catalysed by the proBNP convertases corin and furin (Semenov et al., 2010). Both ANP and BNP are typically released in response to stretch of the cardiac wall (Kinnunen et al., 1993; Lang et al., 1985), and as such, are released in large quantities in heart failure (Falcao et al., 2004). BNP in particular is often used as a marker of the severity of cardiac dysfunction (Mishra et al., 2014). As the name suggests, one of the main physiological roles of cardiac natriuretic peptides is in natriuresis i.e. the loss of sodium in the urine (Weidmann et al., 1986).

Natriuretic peptides exert their effects on target cells by binding to activated (NPRA) or clearance (NPRC) receptors on the plasma membrane (Suga et al., 1992). NPRA has guanylate cyclase activity and generates second messenger cyclic guanosine monophosphate (cGMP) (Suga et al., 1992). Increased cGMP then activates protein kinase G (Haas et al., 2009) which modulates the activity of downstream proteins by phosphorylation leading to a cellular response to cardiac natriuretic peptide (NP) binding. In contrast, NPRC does not initiate downstream signalling but is responsible for degradation of NP and removal from the circulation (Maack et al., 1987).

It had previously been observed that ANP and BNP increased the rate of lipolysis in primate adipose tissue, however this was largely considered to be a species-specific effect as no effect was observed in rodent models (Sengenes et al., 2002). It is thought that this is due to rodents possessing a large abundance of the NPRC compared to NPRA leading to rapid degradation of these hormones (Sengenes et al., 2002). This differs from humans, as NPRA abundance is significantly higher than NPRC (Sengenes et al., 2002). In $NPRC^{-/-}$ mice, UCP1 is upregulated in interscapular brown adipose tissue (iBAT) but also in epididymal and inguinal adipose tissue depots, suggesting that increased cardiac natriuretic peptide signalling due to loss of NPRC is able to promote BAT activity and adipose tissue browning (Bordicchia et al., 2012). Plasma BNP concentrations significantly increase in cold-exposed mice with an increase in NPRA mRNA and a decrease in NPRC mRNA suggesting a possible increase in NP signalling during cold exposure, upregulating UCP1 (Bordicchia et al., 2012). When mice are infused

with BNP to increase plasma concentrations significantly compared to saline infused control animals (but still within a physiological range), UCP1 and other thermogenic genes are significantly increased (Bordicchia et al., 2012).

Haas et al. had previously elucidated some components of the protein kinase G pathway in brown adipocytes. This involves the protein kinase G I (PRKGI) isoform which inhibits RhoA and Rho-associated kinase (ROCK) which are inhibitors of insulin signalling (Haas et al., 2009). Insulin signalling is then increased leading to the differentiation of brown pre-adipocytes and mitochondrial biogenesis (Haas et al., 2009). Similar to PKA, PRKGI also phosphorylates p38 MAPK (Bordicchia et al., 2012). Interestingly natriuretic peptides and catecholamines (i.e. PKA and PRKGI signalling) have a synergistic effect (Bordicchia et al., 2012), raising the possibility of utilising both signalling pathways in combination to upregulate UCP1 and increase thermogenesis. Given the contiguity of epicardial adipose tissue and the myocardium it is possible that paracrine effects of cardiac natriuretic peptides could strongly influence thermogenesis in this depot. Currently however, little is known about the effects of cardiac natriuretic peptides on adipose tissue surrounding the heart and it will be an interesting topic for further study. An overview of cardiac natriuretic peptides on downstream PRKGI and UCP1 upregulation is shown in Figure 1.10.

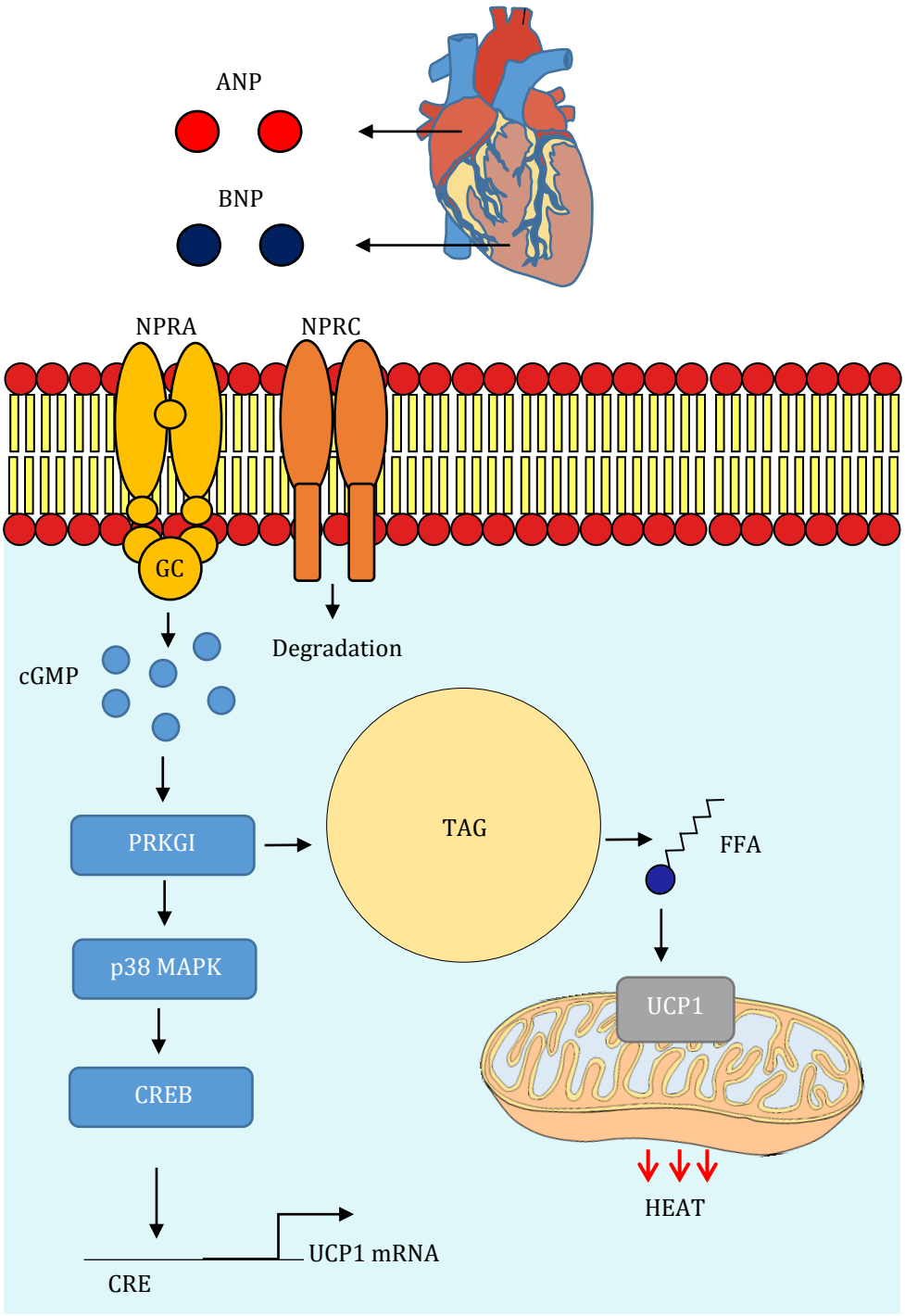


Figure 1.10 Effects of cardiac natriuretic peptides on adipose tissue thermogenesis. *Atrial natriuretic peptide (ANP) is released from the atria of the heart and B-type natriuretic peptide from the ventricles. ANP and BNP can bind to activated (NPRA) or clearance (NPRC) receptors. NPRA initiates a downstream signalling cascade through cyclic guanosine monophosphate (cGMP) and protein kinase G I (PRKGI). PRKGI phosphorylates p38 mitogen activated kinase (p38 MAPK) which phosphorylates cyclic adenosine monophosphate response element binding protein (CREB) which acts as a transcription factor binding to the cyclic adenosine monophosphate response element (CRE). PRKGI can also stimulate lipolysis providing free fatty acids (FFA) for UCP1 thermogenesis. NPRC degrades ANP and BNP and removes them from the circulation.*

1.7 Clinical significance of human brown adipose tissue on energy balance and insulin sensitivity

As animal models have shown promising effects of UCP1 on energy balance and metabolic health, the finding of UCP1 positive BAT in adult humans has sparked great interest in its use as therapy against obesity and diabetes. Initial ^{18}F-FDG PET-CT studies found that the BAT activity was inversely correlated to BMI (Lichtenbelt et al., 2009; Ouellet et al., 2011; Saito et al., 2009), suggesting some involvement in obesity and energy balance. Studies have also found that obese individuals who lose weight also have an increased amount of detectable BAT after weight loss (Vijgen et al., 2012). BAT activation after a 2 hour cooling protocol that minimised shivering increased mean total energy expenditure by 250 kcal (Ouellet et al., 2012) suggesting a significant effect on overall energy balance. Subjects taking 200 mg of mirabegron, (a β-3 agonist) for 2 days showed increased resting metabolic rate concomitant with increased BAT activity (Cypess et al., 2015). However, given that only small deficits in energy balance may be sufficient to cause weight loss (Hill et al., 2003) and that moderate weight loss of 5% of total bodyweight significantly improves metabolic health (Magkos et al., 2016), the increase in energy expenditure associated with BAT activation could be beneficial in human weight management.

However demonstrating a causal role for activated BAT in weight loss is difficult in humans and few long-term studies have been conducted to assess changes in bodyweight. Initial results have been somewhat disappointing, as healthy

volunteers exposed to 19°C for 10 hours every night for 1 month did not show any change in bodyweight or composition despite increased BAT activity (Lee et al., 2014). Caloric intake was unchanged (Lee et al., 2014) suggesting that hyperphagia due to cold exposure was not a confounding factor. It is possible that a more severe cold challenge is needed; however, it is important that in these studies the subjects do not start to shiver. To my knowledge, this is the only study to date conducted over a sufficient time period for potential effects of BAT activity on weight loss to be observed as many other studies have used short-term cold exposure protocols.

Despite the lack of observed effects on weight loss, activated BAT may have significant clinical applications in improving insulin sensitivity in humans. Lee et al found 1 month overnight cold exposure improved insulin sensitivity in healthy males, an effect that not maintained when subjects were exposed to 24°C for the following month (Lee et al., 2014). The clinical relevance is particularly evident in a study reporting improved insulin sensitivity in subjects with type II diabetes. Cold exposure (10°C) for 10 days caused a small but statistically significant increase in glucose uptake into supraclavicular BAT with an accompanying increase in insulin sensitivity measured by hyperinsulinemic-euglycaemic clamp (Hanssen et al., 2015). Glucose uptake was also increased into skeletal muscle and an upregulation of GLUT4 protein was also observed, suggesting that activated BAT may not be solely responsible for these effects. A study conducted with BAT positive and negative subjects of similar adiposity, age and BMI showed improved insulin sensitivity to 5-8 hours of cold exposure but only in the BAT positive group (Chondronikola et al., 2014). In addition to these cold exposure

studies, Cypess et al showed that pharmacological treatment of subjects with 200 mg mirabegron showed decreased HOMA-IR as a marker of insulin resistance in addition to increased BAT activity (Cypess et al., 2015). Together these findings suggest that even short term cold exposure or pharmacological treatment can improve insulin sensitivity in healthy and type II diabetic patients, an affect possibly mediated through BAT activation. These results are in accordance with the role for BAT in improved insulin sensitivity observed in animal models discussed in section 1.5.

1.8 Pheochromocytoma as a model of chronic adrenergic stress and adipose tissue browning

One of the first indications of BAT activation in humans was in patients with pheochromocytoma (Ricquier et al., 1982). A pheochromocytoma is defined as a tumour of the chromaffin cells located in the adrenal medulla that secrete catecholamines into the circulation (Lenders et al., 2014). It is relatively rare, with an estimated prevalence of 1:2,500-1:6,500 patients in western countries (Pacak and Del Rivero, 2000). Patients often present with hypertension (Zuber et al., 2011) headaches, nausea and diaphoresis (Ariton et al., 2000). The symptoms can be episodic due to the pulsatile nature of catecholamine release from the tumour (Lenders et al., 2005). Although not fatal in itself, if left untreated it is likely to lead to CVD due to prolonged hypertension (Garg et al., 2011).

As catecholamines are well established to stimulate thermogenesis in BAT and cause WAT browning (Thomas and Palmiter, 1997), pheochromocytoma provides a model of adipose tissue response to chronic adrenergic stress. Browning of perirenal adipose tissue close to the tumour has been noted in several studies (Betz et al., 2013; Nagano et al., 2015; Puar et al., 2016). Interestingly, although pheochromocytoma is often unilateral (i.e. occurring on only one adrenal gland), bilateral glucose uptake to periadrenal adipose tissue is observed by ^{18}F-FDG PET-CT, suggesting effects on distal adipose tissue depots (Park et al., 2014; Puar et al., 2016). Local effects of catecholamine secretion by the tumour on ipsilateral periadrenal adipose tissue cannot be ruled out however (Puar et al., 2016). Browning of the omental adipose tissue depot has been noted in 6 out of 12 subjects with pheochromocytoma (Frontini et al., 2013), suggesting typical white fat depots, such as omental fat (Frontini et al., 2013; Walden et al., 2012) are capable of browning in some humans in response to catecholamines. Less is known about the browning of subcutaneous adipose which could be particularly important as, in females at least, it comprises approximately 85% of total body fat (Fowler et al., 1991). Further studies are needed to characterise possible browning of this depot in humans.

1.9 Age related BAT atrophy or adipose tissue 'whitening'

In humans and many other mammalian species, it has been observed that the amount of BAT peaks during early life and diminishes with increasing age. For example, in large mammals such as sheep and goats BAT is present in the first days after birth but lost relatively quickly, typically over 3-4 weeks (Basse et al.,

2015; Nicol et al., 1994; Pope et al., 2014). Rodents also show a loss of UCP1 with age in perirenal adipose tissue but this time period is dependent the strain of mice (Xue et al., 2007). In contrast, the large interscapular BAT depot in rodents does not change markedly over the lifespan (Xue et al., 2007). Heaton et al observed in human cadavers that BAT (or multilocular adipocytes) is present in many depots in the first decade of life and is lost gradually after the third decade to be replaced by more unilocular adipocytes (Heaton, 1972). More recent studies in humans have also found reduced BAT activity with age by PET-CT detection methods (Cypess et al., 2009; Yoneshiro et al., 2011).

The development and activity of BAT during childhood and adolescence has received little attention, possibly due to the invasive nature of PET-CT scans and the radiation exposure. Interestingly, although is it well known that BAT is found in children in the first decade of life, recent studies suggest an activation of BAT during puberty (Gilsanz et al., 2011; Gilsanz et al., 2012). The activation of BAT correlates with muscle volume (Gilsanz et al., 2011) suggesting a possible interplay between muscle and adipose tissue or an effect of sex steroids. It should be noted that the subjects who participated in these studies had previously had malignancies and may therefore not be representative of the healthy adolescent population. Therefore studies on healthy volunteers using imaging modalities that can be performed non-invasively would be informative for future studies.

The molecular mechanism of age-related adipose tissue 'whitening' is not currently known at present and has not been as extensively studied as adipose

tissue browning. As discussed in section 1.6.1, human adipose tissue has been suggested to express mRNA markers of beige adipocytes (Wu et al., 2012). As beige adipocytes in rodents have been found to take on characteristics of white adipocytes on rewarming after cold exposure (Rosenwald et al., 2013), it is possible that beige to white adipocyte transdifferentiation may occur with age resulting in the loss of UCP1 positive brown adipocytes. An early lineage tracing study suggested that the inguinal adipose tissue of 12-14 week old mice did not possess adipocytes that had previously expressed UCP1 (Moulin et al., 2001). Given that the inguinal adipose tissue depot of mice is UCP1 positive 21 days after birth even in mice housed at thermoneutrality (Chabowska-Kita et al., 2015); the results suggest that brown or beige adipocyte transdifferentiation does not occur with increasing age. In contrast, retroperitoneal adipocytes from 12-14 week old mice showed the presence of former UCP1-positive adipocytes (Moulin et al., 2001) despite the fact that UCP1 protein is not detectable in the retroperitoneal adipose tissue from mice of a similar age (Xue et al., 2007). It is possible that the loss of brown adipocytes could occur by different mechanisms depending on the adipose tissue depot. Further work will be required to determine the fate of UCP1-positive adipocytes on age-related whitening and if the mechanisms in animal models are similar to that in humans.

1.10 Sheep as an animal model of BAT development and whitening

Similar to human newborns, sheep have abundant BAT and UCP1 in early life which is lost with age. Other similarities with humans include relatively small litter sizes (of 1-3 lambs), a long gestation period (143 days) (Pope et al., 2014),

and that adipose tissue constitutes a similar proportion of weight in both the newborn sheep and human of 1-2% (Alexander and Bell, 1975). Rodents, in contrast, although offering powerful and informative genetic approaches (Lusis et al., 2016; Seale et al., 2011), have constituently active interscapular BAT throughout the lifespan (Xue et al., 2007) which makes up a much larger proportion of bodyweight than BAT depots in humans. Although rodents also display abundant UCP1 in interscapular BAT at birth, the inguinal adipose tissue does not undergo browning to cold exposure until 10 days after birth (Xue et al., 2007). This may suggest that some aspects of adipose tissue thermogenesis are not functional until a few days after birth. Therefore, a large animal model such as sheep may be more appropriate for assessing adipose tissue thermogenesis at birth.

The loss of BAT in sheep occurs over the first month of postnatal life (Pope et al., 2014), which, although likely lost at a faster rate than in humans (Heaton, 1972), is practical for observing this process over a relatively short study period. The amount of adipose tissue present in young sheep also provides the advantage of studying depots such as epicardial and paracardial fat during early life which may not be present in adequate amounts for analysis in rodents.

1.11 Aims and Hypotheses

Both studies in this thesis aimed to compare adipose tissue depots in terms of brown or beige adipocyte composition and possible function as thermogenic fat. Currently, little is known about the role of epicardial and paracardial adipose

tissue and their developmental transition during early life. Therefore the aim of my first study was to investigate the development of epicardial and paracardial adipose tissue in comparison to the classical white omental fat depot during the first 28 days of life in sheep. It was hypothesised that epicardial and paracardial fat depots will show a brown to white adipose tissue transition over the first 28 days of life and will show expression of genes involved in brown/beige thermogenesis which will not be observed in omental fat.

Although in rodents, inguinal subcutaneous adipose tissue readily undergoes browning, it is not clear if human subcutaneous adipose tissue undergoes similar adipose tissue remodelling. Therefore the aim of my second study was to assess adipose tissue browning in subcutaneous compared to periadrenal fat biopsies from patients with pheochromocytoma as a model of chronic adrenergic stress or patients with non-catecholamine secreting tumours as a control group. The hypothesis was that subcutaneous and periadrenal adipose tissue would undergo browning in the pheochromocytoma group and would not be observed in the control group.

Chapter 2 Materials and methods

My thesis consists of projects completed at two different locations. Sheep studies (Chapter 3 & 4) and subsequent laboratory and data analyses were conducted between October 2012-September 2016 at the Department of Child Health, University of Nottingham under the primary supervision of Professor Michael Symonds and Professor Helen Budge. From September 2014 - July 2015 I worked on a human pheochromocytoma study (Chapter 5) as a Visiting Graduate Researcher at the laboratory of Professor Karen Reue at the University of California, Los Angeles. This was primarily supervised by Dr Laurent Vergnes and Professor Harold Sacks. Similar laboratory protocols were used throughout but due to the different locations, some minor amendments were made to protocols for different reagents and equipment used in the respective laboratories. Where protocols and laboratory techniques overlap, they are given for the Nottingham studies and any modifications in the technique when performed for the human study are noted briefly.

2.1 Sheep study

Animal procedures for sheep studies were conducted at Sutton Bonington Campus, University of Nottingham in accordance with the UK Animals (Scientific Procedures) Act, 1986 with prior approval from the local Ethics Committee of the University of Nottingham (Nottingham, United Kingdom). The first sheep study was conducted in 2011 by Professor Michael Symonds, Miss Rachel Woods and

Dr Mark Birtwistle. The second sheep study (samples used for histology) was conducted in 2013 by Professor Michael Symonds and assisted by Dr Mark Birtwistle, Dr Viv Perry and myself.

2.1.1 Experimental design and sampling

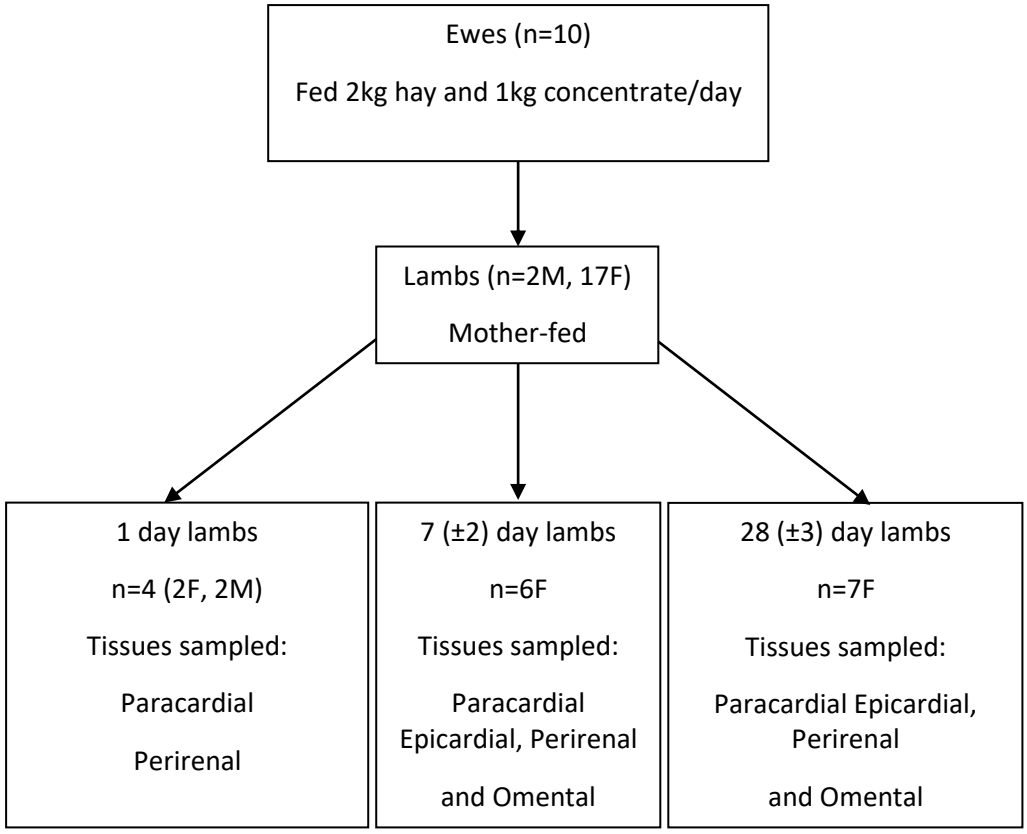
Zworval ewes were mated with a Charolais ram at the same time of year (Spring) so that all lambs were born and sampled as a single cohort. Pregnant ewes (n=10) were fed to requirements for metabolism and lactation with 2kg hay and 1kg concentrate per day and gave birth normally at term. Lambs suckled with their mothers and were housed together in a barn for the duration of the study. Singleton lambs were excluded from the study. Lambs born from the same ewe were randomly selected for sampling at either 7±2 (7 day group) or 28±3 days (28 day group). The remaining triplet lambs were sampled at 1 day (1 day group) for comparison. All lambs sampled at 7 and 28 days were female, whereas the 1 day group comprised two males and two female lambs. The 7 day group comprised of 2 twin animals, 1 triplet and 2 quadruplets whereas the 28 day group comprised of 4 twins, 2 triplets and 1 quadruplet lamb.

Lambs randomly selected for adipose tissue sampling as above (n=4 for 1 day group, n=6 for 7 day group and n=7 for 28 day group) also had blood samples collected prior to euthanasia. Up to 20 ml of blood was taken from the jugular vein of lambs using a syringe and collected into EDTA tubes (Vacutainer, Devon, UK) on ice. Bloods were centrifuged at 1200g for 15 minutes at 4°C and plasma collected into eppendorf tubes and stored at -80 ^{o}C. After blood sampling, lambs

were humanely euthanased with an overdose of barbiturate (i.v. 200 mg/kg pentobarbital sodium, Euthatal: RMB Animal Health, UK) at their allotted sampling age for adipose tissue sampling. Paracardial adipose tissue was excised at 1, 7 and 28 days whereas epicardial and omental adipose tissues were only sampled at 7 and 28 days due to the lack of adequate amounts of fat in these depots in 1 day old lambs. At the time of tissue excision, omental and paracardial fat were weighed. This was not performed with epicardial fat as it was not possible to excise this entire tissue depot completely. Adipose tissue samples were snap frozen in liquid nitrogen and stored at -80°C until further analysis.

After commencing gene expression and protein analysis from the above animals, a separate group of lambs, offspring from Blue-faced Leicester cross Swaledale ewes mated with a Texel ram, were sampled for histology as the cardiac adipose tissues were not fixed from lambs in the previous study. Also, most of the epicardial adipose tissue from the first group of lambs had been used for RNA, DNA and protein extraction and no tissue was remaining for cryosectioning. The experimental design was the same as the previous study. Epicardial, paracardial and perirenal adipose tissue samples were taken from female lambs at 1, 7±1 and 28±3 days (n=4 per depot and time point). There was a small amount of epicardial adipose tissue present in 1 day old lambs that could be taken for histology; however, omental adipose tissue was not visible in 1 day old lambs. Therefore omental adipose tissue samples were taken at 7±1 and 28±3 days. Samples were stored in 10% formalin before processing for histology and immunohistochemistry. A summary diagram of the experimental design is shown below.

A



B

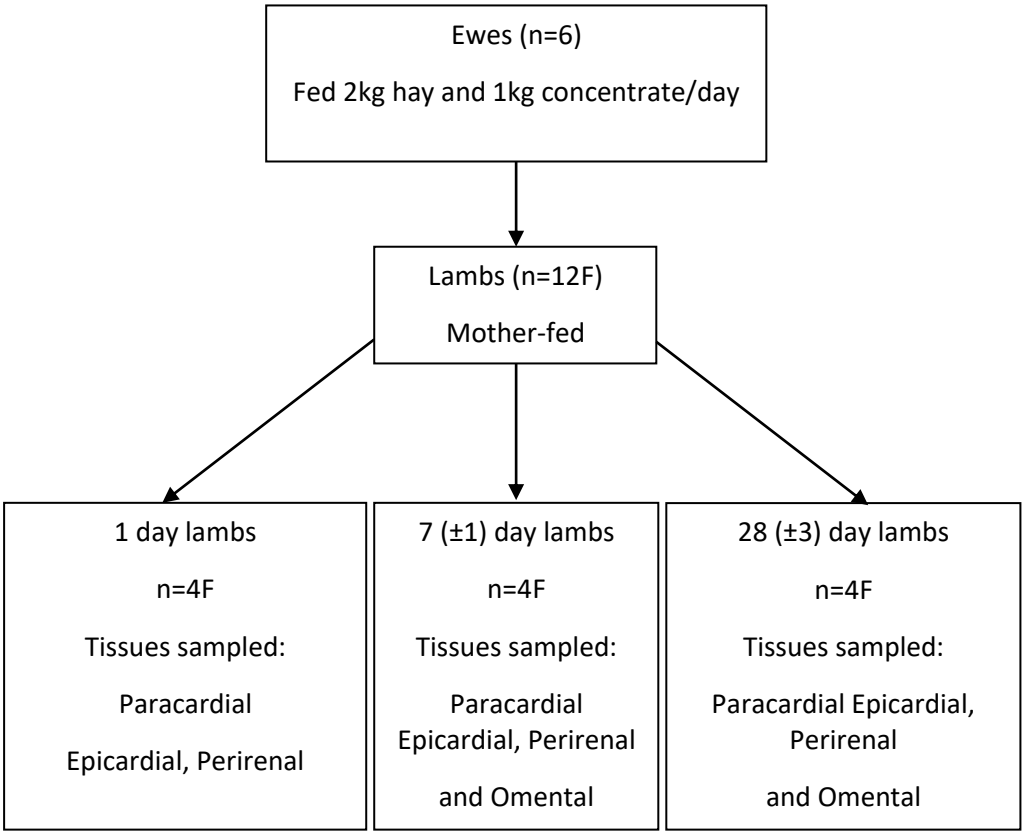


Figure 2.1 Schematic diagram of overall study design and tissue sampling.

(A) Sheep study where samples were collected for qPCR and western blot analysis; (B) Sheep study where adipose tissues were sampled for histology M=Male, F= Female

2.2 Laboratory procedures

2.2.1 Plasma BNP Analysis by Enzyme Immunoassay

An enzyme immunoassay works by competitive binding of spiked biotinylated BNP and endogenous BNP to an anti-BNP antibody. Once the biotinylated BNP binds to the capture (anti-BNP) antibody it is linked to HRP-Streptavidin which catalyses a colourimetric reaction. Therefore the intensity of the colourimetric reaction is inversely proportional to the amount of endogenous BNP in a sample. The amount of endogenous BNP is extrapolated from a standard curve where known concentrations of endogenous BNP are spiked with biotinylated BNP which must remain constant between all standards and samples. A schematic diagram of the steps in the assay is shown in Figure 2.2.

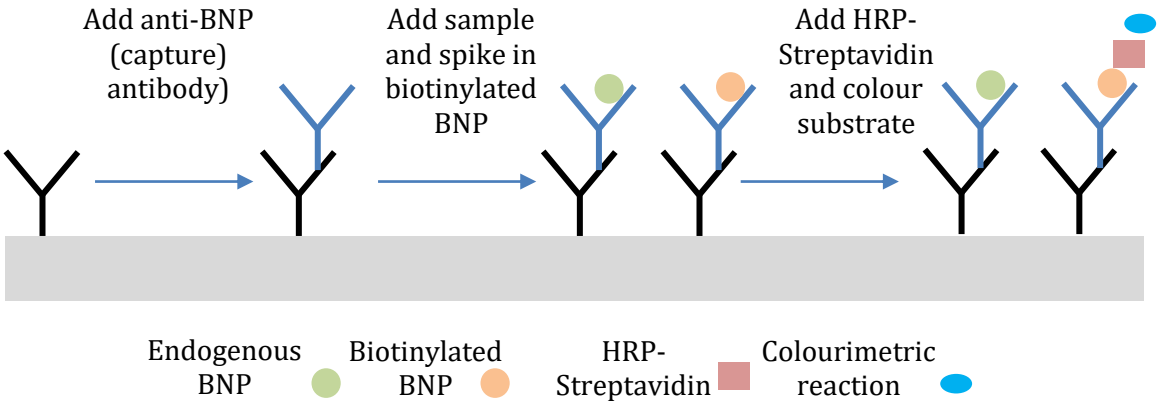


Figure 2.2 Schematic diagram of the principle of enzyme immunoassay

Plasma BNP was assessed using a BNP Enzyme Immunoassay kit (EIA-BNP, Ray Biotech). Reagents were prepared according to the kit protocol. 100 µl anti-BNP was added to each well of a coated microplate provided in the kit and incubated

for 1.5 hours at room temperature. A 1:10 Standard dilution series was prepared from 1000 pg/ml to 0 pg/ml BNP (diluent only). Samples were diluted 1:2 with assay diluent and 10 pg/ml biotinylated antibody was added to both standards and samples. 100 µl standard and sample diluted 1:2 was added to the plate in duplicate and incubated for 2.5 hours at room temperature. 100 µl of streptavidin solution was added to each well and incubated at room temperature for 45 minutes. 100 µl TMB One-Step Substrate Reagent was adder to each well and incubated for 30 minutes at room temperature. 50 µl of stop solution was then added to each well and read immediately on a spectrophotometer (Benchmark Microplate Reader, Biorad, Hercules, CA, USA) at 450nm. Concentrations were calculated from a line of best fit through the standard curve (Figure 2.3) using four-parameter logistic regression software Microplate Manager® (Biorad, Hercules, CA, USA). Overall intra-assay coefficient of variation was 10.2%, slightly higher than the <10% recommendation, possibly caused by pipetting error. However there were no wells remaining to repeat samples with high variation between replicates and this would have required the purchase of another kit. The results were analysed and found to be within the range of a previous study in lambs (Oishi et al., 2007) and were deemed suitable for analysis.

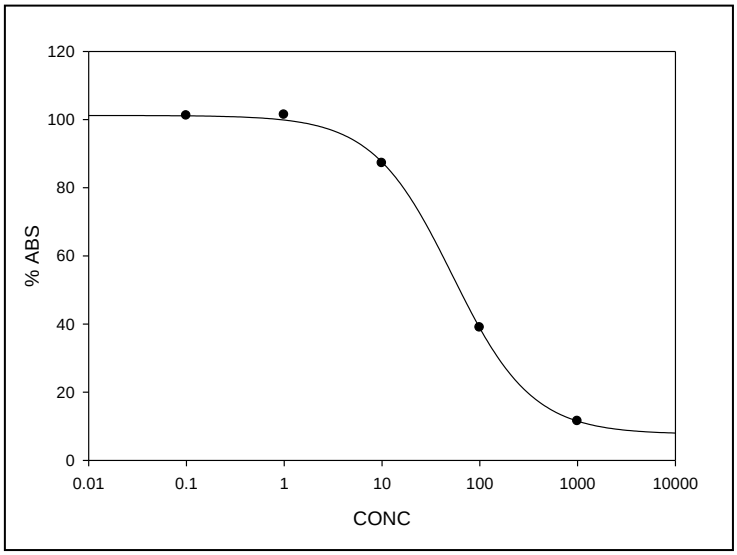


Figure 2.3 Standard curve of BNP EIA showing absorbance and concentration for extrapolation of unknown samples

2.2.2 RNA isolation

Using a variation of the phenol chloroform extraction method it is possible to extract RNA from tissue samples. The tissue is ruptured through homogenization which allows the release of macromolecules within the cells including RNA. Guanidine thiocyanate is commonly used which facilitates this process and inhibits endogenous RNAses present into the tissue (Griffin et al., 2012). The addition of chloroform to the tissue homogenate allows the separation of macromolecules into 3 phases: a top aqueous RNA layer, a white interphase of DNA and a lower protein layer (Chomczynski and Sacchi, 2006). The top layer containing the RNA can then be removed and purified by several washing steps with ethanol to yield RNA for molecular biology techniques such as reverse transcription and qPCR. The elimination of genomic DNA can also be useful to ensure amplification in PCR is from cDNA (Grillo and Margolis, 1990) and is part

of many RNA extraction kits. The purity of RNA extracted can be analysed using a spectrophotometer which uses wavelength absorption to determine the amount of RNA present in a sample. It can also give an estimation of RNA purity, as nucleic acids absorb light at 260nm and the presence of contaminants such as protein or guanidine thiocyanate residues can be detected due to their absorption of light at 280nm.

Prior to RNA analysis, benches were cleaned with RNAase Zap® (Ambion, California, USA) and Spiriclens® hard surface spray containing 70% denatured ethanol v/v (Ecolab, Surrey, UK). Tissue samples were transferred from the -80°C freezer to dry ice for tissue cutting. Approximately 100 mg of frozen tissue was cut from the whole excised tissue and put into a gentleMACS™ tube (Miltenyi Biotec, Surrey, UK) for RNA extraction. An RNeasy® Plus Mini Kit (Qiagen, Hilden, Germany) was used for all RNA extractions. 500 µl TRI Reagent® (Sigma-Aldrich, Gillingham, UK) was added to 100 mg of tissue and thawed on ice. Samples were homogenised on a Dispomix® drive homogeniser (Medic Tools AG, Lussiweg, Switzerland) and centrifuged for 30 seconds at 3220g. The gentleMACS™ tubes were then placed in a 37°C water bath for 2 minutes, vortexed for 30 seconds and the homogenate centrifuged for 5 minutes at 3220g. The solution was transferred to a sterile 2 ml tube. 100 µl chloroform was added per 100 mg of tissue sample and inverted to mix. The samples were incubated for 10 minutes at room temperature and then centrifuged at 12000g for 15 minutes at 4°C for phase separation The RNA layer was removed and added to a gDNA eliminator column, centrifuged for 30 seconds at 12000g and the flow through collected.

The eliminator column was discarded and 100 µl of 70% ethanol was added per 100 mg of tissue sample and pipette mixed thoroughly. 700 µl of sample was added to the RNeasy spin column, centrifuged for 15 seconds at 8000g and the flow-through discarded. 700 µl of Buffer RW1 was added to the column and centrifuged for 15 seconds at 8000g and the flow-through discarded. 500 µl Buffer RPE was added to the column and centrifuged for 15 seconds at 8000g and the flow-through discarded. The column was transferred to a new sterile 2 ml tube and centrifuged for 1 minute at 8000g to remove all RPE buffer. The column was then transferred to a new sterile 1.5 ml eppendorf tube. 50 µl nuclease free water was added to the column to elute the RNA. Samples were centrifuged at 8000g for 1 minute and the samples stored on ice. RNA concentration was determined using a Nanodrop (Thermo Scientific, Wilmington, USA). The samples were stored at -80°C for further processing in an RNA-only freezer to prevent contamination.

2.2.3 Reverse Transcription

RNA was diluted to 1 µg in 9 µl of nuclease free water. A high capacity RNA to cDNA kit (Applied Biosystems, Foster City, California, USA) was used for reverse transcription. 10 µl of RT Buffer and 1 µl of RT enzyme mix were added to the RNA samples. A non-template control (NTC) was included where 9 µl of water was added to an eppendorf instead of an RNA sample, and a random sample was used as a non-reverse transcriptase control (NRTC) where 10 µl of RT Buffer was added and 1 µl nuclease-free water was used in place of the RT enzyme mix. The

tubes were placed in a Techne touchgene gradient thermocycler (Bibby Scientific Ltd., Staffordshire, UK) with the following program settings: 37°C for 1 hour, 95°C for 5 minutes and held at 8°C. After reverse transcription, cDNA samples were diluted 1:10. The remaining template and diluted cDNA samples were stored at -20°C.

2.2.4 End-point PCR

The polymerase chain reaction (PCR) has been a revolutionary technique in molecular biology and allows for the amplification and analysis of specific DNA sequences. A single or double stranded region of DNA is amplified by thermocycling. DNA is heated to approximately 95°C for 15 seconds which denatures the hydrogen bonds between the double helix. The reaction is then cooled to approximately 54°C to allow binding of primers: short sequences of single stranded DNA between 20 to 30 nucleotides long (Berg, 2007). The annealing temperature is dependent on the primers used (Kubista et al., 2006). Primers flank the cDNA sequence of interest. The reaction is heated to approximately 72°C which is the optimal temperature for heat-stable Taq DNA polymerase which adds free nucleotides and elongates both forward and reverse primers in the 5' to 3' direction (Berg, 2007). A schematic diagram of the steps in the polymerase chain reaction is shown in Figure 2.4.

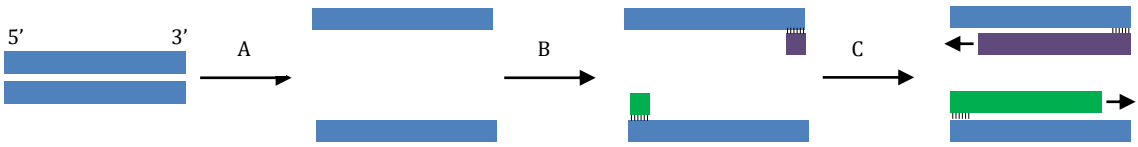


Figure 2.4 Schematic diagram of the polymerase chain reaction.

(A) Double stranded DNA is denatured at 94-96°C; (B) Forward and reverse primers are anneal to the target gene at approximately 60°C; (C) Primers are extended by Taq DNA Polymerase at approximately 72°C. These steps are repeated for 30-40 cycles which allows for exponential amplification of DNA.

2.2.5 Primer design and testing

Primers were designed for PCR and qPCR experiments using Primer3 software (Untergasser et al., 2012) or from previous publications. For sheep studies they were designed in Primer3 to the sheep genome on Ensembl. At least one of each pair of primers per target gene was designed to cross an exon-exon boundary and thereby avoiding the amplification of genomic DNA due to the presence of introns. Primer specifications used were:

- Primer length of 18-30bp
- Product length of 80-220bp
- 40-60% GC content
- Annealing temperature of approximately 60°C

For each primer pair analysed, qPCR standard curves were used in a 1:10 dilution series to determine assay efficiency. This required the use of end-point PCR to amplify the product and then gel electrophoresis to ensure the product

was of the expected size. The primer sequences used for qPCR in sheep studies are shown in table 2.1.

Gene	Publication or NCBI sequence	Forward primer (5'-3')	Reverse primer (5'-3')	Amplicon length (bp)
IPO8 *(ref)*	(Pope et al., 2014)	GCCCTTGCTCTTCAGTCATT	GTGCAACAGCTCCTGCATAA	99
RPLP0 *(ref)*	(Robinson et al., 2007)	CAACCCTGAAGTGCTTGACAT	AGGCAGATGGATCAGCCA	227
YWHAZ *(ref)*	NM_001267887.1	TGTAGGAGCCCGTAGGTCA	TTCTCTCTGTATTCTCGAGCCATCT	102
Cyclophillin *(ref)*	(Fletcher et al., 2007)	CCTGCTTTCACAGAATAATTCCAG	CATTTGCCATGGACAAGATGCCAG	156
UCP1	NM_001166528.1	GGGCTTTGGAAAGGGACTA	CAGGGCACATCGTCTGCTAAT	128
DIO2	(Pope et al., 2014)	AGCCGCTCCAAGTCCACTC	TTCCACTGGTGTCACCTCCT	175
PGC1α	XM_004009738.3	GATTGGCGTCATTCAGGAGC	CCAGAGCAGCACACTCGAT	84
ADRβ3	NM_174232.2	AGAGAGCGAAAACCCACTTG	TTCCTGCGGACTTTCTTAGG	209
RIP140	(Pope et al., 2014)	CGAGGACTTGAAACCAGAGC	TCTTAGGGACCATGCAAAGG	179
Leptin	(Pope et al., 2014)	CCAGGATGACACCAAAACC	TGGACAAACTCAGGAGAGG	140
PPARγ	(Pope et al., 2014)	GACCCGATGGCTCCGTTA	TGAGGGAGTTGGAAGGCTCT	145
TCF21	XM_004011346.3	ATCCTGGCCAACGACAAGTA	TCAGGTCACTCTCGGGTTTC	94

Gene	Publication or NCBI sequence	Forward primer (5'-3')	Reverse primer (5'-3')	Amplicon length (bp)
CD137	NM_001035336.2	TGAGAGGACACGATCACTGC	CACTTTCTGCATATGTCACAGGA	147
SHOX2	NM_001205527.1	CGCCTTTATGCGTGAAGAAC	TTGGCTGGCAGCTCCTAT	142
ATGL	NM_001308576.1	CTAGGCATCTCTCTGACCCG	TGCAGACATTGGCCTGGATA	182
HSL	NM_001128154.1	AGCACTACAAACGCAACGAG	GCCATGTTTGCTAGAGACGA	193
PLIN1	NM_001113773.1	TCCTCCTGAAAAGATCGCCT	TGTCTGAAGTGCTGGCAATG	100
NPR A	XM_015092256.1	AGACAGCGTATTATAAGGGCAAC	GCTCCCACAAACCTGGTCAA	139
NPR C	XM_015101328.1	CAGTGAGGAAGATTACGTGAACA	GTTCGGTTCCAAGTCTGCTG	144
PRKGI	XM_004020002.3	GGCCCCAGAGATCATCCTGA	TGAGAAAGGTGGGCTGCCA	103

Table 2.1 Primers used for ovine reference (ref) and target gene mRNA quantification

2.2.6 Gel electrophoresis of PCR products

A 2% w/v agarose gel was made using 1g of agarose powder dissolved in 50 ml of 1x Tris(hydroxymethyl)aminomethane base (Tris), glacial acetic acid (Fisher Scientific), EDTA buffer (TAE) buffer with 5 µl of ethidium bromide. 5 µl DNA ladder was added to the first well and 20 µl of amplified product from end-point PCR to the other wells. The gel was run at 100 V (400 mA) for 30 minutes. Gels were imaged using a Fujifilm LAS-1000 cooled CCD camera (Fuji Photo Film Co, Ltd, Tokyo, Japan) detecting ethidium bromide fluorescence.

2.2.6 Gel Extraction

Gel bands visualised with UV light for ethidium bromide staining were excised with gel extraction tips. Gel extraction was performed using a QIAquick® gel extraction kit (Qiagen, Hilden, Germany). The gel slice was weighed and 3 volumes of Buffer QG added to the gel volume (e.g. 100 mg gel slice – 300 µl of Buffer QG). The solution was incubated at 50°C for 10 minutes. A volume equal to the weight of the tissue in milligrams (e.g. 100 µl per 100 mg of gel slice weight) was added and pipette mixed thoroughly. A QIAquick spin column was placed in a 2 ml collection tube and the solution added. The column was centrifuged for 1 minute at 11,000g and the flow-through discarded. 500 µl Buffer QG was added to the QIAquick column and centrifuged for 1 minute at 11000g and the flow-through discarded. 750 µl Buffer PE was added to the QIAquick column and centrifuged for 1 minute and the flow-through discarded. Centrifugation was

repeated for 1 min at 11000g. The column was placed into a new 1.5 ml tube. 30 µl Buffer EB was added to elute the cDNA and centrifuged for 1 minute at 11000g. cDNA quantity was determined using a Nanodrop and the solution diluted to 1 ng/µl with nuclease-free water in a total volume of 20 µl.

2.2.7 Quantitative Reverse Transcription PCR (qPCR)

Quantitative Reverse Transcription PCR (qPCR) provides a powerful tool for the analysis of the transcriptome (Kubista et al., 2006) and can be quantitative to levels exceeding that of traditional end-point PCR. The thermocycling reaction remains the same as traditional end-point PCR but reporters or dyes are often used which bind to the product and fluoresce (Kubista et al., 2006). An increase in fluorescence is therefore proportional to the quantity of product formed (Kubista et al., 2006). The difference in fluorescence between samples is analysed during the exponential phase of the reaction, which allows comparisons of initial starting quantities of mRNA. Samples are compared in the number of cycles needed for a fluorescence threshold to be reached, known as the Ct value (Kubista et al., 2006). SYBR Green is a commonly used dye which fluoresces when bound to the minor groove of double stranded DNA so increased fluorescence is observed with increasing product amplification (Kubista et al., 2006). It offers advantages in that it is low in cost and can be used for any primer sequence without probe design which is useful in sheep as the genome has not been fully annotated.

The efficiency of a PCR reaction can be determined by running a standard curve. A 10 fold dilution series for example can be constructed as shown below using a carrier such as tRNA to prevent loss of primer or template at low concentrations (Adams, 2006). Using the log template amount and the number of cycles required to reach a given threshold (Ct value) a line of best fit can be constructed and the efficiency calculated using the equation:

Efficiency= (10 $^{(-1/slope)}$-1 (Adams, 2006)

A theoretical reaction would have an efficiency of 2 i.e. the amount of DNA doubles with each cycle. In practice this does not occur as a clear plateau is always observed in an amplification plot, although it is not currently known why this occurs. The efficiency is therefore calculated in the exponential phase of the qPCR reaction. An example of a standard curve amplification plot and line of best fit is shown in Figure 2.5.

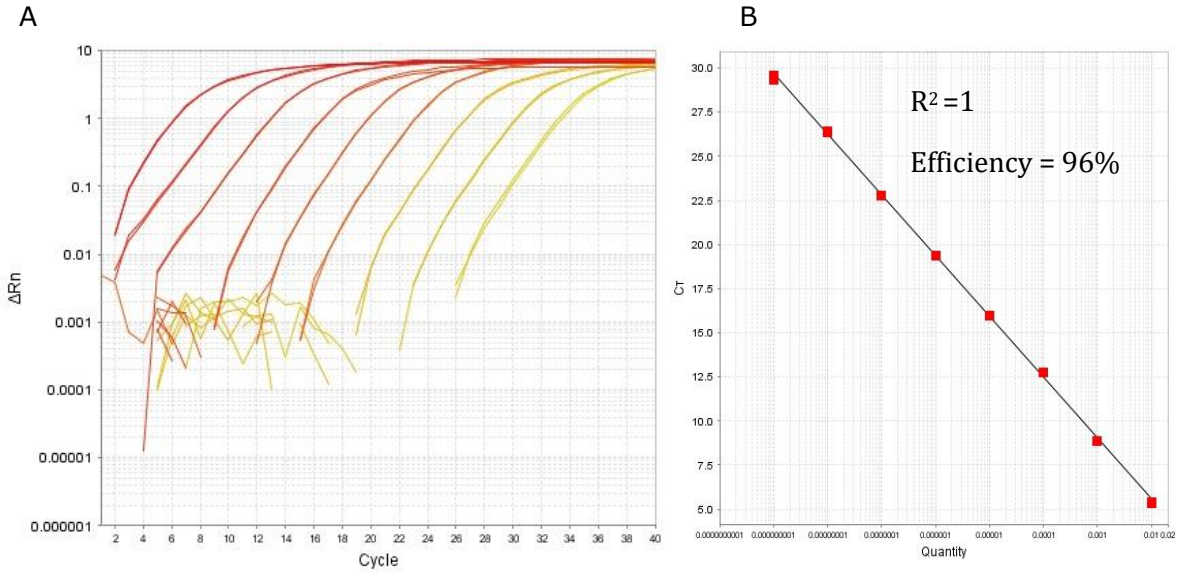


Figure 2.5 qPCR standard curve and efficiency.

A) qPCR amplification plot of standard curve B) Linear graph of standard curve with Ct value plotted against log of template quantity. R^2 and efficiency values are shown. Both graphs were generated from the same primer pair of ovine PGC1α

To ensure that the primers used in the qPCR reaction bind to only one product, a melt curve analysis can be performed. This involves an increase in temperature to around 90°C until the product melts, SYBR Green is released and a decrease in fluorescence is quantified automatically in real-time. A single product produced by the primers will result in a single peak in the melt curve (Ponchel, 2006). An example of this is shown in Figure 2.6.

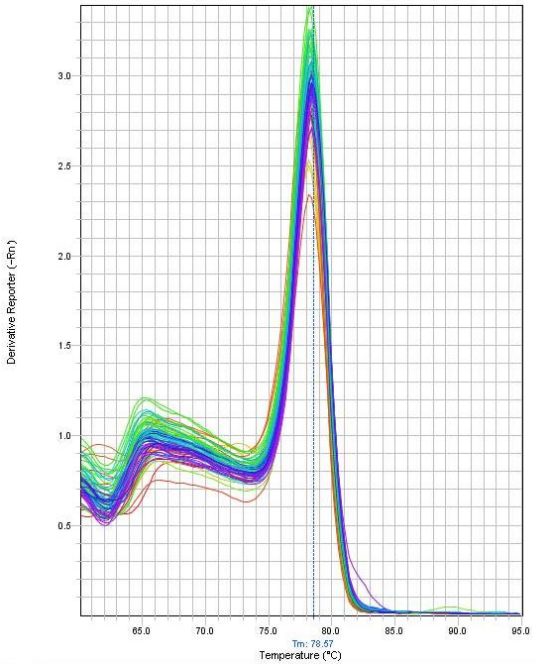


Figure 2.6 Figure 2.6 Melt curve analysis of product (PGC1α) showing a single product is amplified by qPCR

A master mix was made of 5 µl Fast SYBR® Green master mix (Applied Biosystems, Foster City, California, USA), 1 µl of 2.5µM forward primer and 1 µl of 2.5µM reverse primer. Primer sequences are detailed in table 2.1. 7 µl master mix was added to each well with 3 µl of the respective sample. An NRTC and NTC were included on all plates as controls. Standards were made from the cDNA of the gene of interest after end-point PCR and gel electrophoresis as described

above. These were added in duplicate as a 1:10 dilution series to test assay efficiency. Plates were run on a Step-One Plus PCR machine (Applied Biosystems, Life Technologies, Paisley, UK). Amplification curves were analysed to ensure the efficiency of the reaction was over 90%. Replicates were analysed to ensure Ct values did not differ by more than 0.5 cycles. Melt curves were also analysed to ensure a single amplicon was produced during the reaction by the primers. The multicomponent plot was examined to ensure similar levels of passive ROX fluorescence in each well and between replicates. DNA products from PCR amplification were sequenced and matched to the sheep genome to confirm primer specificity.

Reference genes are important for data normalisation by correcting for differences in the quantity and quality of amplifiable RNA or cDNA as well as variation in reverse transcription efficiency (Radonic et al., 2004). It has been established that the use of multiple reference genes provides a more accurate normalisation method than single reference genes alone (Vandesompele et al., 2002) and that mRNAs are most suitable for this purpose (Radonic et al., 2004). To this end, the geNorm algorithm (Vandesompele et al., 2002) was used on a panel of four reference genes importin 8 (IPO8), cyclophillin, 14-3-3 protein zeta/delta (YWHAZ) and ribosomal protein lateral stalk subunit P0 (RPLP0). geNorm uses pairwise variation to calculate a stability or M value for each of the reference genes. The two reference genes with the lowest M values (i.e. the most stable) were used for normalisation which in this case were IPO8 and RPO. Target gene relative quantities are divided by the geometric mean of the most

stable reference genes to produce an output value for analysis. Reference gene selection and relative expression were determined by using the geNorm method performed on geNorm software v3.5 (Primer Design Ltd, Southampton, UK) which takes into account the efficiency of multiple assays.

2.2.8 Mitochondrial DNA to nuclear DNA ratio

Analysis of the expression ratio of mitochondrial DNA (mtDNA) to nuclear DNA (nDNA) has often been used to give an estimation of mitochondrial biogenesis in adipose tissue (Basse et al., 2015; Rong et al., 2007) and has been observed in the browning response (Zhang et al., 2014). This requires the cellular DNA extraction and primers for regions of mtDNA and nDNA. The amount of product can then be assessed through qPCR.

2.2.8.1 Cellular DNA Extraction

DNA was extracted from a small amount of tissue from the same samples that were used for qPCR analysis. Tissue pieces were incubated in 500 µl Extraction Buffer with 3 µl of proteinase K (20 mg/ml) overnight at 55°C. 500 µl of phenol/chloroform/isomyl alcohol (24:24:1) was added to the tube and mixed. Samples were centrifuged for 10 minutes at 10000g at room temperature and the upper phase transferred to a new eppendorf tube. 200 µl of 7.5 M ammonium acetate was added to each tube and 800 µl of ice-cold 100% ethanol. Centrifugation was performed at 16000g for 15 minutes and the resulting supernatant removed. 700 µl of 75% ethanol was added and the centrifugation

step repeated at 16000g for 15 minutes. The supernatant was removed and the DNA pellet air-dried at room temperature. The pellet was re-suspended in 30 µl of Ambion nuclease free water and dissolved by incubating at 50°C for 1 hour with shaking. Prior to qPCR analysis, DNA was diluted to 15 ng with nuclease free water.

2.2.8.2 qPCR

qPCR was performed as described above using primers for mtDNA sequences MTCO1 F – ATCGGTGGATTCGGCAACTGA, R -GGAGTAACAGGAAAGATGGGGGAAG (Basse et al., 2015) and nDNA 18S F – GATGCGGCGGCGTTATTCC, R – CTCCTGGTGGTGCCCTTCC (Begum et al., 2012). The relative quantity of MTCO1 for each sample was divided by the relative quantity of 18S to determine the mtDNA/nDNA ratio.

2.2.9 Mitochondrial Protein Extraction Procedure

A mitochondrial protein extraction procedure was used prior to western blotting as the target proteins UCP1 and cytochrome c are located within the mitochondria and enrichments for the particular organelles can reduce background and non-specific binding in subsequent western blots. Protein extraction was achieved using differential centrifugation in a sucrose solution, which helps to preserve mitochondria integrity (Clayton and Shadel, 2014).

100 mg of frozen tissue was chopped and placed in a dispomix tube with 1 ml mitochondrial homogenisation buffer. Samples were homogenised on a Dispomix® drive homogeniser (Medic Tools AG, Lussiweg, Switzerland), centrifuged at 3220g for 1 minute at 4°C and transferred to an Eppendorf tube. The homogenate was then further homogenised using a Potter-Elvehjem homogeniser 10 times. 100 µl was aliquoted for total protein. The remaining homogenate was centrifuged at 1500g for 10 minutes at 4°C. The supernatant was removed and transferred to a new tube. Samples were centrifuged at 13000g for 60 minutes at 4°C. The supernatant was removed and the mitochondrial pellets were re-suspended in 120 µl of mitochondrial homogenisation buffer.

2.2.10 Protein quantification by Bicinchoninic acid assay

A Bicinchoninic acid (BCA) assay allows the quantification of protein based on the reduction of Cu^{2+} to Cu^{+} in the presence of protein when in an alkaline environment (Walker, 1994). BCA acts as a chelating agent with Cu^{+} to give a colourimetric reaction resulting in a dark purple colour in aqueous solution (Walker, 1994). Two reagents were prepared prior to running the BCA assay: Reagent A (1% (w/v) BCA, 2% (w/v) sodium carbonate, 0.16% sodium tartrate and 0.4% (w/v) sodium hydroxide, pH 11.25) and Reagent B (4% (w/v) copper sulphate. The final working reagent (Reagent C) was made by mixing Reagent A with reagent B (100:2). Standards of 1, 0.8, 0.6, 0.4, 0.2, 0.1 and 0.05 (mg/ml) bovine serum albumin (BSA), diluted in 0.9% saline were loaded in duplicate into a 96 well microtitre plate with unknown samples diluted 1:20 with 0.9% saline also loaded in duplicate. 200 µl of reagent C was added to each well and

incubated at 37°C for 30 minutes with gentle shaking. Absorbance was measured at 570 nm using a spectrophotometer. The sample dilutions were multiplied by the dilution factor to determine the final protein concentration present in the sample. Samples where the %CV of replicates was >5% were repeated.

2.2.11 Western Blotting

Western blotting is a technique for quantifying the amount of protein in a sample using specific antibodies to a protein of interest (Jensen, 2012). Once the total protein or fractionated organelle protein (e.g. mitochondria) has been extracted from a tissue, it is first denatured by heating and the addition of a reducing agent such as β-mercaptoethanol that cleaves disulphide bonds in peptide sequences. Proteins are then used for sodium dodecyl sulphate -polyacrylamide gel electrophoresis (SDS-PAGE). SDS binds to hydrophobic regions of proteins causing them to unfold and also donates a negative charge to the proteins so they migrate through the gel when subjected to an electrical field (Jensen, 2012). The polyacrylamide gel is a highly cross-linked structure that retards large protein migration compared to smaller proteins. This allows proteins to be separated by size, with smaller polypeptides migrating faster down the gel. Ladders of known protein sizes are typically included on gels so that bands seen with the addition of antibody are of the expected size. Once proteins have been separated by SDS-PAGE they are transferred from the gel to a nitrocellulose membrane by electrical force. A schematic diagram of this process is shown in Figure 2.7.

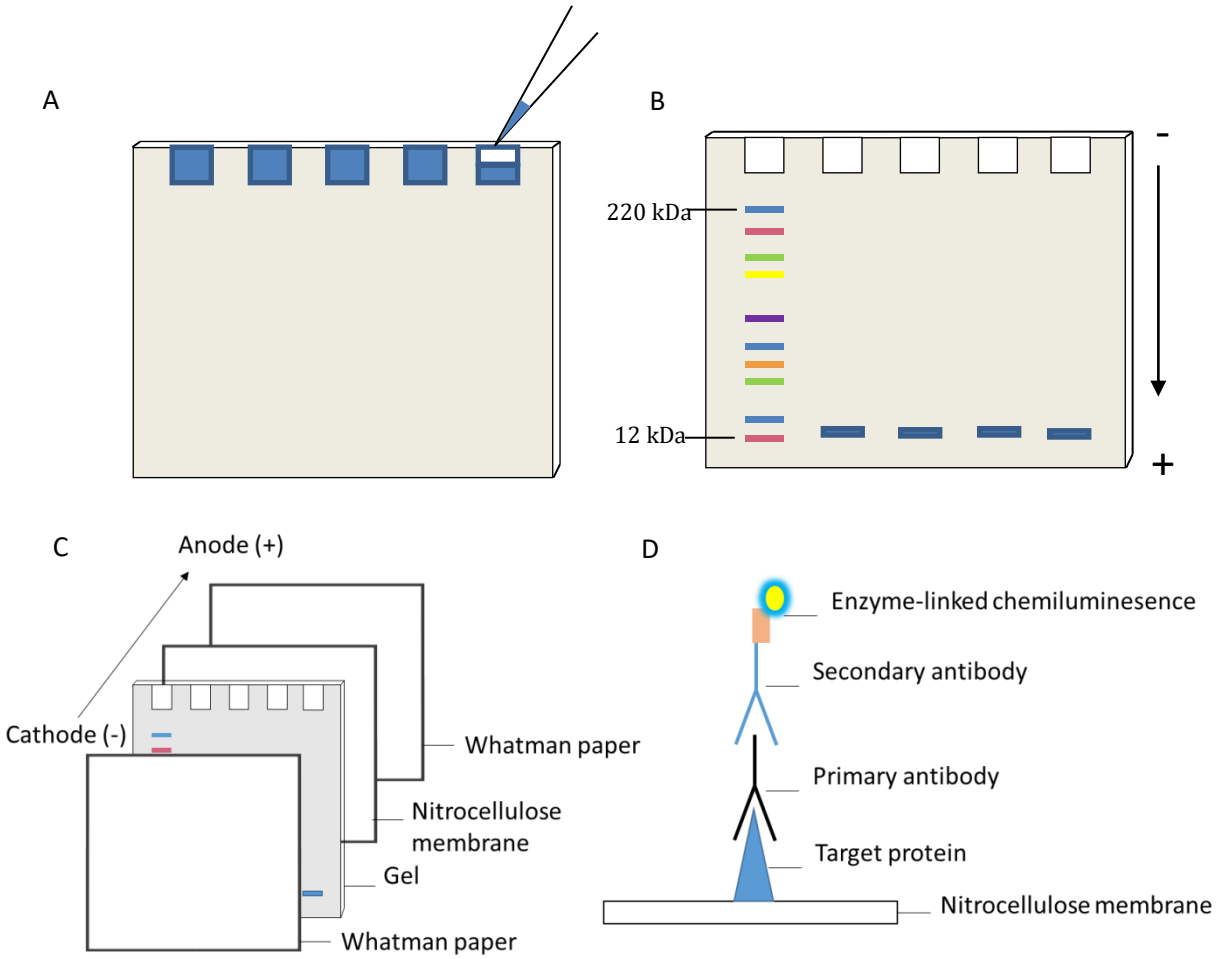


Figure 2.7 Schematic diagram of the principal steps in western blotting.

A) Loading of protein samples into wells of polyacrylamide gel B) SDS-PAGE. Proteins migrate towards the anode (+) in order of size as shown by molecular marker on left C) Transfer of protein from gel to nitrocellulose membrane through an electrical field. Samples move towards anode (+) D) Detection of target protein on nitrocellulose membrane by immunoblotting and chemiluminesence

Ponceau S staining can be used to check for the transfer of protein from gel to membrane and stains non-specific protein a red colour after washing in water. This reversible staining can be removed through detergent based solutions. Membranes are typically blocked in a solution of milk protein or BSA to prevent non-specific binding of antibodies to the membrane in subsequent steps. After

blocking, a primary antibody solution is then added to the membrane which binds to the target protein. After washing steps to remove unbound antibody, a secondary antibody that binds to the primary antibody is added and is linked to chemilumiescent reagents which allow the visualisation of protein bands on the membrane at certain wavelengths of light. The intensity of the bands seen can then be quantified using densitometry to give an indirect method for the abundance of protein within a sample.

Protein samples were diluted to 4.2 µg/µl with mitochondrial homogenisation buffer in a total volume of 20 µl. 14 µl of glycerol bromophenol blue and 50 µl protein dissociation buffer (50 mM tris, 10 (w/v) % glycerol, 2 (w/v) % SDS, 5 (w/v) % 3-mercaptoethanol). Electrophoresis and blotting were run using a Mini-PROTEAN 3 Cell kit (Bio-Rad, Hercules, CA, USA). A 12% resolving gel (30% polyacrylamide mix (37:5:1) 3.3 ml, Distilled water 4 ml, 1.5 M Tris pH 8.8 (2.5 ml), 10% SDS 100 µl, 10% ammonium persulphate (APS), Tetramethlethylenediamine (TEMED) 4 µl) was made for 2 gels into the cast. After the gel had set, a stacking gel containing 3.4 ml distilled water, 30% polyacrylamide mix (37:5:1) 850 µl, 1M Tris (pH 6.8) 625 µl, 10% SDS 50 µl, 10% APS 50 µl, 5 µl TEMED was added to the top of the resolving gel to fill the chamber. A 15 well comb was then added and the gel allowed to polymerise. Protein samples were incubated at 95°C for 10 minutes to disassociate the proteins and placed immediately on ice. The gel was removed from the casting stand and placed in the electrophoresis apparatus. The lower chamber was filled with approximately 200 ml 1x running buffer and the inner chamber with 100 ml

running buffer. The comb was removed and 10 µg (10 µl) of previously diluted sample mitochondrial protein solution was added for each sample in duplicate into the wells. A protein ladder was included on each gel plus a 7 day perirenal sample to serve as a calibrator between gels.

The electrophoresis was run for 1 hour at 150 V. Wet transfer using a gel electrophoresis tank (Bio-Rad) onto a nitrocellulose membrane (Amersham Hybond ECL Nitro-cellulose Membrane, GE Healthcare, Buckinghamshire, UK) and the membrane stained with Ponceau S stain to visualise protein transfer and gel loading. Protein ladder bands were marked with an antigen-antibody pen for rabbit primary antibodies (Alpha diagnostics, San Antonio, TX, USA) to be visualised with chemiluminesence. Membranes were blocked in 10% (w/v) milk powder (Marvel; Premier Foods, Spalding, Lincolnshire, UK) in Tween 20 tris-buffered saline (TTBS) for 1 hour with shaking. The primary antibodies were used at 1:10,000 dilution and membranes were incubated overnight with an in-house anti-UCP1 antibody as previously described (Schermer et al., 1996) at a 1:10,000 dilution and anti-Cytochrome c ((H104) sc-7159, Santa Cruz Biotechnology, Santa Cruz, USA) in 3% (w/v) milk powder. Membranes were then washed with TTBS for 30 minutes and incubated with a swine anti-rabbit secondary antibody (P0217, Dako Ltd., Cambridge, UK) at a 1:20,000 dilution in 3% (w/v) milk for 1 hour at room temperature with shaking. After secondary antibody incubation, the membranes were washed in TTBS for 30 minutes at room temperature followed by Tris-buffered saline (TBS) incubation at room temperature with shaking for 30 minutes and 45 minutes without shaking.

Immobilon Western Chemiluminescent HRP Substrate (WBKLS0500, Merck Millipore, Watford, UK) reagents were divided into aliquots and brought to room temperature 10 minutes before use. 1 ml of Reagent A and 1ml of Reagent B were used per membrane. After addition of ECL reagents the membrane was incubated for 5 minutes at room temperature and visualised on a Fujiflim LAS-3000 CCD camera. Band densities were determined using AIDA software by subtracting background staining intensity and expressed as a percentage of the calibrator run on every gel.

2.2.12 Histology

Histology is the study of microscopic tissue sections or cells. Tissue structure and integrity must be conserved through fixing of the tissue where immersion in formalin forms cross-links between proteins (Gordon, 1990). The tissue pieces must then be dehydrated through immersion in ethanol solutions to remove aqueous fixative, the dehydrating reagent removed through a 'clearing reagent' such as xylene before being embedded in paraffin wax which provides a solid support for thin sections to be cut with a microtome (Gordon, 1990). Once sections have been obtained from a tissue they are attached to a microscope slide and a variety of stains can be utilised to visualise different organelles and structures within the cell. A commonly used combination of stains to determine adipose tissue morphology (as well as other tissue types) is haematoxylin and eosin staining. Harris's Haematoxylin is a basic compound that stains acidic parts (or basophilic components) of the cell dark blue when washed in weak alkaline

solutions. This generally includes the nucleus as nucleic acids incorporate the stain. Eosin is an acid which stains dyes basic (acidophilic) components of the cell a red/pink colour. Many of the components of the cells cytoplasm have a basic pH and will therefore be stained. A combination of these two stains allows the nucleus and cytoplasm to be easily distinguished and therefore tissue morphology can be determined by brightfield microscopy.

2.2.12.1 Tissue processing and sectioning

At the time of dissection tissues were placed in 10% formalin. The samples analysed were taken from a separate study as the epicardial and paracardial samples used for qPCR and western blot were not fixed for histology. The animals in the study for histology were sampled at the same time points of 1, 7±1 and 28±3 days and only adipose tissue from female lambs were selected. The sheep were a different breed however and were lambs from Bluefaced Leicester cross Swaledale mule ewes crossed with a Texel ram.

A small piece of formalin fixed tissue was cut and placed into a Histocassette (Simport Scientific, Beloeil, QC, Canada). The cassettes were stored in 70 % IMS and processed overnight in a Shandon Excelsior advanced tissue processor (Thermo Shandon Ltd, Runcorn, Cheshire, UK). A processing programme of six cycles of increasing concentrations of IMS (75, 90, 95, 100, 100, 100% respectively) at 20 °C for 1 hour, three cycles of xylene at 20 °C for 1 hour, and three cycles of wax at 62 °C for 1 hour 20 minutes. After completion of tissue

processing, each sample was then embedded in paraffin wax using a Tissue-Tek III Embedding Center (Sakura Finetek, Torrance, CA, USA). Epicardial and paracardial samples had previously been processed by Mrs Victoria Wilson and Miss Gloria Gusman. Perirenal samples were processed by Mrs Reham Algal. Embedded tissue samples were sectioned at 5 μm using a sledge microtome with sections being floated in a water bath at 37°C. Sections were placed onto Thermo superfrost slides and placed on a heated rack at 45°C for 30 minutes. Slides were then baked in an oven at 37°C for a minimum of 24 hours for proper attachment of sample to the slide.

2.2.12.2 Haematoxylin and eosin staining protocol

Slides were placed into a slide rack and stained using the protocol shown below (Table 2.2). I was assisted in these experiments by Urmila Cockerill, a BMedSci student conducting a research project under my supervision.

Reagent	Time (seconds)
Xylene I	180
Xylene II	180
100% IMS I	180
100% IMS II	180
70% IMS	180
Distilled Water	180
Harris' Hameatoxylin	300
Running tap water	300
Acid Alcohol (1% v/v HCl in 70% IMS)	15
Scott's tap water	90
Running tap water	300
0.1% Eosin	300
Running tap water	90
100% IMS III	120
100% IMS IV	120
Xylene III	120
Xylene IV	180

Table 2.2 Protocol for haematoxylin and eosin staining of adipose tissue sections

2.2.13 Immunohistochemistry

Immunohistochemistry (IHC) allows the detection of a protein on a tissue section and is therefore useful in determining the localisation of a particular protein within a cell. The principles are similar to that of immunoblotting where a primary antibody recognises the protein of interest and a secondary antibody binds to the primary antibody. Instead of chemiluminescence, the secondary

antibody can be coupled to an enzyme-linked colourimetric reaction using 3,3'-Diaminobenzidine (DAB) as a substrate. This can produce a brown colour where the target protein is detected. There are other methods of detection available such as fluorescence; however the reagents readily available within the laboratory were DAB staining and can be assessed through brightfield microscopy, with the advantage that they do not fade greatly over time.

IHC was performed on a 5µm thick tissue sections (as described above) using Leica BondMax™ IHC slide processor (Leica Microsystems). An automated programme was used with the following steps: 1 minute xylene and 1 minute ethanol for wax removal and dehydration, 150 µl Epitope retrieval solution 1 incubated at 95°C for 20 minutes, Peroxide block for 5 minutes, 150 µl of 1:500 primary ovine UCP1 antibody incubated for 30 minutes, 150 µl of HRP-conjugated secondary anti-mouse and rabbit antibody polymer incubated for 8 minutes. Slides were then immersed in DAB for 10 minutes and counterstained with Harris' haematoxylin for 5 minutes. Slides were visualised with brightfield microscopy and several images were taken of each slide.

2.2.14 TUNEL assay

One of the hallmarks of apoptosis is the fragmentation of cellular DNA (Kyrylkova et al., 2012). A Terminal deoxynucleotidyl transferase (TdT) dUTP Nick-End Labeling (TUNEL) assay can detect possible apoptotic cells with fragmented DNA by the incorporation of biotinylated nucelotides into DNA strand breaks by TdT (Kyrylkova et al., 2012). Biotin labelling is used with

horseradish peroxidase and streptavidin to initiate a colourimetric reaction using DAB as a substrate. Therefore localisation and identification of DNA with strand breaks is identified by a brown precipitate which can be visualised through brightfield microscopy (Figure 2.8).

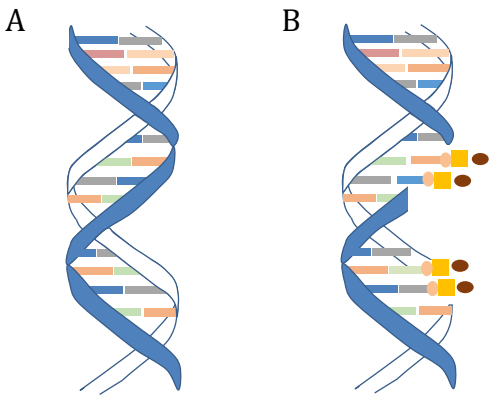


Figure 2.8 Schematic diagram of TUNEL assay principle.
(A) Normal un-fragmented DNA does not show any staining; (B) Apoptotic fragmented DNA incorporates free biotinylated dNTPs with Enzyme linked HRP-Strep which causes a colourimetric reaction using DAB as a substrate leading to a brown precipitate on tissue sections

A TUNEL assay was performed using a commercially available TACS® 2 TdT-DAB *In Situ* Apoptosis Detection Kit (Cat# 4810-30-K, Trevigen®, Gaithersburg, MD, USA) according to the manufacturer's instructions. Tissue blocks were sectioned at 5µm and attached to superfrost plus slides and baked overnight. Slides were dewaxed by immersing in Xylene I & II, 100% IMS I & II and 70% IMS as described for H&E staining above. Slides were immersed in 50 ml PBS in a coplin jar for 10 minutes. The slide surrounding the sample was dried and 50 µl Proteinase K was added to the sample and incubated at room temperature for 30 minutes. This was completed in a humidity chamber to avoid dehydration of

samples. Slides were washed twice in 50 ml of deionised water for 2 minutes each. Samples were immersed in 50 ml of Quenching solution containing 45 ml methanol and 5 ml hydrogen peroxide. Samples were washed in PBS for 1 minute. In a separate step, positive control samples were treated with 50 µl of 1:50 TACS Nuclease (diluted in TACS Nuclease buffer) and incubated for 15 minutes at 37°C in a humidity chamber. A rat thymus slide (4800-30-41, Trevigen®, Gaithersburg, MD, USA) was treated with TACS nuclease as a positive control or untreated as a negative control. A positive control was also generated from sheep sections by treating with TACS Nuclease. The positive control slides were washed twice in 1x PBS and all samples were then covered with 50 µl of labelling reaction. The negative control slides were also used with TdT enzyme omitted from the labelling reaction. All slides were incubated for 1 hour at 37°C in a humidity chamber. Samples were then immersed in 50 ml stop buffer for 5 minutes to stop the labelling reaction and washed twice in deionised water for 5 minutes each. Samples were then covered with 50 µl Streptavidin-HRP solution and then washed twice in 50 ml 1x PBS for 5 minutes each. Samples were immersed in DAB solution for 2 minutes, counterstained with haematoxylin for 5 minutes and dehydrated and coverslips applied as described for H&E staining. Haematoxylin was used as a counterstain as provided methyl green did not stain nuclei in adipose tissue samples.

2.3 Human Pheochromocytoma study

The collection of samples and subsequent analysis was performed at the University of California, Los Angeles. This was approved by the University of California Los Angeles Medical Institutional Review Board and written patient consent was taken by Dr Laurent Vergnes. I received anonymised clinical data for each of the patients.

2.3.1 Study subjects and sampling procedures

Blood samples were obtained from patients between 7am-10am after overnight fasting. Bloods were centrifuged at 1200g for 15 minutes at 4°C and plasma collected into eppendorf tubes and stored at -80 ^{o}C. Adipose tissue samples were resected from patients during adrenalectomy at the Division of Endocrine Surgery at UCLA Ronald Reagan Hospital, Los Angeles performed by surgeon Dr Michael Yeh. Of the patients studied 8 had non-functioning tumours, 3 had aldosterone secreting tumours, 2 had Cushing's syndrome and 13 had pheochromocytoma. Biopsies were stored on ice, and were cut into three parts: one piece of fresh tissue was used immediately for mitochondrial isolation and subsequent mitochondrial respiration analysis, one piece was snap frozen in liquid nitrogen and frozen at -80°C for RNA and protein extraction and one piece was fixed in formalin and used for H&E histology.

2.3.2 Exclusion Criteria

For both the control and pheochromocytoma group, patients were excluded that had type 2 diabetes treated with thiazolidinedione (pioglitazone or rosiglitazone) as these compounds have been shown to up-regulate UCP1 (Petrovic et al., 2010) and promote adipocyte differentiation (Fischer et al., 2002) that may confound the results. Patients who had untreated hyper or hypothyroidism were also excluded as thyroid hormones have been established to increase UCP1 activation (Bianco and Silva, 1987). Patients who had malignancies were also excluded due to effects of cancer cachexia on adipose tissue browning (Petruzzelli et al., 2014). Patients with paraganglioma were also excluded. The full clinical details of subjects studied including prescribed medications are included in the appendix.

2.4 Laboratory Procedures

All analyses were conducted in the laboratory of Prof. Karen Reue in the Department of Human Genetics, University of California, Los Angeles (UCLA) and performed by myself under the supervision of Dr Laurent Vergnes unless otherwise stated.

2.4.1 Catecholamine Plasma analysis

Analyses of plasma catecholamines (noradrenaline, adrenaline, normetadrenaline and metadrenaline) were outsourced from the lab and

measured by Quest Diagnostics. The results from the analysis were then forwarded to Prof. Harold Sacks who supplied me with the data.

2.4.2 Glucose Plasma analysis

Glucose analysis was performed using a commercial available glucose assay kit (GAGO-20, Sigma Aldrich). The kit uses glucose oxidase to oxidise glucose to gluconic acid and hydrogen peroxide. The resulting hydrogen peroxide can then react with o-dianisidine to form oxidised o-dianiside in the presence of peroxidase. Sulphuric acid is then added to form a pink coloured product. The intensity of the pink colour proportional to the amount of glucose present in the sample can be measured by a spectrophotometer at 540 nm.

10 µl of 1:5 diluted plasma samples were added in duplicate to a 96 well plate. Previous optimisation steps determined this plasma dilution. A standard curve was made of 0, 2, 4, 6 and 8 mg of glucose from a 1 mg/ml stock. 80 µl of Assay reagent was to each well and mixed. The plate was incubated at 37°C for 30 minutes with shaking at room temperature. 80 µl of 12N Sulphuric acid was added to each tube and mixed. Optical densities were measured at 540 nm and sample concentrations were extrapolated from the linear standard curve.

2.4.3 Non-esterified Fatty Acid Plasma Analysis

Non-esterified fatty acids (NEFA) present in the plasma were analysed using a commercially available reagent (NEFA-HR(2), Wako). The Wako kit uses a series of enzymatic reactions to determine NEFA plasma concentrations. The first reaction is the conversion of NEFA to Acyl-CoA, AMP and PPi using Acyl-CoA synthetase. ATP and coenzyme A are provided as substrates in this reaction. Acyl-CoA is then oxidised in the presence of Acyl-CoA oxidase to form 2,3-trans-Enoyl-CoA. A colorimetric reaction then occurs with the addition of peroxidase and the absorbance can then be measured using a spectrophotometer.

10 µl of standard or sample were added in duplicate to a 96 well plate. 10mM of palmitate was used as the standard from 0 µl as blank to 3.5 µl in 0.5 µl increments. 120 µl of reagent 1 (HR Series NEFA-HR (2) Reagent 1) was added to each well and incubated at room temperature with shaking for 10 minutes. 40 µl of reagent 2 (HR Series NEFA-HR (2) Reagent 2) was added to each well and analysed on a spectrophotometer at 550 nm.

2.4.4 FGF21 Plasma Analysis

Plasma FGF21 was measured using an Enzyme-linked Immunoassay (ELISA) kit (Cat#: ELH-FGF21). Reagents were re-constituted according to the manufacturer's instructions. FGF21 standard dilutions from 2000 pg/ml to 0 pg/ml (blank) were made up from the stock provided in the kit and 100 µl of standard or diluted sample was added in duplicate to coated wells of a

microplate. The sample dilution was determined empirically and was found to be optimal for human plasma samples in this study at a 1:10 dilution. The wells were covered and incubated at room temperature for 2.5 hours with gentle shaking. The solution was washed four times with 1x Wash Solution. 100 µl of 1x biotinylated antibody was added to each well and incubated for 1 hour at room temperature with gentle shaking. The solution was discarded and the previous wash step repeated. 100 µl of Streptavidin solution was then added to each well and incubated for 45 minutes at room temperature with gentle shaking. The solution was discarded the washing steps repeated. 100 µl of TMB One-Step substrate was added to each well and incubated for 30 minutes wrapped in aluminium foil at room temperature with gentle shaking. 50 µl of Stop Solution was added to each well and the absorbance was measured at 450 nm immediately using a spectrophotometer.

2.4.5 ANP Plasma Analysis

Plasma ANP was measured using an Enzyme Immunoassay (EIA) kit (Cat#: EIA-ANP, RayBiotech, Inc.) according to the manufacturer's instructions. 100 µl of anti-ANP antibody (capture antibody) was added to an anti-rabbit IgG coated 96 well microplate provided in the kit, and incubated for 1.5 hours at room temperature with shaking. The solution was then discarded and washed 4 times with 1x Wash solution. A 10 fold dilution series was constructed from the stock ANP peptide from 1000 pg/ml to 0.1 pg/ml. To each standard and sample 10 pg/ml of biotinylated ANP was added. 100 µl of standard was added to the plate and a blank (assay diluent) and positive control (cell culture medium) was also

included. Samples were diluted 1:2: this was previously determined by me to be the optimum dilution for my plasma samples by testing a range of dilutions of sample with standard curves. 100 µl of sample was added to the plate. Due to limited amounts of plasma remaining after previous plasma tests, technical replicates were not possible. The plate was incubated for 2.5 hours at room temperature with shaking. The solution was discarded and the plate washed as before. 100 µl of HRP-Streptavidin solution was added to each well and incubated for 45 minutes at room temperature with shaking. The solution was discarded and washed and 100 µl of TMB one-step substrate reagent was added to each well and the plate covered in aluminium foil and incubated for 30 minutes at room temperature with gentle shaking. 50 µl of stop solution was added to each well and absorbance read immediately at 450 nm on a spectrophotometer. Sample concentrations were extrapolated from the standard curve.

2.4.6 BNP Plasma Analysis

A commercially available human ELISA kit (Catalog #:ELH-BNP, RayBiotech) was used to quantify plasma BNP. This measures total BNP and not pro-BNP specifically. All reagents were diluted according to the manufacturer's instructions. Standards were made from 15.63 pg/ml to 1000 pg/ml as described in the manual. Assay diluent served as a blank. 100 µl of standard was added to the plate and 100 µl of undiluted sample. Due to the limited amount of plasma due to use in previous plasma experiments and cell culture experiments, samples

were added in single replicates. The plate was incubated for 2.5 hours at room temperature with shaking and washing steps described in previous ELISAs above were performed with the supplied wash buffer. 100 µl of biotin antibody was added to each well and incubated for 1 hour at room temperature with shaking. The wash steps were repeated and 100 µl of Streptavidin solution was added to each well and incubated for 45 minutes at room temperature. Washing was repeated and 100 µl of TMB One-step-substrate reagent was added to each well and incubated for 30 minutes at room temperature. 50 µl of Stop solution was added to each well and the absorbance measured immediately on a spectrophotometer at 450 nm. Samples were extrapolated from the standard curve.

2.4.7 Histology

Fixed tissues samples were outsourced from the lab and sent for H&E staining at the Department of Pathology, Centre for Health Science, UCLA; 7µm sections were requested and the slides returned to the Reue lab for microscopic examination and the determination of unilocular or multilocular adipocytes.

2.4.8 Immunohistochemistry

Formalin fixed samples were also outsourced and sent for IHC performed by the histopathology department in the Centre of Health Sciences at UCLA. The principles of the assay and protocols are similar to that described for the sheep studies above. The patient samples sent for analysis were 12 pheo (n= 6

unilocular by H&E and 6 multilocular), 12 controls (lean controls (n=6) and obese controls (n=6)). A UCP1 antibody (662045 Anti-UCP1, Calbiochem®, EMD Millipore) was used at a 1:1000 dilution. Stained slides were transported back to the UCLA Reue lab for imaging by brightfield microscopy.

2.4.9 Cellular bioenergetics analysis

Measurements of oxygen consumption of isolated mitochondria in response to various compounds affecting the electron transport chain allows for the respiration profile of cells to be determined. This can be done through an XF24 Extracellular Flux Analyser (Agilent Technologies, Santa Clara, CA, USA), which works in the same way as the earlier Clark electrodes for measuring oxygen consumption, but allows for a higher throughput and smaller quantities of mitochondria to be used (Divakaruni et al., 2014). A solid state oxygen probe on a sensor cartridge is lowered to 200 μm above a monolayer of mitochondria forming a transient microchamber, allowing the decrease in oxygen within the media to be measured (Rogers et al., 2011). Four drug ports allow for automatic injection of various drug compounds at pre-determined time points and the change in oxygen consumption to be quantified. The individual assays used in this thesis are described in detail below.

Dr Laurent Vergnes optimised this protocol and collected some of the experimental results for human adipose tissue samples prior to my arrival at UCLA. Due to the long procedure of mitochondrial isolation and subsequent

cellular bioenergetics experiments, these were performed jointly between Dr Laurent Vergnes and myself.

2.4.9.1 Mitochondrial isolation

A fresh piece of tissue from the biopsy was cut, weighed, minced and placed on a cell strainer and washed with PBS to remove any blood. The tissue was then placed in a pre-chilled glass dounce and 7 ml of MSHE Buffer added. The tissue was homogenised until tissue pieces were no longer visible (approximately 5-6 times). The homogenate was transferred to a 15 ml Falcon Tube and centrifuged for 10 minutes at 800g, at 4°C. The top layer of fat was aspirated and the supernatant poured through a cell strainer into a separate tube. The pellet was then re-suspended in 7 ml MSHE buffer and re-centrifuged, aspirated and decanted through a filter into the previous tube to combine the supernatants. The combined supernatant was then centrifuged at 8000g for 10 minutes. The supernatant was aspirated the remaining mitochondrial pellet was re-suspended in 5μl of MSHE and pipette mixed to ensure complete re-suspension. 700μl of MSHE was added, the solution pipetted mixed and transferred to a 1.5 ml eppendorf tube and centrifuged for 10 minutes at 8000g at 4°C. The resulting supernatant was aspirated and the pellet re-suspended in 5μl MAS buffer (see appendix) and pipette mixed. 20μl MAS buffer was added and pipette mixed. Mitochondrial protein yield was determined by Bradford assay.

2.4.9.2 Bradford assay

A Bradford assay works by a shift in the absorption wavelength of Coomassie Blue acidic solution from 465 to 595nm when binding to a protein occurs (Noble and Bailey, 2009). This causes a red to dark blue colourimetric reaction. It does not involve an incubation step for the colourimetric reaction to occur unlike a BCA assay. This was an advantage with cellular bioenergetics experiments so that the time from extraction of mitochondria from the adipose tissue to oxygen consumption measurements was as short as possible to maintain viable mitochondria.

An aliquot of mitochondrial protein was added to Protein Triton lysis buffer. 1.6 ml 5x stock Protein Assay Dye Reagent Concentrate (BioRad, CAT# 500-0006) was added to 6.4 ml distilled H_2O to obtain a 1x working solution. Standards were made using a 2 mg/ml BSA stock and 0, 0.5, 1, 1.5, 2, 2.5, 3 or 3.5 µl of stock was added to wells in duplicate. 2 µl of each sample was added to wells in duplicate and 150 µl of Protein Assay Dye Reagent Concentrate added. Absorbance values were read immediately on a plate reader at 595 nm and concentrations of the unknown samples were extrapolated from the standard curve using Microsoft Excel.

2.4.9.3 Coupling Assay

A coupling assay allows both ATP-linked and uncoupled respiration to be determined. Uncoupled respiration is useful when analysing thermogenic

adipose tissue as it can give a functional indication of UCP1 activity. Basal respiration measurements of mitochondria in this assay are complex II driven by adding succinate (complex II substrate) and rotenone (complex I inhibitor) into the media. A saturating concentration of ADP is added to provide substrate for ATP synthesis termed 'State 3 respiration' (Packer, 1960). Oligomycin is then added which inhibits ATP synthase and allows proton leak to be determined (Divakaruni et al., 2014). This is termed pseudo state 4 respiration or 'state 4_o respiration' which occurs when ADP substrate is exhausted (Packer, 1960). Carbonyl cyanide-4-(trifluoromethoxy)phenylhydrazone (FCCP) is then injected which acts as an uncoupler, the mitochondria therefore increase respiration in order maintain membrane potential which allows maximal mitochondrial respiration to be measured (Divakaruni et al., 2014). Antimycin A is injected which inhibits complex III and prevents mitochondrial respiration and gives non-mitochondrial respiration which may result from the presence of peroxisomes (Stackley et al., 2011) remaining from cellular mitochondrial isolation. This is subtracted from oxygen consumption values after each measurement to give mitochondrial oxygen consumption rates. The respiratory control ratio (RCR) can also be calculated from a coupling assay by using state3/state 4_o respiration rates and gives the ratio of coupled to uncoupled mitochondrial respiration (Brand and Nicholls, 2011).

After the determination of mitochondrial protein yield as assessed through a Bradford assay, 50ug periadrenal and 100ug SAT mitochondria were loaded into wells of a 24 well Seahorse plate (Agilent Technologies, Santa Clara, CA, USA) in triplicate. Due to the nature of tissue collection from surgery, each patient's

samples were processed separately however the same amount of mitochondria were loaded across runs. The mitochondria suspensions were diluted in complete MAS buffer to 50 µl total volume. 50 µl of mitochondrial suspension was added to each well with the plate on ice. The plate was then transferred to a centrifuge with a swinging bucket microplate and centrifuged for 20 minutes at 2000g to attach the mitochondria to the bottom of the wells. 450 µl of complete MAS buffer (MAS buffer plus 10 mM succinate and 2 µM rotenone) was then added to each well and the plate placed at 37°C for 60 minutes prior to loading into an XF24 extracellular flux analyser.

A pre-incubated sensor cartridge was then loaded with the following compounds into the each of the appropriate ports: 50 µl of 40 mM ADP (Port A), 55 µl of 25 µM Oligomycin (Port B), 60 µl of 40 µM FCCP (Port C) and 65 µl of 15 µg/ml AA (Port D). After port loading, the sensor cartridge was then placed into the XF24 Extracellular Flux Analyzer for calibration and the cell plate loaded at the end of calibration. The run was conducted using the same programme as published cellular bioenergetics experiments using isolated mitochondria.

2.4.9.4 Electron Flow Assay

An electron flow assay allows sequential analysis of the activity of complexes I-IV of the electron transport chain. It is similar to a coupling assay, however the drugs used for injections differ, as well as the initial conditions of the mitochondrial medium. Basal complex I respiration is measured by the presence

of pyruvate (complex I substrate, malate (complex I substrate) and FCCP (uncoupled) in the media. Complex I is then inhibited by the injection of rotenone and the difference between basal respiration and rotenone inhibited respiration gives the OCR of complex I. Succinate, a complex II substrate is injected and therefore the difference between rotenone inhibited and succinate induced respiration gives complex II OCR. Antimycin A injection then inhibits complex III and therefore the difference between complex II driven respiration and complex III inhibited respiration gives complex III OCR. N,N,N′,N′-tetramethyl-p-phenylenediamine (TMPD), a complex IV substrate and ascorbate (an antioxidant maintaining TMPD in a reduced state) are injected to allow complex IV OCR to be measured.

Mitochondria were prepared as described above and 450 µl of MAS buffer (MAS Buffer plus 10 mM fresh pyruvate, 2 mM malate and 4 µM FCCP) was added to mitochondria. The plate was then incubated in a non- CO_2 incubator for at least 60 minutes before loading into a Seahorse XF24 Extracellular Flux Analyzer. Injections were added to a pre-incubated sensor cartridge as follows: 50 µl of 20µM rotenone (Port A), 55 µl of 100 mM succinate (Port B), 60 µl of 40 µM Antimycin A (Port C) and 65 µl of 1 mM TMPD plus 100 mM ascorbate (Port D).

A schematic diagram of the setup on both coupling and electron flow assays in shown in Figure 2.9. The effect of the compounds on the complexes of the electron transport chain is also illustrated in Figure 2.10.

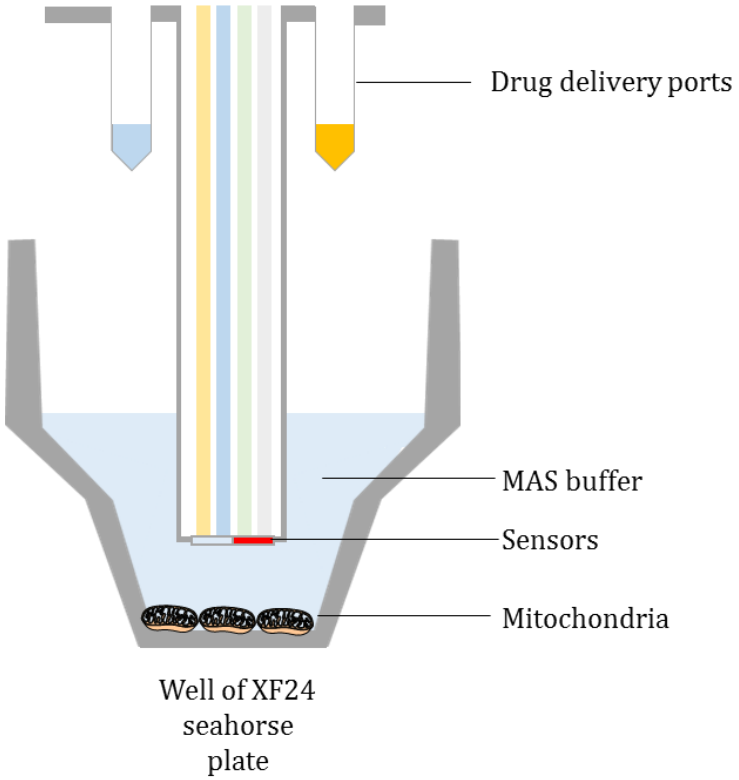


Figure 2.9 Setup of mitochondrial bioenergetics experiments using a Seahorse XF24 Extracellular Flux Analyzer.

Mitochondria from periadrenal and subcutaneous biopsies were seeded in wells of XF24 well plates with appropriate MAS buffer for coupling or electron flow assays. Solid state sensor probes measure oxygen consumption and drug delivery prots allow automatic injections of compounds into the media.

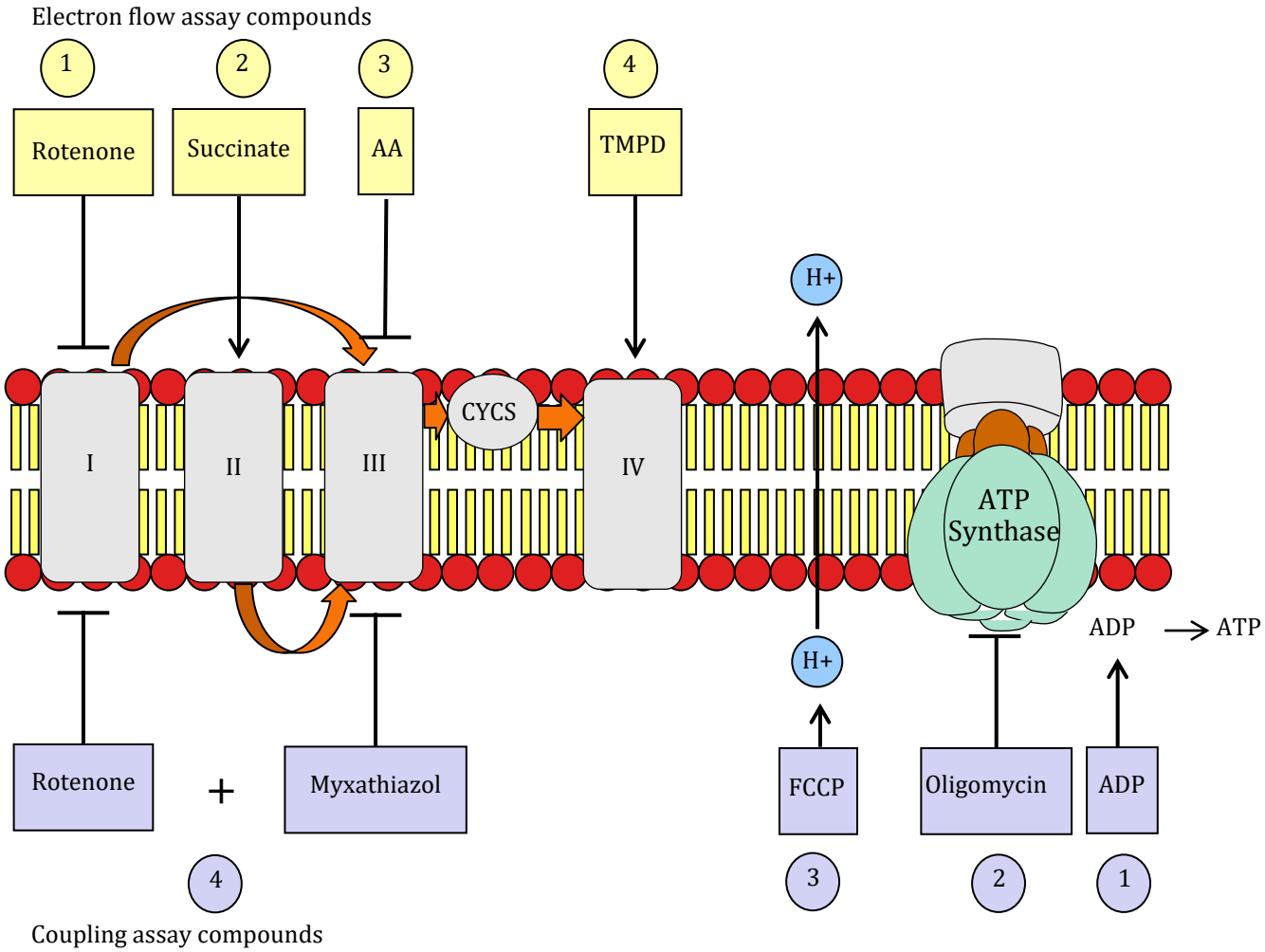


Figure 2.10 Effect of compounds used in coupling and electron flow assays on complexes of the electron transport chain.

Electron flow assay compounds are shown at the top in yellow with numerical order of injection. Rotenone inhibits complex I, succinate stimulates complex II, Antimycin A (AA) inhibits complex II and TMPD stimulates complex IV. Coupling assay compounds are shown at the bottom in purple with numerical order of injection. ADP is a substrate for ATP synthesis, oligomycin inhibits ATP synthase, FCCP allows proton transport across the mitochondrial membrane and a combination of rotenone and myxathiazol inhibit complex I and III respiration

2.4.10 RNA Extraction

RNA extraction was performed from biopsy samples that were previously snap frozen immediately in liquid nitrogen upon arrival and stored at -80°C. All procedures were carried out quickly and samples kept on ice where possible. 1 ml of TRIzol Reagent (Ambion, Life Technologies) was added to each sample and homogenised using a power homogenizer. For RNA extraction from 3T3-L1 cells 0.5 ml Trizol was added and cells lysed by pipette mixing. Following homogenization, the samples were centrifuged at 12000g for 10 minutes at 4°C and the resulting lipid layer on the surface of the supernatant was discarded. The cleared supernatant was then transferred to a new tube. 200 µl of Chloroform was then added to each samples and mixed vigourously by shaking for 30 seconds. The sample was incubated at room temperature for 3 minutes and then centrifuged at 12000g for 15 minutes at 4°C. The top layer containing the RNA was transferred to a new eppendorf tube and care was taken not to disturb the interphase layer.

500 µl isopropanol was added the transferred upper phase and incubated at room temperature for 10 minutes. Centrifugation was then performed at 12000g for 10 minutes at 4°C. The resulting supernatant was then removed, leaving only the RNA pellet. The pellet was washed by the addition of 1 ml of 75% ethanol. The sample was vortexed briefly, centrifuged 7500g for 5 minutes at 4°C and the supernatant discarded. The samples were then air dried for approximately 5 minutes and the RNA was resuspended in 25 µl of Ambion nuclease free water.

Quantification of RNA was completed using a spectrophotometer with a 1:50 dilution of the RNA. The optical density was converted to a quantity in µg/µl using the formula:

conc=OD*4/n

(n= µl of RNA used for the dilution)

This RNA extraction protocol did not include the removal of gDNA from the samples however primers were designed to span or cross an exon boundary and a NRTC was tested to ensure primers did not amplify DNA. Primers were tested with a non-template control for validation.

2.4.11 cDNA synthesis

RNA samples were diluted to 1ug in a total volume of 16 µl nuclease free water. 4 µl iScript (BioRad) was added and the samples incubated at 37°C for 1 hour, 95°C for 5 minutes and held at 8°C on a thermocyler PCR machine. cDNA samples were diluted 1:4 and stored at -20°C until qPCR analysis.

2.4.12 qPCR analysis

A master mix of SYBR Green, forward and reverse primers was made for samples and standards. 3 samples were pooled for use as standard and 1:5 serial dilutions of this were made. 11.6 µl of master mix was added to each well and 2 µl of cDNA sample was added. The plate was sealed and centrifuged briefly and then placed

into a BioRad CFX Connect™ Real-Time System qPCR machine and run at the following programme:

95°C 30 seconds

95°C 10 seconds
55°C 10 seconds
} 45 cycles

65°C 5 seconds

Up to 95°C in 0.5°C increments every 5 seconds

8°C hold

Melt curves were examined to ensure the amplification of a single product by each primer pair and the efficiency analysed to ensure this was >85%. Primer sequences used for human mRNA quantification are shown in Table 2.3.

Gene	Publication or NCBI sequence	Forward Primer (5'-3')	Reverse primer (5'-3')	Amplicon length (bp)
B2M *(ref)*	(Haas et al., 2011)	GTCTTTCAGCAAGGACTGGTC	CAAATGCGGCATCTTCAAACC	173
Cyclophillin (*ref*)	(Chechi et al., 2012)	ATCCTAGAGGTGGCGGATTT	CACTCAGGTCTGAGCCACAA	184
GAPDH *(ref)*	(Sharma et al., 2011)	ATGTTCGTCATGGGTGTGAA	GGTGCTAAGCAGTTGGTGGT	89
PSMB2 *(ref)*	(Kriegova et al., 2008)	AGAGGGCAGTGGAACTCCTT	AGGTTGGCAGATTCAGGATG	72
RPLP0 *(ref)*	(Chechi et al., 2012)	GGATTACACCTTCCCACTTGCT	GCCACAAAGGCAGATGGATCA	66
ACADM	(Alesci et al., 2006)	TTGAGTTCACCGAACAGCAG	AGGGGGACTGGATATTCACC	115
ADRB3	(Dincer et al., 2003)	CCTTCCTCTTCTCGTGATGC	TCTGAACAGAGGCCAGAGGT	307
ASC1	(Ussar et al., 2014)	GTGGCGCTCAAGAAGGAGAT	CCTTGGGCGAGATGAAGAT	91
COX7B	(Croes et al., 2014)	AGGTGTACGTTTCTGGTGGC	CACCTTCACGATGTTTCCCT	103
DIO2	(Chondronikola et al., 2014)	CCTCCTCGATGCCTACAAAC	GCTGGCAAAGTCAAGAAGGT	157
KCNK3	(Mant et al., 2013)	CTACTTCGCCATCACCGTCA	CAGCAGCGCGTAGAACATG	97

Gene	Publication or NCBI sequence	Forward Primer (5'-3')	Reverse primer (5'-3')	Amplicon length (bp)
MTUS1var3	(Shinoda et al., 2015)	AGGAGAAGCACTGTTGTTTTCCAC	GGAGCTGTCTGTGGCTGGATAC	86
NDUF9	NM_001311168.1	CCTTCGCCATATCCTTTTCA	ACCCATCAGCAAAAGGTGTT	115
PAT2	(Ussar et al., 2014)	CCTGCCACTGTATGCACATC	TAGTCCATGCATCACCGTGT	101
PGC1α	XM_017007664.1	GGATACACTTTGCGCAGGTCA	GCTTCTCTGAGCTTCTTTCAG	183
SDHB	(Haq et al., 2013)	AAGCATCCAATACCATGGGG	TCTATCGATGGGACCCAGAC	96
UCP1	NM_021833.4	GCCCAATGAATACTGCCACT	CTACGACACGGTCCAGGAGT	110
UQCRFS1	(Owens et al., 2011)	GGCAACGGCAGTAATAACCA	CCCACACAGACATCAAGGTG	125

Table 2.3 Primer sequences used for human reference (ref) and target gene mRNA quantification by qPCR

2.4.13 Mitochondrial DNA to genomic DNA ratio

Cellular DNA was extracted and mtDNA/nDNA ratio was performed essentially as stated above in Nottingham sheep study protocols. qPCR was performed as described in 2.4.12. A solution of pooled sample DNA was used to generate a standard curve of a 1:5 dilution series to check amplification efficiency. Primers for mtDNA NADH subunit 1 Forward - CCCTAAAACCCGCCACATCT, Reverse - GAGCGATGGTGAGAGCTAAGGT and gDNA LPL Forward - CGAGTCGTCTTTCTCCTGATGAT, Reverse - TTCTGGATTCCAATGCTTCGA were used as previously described (Sparks et al., 2011). The ratio of mtDNA to gDNA was calculated by dividing the quantity of ND1 by the quantity of LPL.

2.4.14 UCP1 promoter SNP sequencing

DNA used for sequencing was the same used to determine mtDNA/gDNA ratio. DNA samples were diluted to 15 ng/µl. Primers were used that flanked -3826bp in the UCP1 promoter F- CCAGTGGTGGCTAATGAGAGAA, R- GCACAAAGAAGAAGCAGAGAGG as previously published (Lindholm et al., 2004). PCR setup was performed by making a master mix of 7 µl H_2O, 10 µl FailSafe™ PCR 2x Premix H (Epicentre, an Illumina Company), 1 µl Forward primer, 1 µl reverse primer and 0.3 µl Velocity DNA Polymerase (Catalogue no. BIO-21098, Bioline). 17 µl of master mix was added to each well and 3 µl of DNA sample was added. Touchdown PCR was performed using the following programme:

94°C for 3 minutes

92°C for 40 seconds

63°C for 40 seconds (-0.5°C at each cycle) } 20 cycles

72°C for 1 minute

92°C for 40 seconds

53°C for 40 seconds } 9 cycles

72°C for 1 minute (+5 seconds at each cycle)

72°C for 3 minutes

4°C hold

5 µl of PCR product was transferred into a new 96 well plate. A master mix was made consisting of Exonuclease I (10.0 unit/µl) and Shrimp Alkaline Phosphatase (2.0 units/µl). 2 µl was added to each well and incubated at 37°C for 15 minutes and the enzymes were inactivated by incubated at 80°C for a further 15 minutes in a thermocycler. This is used as a clean-up of the PCR reaction for sequencing: Exonuclease I removes any remaining single stranded primers and Shrimp Alkaline Phosphatase removes any un-hybridised dNTP left in solution.

2.4.15 Western Blotting

Protein Extractions from mitochondria were performed as described above and protein yields determined by a BCA assay. Mitochondrial pellets were re-suspended in 120 µl of Triton Lysis Buffer. Western blots were performed essentially as previously above with minor amendments. After quantification of mitochondrial protein yield samples were diluted to 8 µg. Mitochondrial protein

extracts from mouse interscapular BAT and liver were included on gels as positive and negative controls respectively. Loading buffer (4% (v/v) β-mercaptoethanol in Nupage 4x Loading buffer) was added at a 1:4 dilution to the volume required for 8µg. Samples were loaded into wells of precast 12% Bis-Tris gels (Novex) with MOPS running buffer. The electrophoresis was run for 1 hour at 150V. Semi-dry transfer to a nitrocellulose membrane was used and the membrane stained with Ponceau to visualise protein transfer and gel loading. Membranes were blocked in 10% (w/v) milk solution overnight. The primary antibodies were used at 1:1000 dilution, UCP1 (662045 Anti-UCP1, Calbiochem®, EMD Millipore) and Cytochrome c (136F3 Cytochrome c, Cell Signalling Technology®) in 3% (w/v) milk or 5% (w/v) bovine serum albumin (BSA) respectively. Membranes were then washed with TTBS for 30 minutes and incubated with a goat anti-rabbit secondary antibody (sc-2030, Santa Cruz Biotechnology®, Inc.) at a 1:20,000 dilution in 3% (w/v) milk for 1 hour at room temperature with shaking. After secondary antibody incubation, the membranes were washed in TTBS for 30 minutes at room temperature followed by TBS incubation at room temperature with shaking for 30 minutes and 45 minutes without shaking. ECL reagents (RPN2232, Amersham™ ECL™ Prime Western Blotting Reagent, GE Healthcare) were divided into aliquots and brought to room temperature 10 minutes before use. 1 ml of Reagent A and 1ml of Reagent B were used per membrane. After addition of ECL reagents the membrane was incubated for 5 minutes at room temperature and visualised on a BioRad imager.

2.4.16 Cell Culture

All cell culture work was performed in a Class II biosafety cabinet and aseptic technique used throughout the protocol. Cell media was heated to 37°C in a water bath before use.

2.4.16.1 3T3-L1 adipocytes

3T3-L1 adipocytes are a commercially available non-immortalised white preadipocyte cell line derived from mouse and are often used as an *in vitro* model of white adipocytes. They are capable of browning and can acquire beige characteristics to external stimuli such as cold temperatures (Ye et al., 2013). They were therefore used in this thesis as a model of white adipocytes to assess browning in response to catecholamines to provide more causal evidence for link between browning in the pheo multilocular group and differences in plasma catecholamine concentration.

3T3-L1 adipocytes (ZenBio, NC, USA) were thawed quickly in a water bath at 37°C. These adipocytes were used at passage 11 (prior to passage 13, according to the Manufacturer's instructions). Cells were added to preadipocyte medium (ZenBio, NC, USA) and the suspension seeded into p100 cell culture plates. At approximately 70% confluence the medium was removed and 5 ml PBS added to wash the cells. The PBS was removed and 3 ml Trypsin was added and incubated for 5 minutes in a 37°C incubator with 5% CO2. The cells were added to 7 ml

preadipocyte medium and the cells counted with a haemocytometer. 3T3-L1 adipocytes were seeded at approximately 500,000 cells per 24 well cell culture plate with 3T3-L1 preadipocyte medium. At confluence, cells were allowed to grow for a further 2 days and then medium changed to differentiation medium for 3 days, with the media changed every other day. Maintenance medium was added for 2 days before the addition of human plasma.

From each of the three groups, 200 ml of plasma from 5 patients was pooled together to make 1 ml of plasma per group. The plasma samples chosen for this were from patients without diabetes and from patients with non-functioning tumours in the control group. The human plasma was filtered through a 0.22 μm Millex GP Filter unit (Millipore, Hertforshire, UK) and then heat treated at 56°C for 30 minutes in accordance with routine heat treatment of FBS to inactivate complement proteins to prevent cell toxicity.

Cells were then treated with either regular 3T3-L1 Maintenance medium, Maintenance medium with 0.5% v/v plasma from control, pheo unilocular or pheo multilocular patients for 6 hours. 0.5% v/v plasma was chosen for these experiments as higher percentages resulted in cell toxicity i.e. cell detachment. A schematic diagram of the experimental design is shown below.

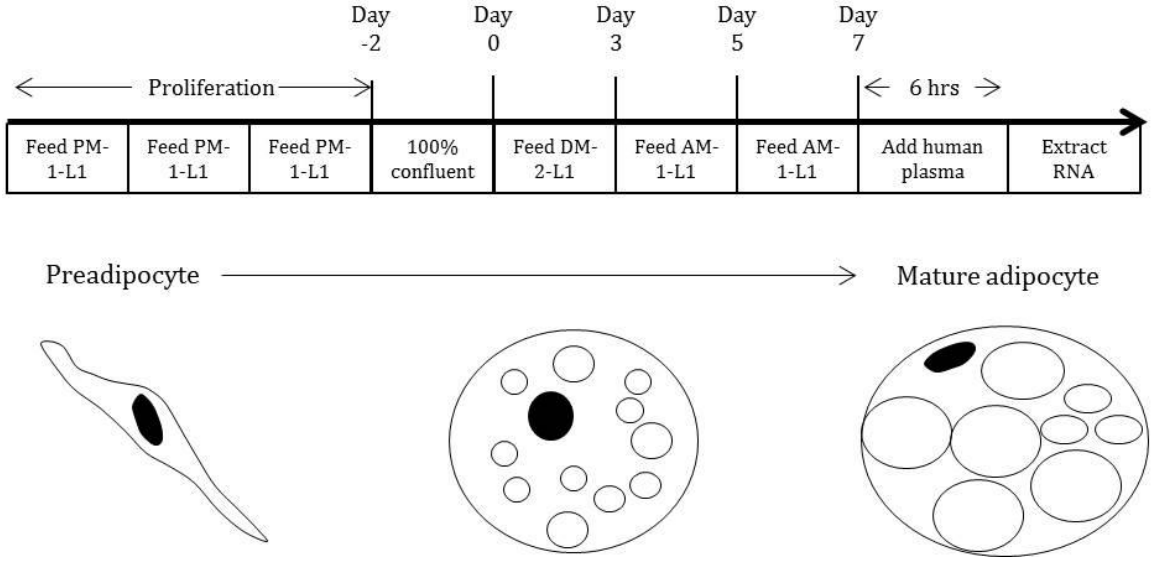


Figure 2.11 Summary of 3T3-L1 experimental design.

RNA extraction and qPCR was performed on these cells as described in the above protocols. UCP1 gene expression by qPCR as described above and normalised to B2M. The murine primer sequences used were B2M (NM_009735.3, reference gene) forward- CAGCATGGCTCGCTCGGTGAC, reverse – CGTAGCAGTTCAGTATGTTCG, amplicon length 143 bp (Donkor et al., 2007) and UCP1 (NM_009463.3) Forward –GGGCCCTTGTAAACAACAAA Reverse – GTCGGTCCTTCCTTGGTGTA, amplicon length 196 bp (Plaisier et al., 2012).

2.4.16.2 Brown adipocytes

An immortalised brown adipocyte cell line from interscapular BAT of wild type mice (Uldry et al., 2006) (a gift to the lab from B. Spiegelman, Harvard), was used to determine the effect of human plasma from the three different patient groups on basal respiration and uncoupling through cellular bioenergetics analysis. This

cell line was chosen as less time is required to obtain differentiated cells than with the 3T3-L1 cell protocol described above and there was less time available. They may also respond differently to 3T3-L1 preadipocytes. Cells were thawed quickly in a water bath at 37°C. The cells were then added to 4 ml of brown adipocyte medium containing 20 nM insulin and 1 nM T3 (Uldry et al., 2006). The resulting cells in medium were centrifuged for 5 minutes at 1000rpm and the supernatant above the cell pellet was aspirated. The pellet was then re-suspended in 3 ml and 0.5 ml of cell suspension was added to a p100 cell culture dish containing 9.5 ml brown adipocyte medium. The cells were incubated in a 37°C incubator with 5% CO_2 until reaching confluence with the medium changed every other day. At confluence the BAT medium was changed to differentiation medium (BAT medium supplemented with 0.5 mM isobutylmethylxanthine, 0.5 µM dexamethasone, and 0.125 mM indomethacin) for 2 days and then differentiation medium used for a further 3 days with the media changed every day.

The cells were then detached from the p100 plate with the addition of 3 ml trypsin EDTA plus 2% v/v collagenase. The number of cells was counted using a haemocytometer and the amount needed for 50,000 cells per well was aliquoted into a new tube. The cells were centrifuged as before, the supernatant aspirated and the cell pellet re-suspended in 2.6 ml of induction medium. 100 µl of cell suspension was then added to each well of a 24 well Seahorse microplate (Agilent Technologies, Santa Clara, CA, USA). Plasma preparation was the same used in the previous 3T3-L1 preadipocyte experiment.

300 µl of 1% v/v human plasma from control, pheo unilocular and pheo multilocular patients was added to cells 2 hours before starting the cellular bioenergetics experiment. Each plasma treatment was performed in 5 replicates. 100 nM CL 316, 243 in 300 µl induction medium served as a positive control and was also added to 5 wells of the plate. Cellular bioenergetics were conducted using a Seahorse XF24 Extracellular Flux Analyzer (Agilent Technologies, Santa Clara, CA, USA) using mix and waiting and measurement times of 5, 2 and 1.5 minutes respectively. Drug compounds used were 75 µl of 5 µM oligomycin (0.5 µM final concentration, Port A), 75 µl of 4 µM FCCP (0.4 µM final concentration, Port B) and 75 µl of 1.5 µM rotenone/myxothiazol (0.15 µM final concentration, Port C). Drug concentrations for this brown adipocyte cell line were previously determined by Dr Laurent Vergnes (Plaisier et al., 2012). A combination of rotenone and myxothiazol (complex I and III inhibitors respectively) inhibit mitochondrial respiration allowing non-mitochondrial respiration to be determined and subtracted from other oxygen consumption rates.

2.4.17 Outdoor temperature analyses

Outdoor temperatures in the month of and month prior to surgery were obtained from the National Weather Service Forecast Office (http://w2.weather.gov/climate/index.php?wfo=lox) with location 'Los Angeles airport'. Average highest temperatures and low temperatures were provided. These results and an average of highest and lowest temperatures as an estimate

of average monthly temperature were used for analysis. A linear regression analysis was performed and data presented as previously described (Betz et al., 2013).

2.6 Statistical Analysis

Data was analysed and graphs were constructed using GraphPad Prism v6.0 (GraphPad Software, California, USA). Parametric tests were used as non-parametric tests are unsuitable for analysing small data sets (Bland and Altman, 2009). The data is presented as scatter plots with individual data points throughout this thesis as it allows for the variation in small sample sizes and outliers within groups to be seen more easily than in bar charts with error bars.

The statistical tests used for both human and sheep studies were one-way ANOVA with *post hoc* Bonferroni correction where comparisons were made between 3 groups or unpaired t test where comparisons were made between 2 groups. For pooled data for correlations, where a larger sample size was used, normal distribution or skewed distribution was detected by a Kolmogorov-Smirnov normality test. Data sets found to have skewed distribution were log(2) transformed, checked that they were normally distributed and were then analysed with parametric tests. This was also performed with plasma catecholamines in Chapter 5 as it had previously been shown in a large study that they were of skewed distribution (Eisenhofer et al., 1998). Results were considered statistically significant when $p<0.05$.

As the planning of these studies occurred prior to my PhD, I was not able to perform power calculations to determine an adequate sample number before commencing the studies. However, these are important when designing an experiment to ensure that an adequate sample size is used so that a difference in effect size can be reliably compared between groups using statistical tests. A power calculation uses the probability of reporting a type I error (i.e. false positive result), often at 20% or less (Charan and Kantharia, 2013). The significance level, effect size and variability (standard deviation) can be used to determine the required sample size which can be calculated using a variety of statistical software packages (Charan and Kantharia, 2013).

Chapter 3 Characterisation of epicardial and paracardial compared to omental adipose tissue during early life in sheep

3.1 Introduction

Epicardial and paracardial adipose tissue depots may be important factors in CVD risk (McKenney et al., 2014; Tanindi et al., 2015). Epicardial adipose tissue has recently been found to possess uncoupling protein 1 (UCP1) (Sacks et al., 2009) and could be composed of beige adipocytes (Sacks et al., 2013). A comparison of epicardial adipose tissue to omental adipose tissue in adult humans reported increased UCP1 and lipoprotein lipase (LPL) mRNA in epicardial adipose tissue, suggesting increased thermogenesis and lipolysis compared to a white fat depot (Fain et al., 2010). My study aimed to further explore the comparison of epicardial and paracardial depots to a more established white adipose tissue depot, omental fat, in terms of thermogenic capacity. UCP1 abundance was also compared to perirenal adipose tissue which has previously been established as possessing UCP1 in early life in sheep (Pope et al., 2014). As well as thermogenesis, white adipose tissue related genes and beige adipocyte gene expression markers were also analysed to assess adipocyte composition of the depots. Epicardial adipose tissue in particular has been found to have high rates of lipid turnover that may be critical for its function (Marchington and Pond, 1990). As the tissue may also be thermogenic which would require lipolysis, the mRNA abundance of genes involved in lipolysis was

also examined to determine if epicardial adipose tissue is different from other visceral depots including known white and BAT depots.

As UCP1 has been found to decrease with age in ovine perirenal adipose tissue over the first 28 days of postnatal life (Pope et al., 2014), the sheep is a useful animal model to investigate adipose tissue 'whitening' with age which is also likely to occur in humans (Wei et al., 2015). This has received relatively little attention compared to the 'browning' of white adipose tissues but is also crucial in developing interventions to prolong BAT activity and delay the loss of UCP1. Little is currently known about the mechanism of adipose tissue whitening with age, although Moulin et al used cell labelling experiments to show that white adipocytes present in mice after whitening were not those that previously expressed UCP1 in the inguinal adipose tissue depot (Moulin et al., 2001). To understand this physiological process further, apoptosis was assessed in the cells of perirenal and epicardial adipose tissues. In many animals, tissues or cells that are no longer required are often removed through the process of apoptosis involving membrane blebbing (Coleman et al., 2001) and DNA fragmentation (Wyllie, 1980). DNA fragmentation as a hallmark of apoptosis was assessed by a TUNEL assay in perirenal and epicardial adipose tissues from lambs at 1, 7 and 28 days as this has not previously been published.

3.1 Hypothesis

The hypothesis for Chapter 3 was that epicardial and paracardial adipose tissue depots would display thermogenic characteristics with increased UCP1 expression compared to omental adipose tissue. Both epicardial and paracardial adipose tissue would express gene markers of beige adipocytes and would also show higher gene expression of lipolytic enzymes. I also hypothesised that UCP1 positive pericardial and perirenal adipose tissues would undergo a brown to white adipose tissue transition between birth and 28 days and apoptotic cells would be observed, particularly in adipose tissues from the 7 day group where adipose tissue is at an intermediate stage between brown (1 day) and white (28 days).

3.2 Methods

Methods were performed as described in Chapter 2. Where possible, tissues were sampled from lambs at 1, 7 and 28 days although insufficient adipose tissue was obtained for RNA or protein extraction at 1 day for epicardial adipose tissue. Omental adipose was entirely absent and therefore could not be analysed at birth. All laboratory procedures and statistical analyses are described in detail in Chapter 2. As described in the Chapter 2, histology (H&E staining, IHC and TUNEL) were performed in a separate group of female lambs at the same time points although they were of different breed.

3.3 Results

3.4.1 The effect of age on lamb bodyweight

As expected lamb bodyweight increased significantly with age between 1 day old and 28 day old lambs. This increase in bodyweight also continued between 7 days and 28 days. No significant bodyweight changes were observed between and 7 day old lambs (Figure 3.1).

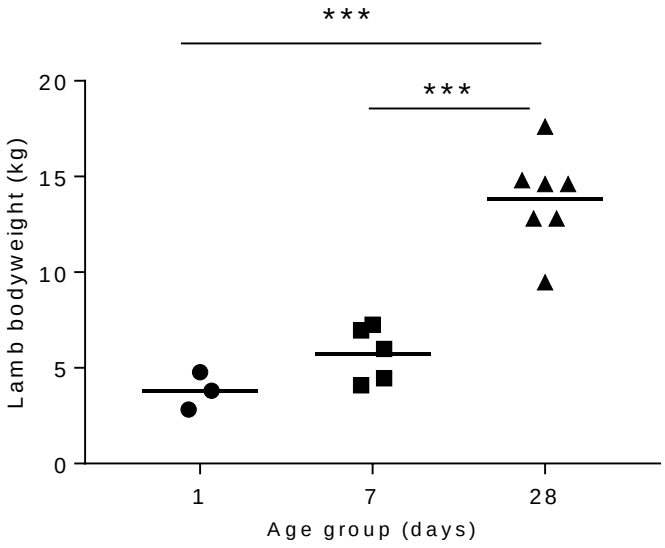


Figure 3.1 Age group comparisons of lamb bodyweights in kilograms.
*Data are presented as individual data points with means from lambs at 1 (n=3), 7 (n=5) or 28 (n=7) days after birth. ***p<0.001*

3.4.2 The effect of age on tissue weight of perirenal, paracardial and omental fat

The weights of paracardial adipose tissue were analysed from 1, 7 and 28 day lambs whereas omental tissue was sampled only at 7 and 28 days as it was not detectable in any 1 day old lambs. As discussed, it was not possible to excise epicardial adipose tissue completely and therefore it could not be included in the analysis of tissue weights. Perirenal adipose tissue was also included as a reference, as it is known to be a major adipose tissue depot in sheep. As expected, the weight of the paracardial adipose tissue depot increased with age between 1 and 28 days in accordance with an increase in total weight of the lambs during the first month of life. A significant increase in paracardial adipose tissue weight was also observed between days 7 and 28 but not between 1 and 7 days of age (Figure 3.2). Omental adipose tissue was not detectable in 1 day old lambs but the tissue weight increased significantly between 7 and 28 days. This increase in tissue weight persists when expressed relative to animal body weight (Figure 3.3.).

Paracardial adipose tissue weight increased significantly between 1 day and 28 day old lambs when expressed relative to the bodyweight of the animal. A significant increase in paracardial adipose tissue weight was also seen between 7 and 28 days of age but not between days 1 and 7 (Figure 3.3). Relative to bodyweight, perirenal adipose tissue weight was significantly increased compared to paracardial adipose at 1, 7 and 28 days. Omental adipose tissue

weight did not differ between perirenal or paracardial adipose tissue at 7 days but was significantly increased compared to paracardial adipose tissue at 28 days.

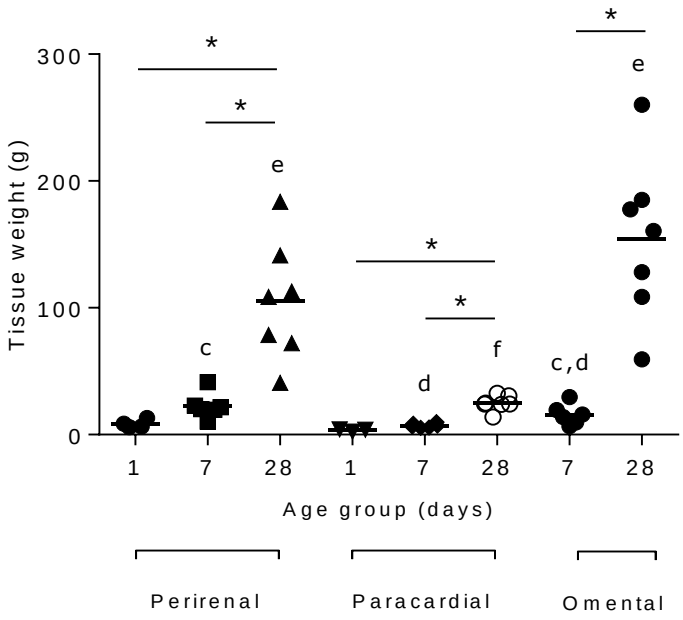


Figure 3.2 Age group comparisons of perirenal, paracardial and omental tissue weights in grams.

*Data is presented as scatter plot with individual data points and group means from lambs at 1 (n=3), 7 (n=5) or 28 (n=7) days after birth. *p<0.05 for individual depot comparisons with age. Letters c and d show significant differences between depots at 7 days where letters differ. Letters e and f show significant differences at 28 days where letters differ.*

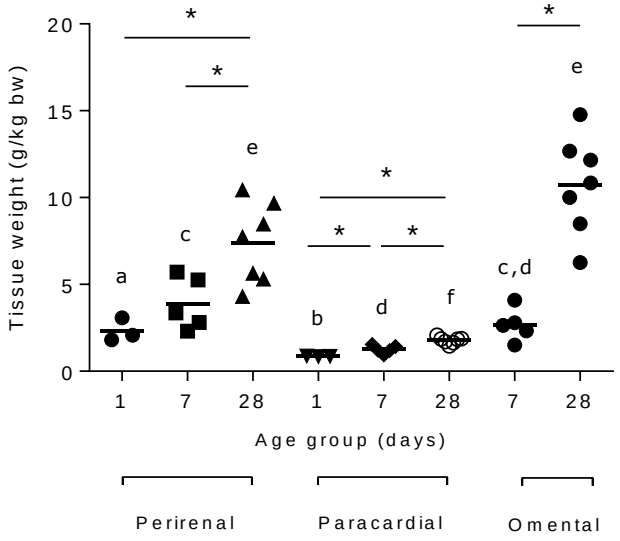


Figure 3.3 Age group comparisons of perirenal, paracardial and omental tissue weights in grams expressed relative to animal bodyweight in kilograms.

*Data is presented as scatter plot with individual data points and group means from lambs at 1 (n=3), 7 (n=5) or 28 (n=7) days after birth. *p<0.05 for individual depot comparisons with age. Letters a and b show significant differences between depots at 1 day where letters differ. from lambs at 1 (n=3), 7 (n=5) or 28 (n=7) days after birth. *p<0.05 for individual depot comparisons with age. Letters c and d show significant differences between depots at 7 days where letters differ. Letters e and f show significant differences at 28 days where letters differ.*

3.4.3 Postnatal age and gene expression modification of paracardial, epicardial and omental adipose tissue depots

3.4.3.1 Thermogenic genes

Gene expression analysis was performed using qPCR. Firstly, genes involved in the thermogenic pathway of UCP1 activation were analysed to provide an indication of non-shivering thermogenesis capability of individual adipose tissue depots with increasing age. Genes included in this pathway were UCP1, PGC1α,

DIO2 and ADRB3. As shown in Figure 3.4 A-C, UCP1, PGC1a and DIO2 showed similar patterns of gene expression and tended to decrease with age. For UCP1 and DIO2 this was statistically significant in all depots studied. Interestingly, epicardial fat had significantly increased UCP1, PGC1a and DIO2 gene expression compared to omental fat at 7 days. Paracardial fat did not differ significantly in UCP1 expression at 7 days compared to epicardial or omental fat depots and had high variation between the samples. Two 7 day paracardial samples in particular showed low gene expression in the majority of genes studied and could be considered outliers. They were not omitted however as it is difficult to determine outliers in small sample sizes and it did not seem that experimental error in qPCR methodology was the cause of this variation. There were no significant depot differences at 28 days for UCP1 gene expression; however PGC1a gene expression was upregulated in paracardial and epicardial adipose tissue compared to the omental depot. DIO2 expression was also significantly increased at 28 days in epicardial, but not paracardial adipose tissue compared to omental adipose tissue.

ADRB3 did not show the same pattern of gene expression as other genes involved in the thermogenic pathway as there was no significant difference in ADRB3 gene expression with age in any of the depots studied. At 7 days there was no difference between the depots although at 28 days there was a significant difference between paracardial and epicardial fat (Figure 3.4 D).

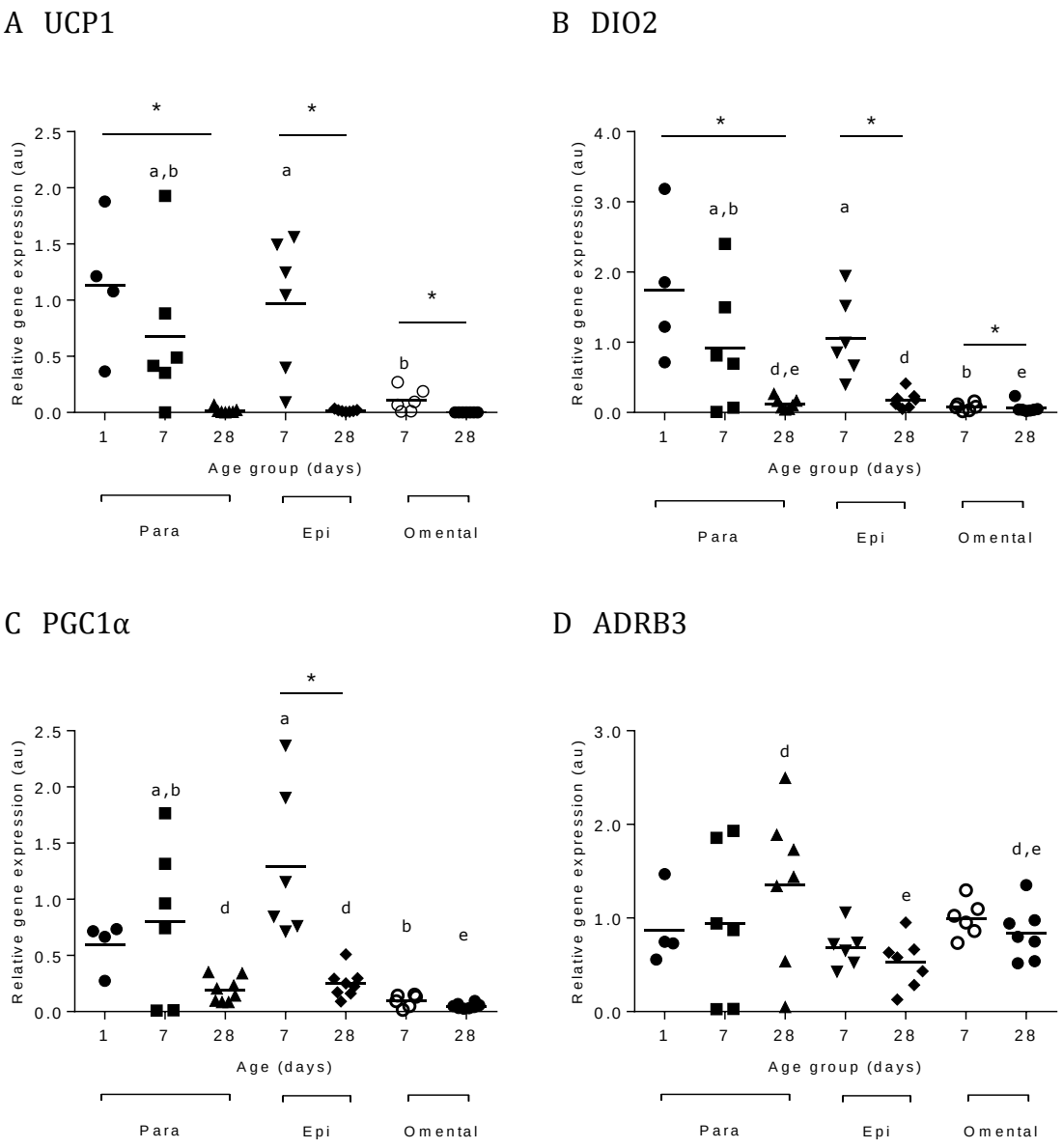


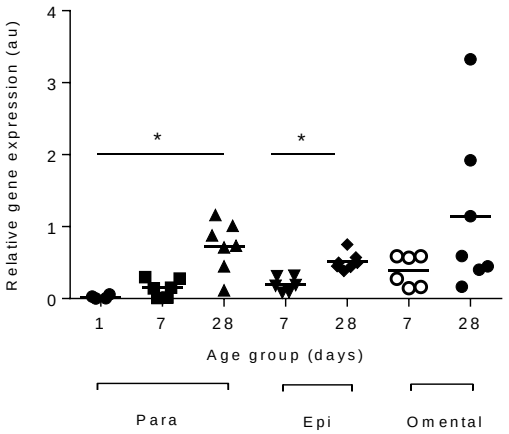
Figure 3.4 Thermogenic gene expression in paracardial, epicardial and omental adipose tissue. A: UCP1 B: DIO2 C: PGC1α D: ADRB3.

*Paracardial (Para) adipose tissue was sampled at 1 day (n=4), 7 days (n=6) and 28 days (n=7). Epicardial (Epi) and omental adipose tissue were both sampled at 7 days (n=6) and 28 days (n=7). Data is presented as a scatter plot with individual data points and group means. * p<0.05 (comparisons with age). Letters a and b show significant differences (p<0.05) between depots at 7 days where letters differ, letters d and e show significant differences (p<0.05) between depots at 28 days where letters differ. Gene expression vales are shown relative to the geometric mean of reference genes importin 8 (IPO8) and ribosomal protein lateral stalk subunit P0 (RPLP0).*

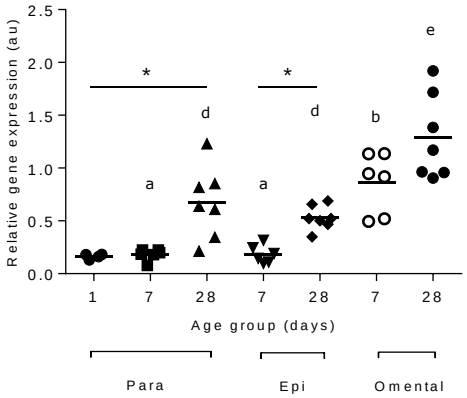
3.4.3.2 White adipose tissue related genes

Leptin and RIP140 are both expressed highly in white adipose tissue and are therefore classed into the same category for this analysis (Figure 3.5). Leptin gene expression increased with age in all depots however this was only statistically significant in paracardial and epicardial depots. Although the mean value was higher for omental fat than paracardial and epicardial fat at 7 and 28 days, it was not statistically significant. RIP140 gene expression also showed a similar trend to increase with age and this was statistically significant in paracardial and epicardial adipose tissue depots. Interestingly RIP140 mRNA was significantly upregulated in omental compared to paracardial and epicardial adipose tissue at both 7 and 28 days. Transcription factor 21 (TCF21) has been suggested to be a white adipocyte marker (de Jong et al., 2015). Epicardial fat had significantly higher expression of TCF21 mRNA compared to both paracardial and omental adipose tissue at both 7 and 28 days (Figure 3.4). There was also a significant increase in TCF21 gene expression between 7 and 28 day groups in epicardial adipose tissue. TCF21 mRNA was significantly higher in omental compared to paracardial adipose tissue at both time points.

A Leptin



B RIP140



C TCF21

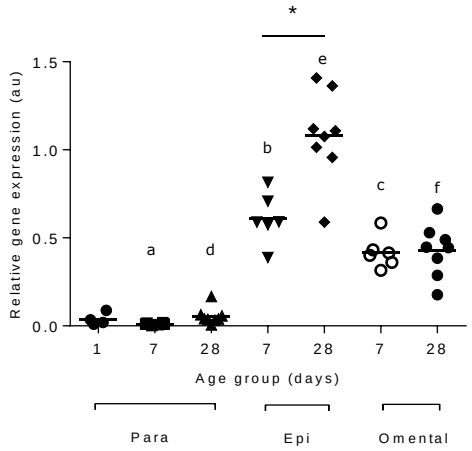


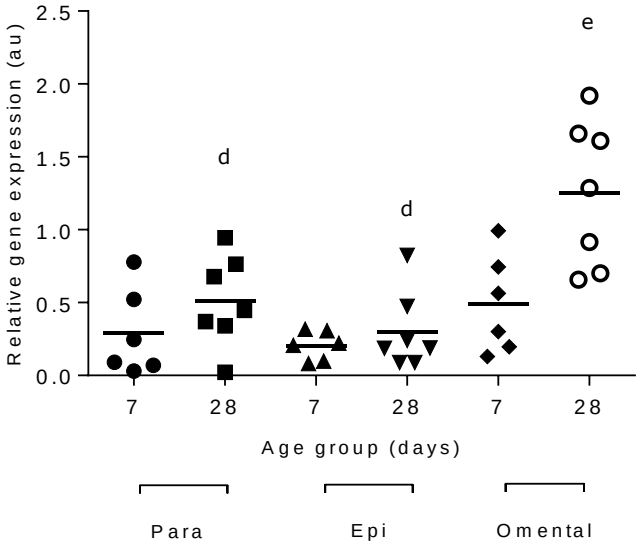
Figure 3.5 WAT related gene expression in paracardial, epicardial and omental adipose tissue. A: Leptin B: RIP140 C: TCF21

*Paracardial (Para) adipose tissue was sampled at 1 day (n=4), 7 days (n=6) and 28 days (n=7). Epicardial (Epi) and omental adipose tissue were sampled at 7 days (n=6) and 28 days (n=7). Data is presented as scatter plots with individual data points and group means. * p<0.05 (comparisons with age), letters a and b show significant differences (p<0.05) between depots at 7 days where letters differ. Letters d and e show significant differences (p<0.05) between depots at 28 days where letters differ. Gene expression vales are shown relative to the geometric mean of reference genes importin 8 (IPO8) and ribosomal protein lateral stalk subunit P0 (RPLP0).*

3.4.3.3 Beige markers

As epicardial fat has been considered to express mRNA transcripts that have been associated with the presence of beige adipocytes (Sacks et al., 2013) it was decided to analyse the mRNA abundance of these genes to see if differences were seen between the depots (Figure 3.6). CD137 gene expression did not differ significantly with age in any of the depots and no depot differences were observed at 7 days. At 28 days however, omental adipose tissue displayed higher CD137 gene expression than both paracardial and epicardial adipose tissue depots. SHOX2 increased significantly in paracardial fat at 28 days compared to fat sampled at 1 day and 7 day groups. No significant differences were observed between depots at 7 days of age. Paracardial adipose tissue also had upregulated SHOX2 expression compared to epicardial and omental adipose tissue at 28 days.

A CD137



B SHOX2

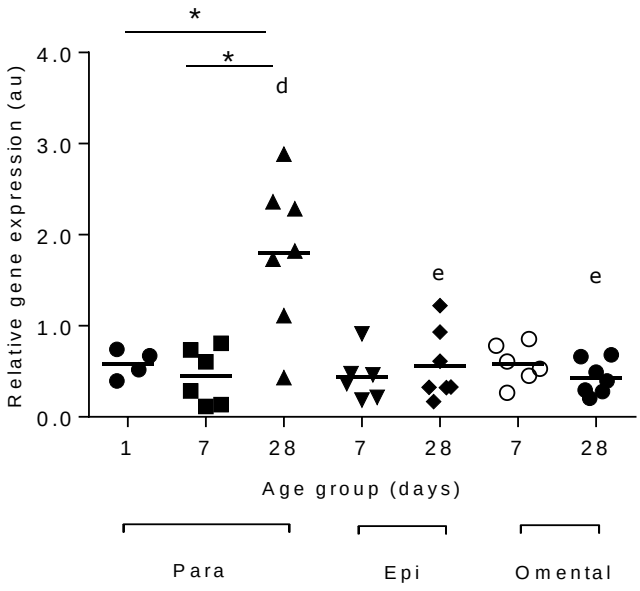


Figure 3.6 Beige adipocyte marker gene expression in paracardial, epicardial and omental adipose tissue. A: CD137 B: SHOX2

*Paracardial (Para) adipose tissue was sampled at 1 day (n=4), 7 days (n=6) and 28 days (n=7). Epicardial (Epi) and omental adipose tissue were both sampled at 7 days (n=6) and 28 days (n=7). Data is presented as scatter plot with individual data points and group means * denote p<0.05 (comparisons with age), letters a and b show significant differences (p<0.05) between depots at 7 days where letters differ, letters d and e show significant differences (p<0.05) between depots at 28 days where letters differ. Gene expression vales are shown relative to the geometric mean of reference genes importin 8 (IPO8) and ribosomal protein lateral stalk subunit P0 (RPLP0).*

3.4.3.4 Adipogenesis

PPARγ increased significantly with age in paracardial adipose tissue between 1 day and 28 day groups and 7 and 28 day groups (Figure 3.7). There was no significant difference between 1 day and 7 day age groups. No significant changes were seen with age in either epicardial or omental depots. Omental adipose tissue has significantly higher PPARγ gene expression at 7 days compared to paracardial but not epicardial adipose tissue. No depot differences were seen in the 28 day age group.

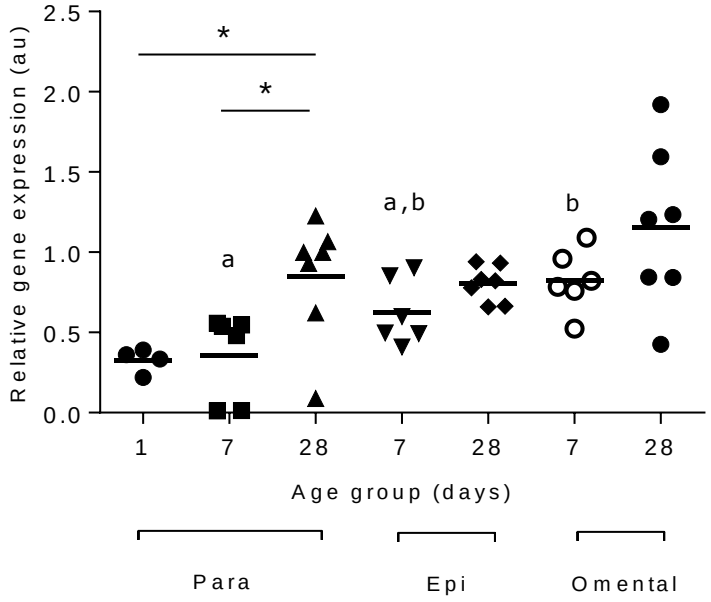


Figure 3.7 PPARγ gene expression in paracardial, epicardial and omental adipose tissue.

*Paracardial (Para) adipose tissue was sampled at 1 day (n=4), 7 days (n=6) and 28 days (n=7). Epicardial (Epi) and omental adipose tissue were both sampled at 7 days (n=6) and 28 days (n=7). Data is presented as scatter plot with individual data points and group mean. * p<0.05 (comparisons with age), letters a and b show significant differences (p<0.05) between depots at 7 days where letters differ. Gene expression vales are shown relative to the geometric mean of reference genes importin 8 (IPO8) and ribosomal protein lateral stalk subunit P0 (RPLP0).*

3.4.3.5 Lipolysis genes

Analysis of genes involved in lipolysis was conducted on a separate batch of cDNA. This was performed by a BMedSci project student Urmila Cockerill under my supervision. cDNA from perirenal adipose tissue from the same animals as used previously for paracardial, epicardial and omental adipose tissue at 7 and 28 day groups was included to see if a major brown fat depot in the sheep had different lipolysis gene expression to those potentially classed as beige (epicardial and paracardial) or white (omental) adipose tissue depots. All three lipolysis genes examined showed a similar pattern of expression (Figure 3.8 A-C). ATGL gene expression increased significantly with age in paracardial adipose tissue. A significant increase in HSL gene expression with age was observed in all depots studied. Paracardial and perirenal adipose tissue had upregulated PLIN1 expression between days 7 and 28.

Interestingly there was a noticeable difference between depots for lipolysis gene expression. Perirenal adipose tissue had significantly higher gene expression of ATGL, HSL and PLIN1 compared to epicardial, paracardial and omental adipose tissue in the 7 day group. PLIN1 gene expression was also significantly higher in perirenal adipose tissue compared to epicardial and omental adipose tissue in the 28 day group.

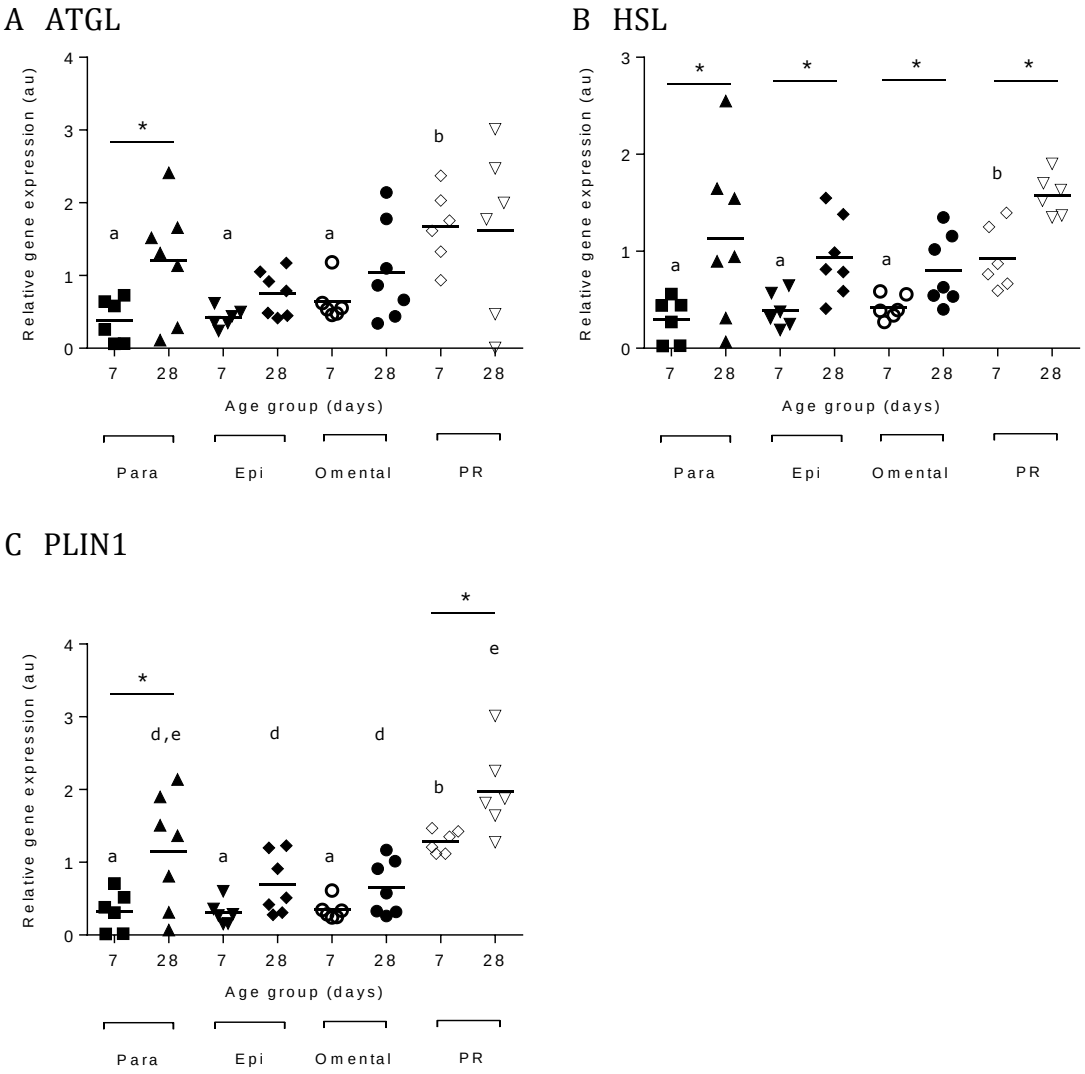


Figure 3.8 Lipolytic gene expression in paracardial, epicardial, omental and perirenal adipose tissue. A: ATGL B: HSL C: PLIN1

*Paracardial (Para), Epicardial (Epi), omental and perirenal (PR) adipose tissue depots were sampled at 7 days (n=6) and 28 days (n=7) after birth. Data is presented as scatter plot with individual data points and group means. * p<0.05 (comparisons with age), letters a and b show significant differences (p<0.05) between depots at 7 days where letters differ, letters d and e show significant differences (p<0.05) between depots at 28 days where letters differ. Gene expression vales are shown relative to the geometric mean of reference genes importin 8 (IPO8) and ribosomal protein lateral stalk subunit P0 (RPLP0).*

3.4.4 UCP1 Western blots

It is important to also measure protein abundance in addition to gene expression, as mRNA is not necessarily translated to protein. To this end, UCP1 and cytochrome c abundance was determined by western blotting as these antibodies have been used previously in the laboratory and are known to work in sheep adipose tissue. An example western blot is shown with UCP1 at approximately 32kDa (see Figure 3.9). Cytochrome c was also run on the same gel due to the much smaller size of the protein at approximately 15kDa. Perirenal adipose tissue from the same 7 day old lambs was included as a known brown fat depot as both a positive control and fat depot comparison. The same perirenal sample was included on each gel for calibration.

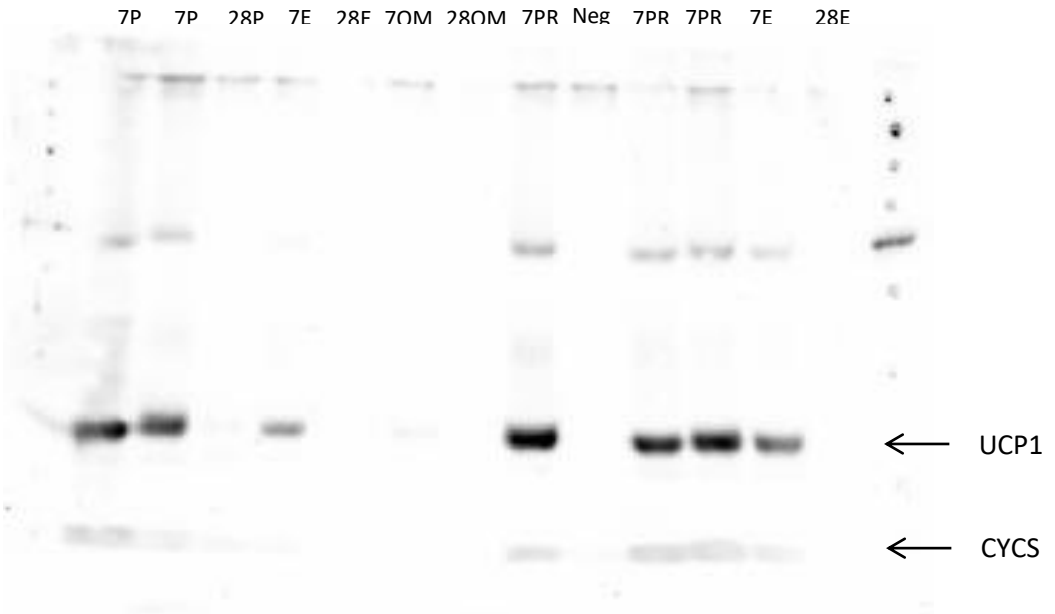


Figure 3.9 Representative image of a western blot with primary antibodies for uncoupling protein 1 (UCP1, 32kDa) and cytochrome c (CYCS, 15kDa). Samples loaded are labelled above each lane with age group (days) and depot: paracardial (P), epicardial (E), omental (OM) and perirenal (PR).

UCP1 protein abundance showed a similar decrease with age to changes observed in UCP1 gene expression and was significantly decreased in paracardial and epicardial adipose tissue between 7 and 28 day groups (Figure 3.10). No significant difference with age was observed in the omental adipose tissue depot. Interestingly perirenal adipose tissue showed the highest denistometry of UCP1 positive bands, which was significantly higher than epicardial and omental adipose tissue at 7 days. There was less variation in UCP1 abundance of perirenal adipose tissue compared to paracardial and epicardial adipose tissue.

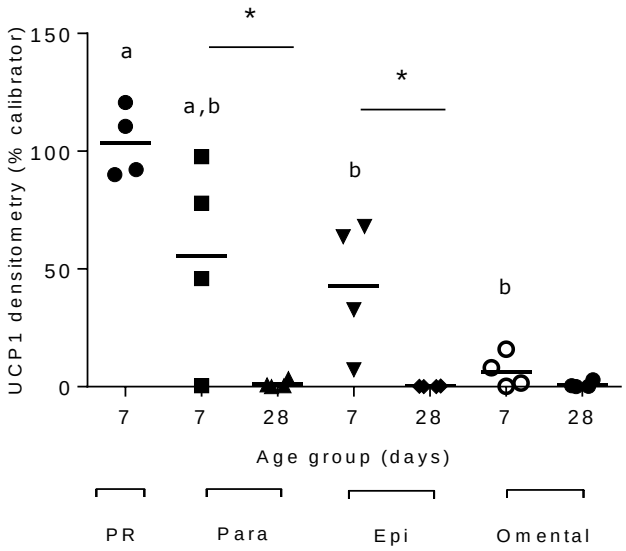


Figure 3.10 UCP1 densitometry in expressed as a percentage of a calibrator 7 day perirenal sample that was loaded on all gels (% calibrator) from Western blots in perirenal (PR) at 7 days, paracardial (Para) epicardial (Epi) and omental adipose tissue at 7 and 28 days

3.4.5 Correlation between UCP1 mRNA and protein

A significant correlation was found between UCP1 mRNA and protein for paracardial, epicardial and omental adipose tissue at 7 and 28 days (Figure 3.11). Samples included for analysis were used for western blot experiments and the UCP1 mRNA abundance from these same animals. The analysis was performed on log transformed data as the pooled data for both variables was not normally distributed.

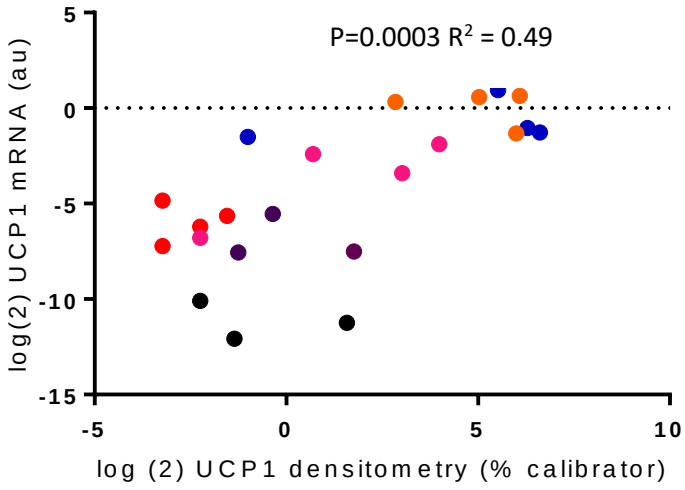
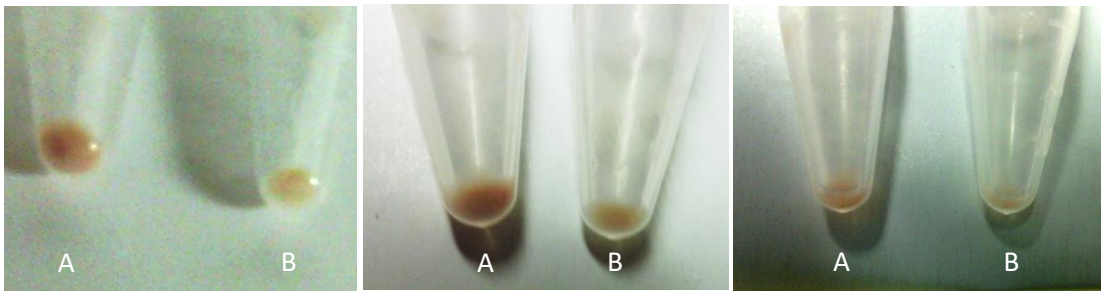


Figure 3.11 Correlation between Log (2) transformed data of UCP1 mRNA and protein.

Samples from paracardial, epicardial and omental adipose tissue depots at 7 and 28 days (n=3-4 per depot and time point) were included in the analysis. Colour coding shows groups: 7 day paracardial (blue), 28 day paracardial (purple), 7 day epicardial (orange), 28 day epicardial (red), 7 day omental (pink) and 28 day omental (black).

3.4.6 Mitochondrial abundance, gene and protein expression

It was observed during mitochondria extraction for western blotting that a difference in colour of the mitochondrial pellet occurred between 7 and 28 day age groups (Fig 3.12). This was particularly evident in mitochondrial pellets from paracardial and epicardial adipose tissue that had a brownish hue compared to a white/yellow colour mitochondria pellets from 28 day old lambs. This colour change between 7 and 28 days was less pronounced in mitochondrial pellets from omental adipose tissue.



Paracardial Epicardial Omental

Figure 3.12 Representative images of mitochondrial pellets observed during mitochondrial isolation.

A) 7 day adipose tissue and B) 28 day paracardial, epicardial and omental adipose tissue depots

3.4.6.4 Cytochrome c qPCR and Western Blots

To assess possible mitochondrial activity, cytochrome c gene expression was quantified using qPCR (Figure 3.13). Similar to thermogenic genes, a decrease was seen between 7 and 28 days which was statistically significant in epicardial and omental adipose tissue. Although the mean cytochrome c gene expression for omental adipose tissue was lower than paracardial and epicardial fat, this

was not significant at 7 days. Paracardial fat had increased cytochrome c gene expression compared to epicardial and omental adipose tissue at 28 days which was statistically significant.

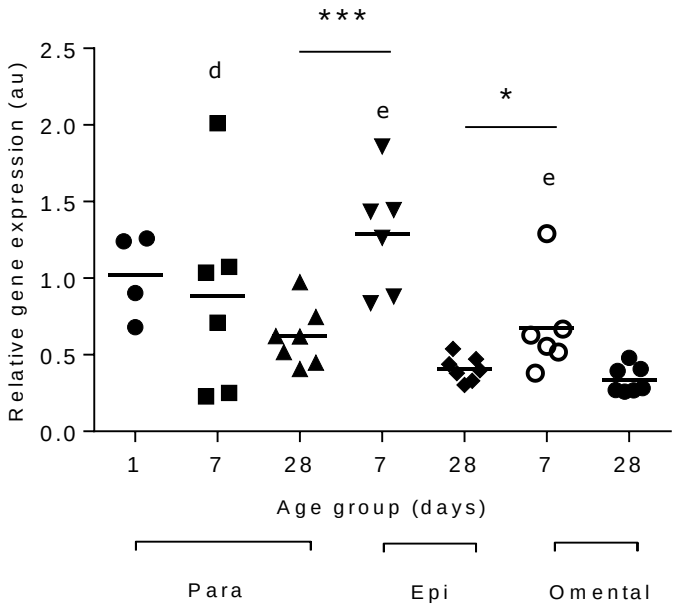


Figure 3.13 Cytochrome c gene expression in paracardial, epicardial and omental adipose tissue.

*Paracardial (Para) adipose tissue was sampled at 1 day (n=4), 7 days (n=6) and 28 days (n=7). Epicardial (Epi) and omental adipose tissue were both sampled at 7 days (n=6) and 28 days (n=7). Data is presented as scatter plot with individual data points and group means. * p<0.05 (comparisons with age), letters a and b show significant differences (p<0.05) between depots at 7 days where letters differ. Gene expression vales are shown relative to the geometric mean of reference genes importin 8 (IPO8) and ribosomal protein lateral stalk subunit P0 (RPLP0).*

To examine this further, cytochrome c protein abundance was measured by western blotting. An example western blot is shown above with cytochrome c bands shown towards the bottom of the gel at 15kDa (Figure 3.9). As stated above, 7 day perirenal samples were run as positive controls and one of these samples was used as a calibrator across gels. A similar pattern of expression was

seen to cytochrome c gene expression, with a decrease in cytochrome c protein observed with increasing age. This was statistically significant only in the epicardial depot. Interestingly there was no difference observed with increasing age in the omental depot. Similar to results seen for UCP1 abundance by western blotting, perirenal adipose tissue showed the highest group mean of all the depots studied at 7 days. There was no significant difference between perirenal, paracardial or epicardial fat in terms of cytochrome c protein abundance although perirenal had significantly increased cytochrome c protein compared to omental adipose tissue (Figure 3.14).

3.4.6.5 Cytochrome c Western Blots

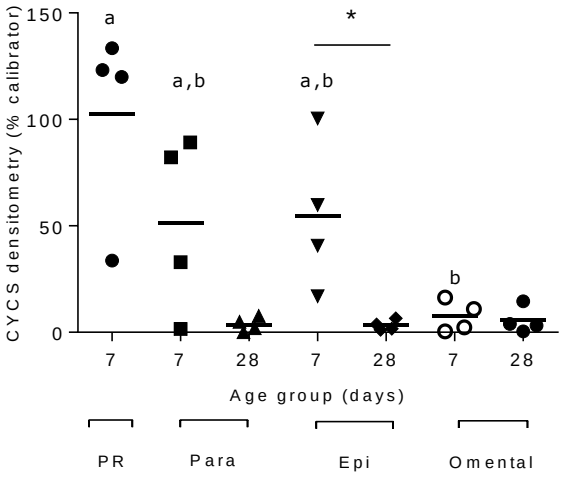


Figure 3.14 Cytochrome c protein abundance in perirenal, paracardial, epicardial and omental adipose tissues at 7 and 28 days.

*Cytochrome c denistometry is expressed as a percentage of a calibrator 7 day perirenal sample that was loaded on all gels (% calibrator) from Western blots in perirenal (PR) at 7 days, paracardial (Para) epicardial (Epi) and omental adipose tissue at days 7 and 28 (n=4 per group). Data is presented as scatter plot with individual data points and group means. *p<0.05 changes within depots with age. a and b denote significant differences (p<0.05) between depots at 7 days where letters differ.*

Due to possible differences in mitochondrial activity between the depots studied, the mitochondrial abundance was then analysed using a ratio of mtDNA to nDNA by qRT-PCR (Figure 3.15). In both paracardial and epicardial adipose tissue there was a significant decrease in mitochondrial abundance between 7 and 28 day age groups. In the omental adipose tissue depot however there was a significant increase with age. At 7 days there was significantly increased mitochondrial abundance in perirenal and epicardial compared to omental adipose tissue. At 28 days there were no significant differences between depots.

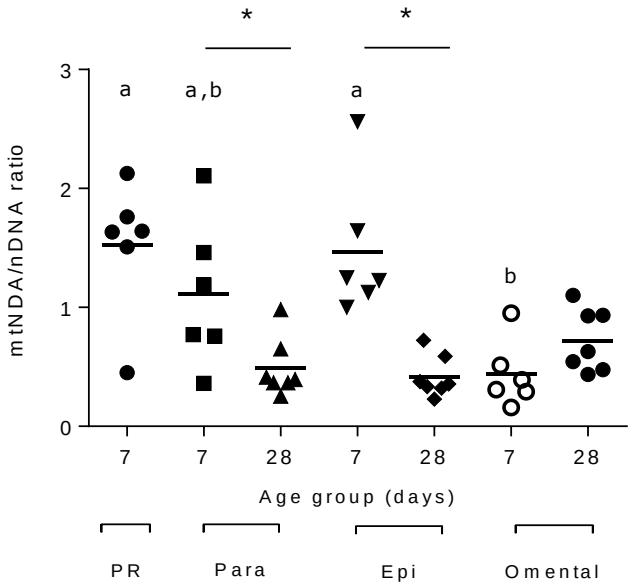


Figure 3.15 Ratio of MTCO1 mitochondrial DNA (mtDNA) to 18S nuclear DNA (nDNA) abundance in perirenal, paracardial, epicardial and omental adipose tissue.

*Perirenal (PR), paracardial (Para), epicardial (Epi) and omental adipose tissue was sampled at 7 (n=6) and 28 days (n=7). Data is presented as scatter plot with individual data points and group means * denote p<0.05 (comparisons with age), letters a and b show significant differences (p<0.05) between depots at 7 days where letters differ.*

There was no correlation between mitochondrial abundance and UCP1 mRNA (Figure 3.16). Paracardial, epicardial and omental samples were included for this analysis at 7 and 28 days. The data was log transformed due to the pooled data not being normally distributed for both variables.

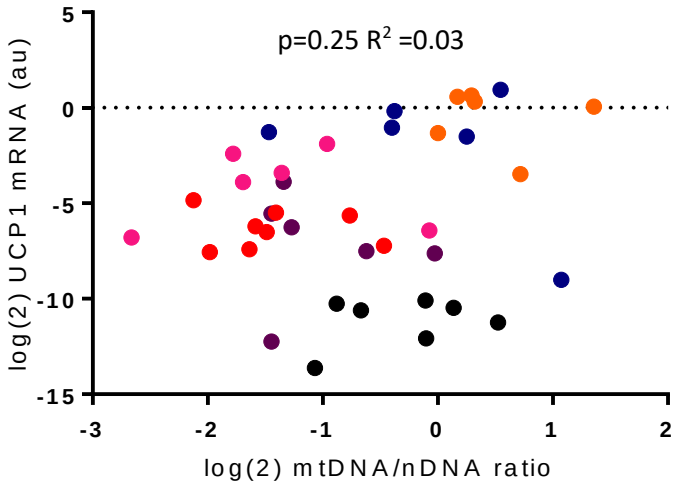


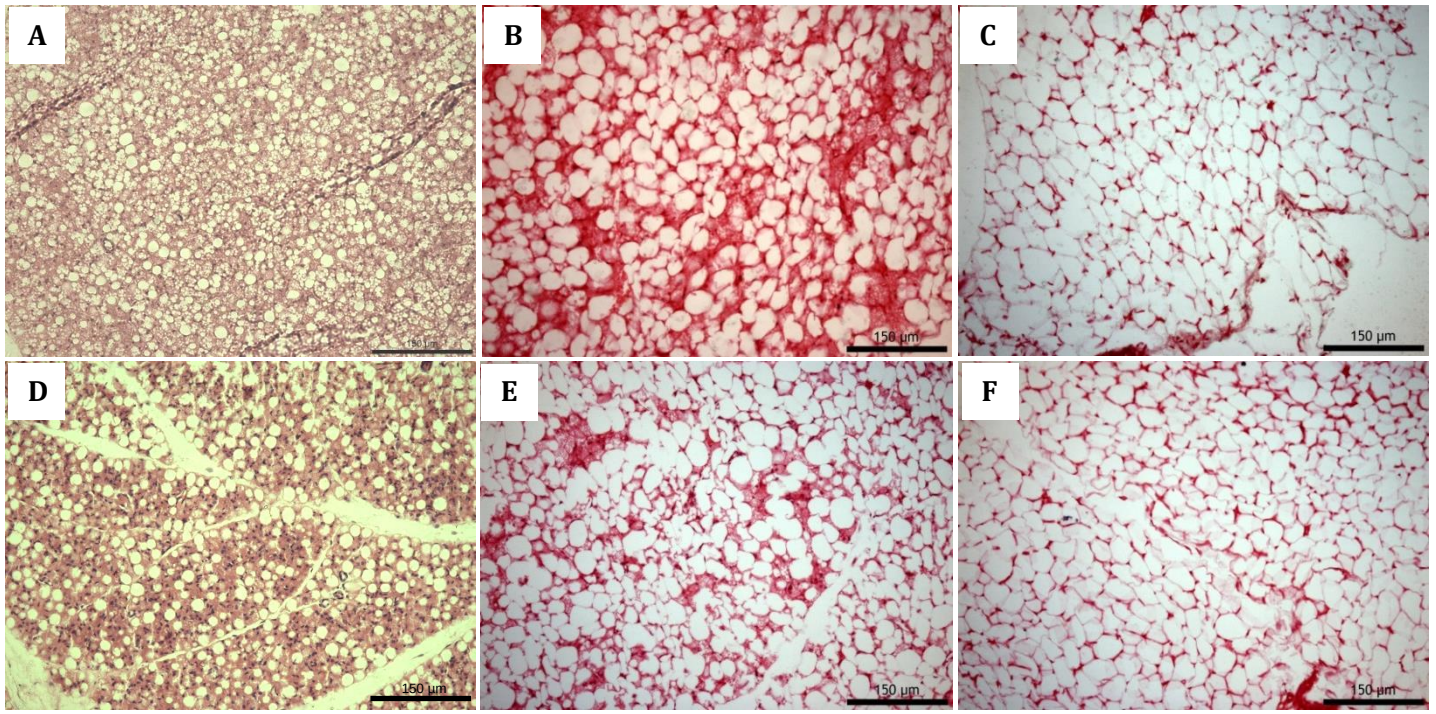
Figure 3.16 Correlation between log(2) transformed UCP1 mRNA and mtDNA/nDNA ratio.

Samples from paracardial, epicardial and omental adipose tissue depots at 7 (n=6 per depot) and 28 days (n=7 per depot) were included in the analysis. Colour coding shows groups: 7 day paracardial (blue), 28 day paracardial (purple), 7 day epicardial (orange), 28 day epicardial (red), 7 day omental (pink) and 28 day omental (black).

3.4.7 Haematoxylin and Eosin stained tissue sections

Tissue sections stained with haematoxylin and eosin showed a marked change in morphology with age and also differences between depots (Figure 3.17). Perirenal adipose tissue showed pockets of multilocular adipocytes dispersed between unilocular adipocytes at 7 days whereas only unilocular adipocytes were observed at 28 days. This same transition with increasing age was also

observed in both epicardial and paracardial adipose tissue sections although there did appear to be fewer pockets of multilocular adipocytes at 7 days in comparison to perirenal adipose tissue. Omental adipose tissue did not show such a striking change in morphology with age and was composed primarily of white unilocular adipocytes at both 7 and 28 days.


A
B
C
D
E
F
150 µm

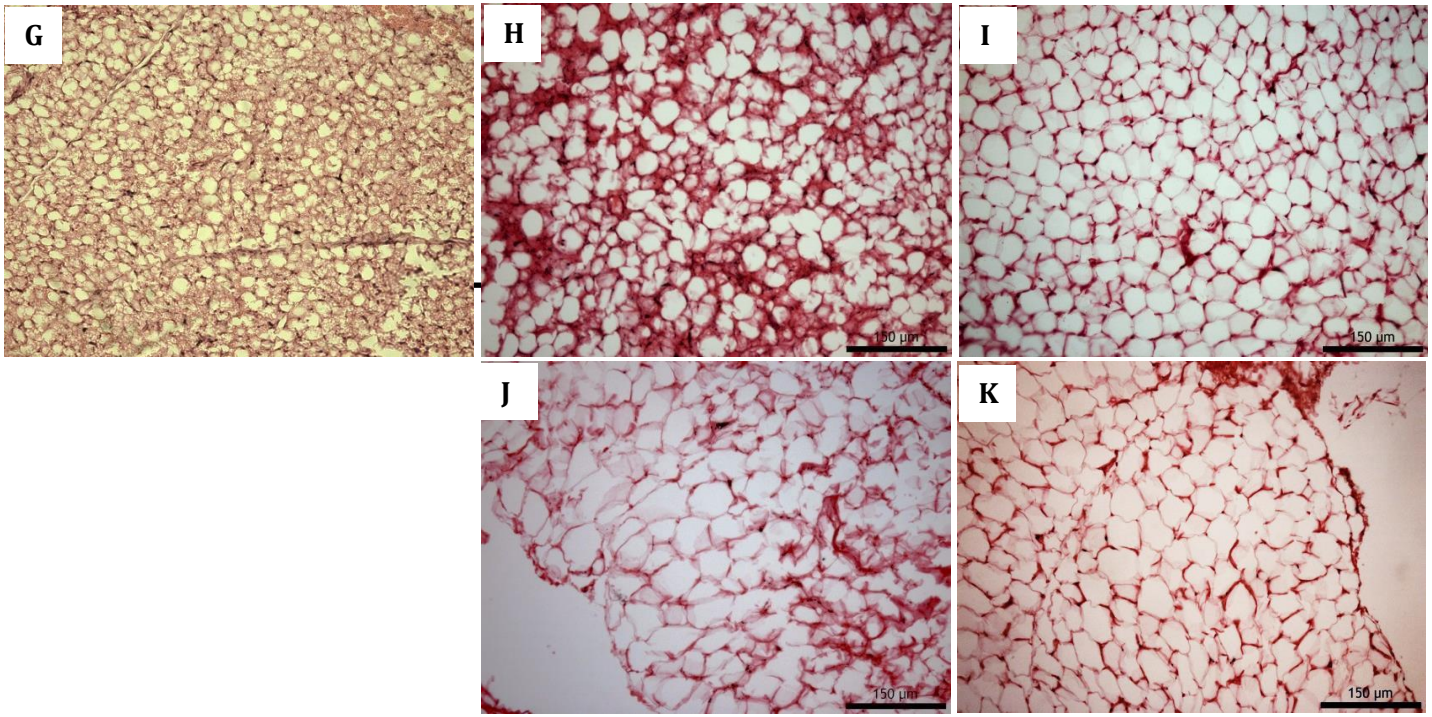
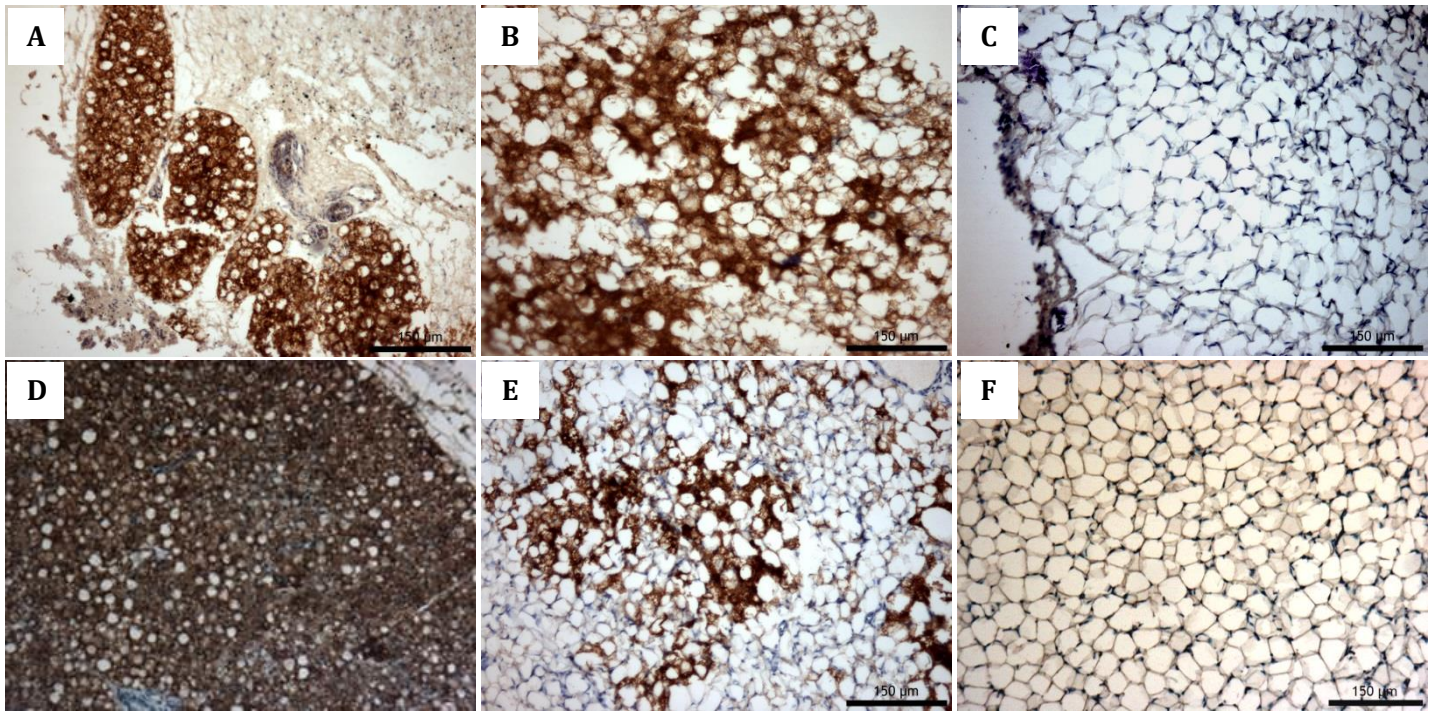


Figure 3.17 Representative images of Haematoxylin and Eosin stained 5µm tissue sections.

A) 1 day perirenal; B) 7 day perirenal; C) 28 day perirenal; D) 1 day paracardial; E)7 day paracardial; F) 28 day paracardial; G) 1 day epicardial; H) 7 day epicardial; I) 28 day epicardial; J) 7 day omental and K) 28 day omental. No omental adipose tissue was present for sampling in 1 day old lambs. Scale bar=150µm

3.4.8 UCP1 Immunohistochemistry

UCP1 immunohistochemistry showed the presence of UCP1 in perirenal, paracardial and epicardial adipose tissue sections at 7 days (Figure 3.18). Perirenal adipose tissue at 7 days showed the most intense staining of all the depots studied. UCP1 staining in paracardial and epicardial sections showed UCP1 positive adipocytes interspersed between white unilocular adipocytes. Some slight staining was observed in omental adipose tissue at 7 days although this may have been background DAB staining. At 28 days there was very little UCP1 staining observed and all of the depots were composed of unilocular white adipocytes.


A
B
C
D
E
F
150 µm
150 µm
150 µm
150 µm
150 µm

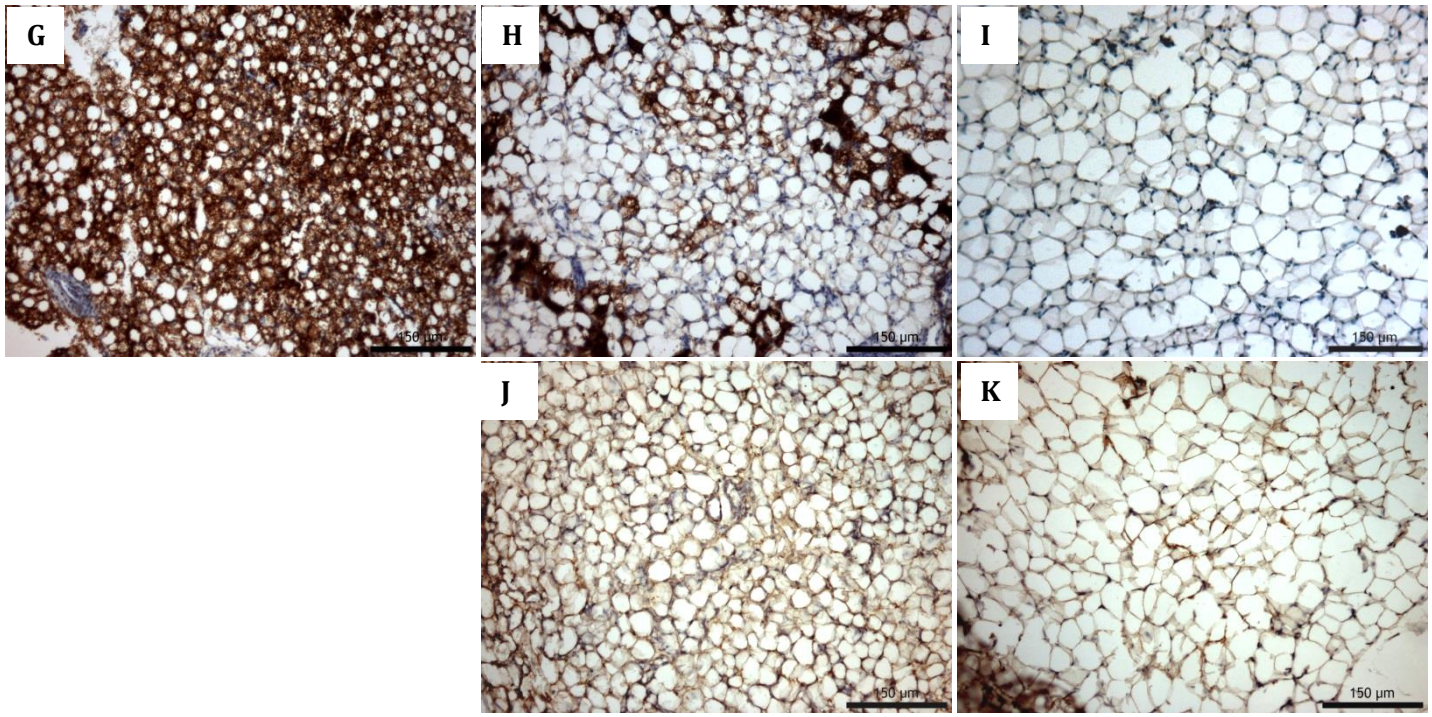
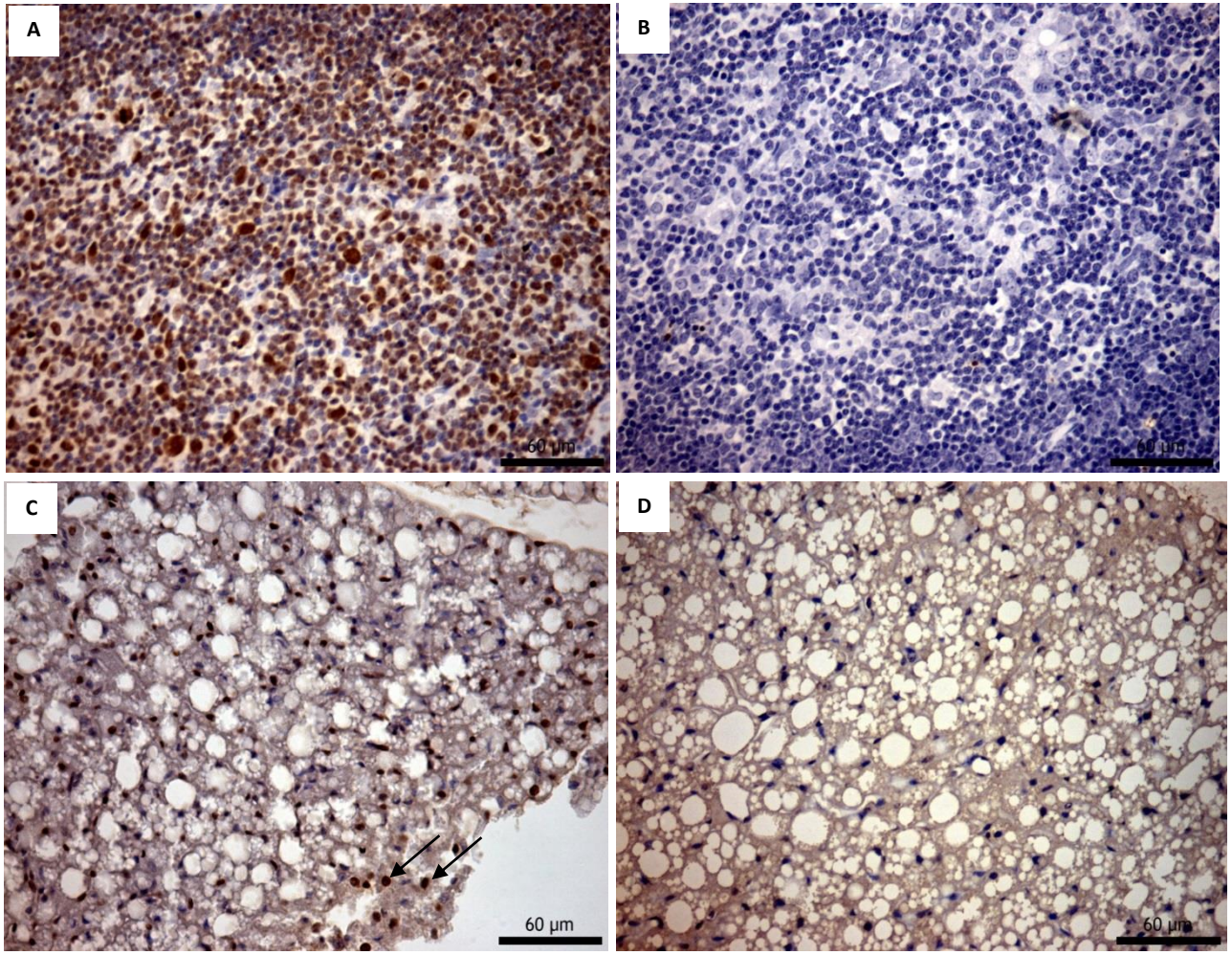


Figure 3.18 Representative images of uncoupling protein 1 stained 5µm tissue sections.

A) 1 day perirenal; B) 7 day perirenal; C) 28 day perirenal; D) 1 day paracardial; E)7 day paracardial; F) 28 day paracardial; G) 1 day epicardial; H) 7 day epicardial; I) 28 day epicardial; J) 7 day omental and K) 28 day omental. No omental adipose tissue was present for sampling in 1 day old lambs. Scale bar=150µm

3.4.9 Assessment of apoptosis during brown to white adipose tissue transition

As there was a decrease in UCP1 with age in perirenal and epicardial adipose tissue as determined by western blotting, a TUNEL assay was performed to determine if there were cells undergoing apoptosis which may be those UCP1 expressing adipocytes present within the adipose tissue almost homogenously at birth which are not present at 28 days. Therefore small amounts of epicardial and perirenal adipose tissue from 1 day, 7 day and 28 day animals were sectioned and analysed. Images were taken at a higher magnification are shown so nuclei can be seen clearly. Rat thymus tissue and 1 day sheep perirenal adipose tissue treated with TACS Nuclease had clear DAB staining showing that kit components were working correctly for nucleotides to be incorporated into fragmented DNA and detected. In both epicardial and perirenal adipose tissue, no apoptotic cells were detected at 1, 7 or 28 days (Figure 3.19).


A
60 µm
B
60 µm
C
60 µm
D
60 µm

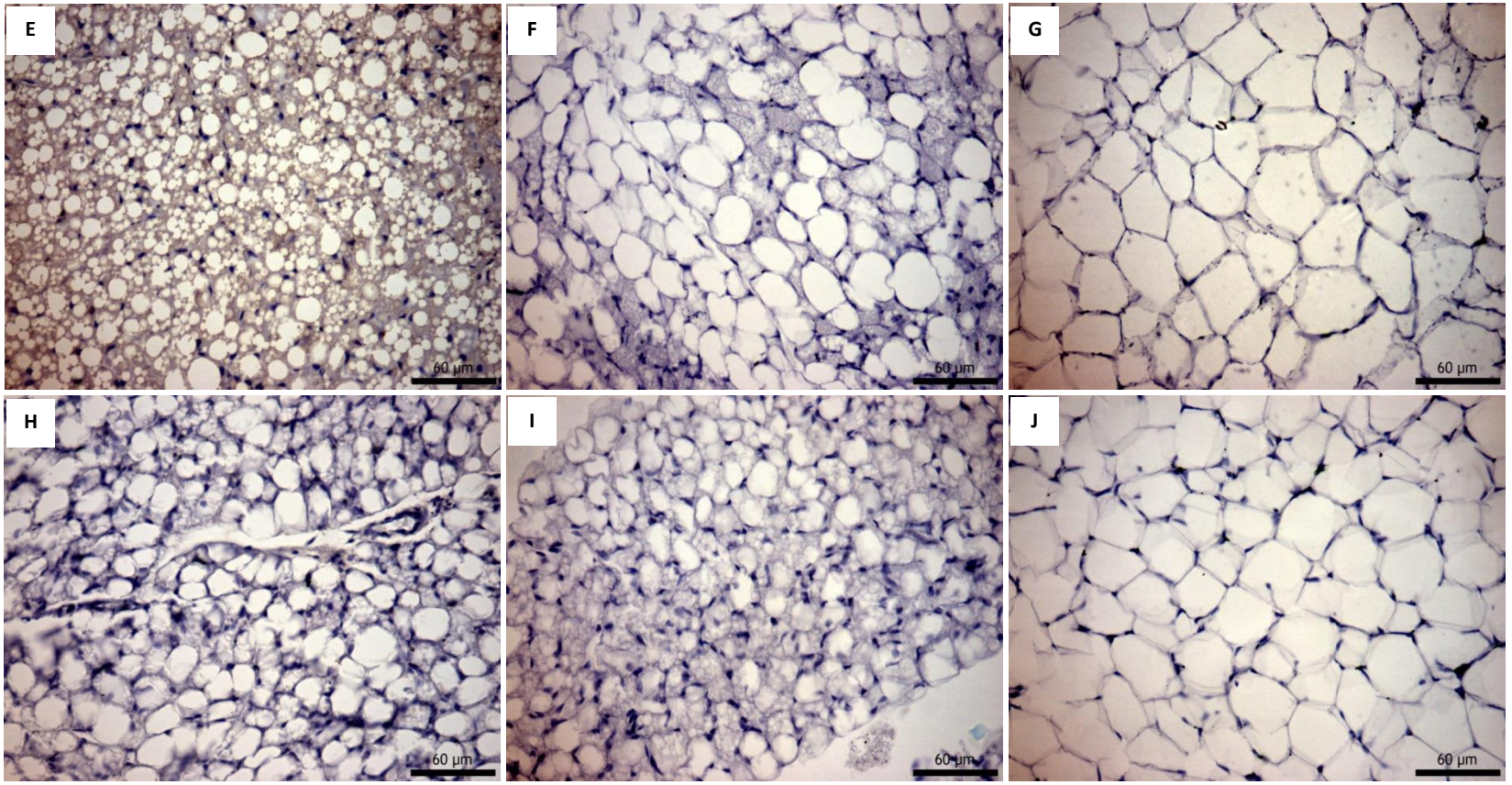


Figure 3.19 Assessment of apoptotic cells in adipose tissue through TUNEL assay.

Representative images of 5µm slides run on a TUNEL assay A) TACS nuclease treated rat thymus with abundant brown staining of cells with fragmented DNA; B) Untreated rat thymus; C) TACS nuclease treated 1 perirenal adipose tissue, nuclei with fragmented DNA are stained brown as shown by arrows; D) 1 day perirenal adipose tissue negative control without TdT enzyme; E) 1 day perienal adipose tissue; F) 7 day perirenal adipose tissue; G) 28 day perirenal adipose tissue; H) 1 day epicardial adipose tissue; I) 7 day epicardial adipose tissue and J) 28 day epicardial adipose tissue. Scale bar=60µm

3.5 Discussion

3.5.1 Epicardial and paracardial adipose tissue express thermogenic genes, possess UCP1 and may be intermediate between known white and brown adipose tissue depots in thermogenic capacity

The data from my study suggests that paracardial and epicardial adipose tissue show similar multilocular adipocyte morphology and abundance of UCP1 mRNA and protein. These findings suggest they may function as thermogenic adipose tissue which is in accordance with UCP1 positive epicardial (Sacks et al., 2009) and paracardial (Cheung et al., 2013) adipose tissue in some adult humans. However the only human study to my knowledge to have analysed paired epicardial and paracardial adipose tissue biopsies from the same patients showed UCP1 positive adipocytes in epicardial but not paracardial adipose tissue by western blot (Sacks et al., 2013). It is worth noting that Cheung et al only detected UCP1 in paracardial adipose tissue in 2 out of 10 patients (Cheung et al., 2013) suggesting it is not common in the adult human population. My study differs in that lambs may show less variation in UCP1 abundance than human paracardial and epicardial fat but also that pericardial fat depots may have a more pronounced thermogenic role in early life. In human newborns and infants undergoing surgery for congenital heart defects, pericardial adipose tissue is composed of multilocular adipocytes and is UCP1 positive in newborns and infants (Ojha et al., 2016) which is in accordance with my findings in sheep.

Similar to a previous comparison in adult humans (Fain et al., 2010), my study demonstrates ovine pericardial adipose tissue has upregulated thermogenic gene expression compared to omental adipose tissue. This suggests adipose tissue differences in thermogenesis, at least in epicardial and paracardial compared to omental adipose tissue, exist in both sheep and humans. My study adds to the work of Fain et al by demonstrating decreased UCP1 protein abundance in omental adipose tissue compared to pericardial adipose tissue as well as further examination of thermogenic gene expression. A summary heatmap of thermogenic, mitochondrial, beige and white adipocyte marker gene expression differences between depots in 7 day old sheep (when thermogenic genes are still abundantly expressed) is shown in Figure 3.20.

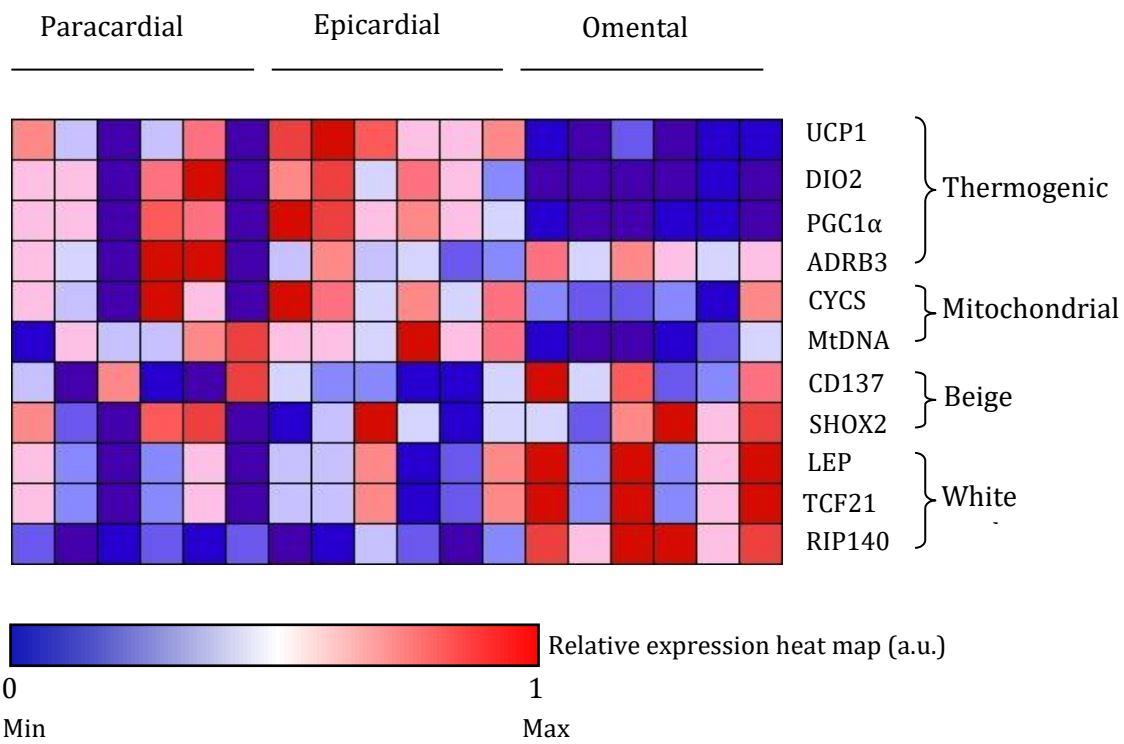


Figure 3.20 Heatmap of thermogenic, mitochondrial, beige and white adipocyte markers. *Samples from 7 day paracardial (n=6), epicardial (n=6) and omental (n=6) adipose tissue depots are shown. Maximum values per row are coloured red and minimum values blue with a gradient for values in between as shown by the legend.*

The role of thermogenic pericardial adipose tissue depots remains speculative (Sacks and Fain, 2011). In early life the main purpose of BAT from an evolutionary perspective is the maintenance of body temperature in the extra uterine environment (Cannon and Nedergaard, 2004). It can be hypothesised that pericardial fat depots may provide essential thermogenesis for the heart or blood flow to the brain through the aorta. Omental adipose tissue may not need to serve this function as surrounding organs such as the stomach may not need equivalent protection. In lambs exposed to cold, it is known that there is a 5 fold increase in blood flow to paracardial adipose tissue, however no results were obtained for omental adipose tissue (Alexander et al., 1973). It is known that blood supply to the digestive organs (reported as stomach) decreases in lambs exposed to cold (Alexander et al., 1973); however these findings may not necessarily apply to the greater omentum surrounding the digestive organs. Omental adipose tissue also develops after birth and may not be exposed to the high concentrations of thyroid hormones possibly upregulating UCP1 in the lamb at birth (Schermer et al., 1996; Symonds et al., 2000) unlike epicardial and paracardial fat depots. This would also result in less thyroid stimulation of omental adipose tissue and may explain the decreased gene expression of DIO2, PGC1α and UCP1 which are regulated through this signalling pathway.

Although epicardial and paracardial adipose tissue depots possess UCP1, they have less UCP1 than perirenal adipose tissue in my study and therefore may be intermediate between that of a white adipose tissue depot such as omental fat and a

brown fat depot. In humans, the most well established thermogenic adipose tissue depot is supraclavicular (Chondronikola et al., 2015) which has been suggested to be composed of both beige and classical brown adipocytes (Jespersen et al., 2013). Sacks et al compared epicardial and paracardial adipose tissue depots to supraclavicular adipose tissue in adult humans and found UCP1 positive adipocytes only in supraclavicular adipose tissue (Sacks et al., 2013). This may be inconclusive however, as epicardial adipose tissue samples showed UCP1 positive bands by western blot but not immunohistochemistry and supraclavicular UCP1 was not assessed through western blots for comparison. As human BAT is typically heterogeneous with pockets of multilocular adipocytes (Lidell et al., 2013), it is possible that regions of UCP1 positive adipocytes could have been missed on sectioning. It is also possible that certain primary antibodies may give better results in western blots compared to immunohistochemistry.

Perirenal adipose tissue was included as a reference BAT depot for comparisons between pericardial and omental adipose tissue depots in my study, as it has been consistently shown to be possess abundant UCP1 in sheep (Basse et al., 2015; Pope et al., 2014). However, the role of perirenal adipose to function as a thermogenic tissue has not been elucidated. One reason may be that in sheep (Alexander et al., 1973; Symonds et al., 1995) and other ruminants such as goats and reindeer (Soppela et al., 1992), perirenal adipose tissue is one of the major adipose tissues in early life and therefore will have the potential to provide heat to nearby internal organs.

Cytochrome c protein abundance showed a significant difference between perirenal and omental adipose tissue suggesting mitochondria activity is increased in the perirenal depot similar to UCP1 expression. If perirenal adipose tissue has increased mitochondrial activity in the electron transport chain, then a greater proton motive force could be generated and possibly used for heat dissipation through UCP1. Basal mitochondrial respiration is increased in hamster primary brown adipocytes compared to white adipocytes when treated with certain browning hormones such as thyroxine (Klaus et al., 1995) which may support this notion. Increased basal respiration was also found in Chapter 5 in mitochondria from UCP1 positive adipose tissue in pheochromocytoma. Unfortunately apparatus for measuring mitochondrial respiration was not available to assess basal respiration (or uncoupling) functionally in sheep tissues.

A decrease in cytochrome c abundance with age was observed in epicardial but not paracardial or omental adipose tissue. In paracardial fat this was probably not significant due to one sample that showed very little cytochrome c abundance by western blotting. In the perirenal adipose tissue of lambs it is known that the activity of citrate synthase as well as cytochrome c mRNA declines between days 1 and 30 with the brown to white adipose tissue transition (Basse et al., 2015). There are many possible reasons why mitochondrial activity could be altered in a brown to white adipose tissue transition. One possibility could be a change in sympathetic innervation or outflow to the adipose tissue. This may be a possibility, as in mice, iBAT has been shown to have increased sympathetic drive compared to inguinal,

epididymal and retroperitoneal white adipose tissue depots (Brito et al., 2007). It is also known that β-3 adrenergic agonists increase mitochondrial function in adipocytes and upregulate PGC1α (Puigserver et al., 1998) which can stimulate mitochondrial biogenesis. Another possibility could be that the energy requirements (i.e. ATP synthesis rates) for growth are greater in the first 7 days of life in lambs which decline by 28 days although this would not be related to the presence of brown or white adipocytes *per se*.

Mitochondrial abundance was significantly higher in epicardial and perirenal adipose tissue in comparison with omental adipose tissue. This is unsurprising given that UCP1 mRNA and protein tended to be higher in epicardial and perirenal adipose tissue as well as the presence of multilocular adipocytes which are known to have numerous mitochondria (Soppela et al., 1992). The results also showed a significant decline in mitochondrial abundance with age in paracardial and epicardial fat depots in line with the loss of UCP1 and multilocular adipocytes. This is in accordance with previous results using the same technique for determining mitochondrial abundance between days 1, 2, 4, 14 and 30 postnatally in perirenal adipose tissue from lambs (Basse et al., 2015). In vitro studies of brown adipocytes have reported the close association of mitochondria to the lipids droplets (Wikstrom et al., 2014) so it is possible that the changes in lipid droplet morphology are related to the loss of mitochondrial abundance if adipocyte transdifferentiation occurs.

A cellular process responsible for the removal of mitochondria is mitochondrial autophagy (or mitophagy), where dysfunctional mitochondria are absorbed by phagophores forming autophagosomes (Kissova et al., 2004) and degraded within autolysosomes (Tong and Sadoshima, 2016). Interestingly a very recent study has demonstrated increased thermogenesis by cold exposure inhibits mitophagy in mice (Cairo et al., 2016). Conversely it may be possible that increased mitophagy inhibits thermogenesis and results in decreased mitochondrial abundance. Partially in support of this notion is evidence from human studies showing increased autophagy in WAT of obese individuals (Kovsan et al., 2011), who would be likely to have decreased prevalence of UCP1 (Vijgen et al., 2011). It could be hypothesised therefore that this process is involved in the loss of BAT or in the brown to white adipose tissue transition. The mitophagy process also degrades mtDNA (Oka et al., 2012) and this would perhaps explain the decrease in mtDNA in perirenal and pericardial adipose tissues between 7 and 28 days in my study. It is currently unknown if this occurs and unfortunately, that study was not published in time to allow me to test qPCR markers of mitophagy in adipose tissues undergoing a brown to white transition. An overall discussion of the fate of brown adipocytes in a brown to white transition is presented in Section 3.5.6.

3.5.2 Beige adipocyte markers do not show a clear pattern of expression between adipose tissue depots or with age in sheep

No clear pattern of gene expression between depots using two putative markers of beige adipocyte abundance was observed. CD137 has been suggested as being a selective marker of 'BRITE' adipose tissue or beige adipocyte precursors (de Jong et al., 2015; Walden et al., 2012; Wu et al., 2012). In the depots studied in this Chapter there was no difference in the 7 day group but at 28 days significant upregulation was seen in omental adipose tissue compared to paracardial and epicardial fat depots, suggesting that omental adipose tissue may have a higher proportion of beige adipocytes. This was somewhat unexpected as CD137 has been found to be highly expressed in epicardial and paracardial adipose tissue depots from adult humans when compared to subcutaneous adipose tissue (SAT) samples from the upper thorax or lower body (Sacks et al., 2013) and that omental adipose tissue has been considered a pure white depot in rodents (Walden et al., 2012). It is known that in humans, omental adipose tissue is able to undergo browning in response to chronically elevated plasma catecholamines in patients with pheochromocytoma (Frontini et al., 2013) which may suggest the presence of beige adipocytes, which are known to be able to undergo browning to increased cyclic adenosine monophosphate (Wu et al., 2012), a signalling molecule upregulated after catecholamine binding (Cao et al., 2001). This may also explain why the basal UCP1 expression is low in omental adipose tissue as UCP1 abundance is similar in unstimulated beige adipocytes to white adipocytes (Wu et al., 2012).

No differences were observed in SHOX2 expression between depots in the 7 day group. At 28 days there was a significant upregulation in paracardial adipose tissue compared to epicardial and omental adipose tissue. SHOX2 has been suggested to be a marker of beige fat due to increased gene expression during the browning of inguinal adipose tissue in mice (Walden et al., 2012). If this is taken to be an accurate marker of beige/BRITE adipocytes, then there appears to be an increase in paracardial adipose tissue beige adipocyte development at 28 days which does not occur in epicardial or omental adipose tissue. It is not clear why this would occur preferentially in paracardial fat but not in other depots such as epicardial adipose tissue located within close proximity. In adult humans undergoing heart surgery, SHOX2 gene expression does not differ between epicardial and paracardial adipose tissue depots (Sacks et al., 2013). As my study analysed depots in early life, it is possible that adipose tissue remodelling that occurs in paracardial adipose tissue in early life may cause a difference in SHOX2 expression and/or beige adipocyte abundance. In addition, paracardial adipose tissue has a different embryological origin from epicardial and omental adipose tissue (Sacks and Fain, 2007) and therefore the population of cells in the depot may differ, although the beige markers analysed did not show consistent results.

There are however, some issues with putative gene expression markers of beige adipocytes. One is that even though many beige markers are upregulated in the inguinal adipose tissue depot of rodents upon cold-induced browning, the increase seen is relative and markers can still be detected by qPCR even where beige

adipocytes are unlikely to be present (de Jong et al., 2015; Wu et al., 2012). CD137 has recently been found to be highly expressed in the stromal vascular fraction (SVF) from murine adipose tissue (Garcia et al., 2016) which may mean in my study, some of the detectable CD137 mRNA was from the SVF rather than mature beige adipocytes within the tissue. This is difficult to determine in my study however as the SVF and mature adipocytes were not separated prior to RNA extraction.

There may also be species differences in these markers of beige adipocytes which would explain why consistent patterns of expression are not seen in this sheep study. Any species differences in beige adipocyte markers however, are not known at present and would require further investigation over a variety of animal models together with human studies to determine their reliability in identifying the presence of beige adipocytes within adipose tissue from *in vivo* studies.

3.5.3 Lipolysis gene expression does not follow thermogenic gene expression and is increased in perirenal adipose tissue compared to other visceral depots studied

As epicardial adipose tissue has been suggested to have high rates of lipid turnover to provide energy substrate for the underlying myocardium (Marchington and Pond, 1990), the expression of genes involved in lipolysis was analysed by qPCR. Epicardial adipose tissue was not found to have increased expression of ATGL, HSL or PLIN1 compared to paracardial or omental depots. In humans epicardial adipose

tissue does have upregulated HSL gene expression compared to sternal SAT but not abdominal SAT (Fain et al., 2010). To my knowledge the gene expression of ATGL, HSL and PLIN1 has not previously been examined in epicardial adipose compared to other visceral depots.

Previous findings in human studies have shown LPL to be 2-fold upregulated in the epicardial compared to omental adipose tissue (Fain et al., 2010) although other lipolysis genes were not analysed. It is known that LPL is highly expressed in BAT upon cold exposure and is responsible for hydrolysis of fatty acids from the circulation for thermogenesis (Bartelt et al., 2011). This would be in accordance with UCP1 being present in epicardial and not omental adipose tissue in this study and in human adults (Sacks et al., 2009). However, LPL is expressed most highly in heart tissue (Enerback and Gimble, 1993) and some contamination of epicardial adipose tissue with underlying myocardium cannot be ruled out in the former study. Unfortunately efforts to design primers for LPL to work in my sheep samples were not successful.

Comparisons of epicardial to perirenal adipose tissue in guinea pigs have shown that fatty acid turnover is higher in epicardial adipose (Marchington and Pond, 1990). Direct measurements of lipolysis in a separate study in guinea pigs found that free fatty acid release was significantly elevated in epicardial adipose tissue compared to paracardial and perirenal adipose tissue although no significant difference was observed between the latter two adipose tissues (Marchington et al., 1989). These

findings may differ from those of my study by the fact that in a large mammal such as sheep, perirenal adipose tissue makes up a vast majority of total adipose tissue weight. Such a large store of adipose tissue in a growing animal would therefore be expected to have a high rate of lipid turnover compared to smaller fat depots possibly to provide FFA (free fatty acid) as substrate for surrounding tissues. Perirenal adipose tissue also showed abundant cytochrome c mRNA and protein suggesting higher mitochondrial activity than other visceral depots analysed. Increased mitochondrial function and lipolysis through β-adrenergic stimulation are coupled (Bukowiecki et al., 1981) and it is possible that increased activity of the mitochondrial electron transport chain is used for lipolysis in perirenal adipose tissue. A definite function for perirenal adipose tissue in a large mammal such as sheep on whole body physiology and metabolism is yet to be elucidated. This could be achieved by surgical removal of the depot in sheep and subsequent assessment of impacts on metabolism and physiology compared to sham operated controls as has been performed in studies of BAT function in rodents, although it is possible that compensatory mechanisms for the adipose tissue removal can occur in other fat depots or skeletal muscle (Rothwell and Stock, 1989).

The expression of lipolysis genes were higher in perirenal adipose tissue in my study but did not follow the same pattern as UCP1 and instead tended to be upregulated at 28 days. Although it is known that lipolysis is required for thermogenesis from adipose tissue-specific conditional ATGL knockout mice (Ahmadian et al., 2011) and ATGL KO adipocytes (Li et al., 2014), little is known

about lipolysis rates between brown and white adipose tissues. A recent study has suggested that fatty acid oxidation is higher in primary human brown adipocytes than white adipocytes (Lee et al., 2016). However it should be noted that the BAT used for SVF isolation was from deep neck adipose tissue and the WAT was from neck SAT. It is known that visceral and subcutaneous adipose tissue can differ in rates of lipolysis (Reynisdottir et al., 1997; Tchernof et al., 2006) and that the samples were taken from those with endocrine disorders or malignancies. It is possible that the difference in lipolysis was between visceral and subcutaneous adipocytes rather than brown and white adipocytes or may have been altered by disease states of patient donors. Studies have found that higher rates of uptake of chylomicrons and lipolysis are observed in BAT compared to gonadal and SAT white adipose tissue of mice (Khedoe et al., 2015) although this may not apply to total lipolysis and much of WAT lipolysis comes from stored intracellular lipid.

A limitation of my study and the analysis of target genes involved in lipolysis however is that gene expression of these enzymes may not be reflective of protein expression and ultimately, lipolysis rates within a tissue (Schweiger et al., 2014). Ideally this would have been performed in conjunction with a lipolysis assay, measuring glycerol and free fatty acid release in the tissues; however fresh tissue is required and these samples were frozen immediately after dissection.

3.5.4 RIP140, a UCP1 inhibitor is upregulated in omental compared to epicardial and paracardial adipose tissue

RIP140 was found to be significantly upregulated in omental adipose tissue compared to epicardial and paracardial adipose tissue. This is interesting as omental adipose tissue was the depot with the lowest abundance of UCP1 and it is known that RIP140 is able to inhibit UCP1 expression through direct binding to an enhancer region upstream of the UCP1 promoter (Christian et al., 2005). The mechanism of action of UCP1 silencing involves the recruitment of DNA and histone methyltransferases resulting in the methylation of the UCP1 promoter (Kiskinis et al., 2007) as well as the inhibition of a microRNA mi30b, known to induce adipose tissue browning (Hu et al., 2015a). Also, in rodents, RIP140 has previously been found to have high mRNA abundance in WAT compared to BAT (Leonardsson et al., 2004). Although this finding from my study is not causal, it can be speculated that an upregulation of RIP140 could result in UCP1 inhibition and could explain in part why UCP1 is less abundant in the omental fat depot than paracardial and epicardial adipose tissue. Interestingly a role for RIP140 has also been described in the inhibition of mitochondrial biogenesis and cytochrome c expression in adipose tissue (Powelka et al., 2006) which is in accordance with decreased mtDNA/nDNA ratio and a trend for lower cytochrome c in omental adipose tissue compared to epicardial adipose tissue in my study.

It has previously been found that in the perirenal adipose tissue of sheep, RIP140 is increased over the first month of life during the BAT to WAT transition (Pope et al., 2014) which was also found across paracardial, epicardial and omental adipose tissues in my study. It therefore may be a key factor in the loss of UCP1 with age in the sheep. Currently however, little is known about factors that regulate RIP140 expression which could explain why RIP140 is upregulated in white adipose tissue such as omental fat. One reason could be that RIP140 mRNA is upregulated in white adipocytes during differentiation (Leonardsson et al., 2004; Soukas et al., 2001). As the adipogenic gene PPARγ was more highly expressed in omental adipose tissue at all time points in my study compared to paracardial and epicardial adipose tissue, it is possible that omental adipose has an increased amount of fully differentiated white adipocytes which express abundant RIP140 mRNA. Further investigation into mechanisms of RIP140 upregulation in particular fat depots may help to explain differences observed in UCP1 abundance and thermogenic capacity.

3.5.5 Other white adipocyte related genes did not show a clear pattern of expression

Leptin gene expression was also examined in my study as it is considered to be released primarily by white adipocytes (Zhang et al., 1994) and is upregulated during adipocyte differentiation (MacDougald et al., 1995). In all depots studied leptin gene expression increased with age although not significantly in omental adipose tissue. It is possible that this is due to increased white adipocyte

differentiation with age although corresponding changes in PPARγ gene expression were not observed. A possible explanation for a lack of significant difference between the depots is that a previous study has suggested that unilocular UCP1 negative adipocytes within BAT are capable of leptin secretion, albeit to a much lesser extent than that of white adipocytes (Cinti et al., 1997). Another study has suggested leptin release by brown adipocytes (Buyse et al., 2001) although this was from a immortalised rat cell line derived from a brown adipose tumour (hibernoma) and therefore may not represent normal endocrine function of BAT in healthy animals. However, as paracardial and epicardial adipose tissues are heterogeneous in their composition of unilocular and multilocular adipocytes as observed by histology in this Chapter, it may result in a less pronounced difference in leptin mRNA expression between UCP1 positive pericardial adipose tissue depots and UCP1 negative omental adipose tissue and therefore no significant difference was observed.

TCF21 has been designated as a white marker in rodent studies (de Jong et al., 2015). In my study it was found to be significantly upregulated in epicardial and omental adipose tissue in comparison to paracardial fat. Similar findings have been reported in a human study where epicardial and omental adipose tissue displayed high TCF21 mRNA expression (Fain et al., 2010). TCF21 is also known as 'epicardin' and has been found to be highly expressed in the heart and other epicardial tissues (Robb et al., 1998). Although this may suggest epicardial and omental adipose tissue depots have higher amounts of white adipocytes compared to paracardial adipose

tissue, it should be noted that TCF21 expression varies depending on anatomical location and at least in rodents, is expressed more highly in posterior adipose tissues (de Jong et al., 2015). It is known that epicardial and omental adipose tissue depots both develop from the splanchnic mesoderm so it is also possible that the lower mRNA abundance of TCF21 in paracardial adipose tissue compared to epicardial and omental adipose tissue is due to the different lineage of paracardial adipose tissue. A possible role for TCF21 in adipose tissue development or metabolism has not been reported. TCF21 deletion results in non-viable murine embryos (Acharya et al., 2012) and therefore the effects on adipose tissue have not been determined. It would therefore be interesting to investigate the role of this transcription factor in adipose tissue-specific (conditional) knockout animals.

3.5.6 A brown to white adipose tissue transition occurs in perirenal and pericardial adipose tissue without evidence of apoptosis

In perirenal, paracardial and epicardial adipose tissue, a clear transition was seen in adipose tissue morphology, UCP1 and mitochondrial abundance between days 1, 7 and 28 consistent with previous reports in sheep (Basse et al., 2015; Pope et al., 2014). However a TUNEL assay did not show any apoptotic cells in perirenal or epicardial adipose tissue between 1, 7 or 28 days. This has previously been reported in sheep in perirenal adipose tissue, although the results were not shown (Lomax et al., 2007). An RNA sequencing approach using sheep as an animal model for the BAT to WAT transition did find differentially expressed upregulated transcripts involved

in apoptosis between the transition and white adipose tissue phase although this contained both pro-apoptotic and anti-apototic genes (Basse et al., 2015). The results from my study suggest that a mechanism other than apoptosis may cause the BAT to WAT transition. As beige adipocytes are capable of reversible transdifferentiation to white adipocytes in rodents (Rosenwald et al., 2013) it is possible that this is responsible for a BAT to WAT transition in the sheep if the UCP1 positive adipocytes are indeed beige. It is also possible that the disappearance of UCP1-positive adipocytes with age occurs by another form of programmed cell death distinct from apoptosis, although no sign of necrotic cells were present by examination of the tissue morphology in my study. A previous study in sheep suggested that the development of white adipocytes in sheep by day 28 is unlikely to occur from the differentiation of white adipocyte precursors due to the lack of upregulation of cell cycle genes in the transition phase (Basse et al., 2015). Further studies are warranted to determine the mechanism of BAT to WAT transition in the sheep and ultimately if this same mechanism is responsible for the loss of BAT in humans with age. Lineage tracing and labelling techniques such as those currently used in rodents, would be a powerful tool to assess cell fate and provide more definitive results. Although not currently used in large mammals, advances in CRISPR/Cas technology for genetic manipulation (Cong et al., 2013) may open this avenue in the future.

A limitation of a TUNEL assay used to detect apoptotic adipocytes in my study is that it only detects late stages of apoptosis where DNA fragmentation begins to occur and

detection of apoptosis *in situ* from *in vivo* experiments is relatively low, therefore other techniques should be used in conjunction to confirm this (Muppidi et al., 2004). IHC using a Caspase 3 antibody unfortunately did not seem specific in adipose tissue sections under the conditions tested and may have required further rounds of optimisation for which there was insufficient time. Also, a general study limitation that is particularly relevant to this apoptosis study is that only 3 time points were assessed at 1, 7 and 28 days. Although this time points do cover those noted previously as maximal UCP1, transition and white adipocyte/lipid storage phases in the ovine BAT to WAT transition (Pope et al., 2014) it is possible that a key stage in apoptosis for example may have been missed and further time points should be taken to examine this process in more detail.

The physiological reasons for the loss of BAT in sheep or humans are not clear at present. In the sheep, a decline in plasma hormones such as thyroxine (Symonds et al., 1996) occurring over the first month of life may lead to less active thermogenic adipocytes. Lambs raised in a cold environment maintain the postpartum surge in thyroid hormones (Symonds et al., 1996) which may suggest BAT could also be maintained with constant stimuli. The sensitivity to cold may decrease over the first month of life as the lamb grows thicker wool to act as insulation. Shorn lambs have been reported to have higher plasma thyroxine concentrations than fully fleeced lambs (Horton, 1981) so it is possible that increased wool growth is involved in BAT loss by 28 days of age in sheep. To my knowledge however shorn and unshorn lambs have not been analysed over the first month of life to test if this directly

affects UCP1 abundance and BAT activity. Although cold exposure probably is not responsible for age-related BAT atrophy in humans due to the general maintenance of thermoneutrality (Speakman and Keijer, 2012), endocrine influences may be present. Using rats as animal models of this process, Valle et al reported the delayed age-related BAT loss in females compared to males was correlated to increased thyroid hormones and estradiol (Valle et al., 2008). Interestingly in humans it has been found that circulating T3 concentrations decrease in the elderly (Corsonello et al., 2010), which could be speculated to result in less active BAT. However other endocrine changes and factors may also be responsible for the loss of BAT with age in humans and animal models. The molecular and physiological mechanisms responsible for age related BAT atrophy are worthy of further investigation to understand how BAT prevalence can be maintained throughout the lifespan.

3.5 Summary and conclusions

This study aimed to characterise epicardial and paracardial adipose tissue compared to omental and perirenal adipose during early life in the sheep. Depot differences in UCP1 and thermogenic gene expression were observed between pericardial and omental adipose tissue suggesting fat depots surrounding the heart have a thermogenic role in early life. They may be intermediate between a brown fat depot (i.e. perirenal) and white fat depot (omental) however, in terms of UCP1 abundance. It is not clear in sheep if these depots are composed of classical brown or beige adipocytes. The results also suggest that in sheep, perirenal adipose tissue may have

higher rates of lipolysis than other visceral depots and that increased lipolysis gene expression is not necessarily associated with the presence of UCP1. Perirenal, paracardial and epicardial adipose tissue undergo a clear brown to white adipose tissue transition over the first 28 days of postnatal life with the loss of UCP1, mitochondria and other thermogenic genes. This brown to white adipose tissue transition occurs without evidence of apoptosis suggesting other mechanisms may be responsible for the loss of BAT in sheep, the elucidation of which may inform the mechanisms of this age related BAT loss in humans.

Chapter 4 Gene expression analysis of cardiac natriuretic peptide signalling in paracardial, epicardial and omental adipose tissue depots

4.1 Introduction

As previously discussed, cardiac natriuretic peptides (ANP and BNP) have been found to increase UCP1 at least in rodents (Bordicchia et al., 2012). As these hormones are primarily released from the heart (Flynn et al., 1983; Saito et al., 1989), I hypothesised that these hormones may have a possible paracrine effect on surrounding epicardial and paracardial adipose tissue. This may in part determine why epicardial adipose tissue has thermogenic potential by possessing abundant UCP1 and mitochondria whereas omental adipose tissue from the same lineage (Ho and Shimada, 1978), perhaps due to its distal location from the heart and less cardiac natriuretic peptide exposure and signalling. Therefore BNP concentrations were measured in plasma to determine if this peaks at birth, in a pattern similar to thyroid hormones (Schermer et al., 1996) possibly stimulating UCP1. To assess possible differences in responsiveness between adipose tissue depots to cardiac natriuretic peptides, the gene expression of natriuretic peptide activated (NPRA) and clearance (NPRC) receptors were examined as well as downstream protein kinase G I (PRKGI).

4.2 Hypothesis

The hypothesis for this Chapter was that epicardial adipose would have a high abundance of NPRA due to the paracrine effects of ANP and BNP released from the underlying myocardium. Conversely, the clearance receptor (NPRC) would be decreased; indicating increased cardiac natriuretic peptide signalling in epicardial adipose tissue compared to depots more distal from the heart such as omental adipose tissue. Due to the lack of UCP1 in omental adipose (reported in Chapter 3), the NPRC receptor would be highly expressed, preventing the thermogenic downstream signalling of cardiac peptides once bound to the activated receptor. Plasma BNP would also be more abundant at birth and in early life but would show a decrease by 28 days suggesting it would participate in maximal UCP1 stimulation at birth.

4.3 Methods

The same experimental protocol and animals used for gene expression analyses above were used for the analyses in this chapter. Plasma BNP analysis was performed as described in Chapter 2.1. Parametric tests were used for comparisons with age and depot comparisons due to small sample size. One-way ANOVA with Bonferroni post hoc correction or unpaired t tests were used where appropriate depending on the number of groups compared and results considered statistically significant at $p<0.05$.

4.4 Results

4.4.1 Plasma BNP concentrations in early life

To assess the possible impact of cardiac natriuretic peptides on the high abundance of UCP1 seen shortly after birth, BNP concentrations were determined in the plasma. Plasma samples were available from two separate studies (studies A and B described in Chapter 2.1.1) with lambs sampled at the same time points of 7 and 28 days with plasma samples also for 1 day animals in study B. There was a trend for decreased BNP plasma concentration between 7 and 28 days in both studies of lambs sampled at the same time points although this was not statistically significant in study A or B ($p=0.06$). In study B, 1 day lambs did not have higher plasma BNP concentrations than 7 or 28 day lambs and there was considerable variation around the 1 day group mean. As there was no significant difference between the two studies at either 7 or 28 day time points and due to the small sample size of the studies, they were pooled together for day 7 and 28 comparisons to give an increased sample number per group. A significant decrease in plasma BNP was observed between pooled day 7 and 28 day animals (Figure 4.1).

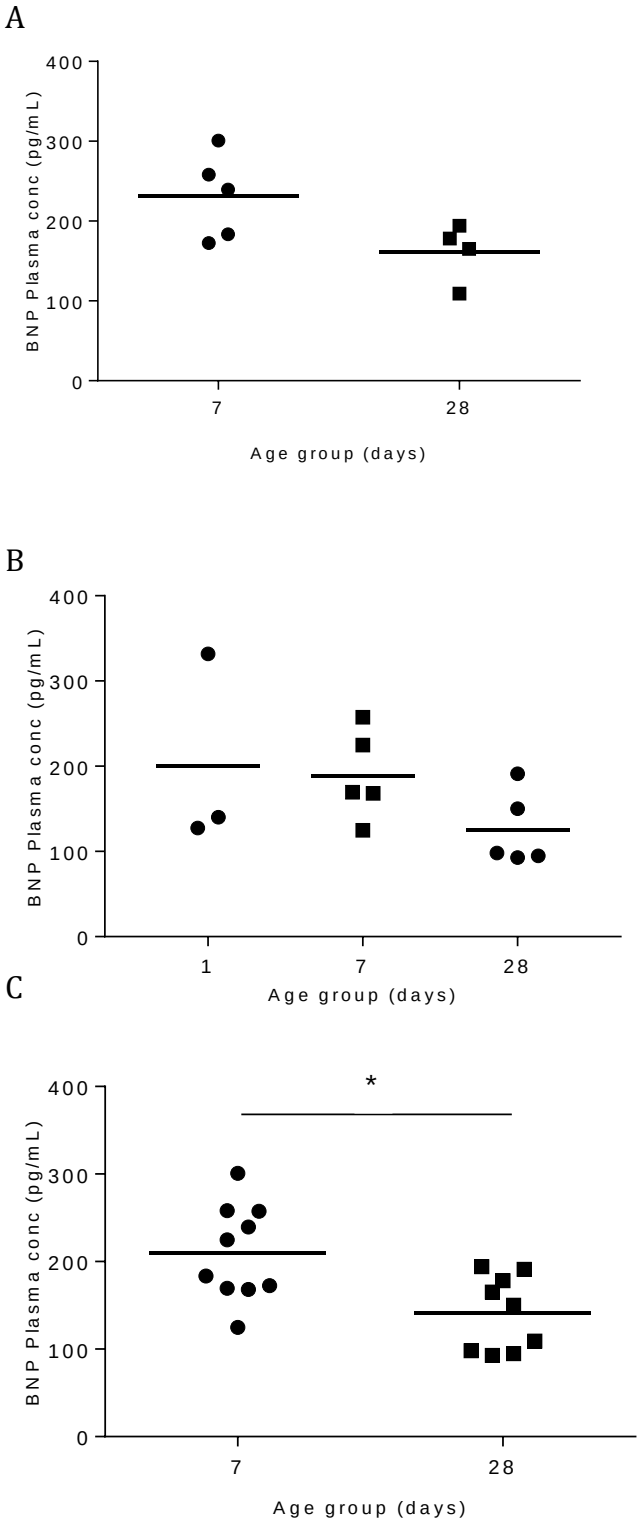


Figure 4.1 Plasma BNP concentrations analysed by enzyme immunoassay (EIA).

*A) Study A - 7 day lambs (n=5) and 28 day lambs (n=4). B) Study B – 1 day lambs (n=3), 7 day lambs (n=5) and 28 day lambs (n=5) C) Pooled data from studies A and B– 7 day lambs (n=10) and 28 day lambs (n=9). Data is presented as a scatter plot with individual data points and group means. * p<0.05 for comparisons with age*

4.4.2 Expression of cardiac peptide receptor mRNA

4.4.2.1 Natriuretic peptide receptor A gene expression

NPRA, the activated form of the receptor for ANP and BNP effects, increased significantly with age in paracardial and epicardial but not omental adipose tissue depots. In paracardial fat this was significant between 1 and 28 and 7 and 28 days. Interestingly there was a significant increase in gene expression of NPRA in omental adipose tissue at 7 days compared to paracardial and epicardial depots.

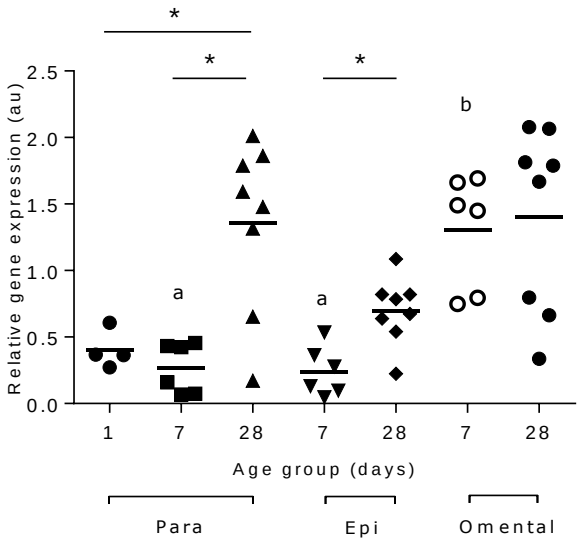


Figure 4.2 NPRA gene expression in paracardial, epicardial and omental adipose tissue.

*Paracardial (Para) adipose tissue was sampled at 1 day (n=4), 7 days (n=6) and 28 days (n=7). Epicardial (Epi) and omental adipose tissue were both sampled at 7 days (n=6) and 28 days (n=7). Data is presented as a scatter plot with individual data points and group means. * denote p<0.05 for comparisons with age, letters a and b show significant differences (p<0.05) between depots at 7 days where letters differ. Gene expression vales are shown relative to the geometric mean of reference genes importin 8 (IPO8) and ribosomal protein lateral stalk subunit P0 (RPLP0).*

4.4.2.2 Natriuretic peptide receptor C gene expression

The clearance receptor (NPRC) for ANP and BNP did not change significantly with age in any depots studied although there were significant differences in gene expression between the depots at both 7 and 28 days of age. Epicardial adipose tissue had significantly higher NPRC gene expression than both omental and paracardial adipose at both 7 and 28 days (Figure 4.3).

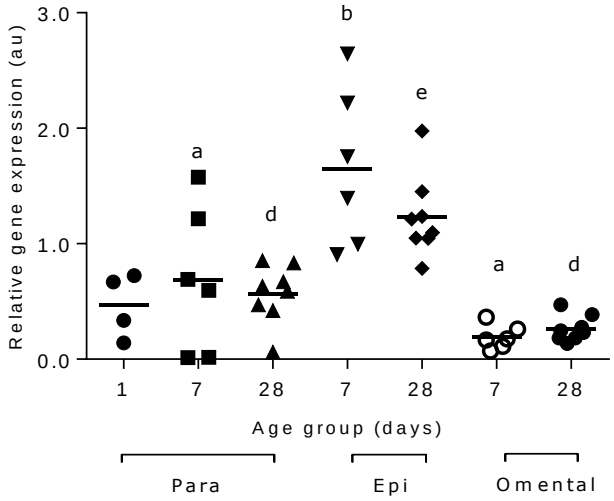


Figure 4.3 Natriuretic peptide receptor type C (NPRC) gene expression in paracardial, epicardial and omental adipose tissue.

*Paracardial (Para) adipose tissue was sampled at 1 day (n=4), 7 days (n=6) and 28 days (n=7). Epicardial (Epi) and omental adipose tissue were both sampled at 7 days (n=6) and 28 days (n=7). Data is presented as a scatter plot with individual data points and group means. * denote p<0.05 for comparisons with age, letters a and b show significant differences (p<0.05) between depots at 7 days where letters differ. Letters d and e show significant differences (p<0.05) between depots at 28 days where letters differ. Gene expression vales are shown relative to the geometric mean of reference genes importin 8 (IPO8) and ribosomal protein lateral stalk subunit P0 (RPLP0).*

4.4.2.3 Natriuretic peptide receptor A to C ratio

As it has been suggested that the NPRA:NPRC ratio suggests the responsiveness of adipose tissue to cardiac natriuretic peptides (Bordicchia et al., 2012) this was calculated from NPRA and NPRC qPCR results. As can be seen in Figure 4.4, there was a significant increase in the NPRA:NPRC ratio in omental adipose tissue compared to epicardial at both time points studied. At 7 days, the NPRA:NPRC ratio was also significantly higher in omental adipose tissue compared to paracardial fat but was not significant at 28 days.

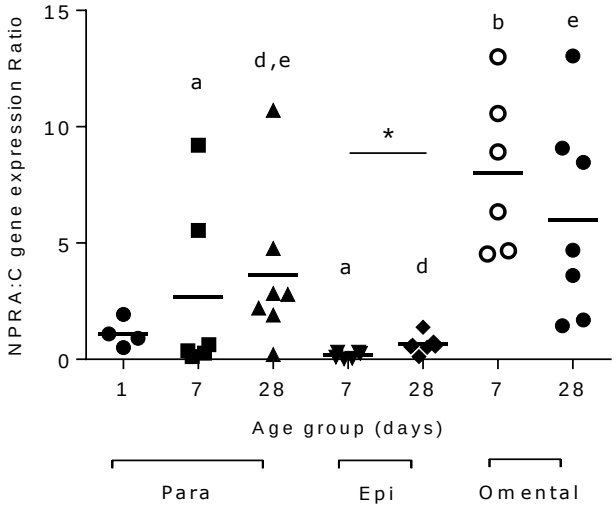


Figure 4.4 Ratio of NPRA:NPRC gene expression in Paracardial, epicardial and omental adipose tissue.

*Paracardial (Para) adipose tissue was sampled at 1 day (n=4), 7 days (n=6) and 28 days (n=7). Epicardial (Epi) and omental adipose tissue were both sampled at 7 days (n=6) and 28 days (n=7). Data is presented as a scatter plot with individual data points and group means. * denote p<0.05 for comparisons with age, letters a and b show significant differences (p<0.05) between depots at 7 days where letters differ. Letters d and e show significant differences (p<0.05) between depots at 28 days where letters differ. Gene expression values relative to the geometric mean of reference genes importin 8 (IPO8) and ribosomal protein lateral stalk subunit P0 (RPLP0) were used in ratio calculations.*

As Protein kinase G I (PRKGI) acts downstream of cGMP activation through NPRA receptors (Bordicchia et al., 2012; Mitschke et al., 2013) gene expression was also analysed by qPCR. Indeed, a similar pattern of expression can be seen as observed for NPRA with omental adipose tissue having significantly elevated PRKGI compared to paracardial and epicardial adipose tissue at both 7 and 28 days.

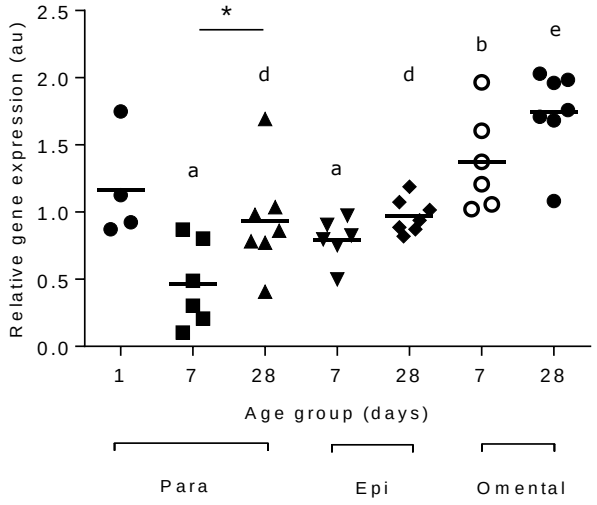


Figure 4.5 Protein kinase G I (PRKGI) gene expression in paracardial, epicardial and omental adipose tissue.

*Paracardial (Para) adipose tissue was sampled at 1 day (n=4), 7 days (n=6) and 28 days (n=7). Epicardial (Epi) and omental adipose tissue were both sampled at 7 days (n=6) and 28 days (n=7). Data is presented as a scatter plot with individual data points and group means. * denote p<0.05 for comparisons with age, letters a and b show significant differences (p<0.05) between depots at 7 days where letters differ. Letters d and e show significant differences (p<0.05) between depots at 28 days where letters differ. Gene expression vales are shown relative to the geometric mean of reference genes importin 8 (IPO8) and ribosomal protein lateral stalk subunit P0 (RPLP0).*

4.4.4 Western blots

Unfortunately attempts to follow up this gene expression work were not successful. Antibodies for both NPRA and NPRC were tested by western blot as there was difficulty in getting sections with fully intact cell membranes for IHC particularly in 28 day tissues. Rat kidney protein was prepared to act as a positive control and crude total protein extracts were used from sheep adipose tissue samples. No bands were present at the respective sizes of proteins expected in any of the tissues. Unfortunately there was insufficient time and costs to purchase alternative primary (or secondary antibodies) and optimise these.

4.5 Discussion

4.5.1 BNP plasma concentrations show a decrease between days 7 and 28

A decrease in BNP plasma concentration was observed between 7 and 28 days. BNP plasma concentrations at 28 days were in line with those previously reported for healthy untreated (control group) lambs at approximately 4 weeks of age (Oishi et al., 2007) suggesting the assay provided valid results. Although Oishi et al observed no difference in plasma BNP concentration between 2 week and 4 week old lambs (Oishi et al., 2007), they did not assess BNP plasma concentrations between birth and 2 weeks of age. This may suggest that the decrease in plasma BNP occurs between days 7 and 14. Although not causal, it may suggest that plasma BNP participates in the increased UCP1 observed at 7 days compared to 28 days in perirenal and pericardial adipose tissue depots. However it did not appear to peak at

birth, as would be expected if it was responsible for UCP1 stimulation in early life. It is known that in mice exposed to cold, plasma BNP concentrations are increased and infusion of physiological concentrations of BNP elicit UCP1 upregulation (Bordicchia et al., 2012). *In vitro* experiments show that human adipocytes treated with ANP undergo significant mitochondrial biogenesis (Bordicchia et al., 2012). The effects of BNP were not reported although it is perhaps likely that these would be similar due to the activation of the same receptor and the ability of both ANP and BNP to upregulate UCP1 and PGC1α. This would be in accordance with results of my study showing a decrease in mitochondrial abundance in epicardial and paracardial adipose tissue with age concomitant with a decline in plasma BNP concentration.

A mechanism for the decline in BNP plasma concentration between days 7 and 28 in sheep is not clear. It is known that the production of BNP is induced in cardiomyocytes by increased pressure and stretch of the ventricular wall (Iwanaga et al., 2006) and possibly hypertension (Kohno et al., 1992). Cold exposure is known to cause an increase in blood pressure (van der Lans et al., 2013) and therefore may be implicated in the increased circulating plasma BNP observed in rodents exposed to cold (Bordicchia et al., 2012). A similar mechanism of acute cold exposure and BNP production may be speculated to occur in lambs during early life possibly playing a role in non-shivering thermogenesis. There may also be other unknown factors also released upon cold exposure that could cause upregulation of BNP, unrelated to increased blood pressure that may warrant further investigation.

The limitations of the experiment are that insufficient numbers of plasma samples were collected from 1 day old lambs to reliably assess if BNP peaks at birth at the time of maximal UCP1 abundance. ANP plasma concentration was not assessed in my study due to time and resource constraints although it would also be interesting to see if a decline in ANP plasma concentrations are observed with increasing age.

4.5.2 Cardiac natriuretic peptide signalling or sensitivity may be increased in omental adipose tissue compared to pericardial fat depots

Interestingly, my study found that NPRA mRNA was significantly increased in omental compared to epicardial adipose tissue. This is in accordance with a human microarray study that found NPRA to be highly expressed in omental adipocytes (Sjoholm et al., 2005). The ratio of NPRA to NPRC mRNA was also significantly greater in omental, compared to both epicardial and paracardial adipose tissue depots. This is interesting as it has been suggested that the mRNA ratio of these two receptors determines, in part, adipose tissue response to both ANP and BNP (Bordicchia et al., 2012). In addition, downstream PRKGI mRNA was also significantly upregulated in accordance with possible increased cardiac natriuretic peptide signalling or sensitivity in omental adipose tissue. Differences between adipose tissue depots in this regard are therefore unknown at present and my study shows novel findings of differences between the depots at the mRNA level. Taken together, my results may suggest that cardiac peptides act on either on white adipose tissues or on fat depots distal to the heart.

Differences is possible responsiveness of different adipose tissue depots could be important as cGMP signalling has been suggested as a promising way of browning white adipose tissue (Haas et al., 2009; Mitschke et al., 2013) and has additive or synergistic effects to cAMP signalling further increasing UCP1 expression (Bordicchia et al., 2012). Previously it has been shown that the NPRA:NPRC ratio is increased in both iBAT and epididymal WAT in mice exposed to cold concomitant with increased UCP1 abundance (Bordicchia et al., 2012); however, fat depot comparisons were not made. BNP infusion does elicit an upregulation of UCP1 in both BAT and WAT (although inducible adipocytes in these depots may be beige) and by western blotting, UCP1 abundance in WAT appeared to be similar to iBAT post-infusion (Bordicchia et al., 2012). It may be that signalling was not increased in omental adipose tissue in my study however, as UCP1 would be hypothesised to be upregulated if this were the case. It has been suggested that both the increased sensitivity (i.e. upregulation of NPRA) and the availability of natriuretic peptide would be required for downstream signalling (Bordicchia et al., 2012). Therefore omental adipose tissue may be more sensitive to the action of cardiac natriuretic peptides but would not display UCP1 upregulation if insufficient ANP and BNP are transported in the circulation to the omental fat depot. Also, an upregulation of inhibitors in omental adipose tissue such as RIP140 (Chapter 3 results) may suppress any UCP1 activation that could be elicited through the action of cardiac natriuretic peptides.

The downstream signalling molecule PRKGI is expressed in adipocytes during differentiation and has a role in adipogenesis (Mitschke et al., 2013). My results showed both a pronounced rate of omental adipose tissue accretion in the growing lamb and high PPARγ gene expression compared to the other depots analysed (Chapter 3 results). Therefore, increased adipogenesis in this depot could explain why PRKGI is highly expressed in omental compared to epicardial and paracardial fat depots. However it has also been reported that PRKGI activation can upregulate UCP1 and mitochondrial biogenesis both *in vitro* (Haas et al., 2009) and *in vivo* (Mitschke et al., 2013) and it is not clear why this is not consistent with my findings in omental adipose tissue. However RIP140 can also inhibit mitochondrial biogenesis in addition to UCP1 stated above and may explain this discrepancy in omental adipose tissue.

It is not clear why the NPRA:NPRC ratio is higher in omental adipose than pericardial depots and is paradoxical to the thermogenic effects of cardiac peptides on adipose tissue. However it has previously been found that endocrine organs such as adrenal tissue have a high NPRA:NPRC ratio (Sarzani et al., 1996). WAT (i.e. omental adipose tissue) could be considered more of an endocrine organ at present than BAT which may be in accordance with these findings but would not offer an explanation for why this occurs. It is known, however, that insulin and glucose exposure causes an upregulation of NPRC in adipose tissue (Bordicchia et al., 2016). As some components of the insulin signalling pathway are upregulated in BAT when undergoing thermogenesis (Gasparetti et al., 2003) and utilises glucose as evidenced

by PET-CT scans (Cypess et al., 2009), it is possible that NPRC is upregulated in thermogenic depots which is independent of cardiac natriuretic peptide stimulation.

Unfortunately, efforts to look at protein abundance of NPRA and NPRC were unsuccessful. NPRC protein did follow gene expression changes in mice exposed to cold in a previous study (Bordicchia et al., 2012); although it is important to consider that protein abundance may not necessarily reflect changes observed at the transcriptional level in my study. Indeed, even if protein abundance reflected gene expression differences it would not show adipose tissue depot responsiveness to cardiac natriuretic peptides functionally. Therefore, further functional investigations would be required to assess downstream effects on UCP1 activation and lipolysis.

4.6 Summary and conclusions

This study investigated B-type cardiac peptide (BNP) plasma concentrations in lambs and the expression of cardiac peptide activated and clearance receptors between depots located proximal (pericardial) and distal (omental) to the heart. The results suggest that BNP decreases from 7 to 28 days of age concomitant with UCP1 loss demonstrated in Chapter 3 which may suggest a role in UCP1 regulation. Cardiac peptide activated receptor is increased in omental compared to paracardial and epicardial adipose tissue depots which suggests that omental adipose tissue may respond more to cardiac peptide signalling and that a paracrine action of

cardiac peptide may not preferentially stimulate epicardial and/or paracardial adipose tissues. Understanding the response of different adipose tissue depots to endocrine stimuli such as cardiac natriuretic peptides may be important to determine their capacity for thermogenesis and to undergo browning.

Chapter 5 Adipose tissue depot specific effects of chronic adrenergic stimulation in humans with pheochromocytoma

5.1 Introduction

β-3 adrenergic stimulation, such as that elicited through catecholamines, is well established to induce a multilocular adipocyte morphology and the upregulation of UCP1 in white adipose tissues (Cannon and Nedergaard, 2004; Mossenbock et al., 2014). This browning is most often reported in the inguinal subcutaneous depot of mice (Rao et al., 2014; Seale et al., 2011) which is predominantly WAT at thermoneutrality (Rosell et al., 2014). Little is currently known about the browning capacity of subcutaneous adipose tissue in humans, which may be an important site to induce browning as it constitutes approximately 85% of total adipose tissue in females (Fowler et al., 1991). Collectively this would present a much larger depot in humans than the upper estimate of 84g of supraclavicular BAT (Ouellet et al., 2012) and therefore would potentially have more significant effects on metabolism and energy expenditure.

Pheochromocytoma (pheo) is defined as an adrenal paraganglioma: a catecholamine-secreting tumour arising from chromaffin cells located within the adrenal medulla (Lenders et al., 2014). These patients have massively elevated

plasma catecholamine concentrations (Lenders et al., 2014) and can be used as a model of adipose tissue browning in response to chronic adrenergic stress. Previous studies conducted in patients with pheo have shown browning of visceral omental (Frontini et al., 2013) and perirenal adipose tissue (Nagano et al., 2015) depots. This study therefore assessed browning in subcutaneous adipose tissue (SAT) as well as visceral periadrenal adipose tissue (pADR) in patients undergoing adrenalectomy in either patients with pheo or benign non-pheo tumours.

5.2 Hypothesis

The hypothesis for chapter 5 was that both pADR and SAT depots would undergo browning in pheo patients but would not be observed in the control (non-pheo) group. This would be evidenced by the presence of multilocular adipocytes, characteristic of beige or brown adipocytes and an upregulation of UCP1 and other thermogenic genes.

5.3 Methods

Laboratory procedures were conducted as detailed in chapter 2 and further information on statistics on individual analyses is given in this chapter where relevant. Sample number used for analysis occasionally differs as this was an ongoing study with continued collection of samples and it was not possible to wait

until all samples had been collected due to the uncertainty when more pheo or non-pheo patients would be undergoing surgery.

5.4 Results

5.4.1 Patient characteristics

A summary of patient characteristics is given in table 5.1. Details of exclusion criteria are stated in Chapter 2. A total of 20 control patients undergoing adrenalectomy for non-functioning, aldosterone or cortisol secreting tumours and 13 pheo patients were studied. Full details of reasons for surgery, co-morbidities and medications of each patient are included in the appendix. No significant differences were seen for age or BMI between control and pheo patients.

	Control	Pheo
n	20	13
Female/male (n)	8/12	8/5
Age	53.6±1.9	54.4±4.0
BMI	30.6±1.7	27.2±1.5

Table 5.1 Summary of patient characteristics for control and pheo patients.
Data are presented as means ± SEM.

5.4.2 Adipose tissue morphology and study groups

Morphological changes in adipocytes were determined using H&E staining and brightfield microscopy. It was observed that 46% of pheo patients (n=6/13 total pheos) displayed pockets of multilocular adipocytes in pADR fat whereas multilocular adipocytes were not observed in the pADR adipose tissue of control (non-pheo, n=20) subjects or remaining pheo patients (n=7). As this may indicate adipose tissue browning, the pheochromocytoma study group was also subdivided for analysis into a 'pheo unilocular' (PU) group, where only unilocular white adipocytes were present and 'pheo multilocular' (PM) where multilocular adipocytes were observed (Figure 5.1). These subgroups were used for all further analysis. No multilocular adipocytes were observed in subcutaneous adipose tissue from any patients including pheos with multilocular adipocytes within the pADR fat depot.

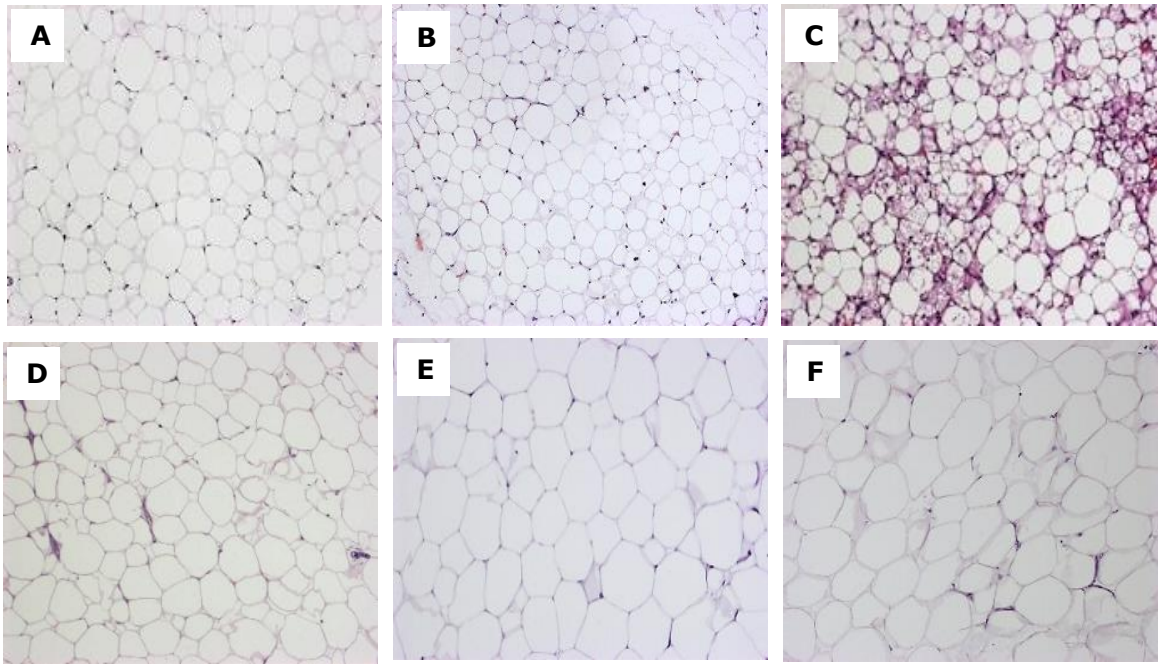


Figure 5.1 Representative images of Haematoxylin and Eosin stained 5µm tissue sections.

A) Control group Periadrenal (pADR) fat B) pADR pheo unilocular C) pADR fat multilocular D) Control group subcutaneous adipose tissue (SAT) E) Pheo unilocular SAT F) Pheo multilocular group SAT

5.4.3 Study group characteristics

Patient characteristics for the study groups based on pADR adipose tissue morphology are shown in table 5.2. No significant differences were observed for age or BMI between the groups.

	Control	PU	PM
n	20	6	7
Female/male (n)	8/12	4/2	4/3
Age	53.6±1.9	49.5±6.7	58.6±4.7
BMI	30.6±1.7	27.8±3.0	26.8±1.4

Table 5.2 Summary of patient characteristics for study groups control, pheo unilocular (PU) and pheo multilocular (PM) based on pADR adipose tissue morphology. *Data presented as means ± SEM.*

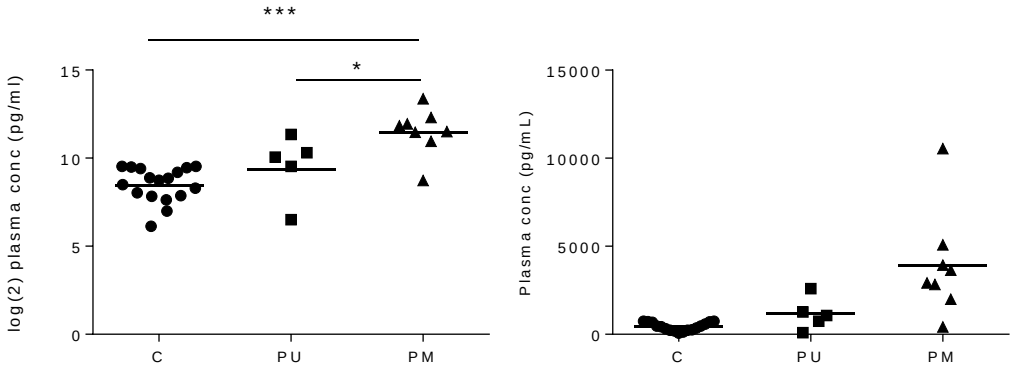
5.4.4 Plasma analyses

5.4.4.1 Catecholamines

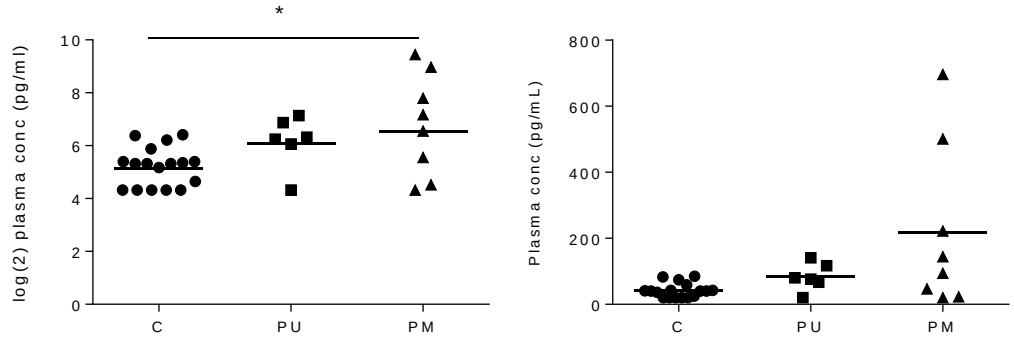
There was a distinct pattern of higher catecholamines (and their metabolites) in the pheo multilocular group compared to pheo unilocular and controls (Figure 5.2). As plasma catecholamines in a large study of pheo patients have been shown to be of skewed distribution, plasma catecholamines were log transformed and analysed with parametric tests and displayed as geometric means as previously described (Eisenhofer et al., 1998). Untransformed data is also shown. For noradrenaline, this was statistically significant between the control and pheo multilocular but not pheo unilocular group. A significant difference was also seen between pheo unilocular and pheo multilocular plasma noradrenaline concentrations. Plasma adrenaline was significantly higher in pheo multilocular patients compared to controls. Normetadrenaline plasma concentrations were significantly increased in pheo unilocular compared to controls and pheo multilocular compared to both pheo

unilocular and controls. Plasma metadrenaline concentrations were significantly increased in pheo multilocular compared to controls. No significant difference was seen between controls and pheo unilocular group compared to controls or pheo multilocular groups.

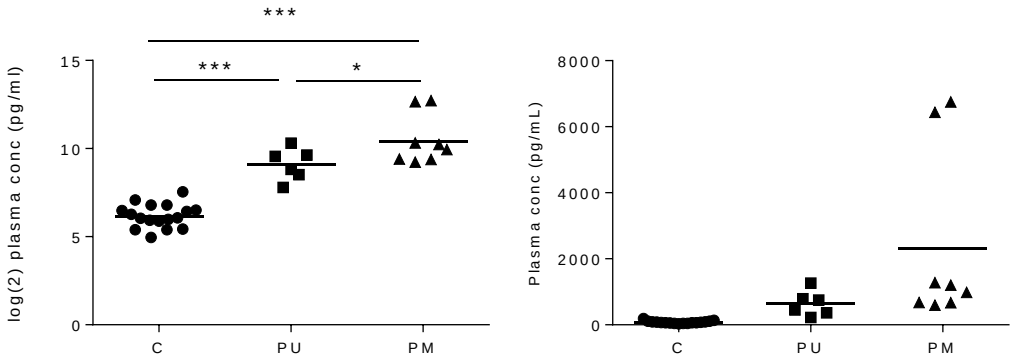
A) Noradrenaline



B) Adrenaline



C) Metnoradrenaline



D) Metadrenaline

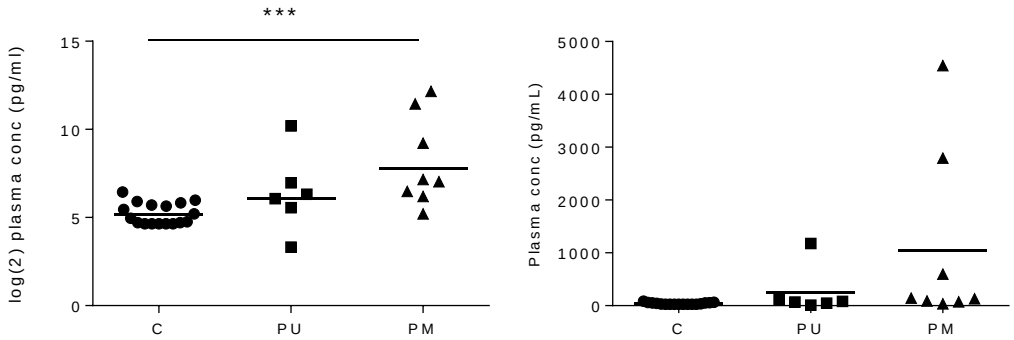


Figure 5.2 Comparison of plasma catecholamine concentrations of control, pheo unilocular and pheomultilocular patients.

*Control (C, n=17), pheo unilocular (PU, n=5-6) and pheo multilocular (PM, n=8) groups. Data on left are shown as log(2) transformed data with group geometric means and analysis with parametric one-way ANOVA. Untransformed data is shown on right with group arithmetic means. A) Noradrenaline B) Adrenaline C) Normetadrenaline D) Metadrenaline. *p<0.05, *** p<0.001*

5.4.4.2 Other plasma hormones and metabolites

No significance was observed between any of the groups for browning hormones ANP, BNP or FGF21 analysed in plasma samples (Table 5.3). Plasma glucose and free fatty acid FFA concentrations showed a trend to be decreased in the pheo multilocular group but were not statistically significant.

Plasma hormone/metabolite	Control	PU	PM
ANP (pg/ml)	33.0±2.2	31.9±4.8	32.4±0.5
BNP (pg/ml)	115.9±19.9	177.4±40.8	102.7±29.1
FGF21 (pg/ml)	638.3±164.2	398.8±265.6	124.1±30.0
Glucose (mmol/l)	6.3±0.4	6.1±0.7	6.0±0.4
FFA (mmol/l)	0.7±0.09	0.5±0.07	0.6±0.1

Table 5.3 Plasma hormone and metabolite concentrations for study groups control, pheo unilocular (PU) and pheo multilocular (PM).

Data presented as means ± SEM for atrial natriuretic peptide (ANP), B-type natriuretic peptide (BNP), fibroblast growth factor 21 (FGF21), glucose and free fatty acid (FFA).

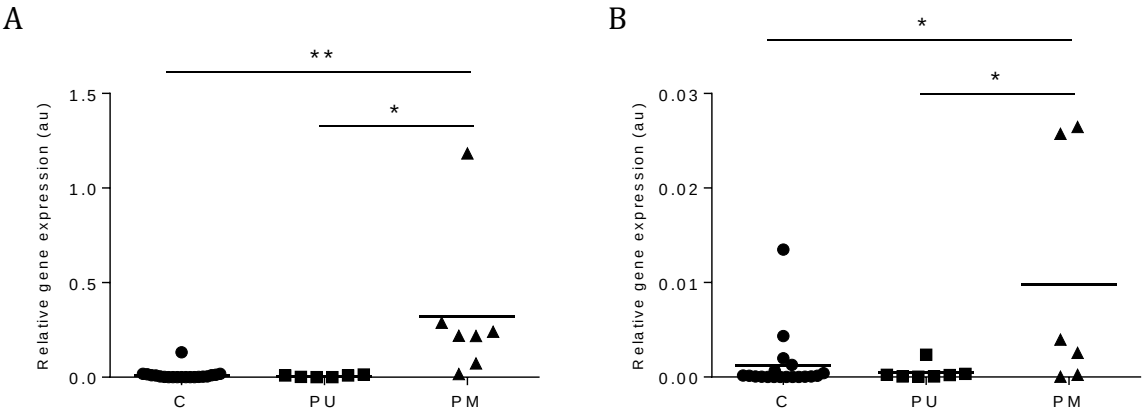
5.4.5. Thermogenic gene expression results

Due to the differences in adipocyte morphology in pADR fat in the pheo group as described above, it was decided to subdivide the pheo group into those with unilocular adipocytes (pheo unilocular, PU) and those with multilocular adipocytes (pheo multilocular, PM) for gene expression analyses. Although reference gene B2M did not vary significantly between groups, it was downregulated in SAT compared to pADR fat. This was also observed in all other reference genes analysed. Therefore comparisons between pADR and SAT were not made for gene expression results and graphs are displayed separately.

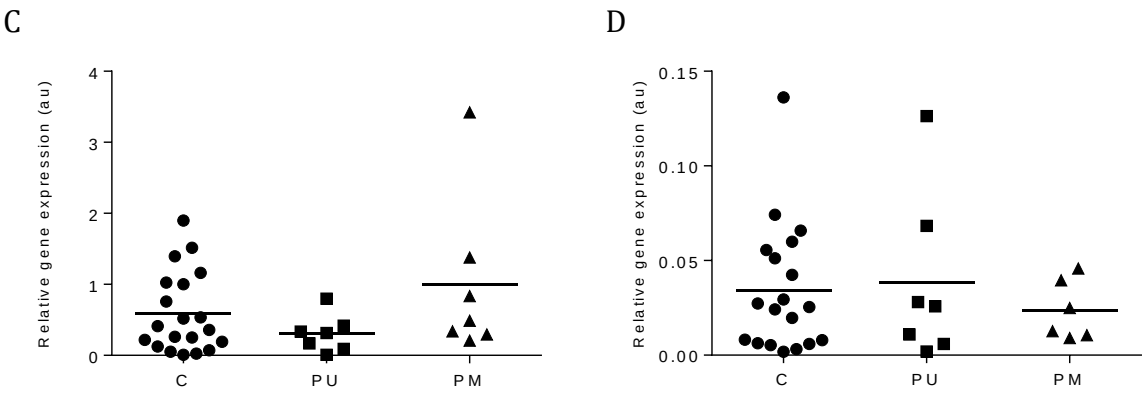
To assess adipocyte browning, thermogenic gene expression was analysed by qPCR (Figure 5.3). Interestingly pADR samples that showed multilocular adipocyte morphology (PM) had significantly elevated UCP1 mRNA compared to those where only white unilocular adipocytes (PU) were observed and the control group (C). A significant upregulation of UCP1 was also noted in the pheo multilocular group in SAT compared to pheo unilocular and controls. PGC1α followed a similar gene expression pattern for pADR fat, with the pheo multilocular group having higher mean gene expression of PGC1α although it was not statistically significant. No significant differences were observed between groups from SAT samples. Higher Ct values were noted for SAT when compared with pADR fat for each group. DIO2 was significantly increased in the pheo multilocular pADR samples compared to pheo unilocular and controls but no significance was observed in SAT samples between

the groups. No significance was observed between the groups for ADRB3 gene expression in either pADR or SAT depots. Higher Ct values were noted for SAT compared to pADR in all groups.

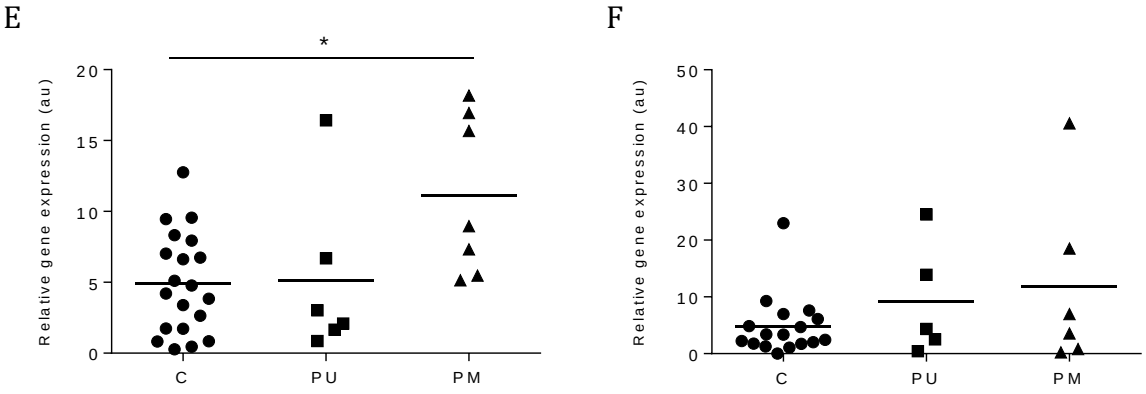
UCP1



PGC1a



DIO2



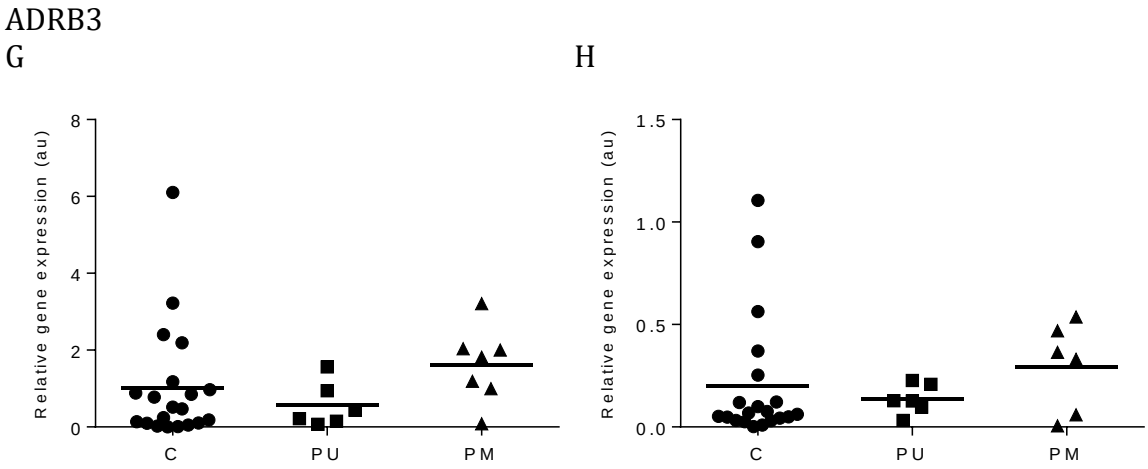


Figure 5.3 Thermogenic gene expression UCP1, PGC1a, DIO2 & ADRB3.

*(A,C,E&G) Periadrenal adipose tissue (pADR) for Control (n=20), pheo unilocular (PU, n=6) and pheo multilocular (PM, n=7) study groups; (B,D,F&H) Subcutaneous adipose tissue (SAT) between Control (n=19), pheounilocular (PU, n=6) and pheo multilocular (PM, n=6) study groups. Scatter plots show individual data points and group means. * p<0.05 **p<0.01. Gene expression values are relative to the reference gene beta 2 microglobulin (B2M)*

5.4.6 Human plasma effects on thermogenesis in brown and white adipocyte cell lines

As there were differences in plasma catecholamine concentrations between the groups, possibly related to differences in adipocyte morphology in pADR adipose tissue and UCP1 gene expression, 3T3-L1 cells capable of displaying browning (Ye et al., 2013) were treated with pooled human plasma from each of the groups or β-3 agonist CL 316,243 as described in Chapter 2 and UCP1 gene expression analysed by qPCR. A trend was seen for an upregulation of UCP1 with pheo multilocular plasma and CL 316,243 treatment but was not statistically significant (Figure 5.4).

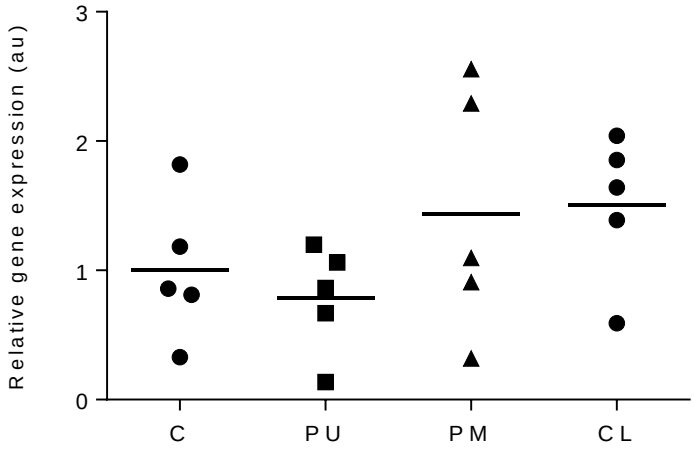


Figure 5.4 UCP1 gene expression in 3T3-L1 adipocytes treated with human plasma.
3T3-L1 adipocytes (n=5 wells per group) were treated with pooled control, pheo unilocular (PU) pheo multilocular (PM) plasma or beta-3 agonist CL 316,243. Results shown as individual data points with group means relative to the expression of reference gene beta 2 microglobulin.

A brown adipocyte cell line available in the laboratory was also treated with human plasma to determine possible differences in the response of white and brown adipocyte cell lines to human plasma treatment. Cellular bioenergetics analyses were performed to assess uncoupled respiration. No significant differences were observed in between cells treated with the 3 groups of pooled human plasma in mitochondrial basal respiration, proton leak or maximal respiration (Figure 5.5). CL 316, 243 served as a positive control and significantly increased mitochondrial basal and maximal respiration compared to DMSO and human plasma treated cells. Proton leak (i.e. uncoupled respiration) was increased in CL 316,243 treated adipocytes compared to DMSO and pheo unilocular plasma treated cells but not control (p=0.052) and pheo multilocular plasma treated cells (p=0.054). Spare respiratory

capacity was not able to be calculated in human plasma treated cells as it was below basal respiration measurements, a result not observed in DMSO or CL treated cells.

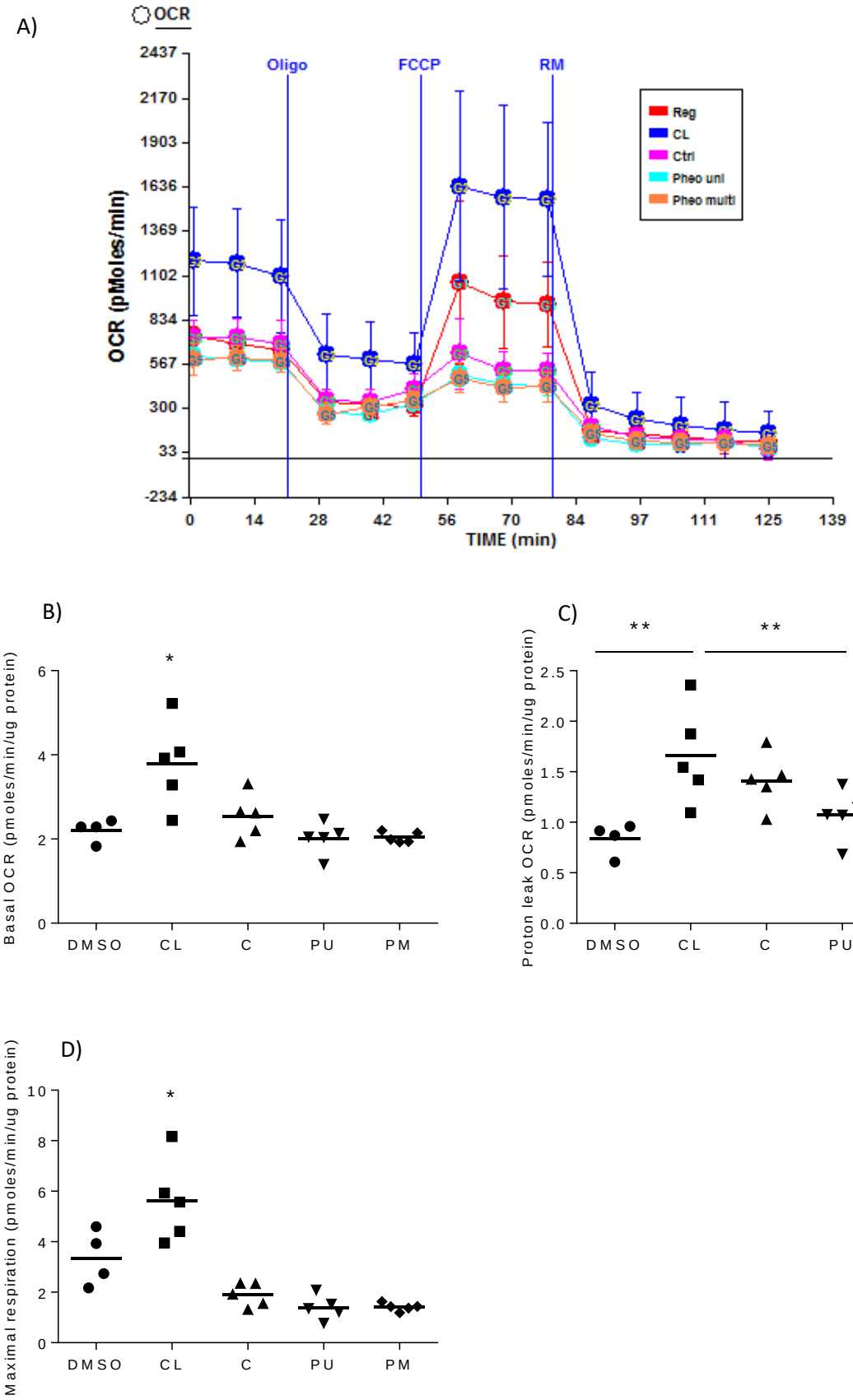

A)
OCR
Oligo
FCCP
RM
Reg
CL
Ctrl
Pheo unl
Pheo multl
OCR (pMoles/mln)
2437
2170
1903
1636
1369
1102
834
567
300
33
-234
0
14
28
42
56
70
84
97
111
125
139
TIME (min)
B)
Basal OCR (pmoles/min/ug protein)
*
DMSO
CL
C
PU
PM
C)
**
**
Proton leak OCR (pmoles/min/ug protein)
D)
Maximal respiration (pmoles/min/ug protein)

Figure 5.5 Cellular bioenergetics analysis of immortalized brown adipocytes treated with human plasma.

Brown adipocytes were treated with DMSO (Reg, n=4) or pooled control (Ctrl or C, n=5), pheo unilocular (PU, n=5) pheo multilocular (PM, n=5) plasma or beta-3 agonist CL 316,243 (CL, n=5). A) Raw data of oxygen consumption measurements between groups, displayed as mean±SD. B) Basal mitochondrial respiration C) Mitochondrial Proton leak D) Maximal mitochondrial respiration. Basal, maximal and proton leak data displayed normalized to total protein per well expressed per µg protein.

5.4.6 Tissue gene expression analysis of beige adipocyte markers

To assess if beige adipocyte abundance may be related to adipose tissue browning, gene expression of PAT2, MTUS variant 3 and KCNK3 were analysed as markers of beige adipocytes within pADR and SAT samples by qPCR (Figure 5.6). PAT2 showed a significant increase in PM pADR adipose tissue samples compared to control and PU. No significant difference was observed between control and pheo unilocular PAT2 gene expression in the pADR depot. PAT2 gene expression did not differ between groups for SAT samples. Gene expression of MTUS variant 3 and KCNK3 did not differ significantly between the groups in either pADR or SAT depots.

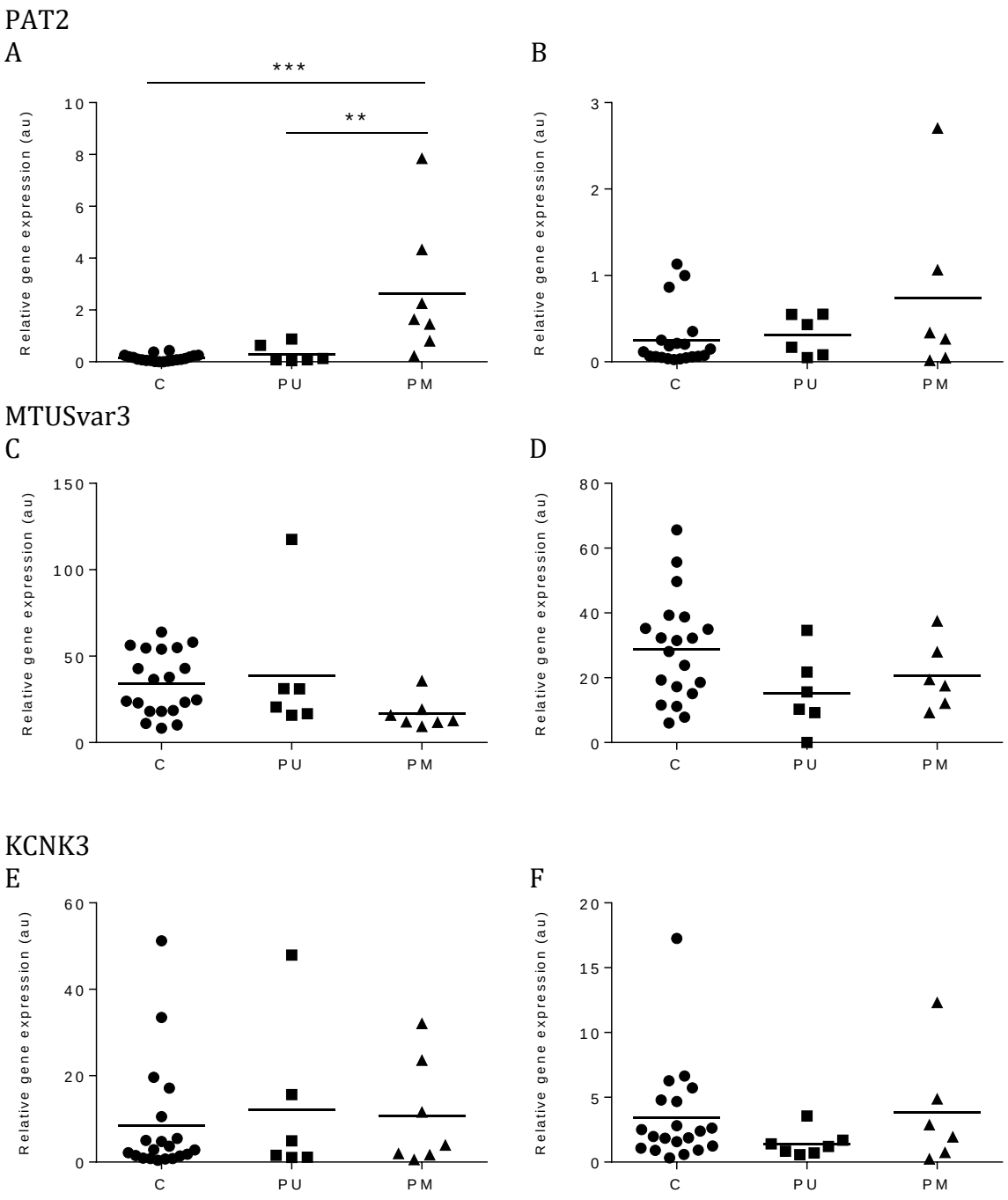


Figure 5.6 Beige marker gene expression PAT2, MTUSvar3 and KCNK3.

*A,C&E) Periadrenal adipose tissue (pADR) for Control (n=20), pheo unilocular (PU, n=6) and pheo multilocular (PM, n=7) study groups B,D&F) Subcutaneous adipose tissue (SAT) between Control (n=19), pheounilocular (PU, n=6) and pheo multilocular (PM, n=6) study groups. Scatter plots show individual data points and group means. * p<0.05 **p<0.01. Gene expression values are relative to the reference gene beta 2 microglobulin (B2M).*

5.4.7 White adipocyte marker ASC-1

A cell surface marker selective for white adipocytes ASC-1, showed a trend to decrease in the pheomultilocular group compared to pheo unilocular and controls but was not statistically significant. Similarly, no significant differences were observed between groups in SAT samples (Figure 5.7).

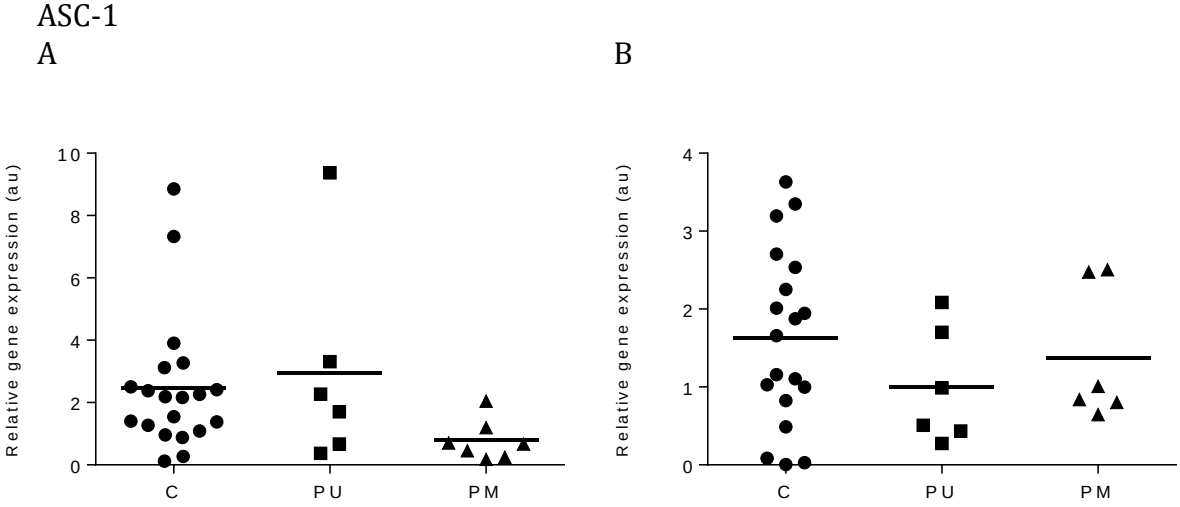


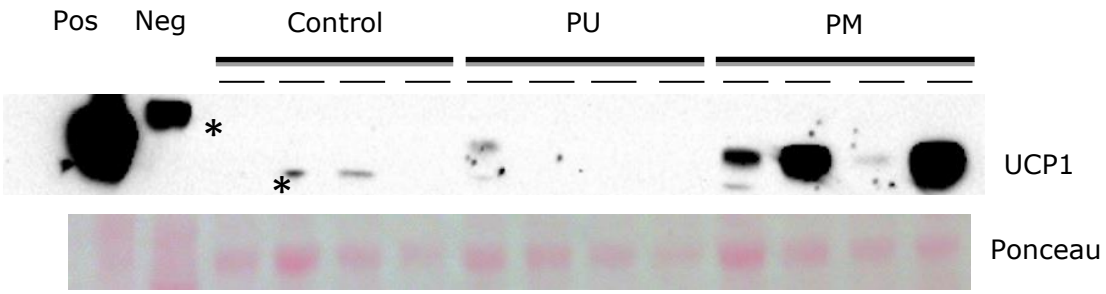
Figure 5.7 White adipocyte marker ASC-1 gene expression.

A) Periadrenal adipose tissue (pADR) for Control (n=20), pheo unilocular (PU, n=6) and pheo multilocular (PM, n=7) study groups and B) Subcutaneous adipose tissue (SAT) between Control (n=19), pheounilocular (PU, n=6) and pheo multilocular (PM, n=6) study groups. Scatter plots show individual data points and group means. Gene expression values are relative to the reference gene beta 2 microglobulin (B2M)

5.4.8 UCP1 Western Blot results

To determine if UCP1 abundance followed the results seen by gene expression analysis, a western blot was performed on pADR fat (n=4 per group) and SAT (control n=3, pheo unilocular n=2, pheo multilocular n=2). Lower sample numbers were run in SAT as there was insufficient tissue to run all of the samples used for pADR adipose tissue. Samples were chosen where there was sufficient tissue to extract protein (for SAT) and the same samples were used for pADR adipose tissue with other samples chosen at random from the three study groups for n=4 per group for pADR adipose tissue. Mouse interscapular BAT (iBAT) and liver mitochondrial protein was extracted using the same methods as human samples and were loaded on gels as positive and negative controls respectively. Clear UCP1 bands were seen in 3 out of the 4 pheo multilocular group in pADR fat with a fainter UCP1 band also seen in one sample (Figure 5.8). These UCP1 bands appear much fainter than mouse BAT which was relatively overexposed compared to UCP1 bands from human samples. Less mitochondrial protein for mouse BAT was loaded on the SAT gel to prevent this. No UCP1 bands were seen in any of the control or pheo unilocular group patients. In SAT no UCP1 bands were seen for any of the patient samples including those showing multilocular adipocyte morphology in pADR fat. A pADR sample was also run on the SAT gel as well as murine BAT and liver (Figure 5.8).

pADR



SAT

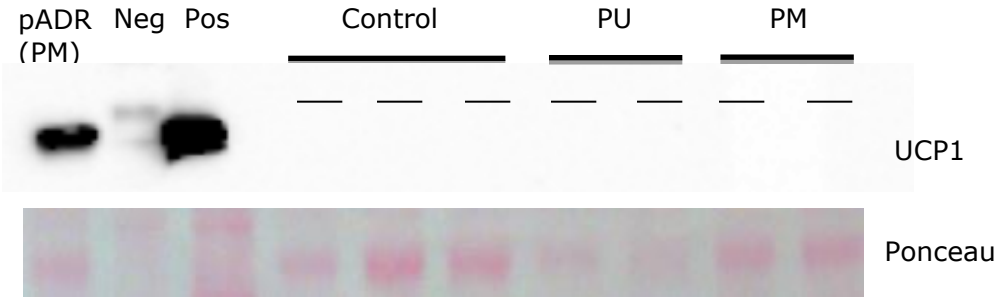


Figure 5.8 Western blot images from A) pADR Control, Phei unilocular (PU) and Pheo Multilocular (PM), n=4 per group. B) SAT Control (n=3), Pheo unilocular (PU, n=2) and Pheo multilocular (PM, n=2).

*6µg mitochondrial protein was loaded per well, Ponceau staining is shown below each sample to show transfer of protein to the membrane. *non-specific bands*

5.4.9 UCP1 IHC results

To further examine UCP1 abundance, immunohistochemistry was also performed on both pADR and SAT samples (n=4 per group) using the same antibody used in the above western blots. This was important to confirm the findings for western blot particularly for SAT samples where limited tissue allowed only a small number of pheo unilocular and multilocular samples to be analysed. UCP1 positive staining was observed in the pheo multilocular group in pADR adipose tissue with no UCP1 staining observed in control or pheo unilocular patient samples. No UCP1 staining was observed in SAT from any of the samples (Figure 5.9).

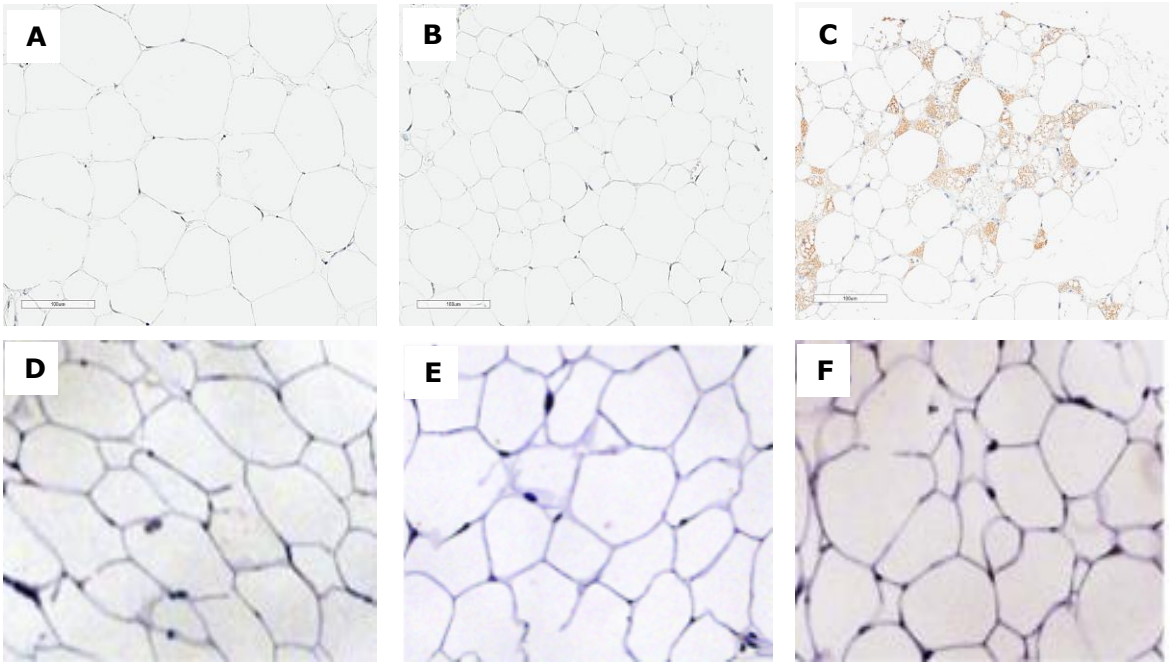


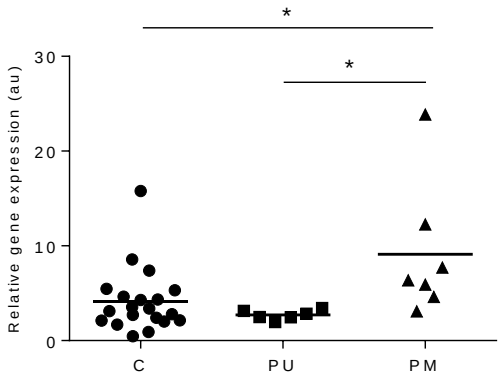
Figure 5.9 Representative images of 5µm thick sections stained with UCP1 antibody.
A) pADR control; B) pADR pheo unilocular; C) pADR pheo multilocular; D) SAT control; E) SAT pheo unilocular and F) SAT pheo multilocular

5.4.10 Mitochondrial gene expression and abundance

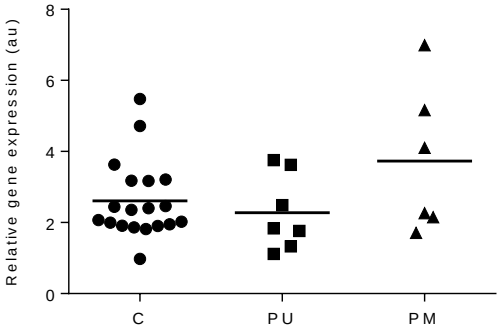
Transcripts of genes involved in mitochondrial activity through the electron transport chain were analysed by qPCR. A similar pattern was seen for NDUFB9 (Complex I), SDHB (Complex II), UQCRFS1 (Complex III) and COX7B (Complex IV) with a significant increase in gene expression in the pheo multilocular group compared to pheo unilocular and controls. No significance was observed between control and pheo unilocular groups in pADR. In SAT no significant differences were observed between any of the groups in the mitochondrial genes analysed.

NDUFB9

A)

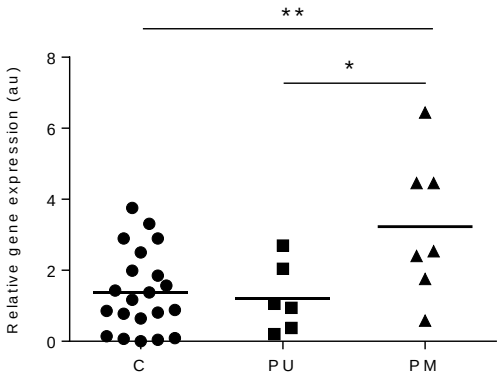


B)

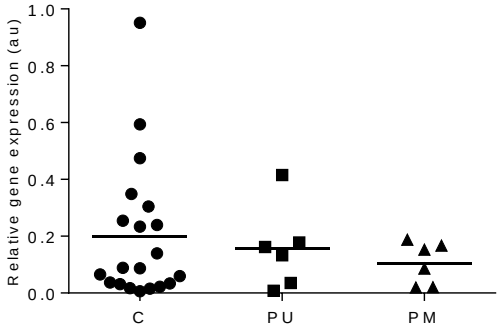


SDHB

C)

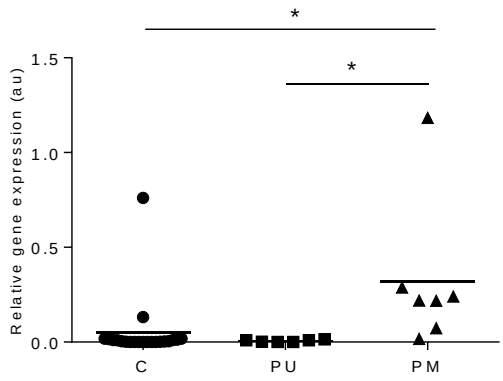


D)

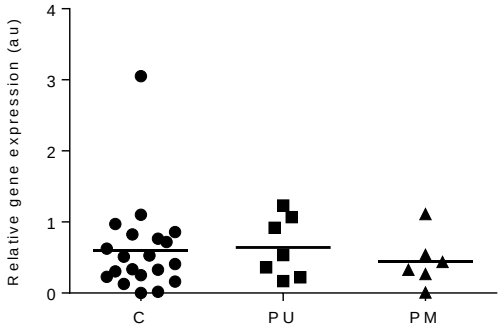


UQCRFS1

E)



F)



COX7B

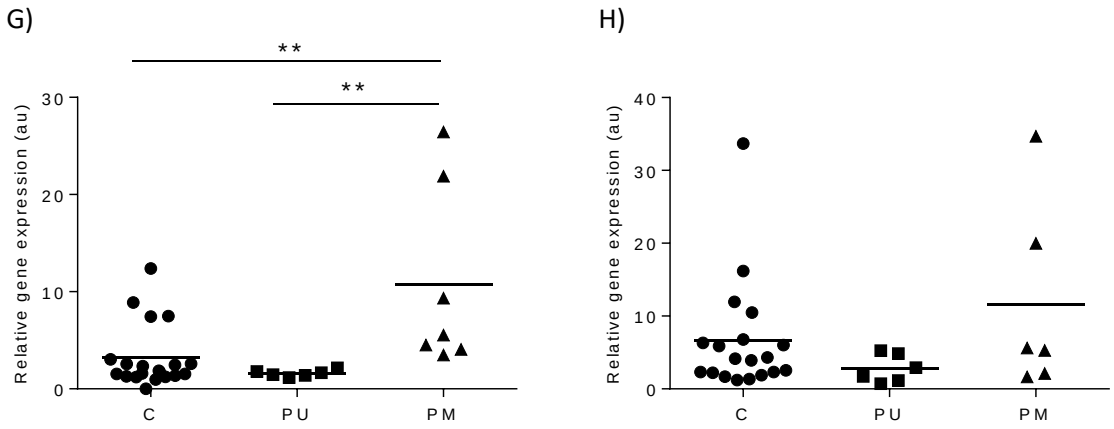


Figure 5.10 Mitochondrial gene expression NDUFB9, SDHB, UQCRFS1 and COX7B.

*A,C,E&G) Periadrenal adipose tissue (pADR) for Control (n=20), pheo unilocular (PU, n=6) and pheo multilocular (PM, n=7) study groups B,D,F&H) Subcutaneous adipose tissue (SAT) between Control (n=19), pheounilocular (PU, n=6) and pheo multilocular (PM, n=6) study groups. Scatter plots show individual data points and group means. * p<0.05 **p<0.01. Gene expression values are relative to the reference gene beta 2 microglobulin*

Increased mitochondrial activity may be due to increased beta oxidation of fatty acids for thermogenesis in the pheo multilocular group and to obtain an indication of this, Acyl-CoA Dehydrogenase, C-4 to C-12 Straight Chain (ACADM, an enzyme involved in the initial step in the beta oxidation pathway) gene expression was analysed by qPCR (Figure 5.11). There was a trend for ACADM to be increased in the pheo multilocular group in pADR although this was not significant (p=0.08). No significance was also observed between groups in SAT samples.

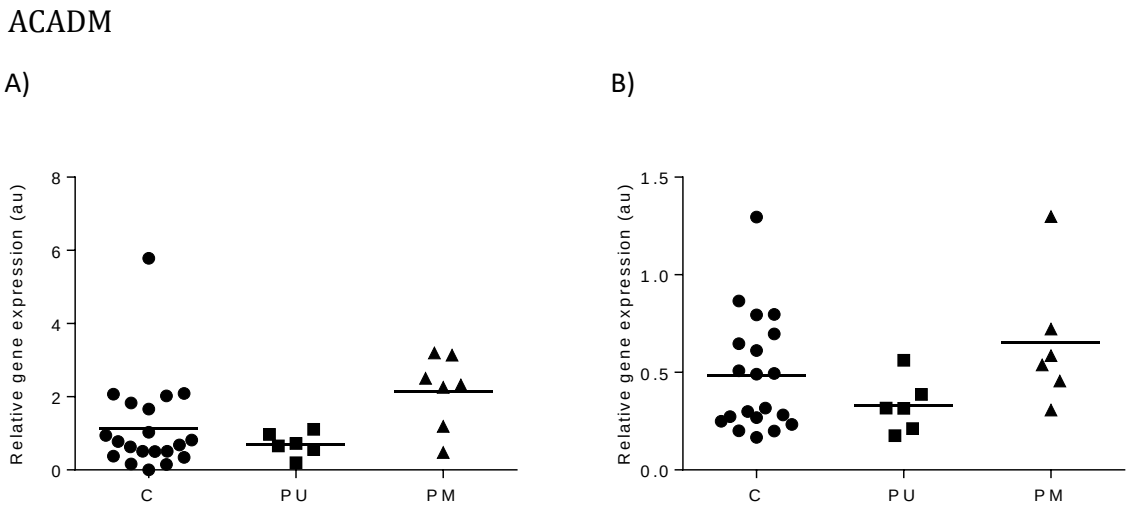


Figure 5.11 ACADM gene expression.

A) Periadrenal adipose tissue (pADR) for Control (n=20), pheo unilocular (PU, n=6) and pheo multilocular (PM, n=7) study groups; B) Subcutaneous adipose tissue (SAT) between Control (n=19), pheounilocular (PU, n=6) and pheo multilocular (PM, n=6) study groups. Scatter plots show individual data points and group means.

To determine whether mitochondrial abundance varied between the groups, mitochondrial abundance was determined by mitochondrial protein yield from samples used for western blots using a BCA assay and mtDNA/nDNA ratios were analysed for pADR samples as previously described. It was hypothesized that pADR samples from the pheo multilocular group would have increased mitochondrial abundance due to the brown adipocytes having abundant mitochondria. No significant differences were observed between any of the groups in mitochondrial protein for pADR samples (Fig 5.12 A). Statistical analysis was not performed for SAT samples due to small sample number for pheo unilocular and multilocular

samples (n=2 per group). No significant differences were observed in mtDNA/nDNA ratio between groups for pADR samples analysed (Figure 5.12 B).

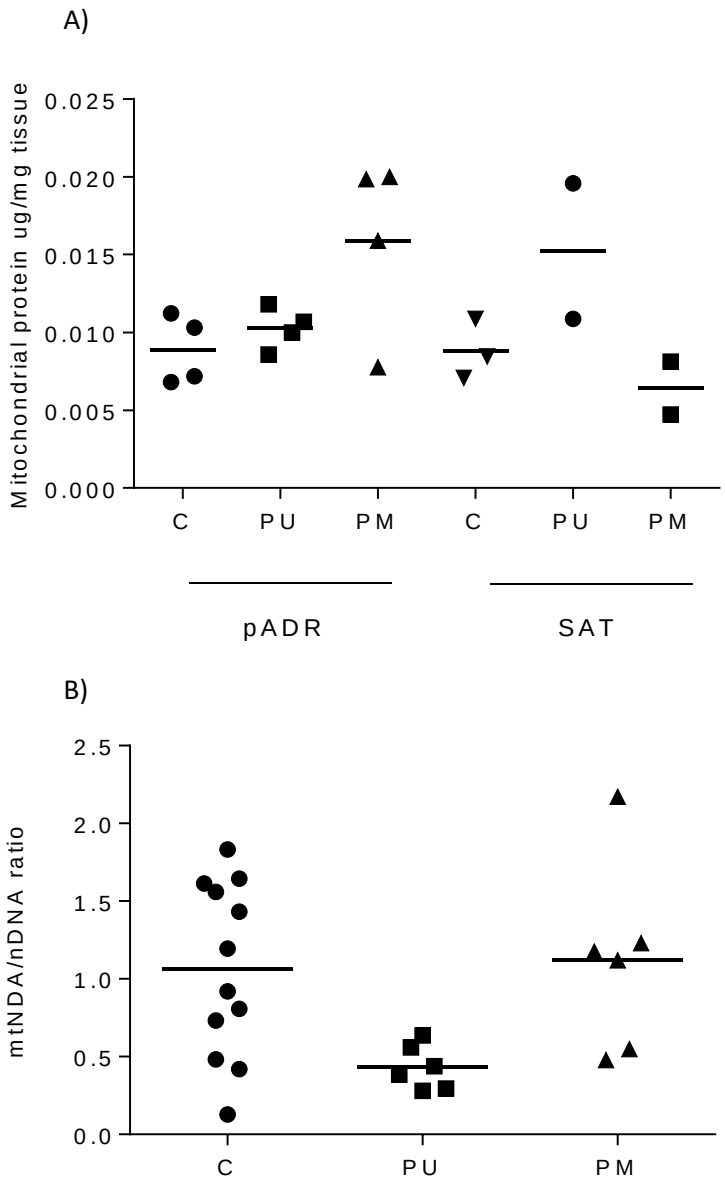


Figure 5.12 Mitochondrial abundance analyses.

A) Mitochondrial protein abundance in pADR control (C, n=4), pheo unilocular (PU, n=4) and pheo multilocular (PM, n=4), and SAT control (C, n=3), pheo unilocular (PU, n=2) and pheo multilocular (PM, n=2); B) mitochondrial DNA (mtDNA) to nuclear DNA (nDNA) ratio in pADR control (n=12), pheo unilocular (PU, n=6) and pheo multilocular (PM, n=6). Data displayed as individual data points and group means.

5.4.11 Cellular bioenergetics analyses

To analyse mitochondrial activity functionally and particularly uncoupled respiration as an indication of UCP1 activity, mitochondria were isolated from adipose tissue biopsies and run using an extracellular flux analyzer using a coupling assay as described in Chapter 2. This allows uncoupled respiration and the RCR to be determined. An example of raw OCR measurements is shown in Figure 5.13 from paired pADR and SAT samples.

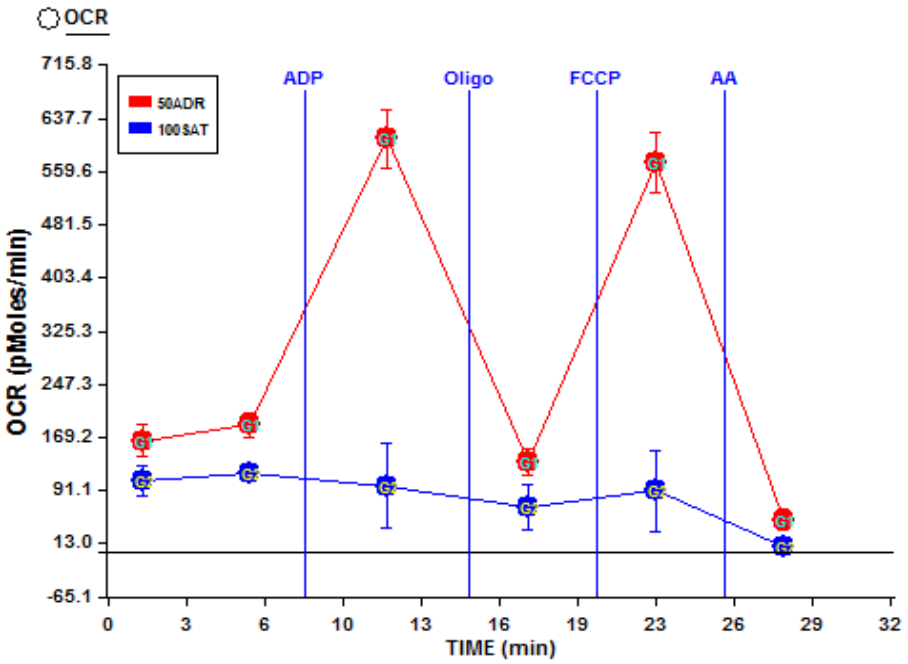


Figure 5.13 Coupling assay: OCR measurements vs Time for paired pADR (red) and SAT (blue) samples from the same patient.

100µg SAT and 50µg were loaded per well to obtain measurable OCR. Raw data shown as mean±SD of technical replicates.

A significant increase in mitochondrial basal respiration was seen in pADR pheo multilocular group compared to pheo unilocular and controls (Figure 5.14 A). SAT had significantly reduced mitochondrial basal respiration compared to pADR for all groups. No significance was seen between groups in SAT samples.

Mitochondrial uncoupled respiration (proton leak) was increased significantly in pADR of pheo multilocular samples compared to pheo unilocular and controls (Figure 5.14 B). SAT samples showed low uncoupled respiration and no significant differences were observed between the groups. When expressed as respiratory control ratio (RCR, calculated as State3/State 4o respiration), a trend was seen for decreased RCR in pADR pheo multilocular compared to pheo unilocular and controls but was not significant (Figure 5.14 C). A possible outlier was noted for the pheo unilocular group although exclusion of this sample from the analysis did not alter statistical significance. No difference was observed between SAT groups. SAT RCR was similar to pADR due to low state 3 respiration. Maximal respiration did not differ significantly between the groups in pADR or SAT samples (Figure 5.14 D).

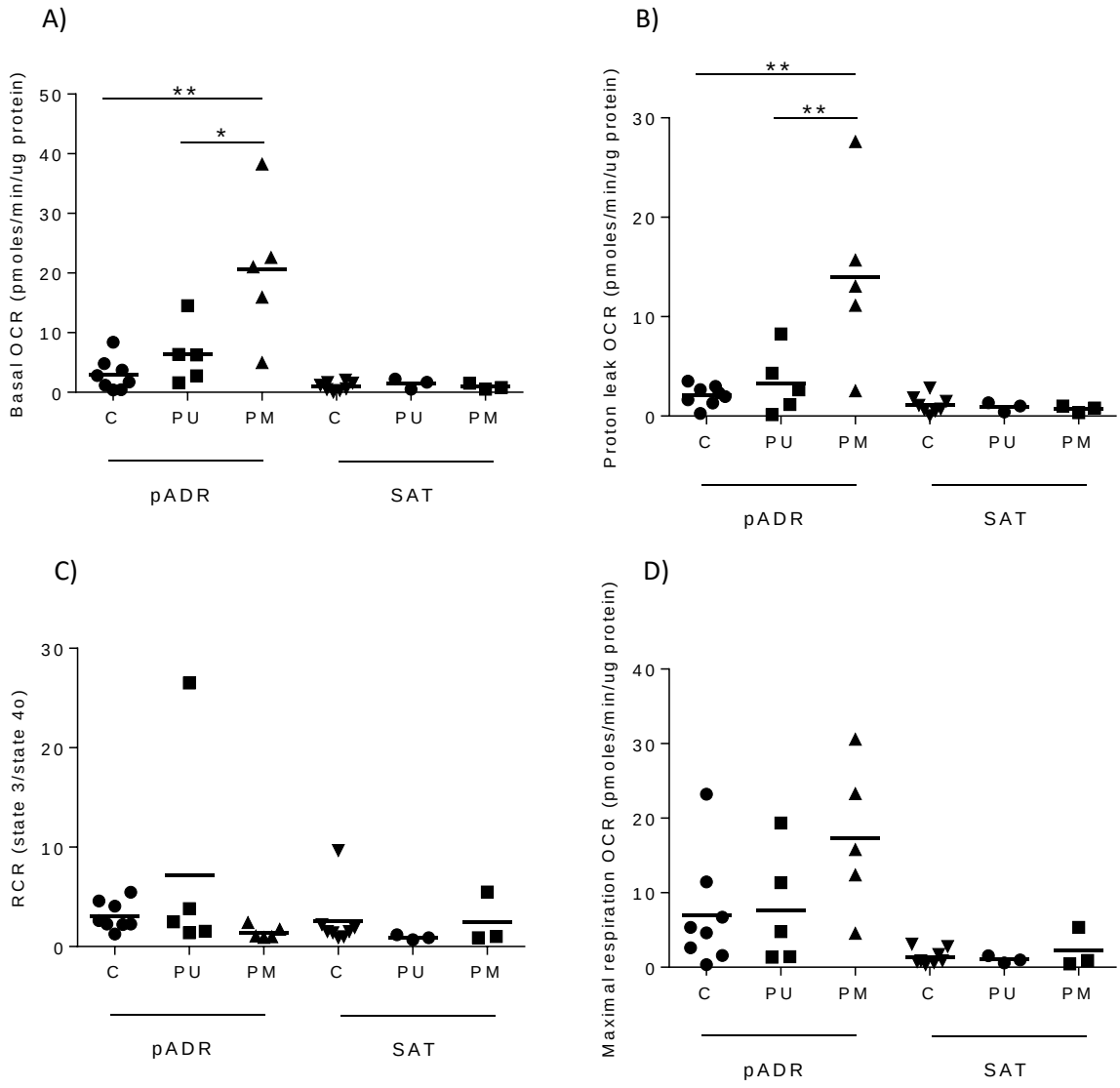


Figure 5.14 Coupling assay oxygen consumption rates (OCR) of isolated mitochondria.

*Samples from periadrenal (pADR) control (C, n=10) pheo unilocular (PU, n=5) and pheo multilocular (PM, n=5) samples and SAT control (C, n=8), pheo unilocular (PU, n=3) and pheo multilocular (PM, n=3) were analysed for A) Basal mitochondrial respiration B) Mitochondrial proton leak (uncoupled respiration) C) Respiratory control ratio D) Maximal respiration. Data is normalized to µg mitochondrial protein and displayed as scatter plots and group means. *p<0.05, **p<0.01*

As basal respiration was increased in pADR adipose tissue samples in the pheo multilocular group compared to pheounilocular and controls, an electron flow analysis was also conducted to assess the activity of electron transport chain complexes I-IV. A representative OCR experiment is shown in Figure 5.15 from paired pADR and SAT samples from showing the different injections used and response of mitochondria.

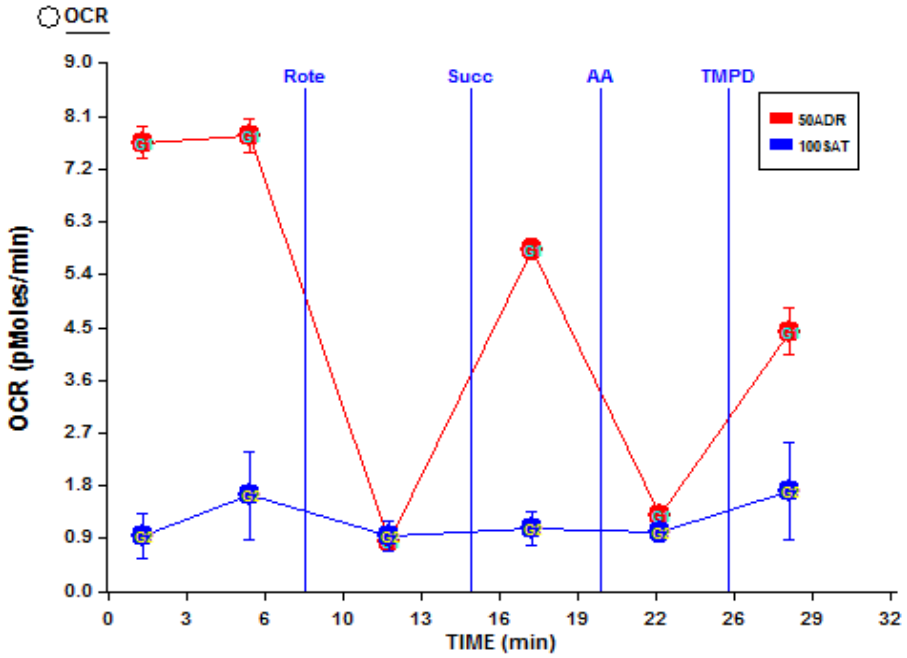


Figure 5.15 Electron flow assay: Oxygen consumption rate (OCR) vs Time for pADR (red) and SAT (blue) samples from the same patient.

100µg SAT and 50µg pADR were loaded per well to obtain measurable OCR. Raw data shown as mean±SD of technical replicates.

Significantly increased complex I, II and IV respiration was observed in pheo multilocular mitochondria compared to pheo unilocular and controls in pADR (Figure 5.16). A trend for increased complex III respiration was seen in the pheo

multilocular group for pADR although it was not statistically significant possible due to high variation seen in the control and pheo unilocular group. Due to the small number of SAT samples used in the electron flow assays, particularly for the pheo unilocular group (n=2), statistical analyses were not performed but individual data points are displayed.

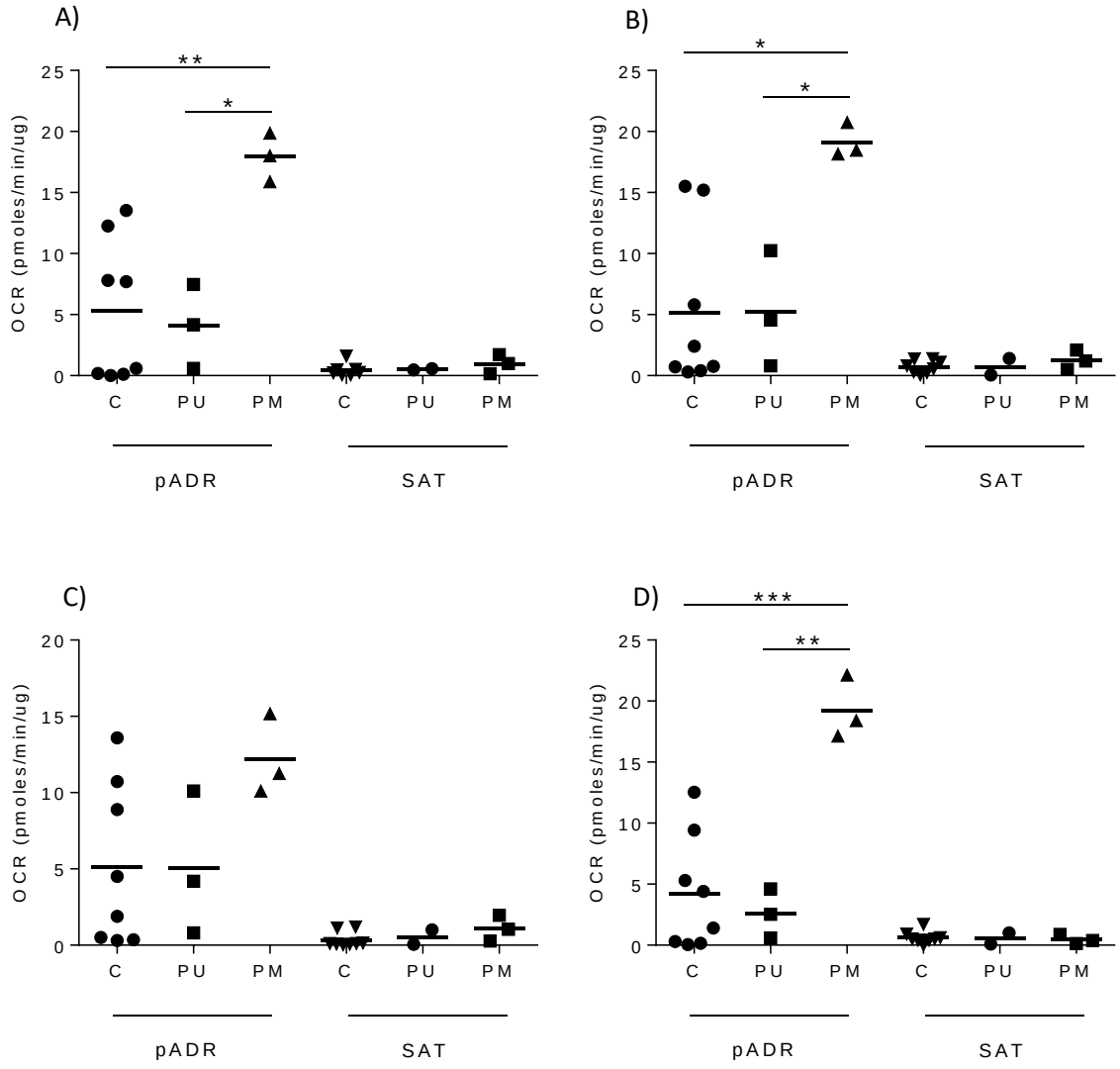


Figure 5.16 Electron flow assay oxygen consumption rates (OCR) of isolated mitochondria.
*Samples from peridrenal (pADR) - control (C, n=10) pheo unilocular (PU, n=5) and pheo multilocular (PM, n=5) samples and SAT - control (C, n=8), pheo unilocular (PU, n=2) and pheo multilocular (PM, n=3). A) Complex I B) Complex II C) Complex III D) Complex IV. Data is normalized to µg mitochondrial protein and displayed as scatter plots and group means. *p<0.05, **p<0.01*

5.4.12 Frequency of-3286A/G UCP1 polymorphism

As a SNP polymorphism in the UCP1 promoter is associated with decreased UCP1 mRNA, the SNP was assessed in samples from control, pheo unilocular and pheo multilocular pADR samples to see if there may be genetic factors resulting in decreased UCP1 rather than differences in plasma catecholamine concentrations. It was hypothesised that those in the pheo unilocular group may have shown decreased UCP1 mRNA compared to the pheo multilocular group due the presence of A/G polymorphism. DNA was extracted from samples and amplified by PCR and sequenced. Examples of sequencing results for the different polymorphisms are shown in Figure 5.17.

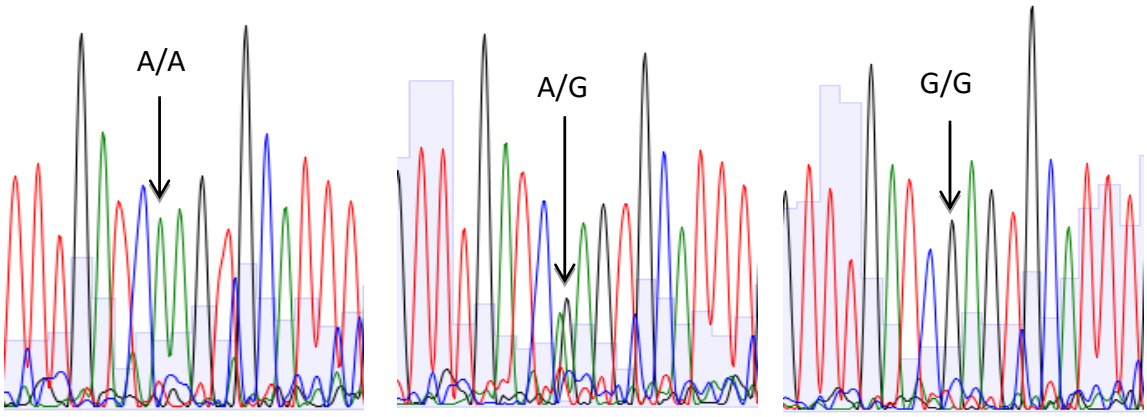


Figure 5.17 Sequencing reads for -3286A/G UCP1 polymorphisms A/A, A/G and G/G. SNP location in shown by an arrow.

Group	Genotype		
	A/A	A/G	G/G
Control (n=12)	3	8	1
Pheo Unilocular (n=5)	4	1	0
Pheo multilocular (n=6)	3	1	2

Table 5.4 Frequency table of genotypes of UCP1 SNP polymorphism

The A/G genotype was present only in 1 of the pheo unilocular group and none had the homozygous minor allele (Table 5.4). Although in a small number of patients, the decreased UCP1 mRNA in the pheo unilocular group is not associated with a UCP1 promoter G/G genotype.

5.4.13 Outdoor temperature analysis

It has previously been reported that in patients with benign adrenal tumours (including pheochromocytoma), reduced UCP1 mRNA is associated with colder outdoor temperatures in the month prior to surgery (Betz et al., 2013). Therefore, it was assessed if there was a correlation between average outdoor temperature in the month of and month prior to, surgery and UCP1 mRNA in this study. Data was analysed and presented as previously described (Betz et al., 2013). No significant linear regression was observed between outdoor temperature and UCP1 mRNA in controls, pheos or all control patients and pheo groups combined (Figure 5.18).

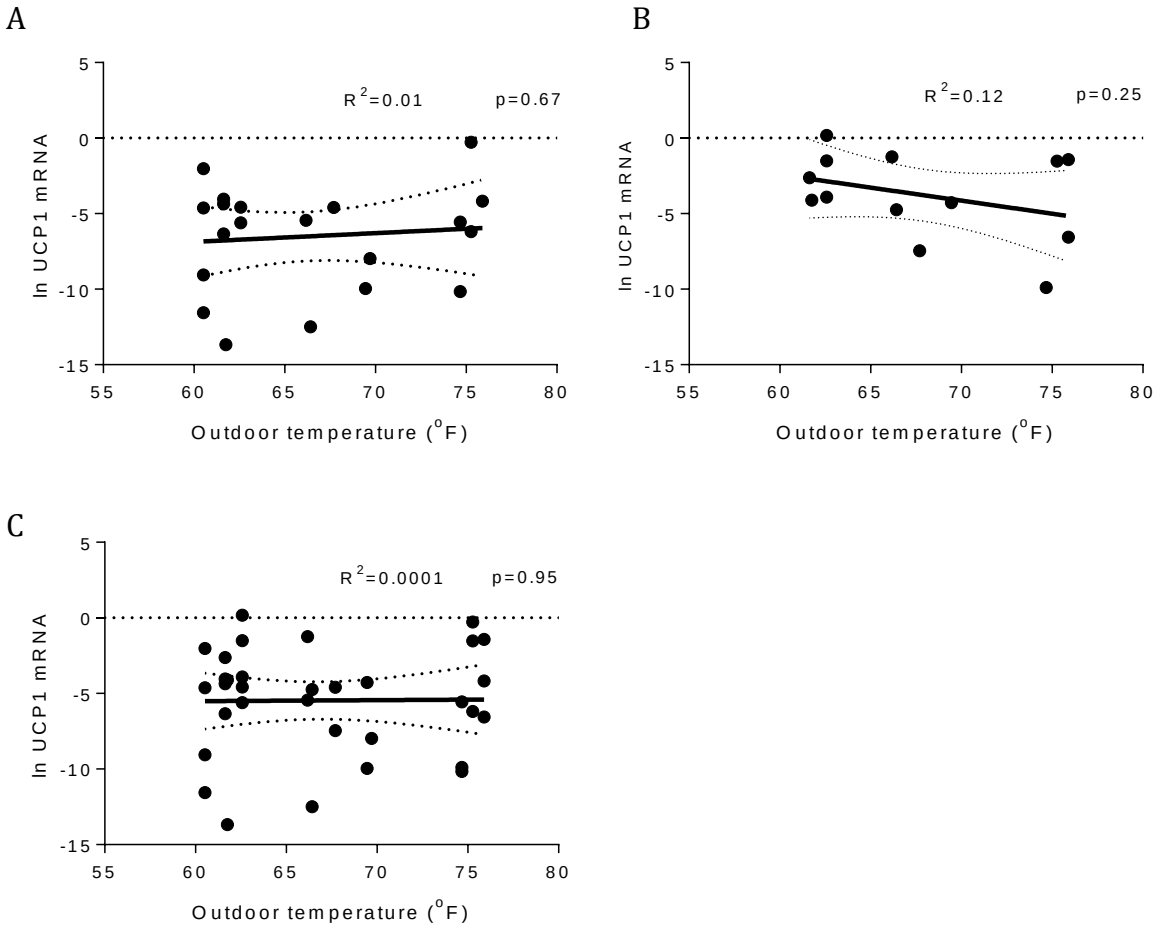


Figure 5.18 Linear regression of ln transformed UCP1 mRNA and average outdoor temperature (°F) in month of and month prior to surgery.

A) Control group (n=20) B) Combined pheo unilocular (n=6) and pheo multilocular (n=7) C) All control and pheo patients (n=34)

5.5 Discussion

5.5.1 Browning of pADR adipose tissue and augmented mitochondrial function occurs in a subset of pheo patients with highest plasma noradrenaline concentrations

In accordance with a previous study analyzing perirenal adipose tissue (Nagano et al., 2015), browning was noted in pADR from 7/13 (54%) pheo patients, based on the presence of UCP1, multilocular adipocyte morphology and increased uncoupled respiration. This is similar to previously reported omental adipose tissue browning rates in pheo patients as Frontini et al found 6/12 (50%) pheo patients had UCP1 positive adipocytes (Frontini et al., 2013). In the perirenal adipose tissue depot, Betz et al reported 5/8 (63%) have adipose tissue browning or UCP1 positive adipocytes.

Interestingly, the pheo patients that exhibited browning of pADR adipose tissue in my study had significantly higher concentrations of noradrenaline and metnoradrenaline (noradrenaline metabolite) than the pheo unilocular group. Noradrenaline is well established to cause adipose tissue browning (Garofalo et al., 1996; Inokuma et al., 2005) so it is therefore a possible factor contributing to the differing adipose tissue morphology between the pheo patients. A previous study reported that only pheo patients with elevated (>185ng/l) total metanephrines (TMN, metnoradrenaline+metanephrine) had increased BAT activity in perirenal adipose tissue based on FDFG uptake by PET-CT scans compared to pheos with normal TMN (Wang et al., 2011). However, both pheo

unilocular and multilocular groups in my study had plasma TMN within their 'high TMN' group of >185ng/l plasma TMN. It is interesting in the study of Wang et al that the two pheo subjects with no BAT activity that had the lowest plasma TMN within the high TMN group (Wang et al., 2011), which may be in accordance with my findings. They also had the highest BMI which cannot be ruled out as a confounding factor. My results may suggest therefore that catecholamine values necessary for browning in pheochromocytoma can be divided further when adipose tissue browning is known, as their paper used 2SD from normal to divide their pheo groups into high and normal TMN before assessing BAT activity (Wang et al., 2011). They also did not report the association of TMN and BAT activity for only their pheo patients as the inclusion of non-pheo patients with normal TMN and low BAT activity may have driven a significant linear regression.

Betz et al however previously reported no difference in plasma metanephrines between BAT positive and negative patients (Betz et al., 2013). This is likely due to their study finding BAT in patients with non-functioning, cortisol and aldosterone secreting tumours without elevated plasma metanephrines and the small number of pheo patients studied which would not allow comparisons of BAT positive and negative patients specifically in those with pheochromocytoma.

Plasma concentrations of other browning hormones (ANP, BNP and FGF21) were not significantly altered in my study with pheochromocytoma. Catecholamines such as noradrenaline have previously been described to increase atrial

secretion of ANP (Schiebinger et al., 1987; Speake et al., 1993); however results in patients with pheo are conflicting. A previous study of 3 pheo patients found plasma ANP concentrations were normal in basal resting conditions prior to surgery but were increased intra-operatively during pheochromocytoma dissection (Donckier et al., 1991). Plasma ANP and BNP have more recently been found to be elevated in patients with untreated pheochromocytoma but are decreased with phenoxybenzamine antihypertensive treatment (Hu et al., 2015b). All patients with pheochromocytoma in my study were taking phenoxybenzamine medication which may have blunted plasma increases in ANP and BNP to elevated plasma catecholamines.

Adipose tissue samples from pheo patients have previously been found to express FGF21 mRNA and protein to a greater extent than samples from non-pheo patients (Hondares et al., 2014). FGF21 mRNA also was reported to be correlated with UCP1 mRNA although it is possible that this was driven by an outlier with high FGF21 and UCP1 mRNA based on their data points. Unfortunately in my study I was unable to obtain suitable primers to assess FGF21 mRNA by qPCR in the samples. FGF21 plasma concentrations were not significantly altered by pheochromocytoma in my study but this was not assessed by Hondares et al, so it is not clear if increased FGF21 production by adipocytes would be detected in the circulation. It could be hypothesized that increased FGF21 production by adipocytes would have autocrine or paracrine effects on the surrounding tissues similar to that suggested in rodents (Fisher et al., 2012) and cannot be ruled out in my study.

As norepinephrine was the only browning hormone studied to be significantly upregulated in pheo patients with multilocular adipocyte morphology, my data suggest that elevated norepinephrine may play a role in the adipose tissue browning observed in a subgroup of pheo patients. Experiments to assess the effects of plasma from the different patient groups on immortalized white and brown adipocyte cell lines did not show any effect on UCP1 mRNA or uncoupled respiration. This may be due to the rodent origin of these cell lines (Green and Kehinde, 1975; Uldry et al., 2006), which may respond differently to human plasma. Unfortunately human adipocyte cell lines were not available which may have been more appropriate for the experiment. Mitochondrial toxicity could also not be ruled out as maximal respiration was decreased in cells treated with human plasma, which has previously been observed with drugs toxic to mitochondria (Beeson et al., 2010). The amount of human plasma to media (%v/v) added to the cells may not have been optimal and the results may be inconclusive to determine if changes in adipose tissue browning are caused by plasma differences in pheo unilocular and multilocular groups.

Other factors may have contributed to the browning difference in pheo groups in addition to differences in plasma hormone concentrations, including environmental factors, although no association was seen in controls or pheos with outdoor temperature prior to surgery. This is in contrast with previous data showing colder outdoor temperatures in the month prior to surgery are associated with increased UCP1 in perirenal adipose tissue of 57 patients with benign adrenal tumours, including 8 patients with pheochromocytoma (Betz et

al., 2013). This may be due to differences in climate and geographical location of the studies. Betz et al studied patients in Munich where the outdoor temperature ranged from approximately -2°C as the coldest average monthly temperature prior to patient surgery to +22°C at the warmest. In contrast, the average outdoor temperature for my study in Los Angeles ranged from 15.6^{o}C (60.1 ^{o}F) at the coldest to 24.4^{o}C (75.9 ^{o}F) at the highest. These warmer temperatures and decreased seasonal variation of temperature may have resulted in no observed association with temperature and UCP1 mRNA in my study. Indeed, a previous studdies reporting increased BAT activity by PET/CT with colder outdoor temperatures showed a large temperature range from -30°C to +30°C (Ouellet et al., 2011) or have been conducted in locations with varying seasonal temperatures such as the UK (Au-Yong et al., 2009).

Colder outdoor temperatures may also be a possible reason for Betz et al finding BAT positive individuals with non-functioning, cortisol and aldosterone secreting tumour groups which were not observed in my study (control group). There are however several issues with BAT positive associations and retrospective outdoor temperature studies. For example, it is not known the degree of outdoor cold exposure an individual is exposed to even if living in a cold environment. It is known that humans maintain thermoneutrality throughout the year by increased clothing and indoor heating (Maloney et al., 2014). Outdoor temperatures are often presented of the locale where patients are undergoing surgery (as in my study) and it is not known if individuals have spent time prior to surgery in this environment. Therefore, cold exposure may explain differences in pADR

browning in patients with non-pheo patients between those reported by Betz et al; however it remains an association and has several limitations. Age may also be a factor in the observed browning of the non-pheo groups studied by Betz et al although they cannot be compared to my study as they were not reported for each of their groups.

Pheo patients with pADR browning (pheo multilocular group) did not have significantly lower BMI and glucose in my study. Other studies have also found that patients with pheochromocytoma do not have significantly lower BMI than patients undergoing adrenalectomy (Frontini et al., 2013). Although not reported for pheo patients specifically, Betz et al found no difference in BMI between BAT positive and negative patients undergoing adrenalectomy for benign adrenal tumours (Betz et al., 2013). This may suggest that the browning observed in these patients is not sufficient to elicit weight loss or improvements in blood glucose concentrations. However, as discussed further in general limitations below, patients included in these studies are not healthy and the findings may differ from browning occurring in healthy populations. Of course it can be argued that overweight or metabolically unhealthy individuals are those that would benefit most from increased BAT activity. A recent study in healthy individuals has reported no change in BMI or total plasma glucose with increased BAT mass and activity after one month of overnight cold exposure, although improvements in insulin sensitivity were observed (Lee et al., 2014). Glucose tolerance tests were not performed in my study so it is not possible to assess this potentially beneficial role of adipose tissue browning.

5.5.2 SAT does not undergo browning in patients with pheochromocytoma

In all SAT samples analysed in my study, browning was not observed due to the lack of UCP1, low uncoupled respiration and unilocular adipocyte morphology. In the course of this project, two studies also found similar results: Di Franco et al found unilocular adipocytes in the SAT of 8 pheo patients and decreased UCP1 compared to pADR adipose tissue (Di Franco et al., 2014) and a case report of a patient with pheochromocytoma by Sondergaard et al did not observe multilocular adipocytes in a SAT biopsy (Sondergaard et al., 2015). My study used a larger number of pheos and controls and also assessed uncoupled respiration functionally in both pADR and SAT providing further evidence to that of Di Franco et al that pheochromocytomas and elevated plasma catecholamines *per se* do not appear to cause SAT browning. A local effect of catecholamines released from the pheo tumour could have an effect on browning adipose tissue located proximally to the adrenal gland although a systemic increase in plasma catecholamines would be hypothesized to affect distal adipose tissues such as abdominal SAT. In accordance with this theory, a case report has shown that a patient with left adrenal pheochromocytoma had increased perirenal BAT activity (assessed by PET-CT) bilaterally (Park et al., 2014), suggesting catecholamine effects occur not only in adipose tissue surrounding the tumour. Fibrous tissue also appears to be present between the pheochromocytoma and perirenal adipose tissue (Park et al., 2014) which could prevent paracrine action of catecholamines.

Therefore differences in browning may be attributable to differences in the adipose tissue depots themselves. In my study there was also a large difference in Ct values in ADRB3 abundance by qPCR between pADR (mean Ct=30.5) and SAT (mean Ct=35.3) suggesting lower gene expression in SAT. This may alter responsiveness to catecholamines acting through beta-3 receptors, as β-adrenergic knockout mice do not show adipose tissue browning in response to CL316243, a β-3 agonist (Ye et al., 2013). In the rat, inguinal SAT was found to have undetectable ADRB3 and did not undergo browning in response to cold exposure whereas iBAT and retroperitoneal WAT with detectable ADRB3, displayed UCP1 upregulation in response to cold (Cousin et al., 1993). It is therefore possible that SAT has less beta 3 receptor-catecholamine binding than pADR adipose tissue, particularly in pheos with excess catecholamines. ADRB3 expression did not differ for pADR samples between pheo unilocular and multilocular; this may be accounted for by differences in catecholamine abundance i.e. receptors are present on control and pheo unilocular pADR adipocytes but there is insufficient catecholamine to cause browning. It is not known however if the protein abundance of the receptor differed between pADR and SAT samples. This would have been interesting to investigate further, however due to time constraints this was not possible. It has also been reported that there are issues with antibody specificity for ADRB3 compared to other beta receptor isoforms (Hamdani and van der Velden, 2009; Pradidarcheep et al., 2009).

Di Franco reported that stem cells isolated from pADR were able to partially differentiate into brown-like cells with beige markers whereas SAT stem cells were only able to differentiate into WAT adipocytes (Di Franco et al., 2014). Therefore if *de novo* development of precursors is responsible for browning as previously suggested (Vegiopoulos et al., 2010) and not the alternative theory of trans-differentiation (Rosenwald et al., 2013), this may explain the browning observed in the pADR of some pheo patients but not in paired SAT specimens.

Some studies have reported browning of SAT in humans however. During the course of this study, two papers reported SAT browning in patients with severe burn injury (Patsouris et al., 2015; Sidossis et al., 2015). Sidossis et al found in both children and adults with third degree burns, a progressive increase in multilocular adipocyte abundance, UCP1 and uncoupled respiration was observed 3 weeks post burn injury. Progressive browning in adults was also noted by Patsouris et al who reported increased UCP1 at 10-21 days post burn compared to 0-3 days. Similar to pheo pathology, burn injury elicits increased catecholamine release and turnover (Patsouris et al., 2015). A rodent model of burn injury failed to show SAT browning when administered propranolol (a non-selective β-receptor antagonist) compared to sham treated controls suggesting browning is dependent on β-adrenergic stimulation (Patsouris et al., 2015) possibly through catecholamines. Urinary catecholamines were measured by Sidossis et al, making it difficult to directly compare with plasma catecholamines values obtained in my study. A previous study in 12 patients with pheochromocytoma found a mean urinary norepinephrine secretion of 1004 ±

289μg/day (Crout and Sjoerdsma, 1960) compared to Sidossis et al reporting 96 ± 48μg/day in burn patients which may suggest catecholamines are not elevated in burn patients compared to pheochromocytoma and would not be responsible for differences in adipose tissue browning. Caution is needed when comparing these urinary norepinephrine values as it is not clear if they were analysed by the same method.

There are however, differences between these studies that may be responsible for discrepancies in SAT browning. Although Sidossis et al largely attribute the adipose tissue browning in burn injury patients to chronic adrenergic stress, significant increases in the release of inflammatory cytokines such as IL-6 and MCP-1 were also observed. IL-6 in particular is responsible for cancer cachexia-induced SAT browning in rodents (Petruzzelli et al., 2014) which could also play a role in SAT browning of burn patients. Indeed, in IL-$6^{-/-}$ mice, burn injury does not stimulate inguinal adipose tissue browning compared to wild-type controls (Patsouris et al., 2015). Propranolol also blunted burn-induced browning in wild-type mice (Patsouris et al., 2015) which may suggest an interplay between IL-6 and β-adrenergic signaling is required for SAT browning in humans. IL-6 plasma concentrations were not measured in my study so it is not known if they increase with pheochromocytoma.

Burn injury removes insulating adipose tissue (Sidossis et al., 2015) and therefore SAT from the site of injury may undergo browning differently to that of SAT from unburned individuals. Healthy female subjects exposed to 15-16°C for

10 days did not display browning of abdominal SAT despite significant increases in plasma catecholamine concentrations (van der Lans et al., 2013). It has been suggested that this time period of adrenergic stress may not be sufficient to cause adipose tissue browning (Sidossis et al., 2015). However, using pheochromocytoma as a model condition in this project allows for the assessment of chronic adrenergic stress on adipose tissue browning where insulating SAT is preserved. It is possible therefore that SAT can undergo browning in certain pathophysiological conditions but is unlikely in patients with elevated plasma catecholamines.

In my study, superficial abdominal SAT was sampled. SAT can be subdivided into superficial and deep subcutaneous adipose tissues separated by the *stroma fascia* (Kelley et al., 2000). Deep SAT displays visceral adipose tissue characteristics in terms of cytokine secretion (Walker et al., 2007) and is implicated in insulin resistance and metabolic syndrome (Kim et al., 2016). In the neck region of humans, it has been shown that UCP1 is more highly expressed in deep adipose tissue compared to superficial SAT (Cypess et al., 2013). It can be hypothesised that the browning capacity may also be altered. This would be in accordance with the findings in my study, that a lack of browning and UCP1 is observed in superficial SAT compared to pADR adipose tissue from pheo patients. The results from my study therefore apply only to superficial abdominal SAT and the browning response to catecholamines may differ for deep SAT.

That SAT does not seem to undergo browning in humans with chronic adrenergic stress (acknowledging the limitations of this study group) would be in contrast to the inguinal SAT of rodents which is often the depot reported to undergo browning to a wide range of factors (Jia et al., 2016; Stine et al., 2016; Wang et al., 2015) including β-3 adrenergic signaling (Ye et al., 2013). This is an important point to consider as it may suggest species differences in SAT browning between rodents and humans, possibly affecting the translational relevance of rodent adipose tissue browning. It is possible that in rodents, inguinal adipose tissue is more similar to human visceral adipose tissue depots in response to browning.

5.5.3 Beige adipocyte markers were not conclusive of increased beige adipocyte abundance in patients with adipose tissue browning

A potential factor influencing the browning capacity of adipose tissue depots to catecholamines could be the abundance of beige adipocytes which can reversibly undergo browning (Rosenwald et al., 2013). Beige markers analysed in my study did not show similar patterns of expression and it is therefore difficult to assess beige adipocyte abundance conclusively within the tissues. PAT2 was the only marker to increase in pheos with multilocular adipocytes and is in accordance with rodent studies that have found it to be upregulated with adipose tissue browning (Ussar et al., 2014). In addition it is expressed highly in UCP1 positive neck fat compared to SAT from the same anatomical location (Ussar et al., 2014). The finding of an increase in PAT2 in the pheo multilocular pADR samples would therefore suggest an increase in brown and beige adipocytes, although PAT2 was

found to be a more selective beige marker. This may explain why adipose tissue browning was seen only in a subset of pheos, as they have adipocytes that are inducible or able to respond to excess catecholamines. Indeed PAT2 is upregulated during browning of adipose tissue in mice treated with β-3 agonists but not with cold exposure and may therefore be suggestive of beta-adrenergic signaling, as other factors in cold may also contribute to browning (Ussar et al., 2014).

KCNK3 and MTUS1 variant 3 have been reported to be markers of brown adipocytes and are upregulated in rodents and humans exposed to cold (Shinoda et al., 2015). They are also highly expressed transcripts in deep compared to superficial SAT in the neck region (Shinoda et al., 2015; Svensson et al., 2011). The discrepancy between results for KCNK3/MTUSvar3 compared to PAT2 in my study may be explained by the fact that PAT2 gene expression is not significantly different between UCP1 positive and negative human adipose tissue samples from the retroperitoneal area in contrast to supraclavicular and mediastinum biopsies (Ussar et al., 2014). My samples obtained from the pADR depot may therefore be similar in anatomical location. This would suggest that this region may have a distinct population of brown/beige adipocytes upon browning or that the marker is not suitable for adipose tissue browning from perirenal or periadrenal fat depots.

5.5.4 Summary and conclusions

This study investigated the browning of adipose tissue in patients with pheochromocytoma or beningn non-pheo tumours. Similar to the findings in the previous chapter, differential gene expression and morphology was noted between adipose tissue depots. Although visceral depots differ in development and thermogenic capacity through UCP1 abundance as found in Chapter 3, differences were observed between pADR (visceral) and abdominal SAT in this study. Excess plasma catecholamines produced by pheochromocytoma only promote adipose tissue browning in pADR but not SAT and there may be a threshold of plasma catecholamines required to induce browning, as those with UCP1 positive adipocytes had the highest plasma catecholamines. Differential browning between depots may be due to differences in beta-3 adrenergic receptor abundance however there are many other factors that may be responsible for differences in browning capacity between the depots. This is interesting to consider in future studies, as understanding the mechanisms of why some depots may be capable of undergoing browning and others lack this responsiveness would be beneficial to developing pharmacological agents to promote browning. It also suggests that there may be species-specific browning in murine inguinal SAT and that this browning may not lead to similar SAT thermogenic adaptations in humans.

Chapter 6 Conclusion

6.1 General aims

This thesis aimed to assess differences between adipose tissue depots in terms of thermogenesis and adipose tissue remodelling during development or in response to chronic adrenergic stress. This was conducted through two separate studies. The first was a sheep study to assess the characteristics of epicardial and paracardial adipose tissue in terms of thermogenesis and development during early life. Epicardial adipose tissue in particular is associated with atherosclerosis therefore it is important to characterise the beneficial thermogenic properties of this tissue. The second study aimed to assess if subcutaneous adipose tissue is capable of browning in humans to chronic adrenergic stress. Human subjects with pheochromocytoma, a catecholamine secreting tumour were used to investigate this. In both studies analyses of adipose tissue morphology, gene expression of white, brown and beige adipocyte markers and UCP1 abundance were assessed. The human pheochromocytoma study also included functional mitochondrial bioenergetics to assess UCP1 activity.

6.2 Summary of study findings

6.2.1 Sheep studies

During early life in the sheep, epicardial and paracardial adipose tissue depots possessed UCP1 and abundantly expressed other genes involved in thermogenesis such as PGC1α and DIO2. They also displayed multilocular adipocytes characteristic of thermogenic adipose tissue. Despite deriving from the same origin as epicardial adipose tissue (Ho and Shimada, 1978), omental adipose tissue did not abundantly express UCP1 and had decreased expression of thermogenic genes than pericardial fat depots. Perirenal adipose tissue, one of the most well characterised BAT depots in the sheep had the highest expression of UCP1 compared to pericardial and omental adipose tissue depots, perhaps suggesting that pericardial adipose tissue depots are intermediate in terms of thermogenesis between current known white and BAT depots. Paracardial, epicardial and perirenal adipose tissue depots showed pronounced adipose tissue remodelling over the first 28 days of life. Multilocular adipocyte morphology and UCP1 expression were observed at 1 day of age and to a lesser extent at 7 days. At 28 days of age these depots showed unilocular white adipocytes, decreased thermogenic gene expression and increased white adipocyte mRNA markers such as leptin and the UCP1 inhibitor RIP140. In contrast, omental adipose tissue was not present at birth and did not show a pronounced brown to white adipose tissue transition between days 7 and 28. A TUNEL assay did not show any apoptotic cells in perirenal or epicardial adipose tissue depots in 1, 7 or 28 day groups suggesting that apoptosis is not the

mechanism responsible for the disappearance of multilocular UCP1 positive adipocytes with increasing age.

Gene expression for cardiac natriuretic peptide signalling revealed an increased NPRA/C ratio in omental compared to epicardial and paracardial adipose tissue. PRKGI was also increased in omental adipose tissue. This may suggest that cardiac natriuretic peptides could elicit a greater thermogenic or lipolytic response in omental adipose tissue than the fat depots located close to the heart. Plasma concentrations of BNP also showed a decrease between 7 and 28 days concomitant with the loss of UCP1 which may suggest BNP has a role in thermogenesis during early life.

6.2.2 Human pheochromocytoma study

Periadrenal adipose tissue biopsies sampled from patients with pheochromocytoma showed multilocular adipocytes in 53% (8/15) of cases. In contrast, periadrenal adipose tissue from patients with non-functioning, cortisol or aldosterone secreting tumours did not show brown adipocyte morphology. Pheo patients with multilocular adipose tissue also had the highest plasma catecholamine concentrations. Other hormones shown to cause adipose tissue browning such as ANP, BNP and FGF21 did not differ between groups. Periadrenal adipose tissue browning in a subset of pheo patients, suggested by the presence of multilocular adipocytes, was confirmed by the expression of UCP1 and increased mitochondrial uncoupled respiration by bioenergetics analyses. Subcutaneous adipose tissue samples did not show browning

characteristics and lacked UCP1 in all patients studied, including those pheochromocytoma patients with browning of periadrenal adipose tissue. These findings suggest that human subcutaneous adipose tissue may not undergo browning in response to chronic adrenergic stress *per se*.

6.3 Limitations of the studies

6.3.1 Sheep as an animal model of human adipose tissue development and thermogenesis

Sheep provide a useful animal model to study epicardial and paracardial adipose which are difficult to study in smaller animals such as rodents due to the small size of these depots (Marchington et al., 1989). The anatomy is also identical in sheep to that found in humans. It should be noted that the function of pericardial adipose tissue as a thermogenic fat depot in early life may differ from humans. A recent study has shown UCP1 positive adipocytes in newborns and infants with a loss of UCP1 with age (Ojha et al., 2016), suggesting the development and function may be conserved across species. Human newborns possess a large interscapular depot (Lidell et al., 2013) however, which is not present in lambs. Therefore, it is possible that the relative contributions of different adipose tissue depots to overall non-shivering thermogenesis in early life may differ. Although BAT is lost with age in sheep (Pope et al., 2014) and humans (Cypess et al., 2009; Heaton, 1972) it is not clear if the molecular mechanism responsible for age-related BAT atrophy is identical in both species.

6.3.2 Technical limitations of the sheep studies

Unfortunately for this ontogeny study not all animals were sampled at exactly 7 and 28 days of age. The slight differences in sampling age in the group may therefore affect the thermogenic properties i.e. adipose tissue samples from a 5 day old animal may show increased expression of thermogenic genes compared to a 9 day old animal (as the 7 day age group was ±2 days). In addition, the use of 3 time points (at 1, 7 and 28 days), although identified to be critical stages in postnatal ovine adipose tissue development (Pope et al., 2014), prevents the elucidation of the exact day of a brown to white adipose tissue transition. For example, it is known that UCP1 and brown adipocyte characteristics are lost in perirenal adipose tissue depots between 7 and 28 days (Pope et al., 2014) but not the exact day when UCP1 is no longer detectable, therefore more time points would allow this to be determined.

Although a sheep genome database exists (Jiang et al., 2014) it is yet to be fully annotated and this may have prevented the successful design of certain primers i.e. ZIC1. The lack of commercial antibodies known to work effectively in sheep was certainly a hindrance in analysing the protein expression of NPRA and NPRC in Chapter 4. Due to the equipment available in this study at Nottingham, a functional assessment of UCP1 activity by mitochondrial bioenergetics was not possible and therefore only UCP1 abundance could be assessed.

The majority of lambs born in Study A were female which not give sufficient numbers to compare the effects of gender on adipose tissue development and thermogenesis. To keep the studies consistent, animals used for histology from study B were also female. It would have been informative to have equal numbers of male and females to allow gender comparisons. It is also possible that differences in litter size may also have affected the results. The lambs were a mixture of twins, triplets and quadruplets as described in Chapter 2. It is known that litter size can affect future development and adiposity. In the sheep, triplet animals are often smaller (Gardner et al., 2007) and have reduced body temperature (Dwyer and Morgan, 2006). Moreover, sheep with lighter birth weights have decrease plasma thyroid hormone concentrations than their heavier littermates (Dwyer and Morgan, 2006). Therefore it is possible that this effects BAT and UCP1 abundance observed in these studies.

6.3.3 Human pheochromocytoma study

Due to ethical considerations is difficult to collect visceral adipose tissue samples from healthy subjects. Although exclusion criteria were established to prevent confounding factors as much as possible, the subjects in this study were all undergoing adrenalectomy, were typically overweight or obese and were taking various medications (full details for each patient are given in the Appendix). As well as having benign tumours of the adrenal gland (either in the pheo or control groups), many also displayed other co-morbidities such as diabetes. It should be noted therefore, that the adipose tissue samples are not collected from healthy individuals and that the properties of the adipose tissue, in terms of

thermogenesis or browning response, may differ from that of healthy subjects. Also, different age groups of patients could not be assessed to ascertain if the browning response may differ depending on the age of subjects. This is largely limited by the pathology however, as catecholamine-secreting pheochromocytoma and paragangliomas are typically diagnosed in individuals at around 44-50 years of age (Eisenhofer et al., 2011). Insufficient numbers of male and females in pheo unilocular and multilocular groups prevented gender comparisons.

6.3.4 Technical limitations of the human pheochromocytoma study

Several primer sequences for beige and brown markers such as ZIC1 and LHX8 taken from previous publications were either not effective on the equipment used or were not highly expressed to be detected reliably by qPCR. In some cases re-designing the primers was also not successful and time constraints prevented further optimisation of these assays. A limitation of the mitochondrial bioenergetics is that they may not be representative of the *in vivo* function (Brand and Nicholls, 2011), and, although uncoupled respiration was assessed, it is not necessarily UCP1 dependent. A UCP1 inhibitor such as GDP (Fedorenko et al., 2012) may have been useful (perhaps in place of FCCP) to more directly assess the uncoupled respiration attributable to the activity of UCP1.

6.4 Future work

6.4.1 Future work based on the findings of sheep studies

The work in this thesis could be extended by the functional assessment of UCP1 activity by cellular bioenergetics to confirm that paracardial and epicardial adipose tissue depots participate in non-shivering thermogenesis during early life. It would also be interesting to assess if adipokine release differs during adipose tissue remodelling. This could be achieved by quantifying various adipokines by ELISA that are released from adipose tissue explants into serum free medium as previously described (Fain et al., 2004). This would allow the possible adverse effects of epicardial adipose tissue whitening on atherosclerosis development in a healthy animal to be further explored. Also, the effects of various factors known to promote browning in humans and animal models such as the β-3 receptor agonist mirabegron (Cypess et al., 2015) could be investigated on the browning of pericardial adipose tissues and effects on atherosclerosis.

The brown to white transition could be further explored possibly through lineage tracing experiments. Given that a transgene with a green fluorescent protein reporter has recently been inserted into the sheep genome using CRISPR/Cas9-mediated genome engineering (Wu et al., 2016), it may be possible to label UCP1 expressing cells in the sheep, similar to the early labelling techniques of UCP1 positive adipocytes in mice (Moulin et al., 2001). This would allow the hypothesis of a brown to white transdifferentiation during aging to be tested directly in a large mammal.

The effect of natriuretic peptides on adipose tissue depot specific effects could be further explored by looking at the protein expression of NPRA and NPRC between pericardial and omental depots. Furthermore, generating primary cells from epicardial, paracardial and omental adipose tissue depots and treating these with ANP and BNP would allow more causal and mechanistic investigations. Experiments could also be performed *in vivo* with ANP or BNP infused sheep (maintaining early life physiological plasma concentrations) to determine if browning effects are noted more in certain adipose tissue depots.

6.4.2 Future work based on human pheochromocytoma study

Differences between periadrenal and subcutaneous adipose tissue depots should be further explored to determine the reason these depots differ in browning capacity. A transcriptomic approach using either a DNA microarray or RNA sequencing may be useful to determine genes that are differentially expressed that may alter responsiveness to chronic adrenergic stress. Indeed, this is also an interesting approach to take using periadrenal samples and comparing those from pheo unilocular and pheo multilocular groups. This could identify new markers of adipose tissue browning or genes involved in either the stimulation or inhibition of UCP1 dependent thermogenesis. The treatment of primary human adipocytes may also allow a possible catecholamine threshold effect on periadrenal adipose tissue browning identified in Chapter 5 to be further explored.

6.5 Final remarks

This thesis has assessed adipose tissue depot differences in thermogenesis and has shown that depots differ in UCP1 expression, development and response to browning stimuli. These findings have contributed further to our knowledge of the function of epicardial and paracardial adipose tissue function in non-shivering thermogenesis during early life in a sheep model. This work has also shown that subcutaneous adipose tissue may not undergo browning to chronic adrenergic stress in humans with pheochromocytoma. Further work will be required to determine the relative contributions of individual fat depots to overall thermogenesis and ultimately, to elucidate if adipose tissue depot browning could be achieved in humans for metabolic benefit.

References

Acharya, A., Baek, S.T., Huang, G., Eskiocak, B., Goetsch, S., Sung, C.Y., Banfi, S., Sauer, M.F., Olsen, G.S., Duffield, J.S., et al. (2012). The bHLH transcription factor Tcf21 is required for lineage-specific EMT of cardiac fibroblast progenitors. Development 139, 2139-2149.

Adamczak, M., and Wiecek, A. (2013). The Adipose Tissue as an Endocrine Organ. Semin Nephrol 33, 2-13.

Adams, P.S., Dovak, M.T. (Ed.) (2006). Real-time PCR (London & New York: Taylor & Francis).

Ahmadian, M., Abbott, M.J., Tang, T., Hudak, C.S., Kim, Y., Bruss, M., Hellerstein, M.K., Lee, H.Y., Samuel, V.T., Shulman, G.I., et al. (2011). Desnutrin/ATGL is regulated by AMPK and is required for a brown adipose phenotype. Cell Metab 13, 739-748.

Akyol, B., Boyraz, M., and Aysoy, C. (2013). Relationship of epicardial adipose tissue thickness with early indicators of atherosclerosis and cardiac functional changes in obese adolescents with metabolic syndrome. J Clin Res Pediatr Endocrinol 5, 156-163.

Alesci, S., Manoli, I., Michopoulos, V.J., Brouwers, F.M., Le, H., Gold, P.W., Blackman, M.R., Rennert, O.M., Su, Y.A., and Chrousos, G.P. (2006). Development of a human mitochondria-focused cDNA microarray (hMitChip) and validation in skeletal muscle cells: implications for pharmaco- and mitogenomics. Pharmacogenomics J 6, 333-342.

Alexander, G., and Bell, A.W. (1975). Quantity and calculated oxygen consumption during summit metabolism of brown adipose tissue in new-born lambs. Biol Neonate 26, 214-220.

Alexander, G., Bell, A.W., and Hales, J.R. (1973). Effects of cold exposure on tissue blood flow in the new-born lamb. J Physiol 234, 65-77.

Alisi, A., Manco, M., Vania, A., and Nobili, V. (2009). Pediatric Nonalcoholic Fatty Liver Disease in 2009. Journal of Pediatrics 155, 469-474.

Altin, C., Sade, L.E., Gezmis, E., Ozen, N., Duzceker, O., Bozbas, H., Eroglu, S., and Muderrisoglu, H. (2016). Assessment of Subclinical Atherosclerosis by Carotid Intima-Media Thickness and Epicardial Adipose Tissue Thickness in Prediabetes. Angiology.

Ariton, M., Juan, C.S., and AvRuskin, T.W. (2000). Pheochromocytoma: clinical observations from a Brooklyn tertiary hospital. Endocr Pract 6, 249-252.

Arner, P., and Ryden, M. (2015). Fatty Acids, Obesity and Insulin Resistance. Obes Facts 8, 147-155.

Atalar, F., Gormez, S., Caynak, B., Akan, G., Tanriverdi, G., Bilgic-Gazioglu, S., Gunay, D., Duran, C., Akpinar, B., Ozbek, U., et al. (2013). Mediastinal adipose tissue expresses a pathogenic profile of 11 beta-hydroxysteroid dehydrogenase Type 1, glucocorticoid

receptor, and CD68 in patients with coronary artery disease. Cardiovasc Pathol 22, 183-188.

Au-Yong, I.T., Thorn, N., Ganatra, R., Perkins, A.C., and Symonds, M.E. (2009). Brown adipose tissue and seasonal variation in humans. Diabetes 58, 2583-2587.

Barrand, M.A., Dauncey, M.J., and Ingram, D.L. (1981). Changes in plasma noradrenaline and adrenaline associated with central and peripheral thermal stimuli in the pig. J Physiol 316, 139-152.

Barreau, C., Labit, E., Guissard, C., Rouquette, J., Boizeau, M.L., Gani Koumassi, S., Carriere, A., Jeanson, Y., Berger-Muller, S., Dromard, C., et al. (2016). Regionalization of browning revealed by whole subcutaneous adipose tissue imaging. Obesity (Silver Spring) 24, 1081-1089.

Bartelt, A., Bruns, O.T., Reimer, R., Hohenberg, H., Ittrich, H., Peldschus, K., Kaul, M.G., Tromsdorf, U.I., Weller, H., Waurisch, C., et al. (2011). Brown adipose tissue activity controls triglyceride clearance. Nat Med 17, 200-U293.

Basse, A.L., Dixen, K., Yadav, R., Tygesen, M.P., Qvortrup, K., Kristiansen, K., Quistorff, B., Gupta, R., Wang, J., and Hansen, J.B. (2015). Global gene expression profiling of brown to white adipose tissue transformation in sheep reveals novel transcriptional components linked to adipose remodeling. BMC Genomics 16, 215.

Beeson, C.C., Beeson, G.C., and Schnellmann, R.G. (2010). A high-throughput respirometric assay for mitochondrial biogenesis and toxicity. Anal Biochem 404, 75-81.

Begum, G., Stevens, A., Smith, E.B., Connor, K., Challis, J.R., Bloomfield, F., and White, A. (2012). Epigenetic changes in fetal hypothalamic energy regulating pathways are associated with maternal undernutrition and twinning. FASEB J 26, 1694-1703.

Berg, F., Gustafson, U., and Andersson, L. (2006). The uncoupling protein 1 gene (UCP1) is disrupted in the pig lineage: a genetic explanation for poor thermoregulation in piglets. PLoS Genet 2, e129.

Berg, J.M., Tymoczko, J.L., Stryer, L. (2007). Biochemistry, Sixth edn (New York: W.H Freeman and Company).

Betz, M.J., Slawik, M., Lidell, M.E., Osswald, A., Heglind, M., Nilsson, D., Lichtenauer, U.D., Mauracher, B., Mussack, T., Beuschlein, F., et al. (2013). Presence of brown adipocytes in retroperitoneal fat from patients with benign adrenal tumors: relationship with outdoor temperature. J Clin Endocrinol Metab 98, 4097-4104.

Bianco, A.C., Sheng, X.Y., and Silva, J.E. (1988). Triiodothyronine amplifies norepinephrine stimulation of uncoupling protein gene transcription by a mechanism not requiring protein synthesis. J Biol Chem 263, 18168-18175.

Bianco, A.C., and Silva, J.E. (1987). Intracellular conversion of thyroxine to triiodothyronine is required for the optimal thermogenic function of brown adipose tissue. J Clin Invest 79, 295-300.

Bing, R.J., Siegel, A., Ungar, I., and Gilbert, M. (1954). Metabolism of the human heart. II. Studies on fat, ketone and amino acid metabolism. Am J Med 16, 504-515.

Bjornholm, M., Kawano, Y., Lehtihet, M., and Zierath, J.R. (1997). Insulin receptor substrate-1 phosphorylation and phosphatidylinositol 3-kinase activity in skeletal muscle from NIDDM subjects after in vivo insulin stimulation. Diabetes 46, 524-527.

Bjorntorp, P. (1990). "Portal" adipose tissue as a generator of risk factors for cardiovascular disease and diabetes. Arteriosclerosis 10, 493-496.

Bland, J.M., and Altman, D.G. (2009). Analysis of continuous data from small samples. BMJ 338, a3166.

Bonnot, E. (1908). The Interscapular Gland. Journal of Anatomy and Physiology 43, 43-58.

Bordicchia, M., Ceresiani, M., Pavani, M., Minardi, D., Polito, M., Wabitsch, M., Cannone, V., Burnett, J.C., Jr., Dessi-Fulgheri, P., and Sarzani, R. (2016). Insulin/glucose induces natriuretic peptide clearance receptor in human adipocytes: a metabolic link with the cardiac natriuretic pathway. Am J Physiol Regul Integr Comp Physiol 311, R104-114.

Bordicchia, M., Liu, D., Amri, E.Z., Ailhaud, G., Dessi-Fulgheri, P., Zhang, C., Takahashi, N., Sarzani, R., and Collins, S. (2012). Cardiac natriuretic peptides act via p38 MAPK to induce the brown fat thermogenic program in mouse and human adipocytes. J Clin Invest 122, 1022-1036.

Boyraz, M., Pirgon, O., Akyol, B., Dundar, B., Cekmez, F., and Eren, N. (2013). Importance of epicardial adipose tissue thickness measurement in obese adolescents, its relationship with carotid intima-media thickness, and echocardiographic findings. Eur Rev Med Pharmacol Sci 17, 3309-3317.

Brand, M.D., and Nicholls, D.G. (2011). Assessing mitochondrial dysfunction in cells. Biochem J 435, 297-312.

Brito, M.N., Brito, N.A., Baro, D.J., Song, C.K., and Bartness, T.J. (2007). Differential activation of the sympathetic innervation of adipose tissues by melanocortin receptor stimulation. Endocrinology 148, 5339-5347.

Bukowiecki, L.J., Follea, N., Lupien, J., and Paradis, A. (1981). Metabolic relationships between lipolysis and respiration in rat brown adipocytes. The role of long chain fatty acids as regulators of mitochondrial respiration and feedback inhibitors of lipolysis. J Biol Chem 256, 12840-12848.

Buyse, M., Viengchareun, S., Bado, A., and Lombes, M. (2001). Insulin and glucocorticoids differentially regulate leptin transcription and secretion in brown adipocytes. FASEB J 15, 1357-1366.

Cairo, M., Villarroya, J., Cereijo, R., Campderros, L., Giralt, M., and Villarroya, F. (2016). Thermogenic activation represses autophagy in brown adipose tissue. Int J Obes (Lond).

Cannon, B., and Nedergaard, J. (2004). Brown adipose tissue: function and physiological significance. Physiol Rev 84, 277-359.

Cannon, B., and Nedergaard, J. (2010). Metabolic consequences of the presence or absence of the thermogenic capacity of brown adipose tissue in mice (and probably in humans). Int J Obes (Lond) 34 Suppl 1, S7-16.

Cao, W., Medvedev, A.V., Daniel, K.W., and Collins, S. (2001). beta-Adrenergic activation of p38 MAP kinase in adipocytes: cAMP induction of the uncoupling protein 1 (UCP1) gene requires p38 MAP kinase. J Biol Chem 276, 27077-27082.

Carbone, F., La Rocca, C., and Matarese, G. (2012). Immunological functions of leptin and adiponectin. Biochimie 94, 2082-2088.

Carr, D.B., Utzschneider, K.M., Hull, R.L., Kodama, K., Retzlaff, B.M., Brunzell, J.D., Shofer, J.B., Fish, B.E., Knopp, R.H., and Kahn, S.E. (2004). Intra-abdominal fat is a major determinant of the national cholesterol education program adult treatment panel III criteria for the metabolic syndrome. Diabetes 53, 2087-2094.

Carvalho, S.D., Bianco, A.C., and Silva, J.E. (1996). Effects of hypothyroidism on brown adipose tissue adenylyl cyclase activity. Endocrinology 137, 5519-5529.

Chabowska-Kita, A., Trabczynska, A., Korytko, A., Kaczmarek, M.M., and Kozak, L.P. (2015). Low ambient temperature during early postnatal development fails to cause a permanent induction of brown adipocytes. FASEB J 29, 3238-3252.

Charan, J., Kantharia, N.D. (2009). How to calculate sample size in animal studies? J Pharmacol Pharmacother, 4(4): 303–306.

Chartoumpekis, D.V., Habeos, I.G., Ziros, P.G., Psyrogiannis, A.I., Kyriazopoulou, V.E., and Papavassiliou, A.G. (2011). Brown adipose tissue responds to cold and adrenergic stimulation by induction of FGF21. Mol Med 17, 736-740.

Chechi, K., Blanchard, P.G., Mathieu, P., Deshaies, Y., and Richard, D. (2013). Brown fat like gene expression in the epicardial fat depot correlates with circulating HDL-cholesterol and triglycerides in patients with coronary artery disease. Int J Cardiol 167, 2264-2270.

Chechi, K., Gelinas, Y., Mathieu, P., Deshaies, Y., and Richard, D. (2012). Validation of reference genes for the relative quantification of gene expression in human epicardial adipose tissue. PLoS One 7, e32265.

Chechi, K., and Richard, D. (2015). Thermogenic potential and physiological relevance of human epicardial adipose tissue. Int J Obes Suppl 5, S28-34.

Cheung, L., Gertow, J., Werngren, O., Folkersen, L., Petrovic, N., Nedergaard, J., Franco-Cereceda, A., Eriksson, P., and Fisher, R.M. (2013). Human mediastinal adipose tissue displays certain characteristics of brown fat. Nutr Diabetes 3, e66.

Chomczynski, P., and Sacchi, N. (2006). The single-step method of RNA isolation by acid guanidinium thiocyanate-phenol-chloroform extraction: twenty-something years on. Nat Protoc 1, 581-585.

Chondronikola, M., Annamalai, P., Chao, T., Porter, C., Saraf, M.K., Cesani, F., and Sidossis, L.S. (2015). A percutaneous needle biopsy technique for sampling the supraclavicular brown adipose tissue depot of humans. Int J Obes (Lond) 39, 1561-1564.

Chondronikola, M., Volpi, E., Borsheim, E., Porter, C., Annamalai, P., Enerback, S., Lidell, M.E., Saraf, M.K., Labbe, S.M., Hurren, N.M., et al. (2014). Brown adipose tissue improves whole-body glucose homeostasis and insulin sensitivity in humans. Diabetes 63, 4089-4099.

Christian, M., Kiskinis, E., Debevec, D., Leonardsson, G., White, R., and Parker, M.G. (2005). RIP140-targeted repression of gene expression in adipocytes. Mol Cell Biol 25, 9383-9391.

Cinti, S. (2012). The adipose organ at a glance. Dis Model Mech 5, 588-594.

Cinti, S., Frederich, R.C., Zingaretti, M.C., De Matteis, R., Flier, J.S., and Lowell, B.B. (1997). Immunohistochemical localization of leptin and uncoupling protein in white and brown adipose tissue. Endocrinology 138, 797-804.

Clayton, D.A., and Shadel, G.S. (2014). Isolation of mitochondria from cells and tissues. Cold Spring Harb Protoc 2014, pdb top074542.

Cleeman, J.I., Grundy, S.M., Becker, D., Clark, L.T., Cooper, R.S., Denke, M.A., Howard, W.J., Hunninghake, D.B., Illingworth, D.R., Luepker, R.V., et al. (2001). Executive summary of the Third Report of the National Cholesterol Education Program (NCEP) expert panel on detection, evaluation, and treatment of high blood cholesterol in adults (Adult Treatment Panel III). Jama-Journal of the American Medical Association 285, 2486-2497.

Coleman, M.L., Sahai, E.A., Yeo, M., Bosch, M., Dewar, A., and Olson, M.F. (2001). Membrane blebbing during apoptosis results from caspase-mediated activation of ROCK I. Nat Cell Biol 3, 339-345.

Cong, L., Ran, F.A., Cox, D., Lin, S., Barretto, R., Habib, N., Hsu, P.D., Wu, X., Jiang, W., Marraffini, L.A., et al. (2013). Multiplex genome engineering using CRISPR/Cas systems. Science 339, 819-823.

Connolly, E., Morrisey, R.D., and Carnie, J.A. (1982). The effect of interscapular brown adipose tissue removal on bodyweight and cold response in the mouse. British Journal of Nutrition 47, 653-658.

Coppari, R., and Bjorboek, C. (2012). Leptin revisited: its mechanism of action and potential for treating diabetes. Nat Rev Drug Discov 11, 692-708.

Corsonello, A., Montesanto, A., Berardelli, M., De Rango, F., Dato, S., Mari, V., Mazzei, B., Lattanzio, F., and Passarino, G. (2010). A cross-section analysis of FT3 age-related changes in a group of old and oldest-old subjects, including centenarians' relatives, shows that a down-regulated thyroid function has a familial component and is related to longevity. Age Ageing 39, 723-727.

Cousin, B., Casteilla, L., Dani, C., Muzzin, P., Revelli, J.P., and Penicaud, L. (1993). Adipose tissues from various anatomical sites are characterized by different patterns of gene expression and regulation. Biochem J 292 (Pt 3), 873-876.

Cousin, B., Cinti, S., Morroni, M., Raimbault, S., Ricquier, D., Penicaud, L., and Casteilla, L. (1992). Occurrence of brown adipocytes in rat white adipose tissue - molecular and morphological characterisation J Cell Sci 103, 931-942.

Croes, K., De Coster, S., De Galan, S., Morrens, B., Loots, I., Van de Mieroop, E., Nelen, V., Sioen, I., Bruckers, L., Nawrot, T., et al. (2014). Health effects in the Flemish population in relation to low levels of mercury exposure: from organ to transcriptome level. Int J Hyg Environ Health 217, 239-247.

Crout, J.R., and Sjoerdsma, A. (1960). Catecholamines in the localization of pheochromocytoma. Circulation 22, 516-525.

Cypess, A.M., Lehman, S., Williams, G., Tal, I., Rodman, D., Goldfine, A.B., Kuo, F.C., Palmer, E.L., Tseng, Y., Doria, A., et al. (2009). Identification and Importance of Brown Adipose Tissue in Adult Humans. N Engl J Med 360, 1509-1517.

Cypess, A.M., Weiner, L.S., Roberts-Toler, C., Franquet Elia, E., Kessler, S.H., Kahn, P.A., English, J., Chatman, K., Trauger, S.A., Doria, A., et al. (2015). Activation of human brown adipose tissue by a beta3-adrenergic receptor agonist. Cell Metab 21, 33-38.

Cypess, A.M., White, A.P., Vernochet, C., Schulz, T.J., Xue, R., Sass, C.A., Huang, T.L., Roberts-Toler, C., Weiner, L.S., Sze, C., et al. (2013). Anatomical localization, gene expression profiling and functional characterization of adult human neck brown fat. Nat Med 19, 635-639.

Dawkins, M.J.R., and Scopes, J.W. (1965). Non-shivering thermogenesis and brown adipose tissue in human new-born infant. Nature 206, 201-&.

de Bold, A.J. (1985). Atrial natriuretic factor: a hormone produced by the heart. Science 230, 767-770.

de Jesus, L.A., Carvalho, S.D., Ribeiro, M.O., Schneider, M., Kim, S.W., Harney, J.W., Larsen, P.R., and Bianco, A.C. (2001). The type 2 iodothyronine deiodinase is essential for adaptive thermogenesis in brown adipose tissue. J Clin Invest 108, 1379-1385.

de Jong, J.M., Larsson, O., Cannon, B., and Nedergaard, J. (2015). A stringent validation of mouse adipose tissue identity markers. Am J Physiol Endocrinol Metab 308, E1085-1105.

Di Franco, A., Guasti, D., Mazzanti, B., Ercolino, T., Francalanci, M., Nesi, G., Bani, D., Forti, G., Mannelli, M., Valeri, A., et al. (2014). Dissecting the origin of inducible brown fat in adult humans through a novel adipose stem cell model from adipose tissue surrounding pheochromocytoma. J Clin Endocrinol Metab 99, E1903-1912.

Dijk, W., Heine, M., Vergnes, L., Boon, M.R., Schaart, G., Hesselink, M.K., Reue, K., van Marken Lichtenbelt, W.D., Olivecrona, G., Rensen, P.C., et al. (2015). ANGPTL4 mediates shuttling of lipid fuel to brown adipose tissue during sustained cold exposure. Elife 4.

Dincer, U.D., Guner, S., Tay, A., Arioglu, E., Tasdelen, A., Aslamaci, S., and Bidasee, K.R. (2003). Decreased expression of beta1- and beta2-adrenoceptors in human diabetic atrial appendage. Cardiovasc Diabetol 2, 6.

Divakaruni, A.S., Humphrey, D.M., and Brand, M.D. (2012). Fatty acids change the conformation of uncoupling protein 1 (UCP1). J Biol Chem 287, 36845-36853.

Divakaruni, A.S., Paradyse, A., Ferrick, D.A., Murphy, A.N., and Jastroch, M. (2014). Analysis and interpretation of microplate-based oxygen consumption and pH data. Methods Enzymol 547, 309-354.

Donckier, J.E., Michel, L.A., Collard, E., Galanti, L., Harvengt, C., Berbinschi, A., Ketelslegers, J.M., and Buysschaert, M. (1991). Plasma atrial natriuretic factor and catecholamines before and during excision of pheochromocytoma. Acta Chir Belg 91, 112-116.

Donkor, J., Sariahmetoglu, M., Dewald, J., Brindley, D.N., and Reue, K. (2007). Three mammalian lipins act as phosphatidate phosphatases with distinct tissue expression patterns. J Biol Chem 282, 3450-3457.

Dulloo, A.G., Young, J.B., and Landsberg, L. (1988). Sympathetic nervous system responses to cold exposure and diet in rat skeletal muscle. Am J Physiol 255, E180-188.

Dwyer, C.M., and Morgan, C.A. (2006). Maintenance of body temperature in the neonatal lamb: effects of breed, birth weight, and litter size. J Anim Sci 84, 1093-1101.

Eisenhofer, G., Keiser, H., Friberg, P., Mezey, E., Huynh, T.T., Hiremagalur, B., Ellingson, T., Duddempudi, S., Eijsbouts, A., and Lenders, J.W. (1998). Plasma metanephrines are markers of pheochromocytoma produced by catechol-O-methyltransferase within tumors. J Clin Endocrinol Metab 83, 2175-2185.

Eisenhofer, G., Timmers, H.J., Lenders, J.W., Bornstein, S.R., Tiebel, O., Mannelli, M., King, K.S., Vocke, C.D., Linehan, W.M., Bratslavsky, G., et al. (2011). Age at diagnosis of pheochromocytoma differs according to catecholamine phenotype and tumor location. J Clin Endocrinol Metab 96, 375-384.

Enerback, S. (2010). Human Brown Adipose Tissue. Cell Metab 11, 248-252.

Enerback, S., and Gimble, J.M. (1993). Lipoprotein lipase gene expression: physiological regulators at the transcriptional and post-transcriptional level. Biochim Biophys Acta 1169, 107-125.

Enerback, S., Jacobsson, A., Simpson, E.M., Guerra, C., Yamashita, H., Harper, M.E., and Kozak, L.P. (1997). Mice lacking mitochondrial uncoupling protein are cold-sensitive but not obese. Nature 387, 90-94.

Fain, J.N., Madan, A.K., Hiler, M.L., Cheema, P., and Bahouth, S.W. (2004). Comparison of the release of adipokines by adipose tissue, adipose tissue matrix, and adipocytes from visceral and subcutaneous abdominal adipose tissues of obese humans. Endocrinology 145, 2273-2282.

Fain, J.N., Sacks, H.S., Bahouth, S.W., Tichansky, D.S., Madan, A.K., and Cheema, P.S. (2010). Human epicardial adipokine messenger RNAs: comparisons of their expression in substernal, subcutaneous, and omental fat. Metabolism-Clinical and Experimental 59, 1379-1386.

Falcao, L.M., Pinto, F., Ravara, L., and van Zwieten, P.A. (2004). BNP and ANP as diagnostic and predictive markers in heart failure with left ventricular systolic dysfunction. J Renin Angiotensin Aldosterone Syst 5, 121-129.

Farmer, S.R. (2009). OBESITY Be cool, lose weight. Nature 458, 839-840.

Fedorenko, A., Lishko, P.V., and Kirichok, Y. (2012). Mechanism of Fatty-Acid-Dependent UCP1 Uncoupling in Brown Fat Mitochondria. Cell 151, 400-413.

Feldmann, H.M., Golozoubova, V., Cannon, B., and Nedergaard, J. (2009). UCP1 ablation induces obesity and abolishes diet-induced thermogenesis in mice exempt from thermal stress by living at thermoneutrality. Cell Metab 9, 203-209.

Finn, D., Lomax, M.A., and Trayhurn, P. (1998). An immunohistochemical and in situ hybridisation study of the postnatal development of uncoupling protein-1 and uncoupling protein-1 mRNA in lamb perirenal adipose tissue. Cell Tissue Res 294, 461-466.

Fischer, P., Moller, P., Bindl, L., Melzner, I., Tornqvist, H., Debatin, K.M., and Wabitsch, M. (2002). Induction of adipocyte differentiation by a thiazolidinedione in cultured, subepidermal, fibroblast-like cells of an infant with congenital generalized lipodystrophy. J Clin Endocrinol Metab 87, 2384-2390.

Fisher, F.M., Kleiner, S., Douris, N., Fox, E.C., Mepani, R.J., Verdeguer, F., Wu, J., Kharitonenkov, A., Flier, J.S., Maratos-Flier, E., et al. (2012). FGF21 regulates PGC-1alpha and browning of white adipose tissues in adaptive thermogenesis. Genes Dev 26, 271-281.

Fletcher, C.J., Roberts, C.T., Hartwich, K.M., Walker, S.K., and McMillen, I.C. (2007). Somatic cell nuclear transfer in the sheep induces placental defects that likely precede fetal demise. Reproduction 133, 243-255.

Flynn, T.G., de Bold, M.L., and de Bold, A.J. (1983). The amino acid sequence of an atrial peptide with potent diuretic and natriuretic properties. Biochem Biophys Res Commun 117, 859-865.

Fowler, P.A., Fuller, M.F., Glasbey, C.A., Foster, M.A., Cameron, G.G., McNeill, G., and Maughan, R.J. (1991). Total and subcutaneous adipose tissue in women: the measurement of distribution and accurate prediction of quantity by using magnetic resonance imaging. Am J Clin Nutr 54, 18-25.

Franks, P.W., Hanson, R.L., Knowler, W.C., Sievers, M.L., Bennett, P.H., and Looker, H.C. (2010). Childhood Obesity, Other Cardiovascular Risk Factors, and Premature Death. N Engl J Med 362, 485-493.

Friedman, J.M. (2009). Leptin at 14 y of age: an ongoing story. Am J Clin Nutr 89, 973S-979S.

Frontini, A., Vitali, A., Perugini, J., Murano, I., Romiti, C., Ricquier, D., Guerrieri, M., and Cinti, S. (2013). White-to-brown transdifferentiation of omental adipocytes in patients affected by pheochromocytoma. Biochim Biophys Acta 1831, 950-959.

Gaborit, B., Venteclef, N., Ancel, P., Pelloux, V., Gariboldi, V., Leprince, P., Amour, J., Hatem, S.N., Jouve, E., Dutour, A., et al. (2015). Human epicardial adipose tissue has a specific transcriptomic signature depending on its anatomical peri-atrial, peri-ventricular, or peri-coronary location. Cardiovasc Res 108, 62-73.

Gammeltoft, S., and Van Obberghen, E. (1986). Protein kinase activity of the insulin receptor. Biochem J 235, 1-11.

Garcia, R.A., Roemmich, J.N., and Claycombe, K.J. (2016). Evaluation of markers of beige adipocytes in white adipose tissue of the mouse. Nutr Metab (Lond) 13, 24.

Gardner, D.S., Buttery, P.J., Daniel, Z., and Symonds, M.E. (2007). Factors affecting birth weight in sheep: maternal environment. Reproduction 133, 297-307.

Garg, M.K., Kharb, S., Brar, K.S., Gundgurthi, A., and Mittal, R. (2011). Medical management of pheochromocytoma: Role of the endocrinologist. Indian J Endocrinol Metab 15 Suppl 4, S329-336.

Garlid, K.D., Orosz, D.E., Modriansky, M., Vassanelli, S., and Jezek, P. (1996). On the mechanism of fatty acid-induced proton transport by mitochondrial uncoupling protein. J Biol Chem 271, 2615-2620.

Garofalo, M.A., Kettelhut, I.C., Roselino, J.E., and Migliorini, R.H. (1996). Effect of acute cold exposure on norepinephrine turnover rates in rat white adipose tissue. J Auton Nerv Syst 60, 206-208.

Gasparetti, A.L., de Souza, C.T., Pereira-da-Silva, M., Oliveira, R.L., Saad, M.J., Carneiro, E.M., and Velloso, L.A. (2003). Cold exposure induces tissue-specific modulation of the insulin-signalling pathway in Rattus norvegicus. J Physiol 552, 149-162.

Gibney, M.J., Vorster, H.H., and Kok, F.J (2002). Introduction to human nutrition (Oxford; Malden, MA: Blackwell Science).

Gierut, J.J., Jacks, T.E., and Haigis, K.M. (2014). Strategies to achieve conditional gene mutation in mice. Cold Spring Harb Protoc. (4):339-49.

Gilsanz, V., Chung, S.A., Jackson, H., Dorey, F.J., and Hu, H.H. (2011). Functional brown adipose tissue is related to muscle volume in children and adolescents. J Pediatr 158, 722-726.

Gilsanz, V., Smith, M.L., Goodarzian, F., Kim, M., Wren, T.A., and Hu, H.H. (2012). Changes in brown adipose tissue in boys and girls during childhood and puberty. J Pediatr 160, 604-609 e601.

Golozoubova, V., Hohtola, E., Matthias, A., Jacobsson, A., Cannon, B., and Nedergaard, J. (2001). Only UCP1 can mediate adaptive nonshivering thermogenesis in the cold. FASEB J 15, 2048-2050.

Goodyear, L.J., Giorgino, F., Sherman, L.A., Carey, J., Smith, R.J., and Dohm, G.L. (1995). Insulin receptor phosphorylation, insulin receptor substrate-1 phosphorylation, and phosphatidylinositol 3-kinase activity are decreased in intact skeletal muscle strips from obese subjects. J Clin Invest 95, 2195-2204.

Gordon, C.J. (2012). Thermal physiology of laboratory mice: Defining thermoneutrality. Journal of Thermal Biology 37, 654-685.

Gordon, K.C., Bancroft J.D. (Ed.), Stevens, A. (Ed.) (1990). Theory and Practice of Histological Techniques (Edinburgh, London, Melbourne & New York: Churchill Livingstone).

Gordon, R.S., Jr. (1957). Unesterified fatty acid in human blood plasma. II. The transport function of unesterified fatty acid. J Clin Invest 36, 810-815.

Gordon, R.S., Jr., and Cherkes, A. (1956). Unesterified fatty acid in human blood plasma. J Clin Invest 35, 206-212.

Granneman, J.G., Lahners, K.N., and Chaudhry, A. (1991). Molecular cloning and expression of the rat beta 3-adrenergic receptor. Mol Pharmacol 40, 895-899.

Graves, R.A., Tontonoz, P., Platt, K.A., Ross, S.R., and Spiegelman, B.M. (1992). Identification of a fat cell enhancer: analysis of requirements for adipose tissue-specific gene expression. J Cell Biochem 49, 219-24.

Green, H., and Kehinde, O. (1975). An established preadipose cell line and its differentiation in culture. II. Factors affecting the adipose conversion. Cell 5, 19-27.

Griffin, M., Abu-El-Haija, M., Abu-El-Haija, M., Rokhlina, T., and Uc, A. (2012). Simplified and versatile method for isolation of high-quality RNA from pancreas. Biotechniques 52, 332-334.

Griffin, M.E., Marcucci, M.J., Cline, G.W., Bell, K., Barucci, N., Lee, D., Goodyear, L.J., Kraegen, E.W., White, M.F., and Shulman, G.I. (1999). Free fatty acid-induced insulin resistance is associated with activation of protein kinase C theta and alterations in the insulin signaling cascade. Diabetes 48, 1270-1274.

Grillo, M., and Margolis, F.L. (1990). Use of reverse transcriptase polymerase chain reaction to monitor expression of intronless genes. Biotechniques 9, 262, 264, 266-268.

Guauque-Olarte, S., Gaudreault, N., Piche, M.E., Fournier, D., Mauriege, P., Mathieu, P., and Bosse, Y. (2011). The transcriptome of human epicardial, mediastinal and subcutaneous adipose tissues in men with coronary artery disease. PLoS One 6, e19908.

Guerra, C., Koza, R.A., Yamashita, H., Walsh, K., and Kozak, L.P. (1998). Emergence of brown adipocytes in white fat in mice is under genetic control. Effects on body weight and adiposity. J Clin Invest 102, 412-420.

Guerra, C., Roncero, C., Porras, A., Fernandez, M., and Benito, M. (1996). Triiodothyronine induces the transcription of the uncoupling protein gene and stabilizes its mRNA in fetal rat brown adipocyte primary cultures. J Biol Chem 271, 2076-2081.

Haas, B., Mayer, P., Jennissen, K., Scholz, D., Berriel Diaz, M., Bloch, W., Herzig, S., Fassler, R., and Pfeifer, A. (2009). Protein kinase G controls brown fat cell differentiation and mitochondrial biogenesis. Sci Signal 2, ra78.

Haas, B.E., Weissglas-Volkov, D., Aguilar-Salinas, C.A., Nikkola, E., Vergnes, L., Cruz-Bautista, I., Riba, L., Stancakova, A., Kuusisto, J., Soininen, P., et al. (2011). Evidence of how rs7575840 influences apolipoprotein B-containing lipid particles. Arterioscler Thromb Vasc Biol 31, 1201-1207.

Haemmerle, G., Zimmermann, R., Hayn, M., Theussl, C., Waeg, G., Wagner, E., Sattler, W., Magin, T.M., Wagner, E.F., and Zechner, R. (2002). Hormone-sensitive lipase deficiency in mice causes diglyceride accumulation in adipose tissue, muscle, and testis. J Biol Chem 277, 4806-4815.

Haines, L., Wan, K.C., Lynn, R., Barrett, T.G., and Shield, J.P. (2007). Rising incidence of type 2 diabetes in children in the U.K. Diabetes Care 30, 1097-1101.

Halaas, J.L., Boozer, C., Blair-West, J., Fidahusein, N., Denton, D.A., and Friedman, J.M. (1997). Physiological response to long-term peripheral and central leptin infusion in lean and obese mice. Proc Natl Acad Sci U S A 94, 8878-8883.

Halaas, J.L., Gajiwala, K.S., Maffei, M., Cohen, S.L., Chait, B.T., Rabinowitz, D., Lallone, R.L., Burley, S.K., and Friedman, J.M. (1995). Weight-reducing effects of the plasma-protein encoded by the obese gene Science 269, 543-546.

Hamdani, N., and van der Velden, J. (2009). Lack of specificity of antibodies directed against human beta-adrenergic receptors. Naunyn Schmiedebergs Arch Pharmacol 379, 403-407.

Hanssen, M.J., Hoeks, J., Brans, B., van der Lans, A.A., Schaart, G., van den Driessche, J.J., Jorgensen, J.A., Boekschoten, M.V., Hesselink, M.K., Havekes, B., et al. (2015). Short-term cold acclimation improves insulin sensitivity in patients with type 2 diabetes mellitus. Nat Med 21, 863-865.

Haq, R., Shoag, J., Andreu-Perez, P., Yokoyama, S., Edelman, H., Rowe, G.C., Frederick, D.T., Hurley, A.D., Nellore, A., Kung, A.L., et al. (2013). Oncogenic BRAF regulates oxidative metabolism via PGC1alpha and MITF. Cancer Cell 23, 302-315.

Hashimoto, O., Ohtsuki, H., Kakizaki, T., Amou, K., Sato, R., Doi, S., Kobayashi, S., Matsuda, A., Sugiyama, M., Funaba, M., et al. (2015). Brown adipose tissue in cetacean blubber. PLoS One 10, e0116734.

Hassan, M., Latif, N., and Yacoub, M. (2012). Adipose tissue: friend or foe? Nat Rev Cardiol 9, 689-702.

Hatai, S. (1902). On the presence in human embryos of an interscapular gland corresponding to the so-called hibernating gland of lower mammals. Anal Anz 21, 369.

Heaton, G.M., Wagenvoord, R.J., Kemp, A., and Nicholls, D.G. (1978). Brown adipose-tissue mitochondria - photoaffinity labeling of regulatory site of energy-dissipation Eur J Biochem 82, 515-521.

Heaton, J.M. (1972). Distribution of brown adipose-tissue in the human. . J Anat 112, 35.

Heymsfield, S.B., Greenberg, A.S., Fujioka, K., Dixon, R.M., Kushner, R., Hunt, T., Lubina, J.A., Patane, J., Self, B., Hunt, P., et al. (1999). Recombinant leptin for weight loss in obese and lean adults: a randomized, controlled, dose-escalation trial. JAMA 282, 1568-1575.

Hill, J.O., Wyatt, H.R., Reed, G.W., and Peters, J.C. (2003). Obesity and the environment: where do we go from here? Science 299, 853-855.

Himms-Hagen, J., Melnyk, A., Zingaretti, M.C., Ceresi, E., Barbatelli, G., and Cinti, S. (2000). Multilocular fat cells in WAT of CL-316243-treated rats derive directly from white adipocytes. Am J Physiol Cell Physiol 279, C670-681.

Ho, E., and Shimada, Y. (1978). Formation of the epicardium studied with the scanning electron microscope. Dev Biol 66, 579-585.

Hondares, E., Gallego-Escuredo, J.M., Flachs, P., Frontini, A., Cereijo, R., Goday, A., Perugini, J., Kopecky, P., Giralt, M., Cinti, S., et al. (2014). Fibroblast growth factor-21 is expressed in neonatal and pheochromocytoma-induced adult human brown adipose tissue. Metabolism 63, 312-317.

Hondares, E., Iglesias, R., Giralt, A., Gonzalez, F.J., Giralt, M., Mampel, T., and Villarroya, F. (2011). Thermogenic activation induces FGF21 expression and release in brown adipose tissue. J Biol Chem 286, 12983-12990.

Horton, G.M. (1981). Responses of shorn and full-fleeced lambs given two levels of feed intake and exposed to warm and cold temperatures. Am J Vet Res 42, 2151-2154.

Hotamisligil, G.S., Arner, P., Caro, J.F., Atkinson, R.L., and Spiegelman, B.M. (1995). Increased adipose tissue expression of tumor necrosis factor-alpha in human obesity and insulin resistance. J Clin Invest 95, 2409-2415.

Houseknecht, K.L., Baile, C.A., Matteri, R.L., and Spurlock, M.E. (1998). The biology of leptin: a review. J Anim Sci 76, 1405-1420.

Hu, F., Wang, M., Xiao, T., Yin, B., He, L., Meng, W., Dong, M., and Liu, F. (2015a). miR-30 promotes thermogenesis and the development of beige fat by targeting RIP140. Diabetes 64, 2056-2068.

Hu, W., Shi, L., Zhou, P.H., and Zhang, X.B. (2015b). Plasma concentrations of adrenomedullin and atrial and brain natriuretic peptides in patients with adrenal pheochromocytoma. Oncol Lett 10, 3163-3170.

Huang, S.G., and Klingenberg, M. (1996). Two-stage nucleotide binding mechanism and its implications to H+ transport inhibition of the uncoupling protein from brown adipose tissue mitochondria. Biochemistry 35, 7846-7854.

Hubert, H.B., Feinleib, M., McNamara, P.M., and Castelli, W.P. (1983). Obesity as an independent risk factor for cardiovascular disease: a 26-year follow-up of participants in the Framingham Heart Study. Circulation 67, 968-977.

Hull, D., and Segall, M.M. (1965). Contribution of brown adipose tissue to heat production in new-born rabbit J Physiol-London 181, 449-&.

Iacobellis, G., di Gioia, C.R., Di Vito, M., Petramala, L., Cotesta, D., De Santis, V., Vitale, D., Tritapepe, L., and Letizia, C. (2009). Epicardial adipose tissue and intracoronary adrenomedullin levels in coronary artery disease. Horm Metab Res 41, 855-860.

Iacobellis, G., Malavazos, A.E., and Corsi, M.M. (2011). Epicardial fat: from the biomolecular aspects to the clinical practice. Int J Biochem Cell Biol 43, 1651-1654.

Iacobellis, G., Pistilli, D., Gucciardo, M., Leonetti, F., Miraldi, F., Brancaccio, G., Gallo, P., and di Gioia, C.R. (2005). Adiponectin expression in human epicardial adipose tissue in vivo is lower in patients with coronary artery disease. Cytokine 29, 251-255.

Ingalls, A.M., Dickie, M.M., and Snell, G.D. (1950). Obese, a new mutation in the house mouse J Hered 41, 317-318.

Inokuma, K., Ogura-Okamatsu, Y., Toda, C., Kimura, K., Yamashita, H., and Saito, M. (2005). Uncoupling protein 1 is necessary for norepinephrine-induced glucose utilization in brown adipose tissue. Diabetes 54, 1385-1391.

Ishibashi, J., and Seale, P. (2010). Medicine. Beige can be slimming. Science 328, 1113-1114.

Iwanaga, Y., Nishi, I., Furuichi, S., Noguchi, T., Sase, K., Kihara, Y., Goto, Y., and Nonogi, H. (2006). B-type natriuretic peptide strongly reflects diastolic wall stress in patients with chronic heart failure: comparison between systolic and diastolic heart failure. J Am Coll Cardiol 47, 742-748.

Jensen, E.C. (2012). The basics of western blotting. Anat Rec (Hoboken) 295, 369-371.

Jespersen, N.Z., Larsen, T.J., Peijs, L., Daugaard, S., Homoe, P., Loft, A., de Jong, J., Mathur, N., Cannon, B., Nedergaard, J., et al. (2013). A classical brown adipose tissue mRNA signature partly overlaps with brite in the supraclavicular region of adult humans. Cell Metab 17, 798-805.

Jezek, P., Costa, A.D., and Vercesi, A.E. (1996). Evidence for anion-translocating plant uncoupling mitochondrial protein in potato mitochondria. J Biol Chem 271, 32743-32748.

Jia, R., Luo, X.Q., Wang, G., Lin, C.X., Qiao, H., Wang, N., Yao, T., Barclay, J.L., Whitehead, J.P., Luo, X., et al. (2016). Characterization of cold-induced remodeling reveals depot-specific differences across and within brown and white adipose tissues in mice. Acta Physiol (Oxf).

Jiang, Y., Xie, M., Chen, W., Talbot, R., Maddox, J.F., Faraut, T., Wu, C., Muzny, D.M., Li, Y., Zhang, W., et al. (2014). The sheep genome illuminates biology of the rumen and lipid metabolism. Science 344, 1168-1173.

Jovanovic, Z., and Yeo, G.S.H. (2010). Central leptin signalling: Beyond the arcuate nucleus. Auton Neurosci-Basic Clin 156, 8-14.

Kabir, M., Catalano, K.J., Ananthnarayan, S., Kim, S.P., Van Citters, G.W., Dea, M.K., and Bergman, R.N. (2005). Molecular evidence supporting the portal theory: a causative link between visceral adiposity and hepatic insulin resistance. Am J Physiol Endocrinol Metab 288, E454-461.

Kajimura, S., Seale, P., and Spiegelman, B.M. (2010). Transcriptional Control of Brown Fat Development. Cell Metab 11, 257-262.

Kamp, F., and Hamilton, J.A. (1992). pH gradients across phospholipid membranes caused by fast flip-flop of un-ionized fatty acids. Proc Natl Acad Sci U S A 89, 11367-11370.

Kamp, F., Hamilton, J.A., Kamp, F., Westerhoff, H.V., and Hamilton, J.A. (1993). Movement of fatty acids, fatty acid analogues, and bile acids across phospholipid bilayers. Biochemistry 32, 11074-11086.

Keipert, S., and Jastroch, M. (2014). Brite/beige fat and UCP1 - is it thermogenesis? Biochim Biophys Acta 1837, 1075-1082.

Kelley, D.E., Thaete, F.L., Troost, F., Huwe, T., and Goodpaster, B.H. (2000). Subdivisions of subcutaneous abdominal adipose tissue and insulin resistance. Am J Physiol Endocrinol Metab 278, E941-948.

Kershaw, E.E., and Flier, J.S. (2004). Adipose tissue as an endocrine organ. Journal of Clinical Endocrinology & Metabolism 89, 2548-2556.

Khedoe, P.P., Hoeke, G., Kooijman, S., Dijk, W., Buijs, J.T., Kersten, S., Havekes, L.M., Hiemstra, P.S., Berbee, J.F., Boon, M.R., et al. (2015). Brown adipose tissue takes up plasma triglycerides mostly after lipolysis. J Lipid Res 56, 51-59.

Kim, S.H., Chung, J.H., Song, S.W., Jung, W.S., Lee, Y.A., and Kim, H.N. (2016). Relationship between deep subcutaneous abdominal adipose tissue and metabolic syndrome: a case control study. Diabetol Metab Syndr 8, 10.

Kinnunen, P., Vuolteenaho, O., and Ruskoaho, H. (1993). Mechanisms of atrial and brain natriuretic peptide release from rat ventricular myocardium: effect of stretching. Endocrinology 132, 1961-1970.

Kiskinis, E., Hallberg, M., Christian, M., Olofsson, M., Dilworth, S.M., White, R., and Parker, M.G. (2007). RIP140 directs histone and DNA methylation to silence Ucp1 expression in white adipocytes. EMBO J 26, 4831-4840.

Kissova, I., Deffieu, M., Manon, S., and Camougrand, N. (2004). Uth1p is involved in the autophagic degradation of mitochondria. J Biol Chem 279, 39068-39074.

Klaus, S., Ely, M., Encke, D., and Heldmaier, G. (1995). Functional assessment of white and brown adipocyte development and energy metabolism in cell culture. Dissociation of terminal differentiation and thermogenesis in brown adipocytes. J Cell Sci 108 (Pt 10), 3171-3180.

Klein, S., Allison, D.B., Heymsfield, S.B., Kelley, D.E., Leibel, R.L., Nonas, C., and Kahn, R. (2007). Waist circumference and cardiometabolic risk - A consensus statement from shaping America's health: Association for Weight Management and Obesity Prevention; NAASO, The Obesity Society; The American Society for Nutrition; And the American Diabetes Association. Diabetes Care 30, 1647-1652.

Klingenberg, M., Echtay, K.S., Bienengraeber, M., Winkler, E., and Huang, S.G. (1999). Structure-function relationship in UCP1. Int J Obes Relat Metab Disord 23 Suppl 6, S24-29.

Kohn, A.D., Summers, S.A., Birnbaum, M.J., and Roth, R.A. (1996). Expression of a constitutively active Akt Ser/Thr kinase in 3T3-L1 adipocytes stimulates glucose uptake and glucose transporter 4 translocation. J Biol Chem 271, 31372-31378.

Kohno, M., Horio, T., Yokokawa, K., Murakawa, K., Yasunari, K., Akioka, K., Tahara, A., Toda, I., Takeuchi, K., Kurihara, N., et al. (1992). Brain natriuretic peptide as a cardiac hormone in essential hypertension. Am J Med 92, 29-34.

Kopecky, J., Clarke, G., Enerback, S., Spiegelman, B., and Kozak, L.P. (1995). Expression of the mitochondrial uncoupling protein gene from the aP2 gene promoter prevents genetic obesity. J Clin Invest 96, 2914-2923.

Kovsan, J., Bluher, M., Tarnovscki, T., Kloting, N., Kirshtein, B., Madar, L., Shai, I., Golan, R., Harman-Boehm, I., Schon, M.R., et al. (2011). Altered autophagy in human adipose tissues in obesity. J Clin Endocrinol Metab 96, E268-277.

Kozak, L.P., and Anunciado-Koza, R. (2008). UCP1: its involvement and utility in obesity. Int J Obes 32, S32-S38.

Kramarova, T.V., Shabalina, I.G., Andersson, U., Westerberg, R., Carlberg, I., Houstek, J., Nedergaard, J., and Cannon, B. (2008). Mitochondrial ATP synthase levels in brown adipose tissue are governed by the c-Fo subunit P1 isoform. FASEB J 22, 55-63.

Kriegova, E., Arakelyan, A., Fillerova, R., Zatloukal, J., Mrazek, F., Navratilova, Z., Kolek, V., du Bois, R.M., and Petrek, M. (2008). PSMB2 and RPL32 are suitable denominators to normalize gene expression profiles in bronchoalveolar cells. BMC Mol Biol 9, 69.

Kubista, M., Andrade, J.M., Bengtsson, M., Forootan, A., Jonak, J., Lind, K., Sindelka, R., Sjoback, R., Sjogreen, B., Strombom, L., et al. (2006). The real-time polymerase chain reaction. Mol Aspects Med 27, 95-125.

Kvetnansky, R., Gewirtz, G.P., Weise, V.K., and Kopin, I.J. (1971). Catecholamine-synthesizing enzymes in the rat adrenal gland during exposure to cold. Am J Physiol 220, 928-931.

Kyrylkova, K., Kyryachenko, S., Leid, M., and Kioussi, C. (2012). Detection of apoptosis by TUNEL assay. Methods Mol Biol 887, 41-47.

Lang, R.E., Tholken, H., Ganten, D., Luft, F.C., Ruskoaho, H., and Unger, T. (1985). Atrial natriuretic factor--a circulating hormone stimulated by volume loading. Nature 314, 264-266.

Leary, C., Leese, H.J., and Sturmey, R.G. (2015). Human embryos from overweight and obese women display phenotypic and metabolic abnormalities. Hum Reprod 30, 122-132.

Lee, P., Bova, R., Schofield, L., Bryant, W., Dieckmann, W., Slattery, A., Govendir, M.A., Emmett, L., and Greenfield, J.R. (2016). Brown Adipose Tissue Exhibits a Glucose-Responsive Thermogenic Biorhythm in Humans. Cell Metab.

Lee, P., Smith, S., Linderman, J., Courville, A.B., Brychta, R.J., Dieckmann, W., Werner, C.D., Chen, K.Y., and Celi, F.S. (2014). Temperature-acclimated brown adipose tissue modulates insulin sensitivity in humans. Diabetes 63, 3686-3698.

Lee, P., Swarbrick, M.M., and Ho, K.K. (2013). Brown Adipose Tissue in Adult Humans: A Metabolic Renaissance. Endocr Rev.

Lee, P., Zhao, J.T., Swarbrick, M.M., Gracie, G., Bova, R., Greenfield, J.R., Freund, J., and Ho, K.K. (2011). High prevalence of brown adipose tissue in adult humans. J Clin Endocrinol Metab 96, 2450-2455.

Lenders, J.W., Duh, Q.Y., Eisenhofer, G., Gimenez-Roqueplo, A.P., Grebe, S.K., Murad, M.H., Naruse, M., Pacak, K., and Young, W.F., Jr. (2014). Pheochromocytoma and paraganglioma: an endocrine society clinical practice guideline. J Clin Endocrinol Metab 99, 1915-1942.

Lenders, J.W., Eisenhofer, G., Mannelli, M., and Pacak, K. (2005). Phaeochromocytoma. Lancet 366, 665-675.

Leonardsson, G., Steel, J.H., Christian, M., Pocock, V., Milligan, S., Bell, J., So, P.W., Medina-Gomez, G., Vidal-Puig, A., White, R., et al. (2004). Nuclear receptor corepressor RIP140 regulates fat accumulation. Proc Natl Acad Sci U S A 101, 8437-8442.

Lepper, C., and Fan, C.M. (2010). Inducible lineage tracing of Pax7-descendant cells reveals embryonic origin of adult satellite cells. Genesis 48, 424-436.

Li, Y., Fromme, T., Schweizer, S., Schottl, T., and Klingenspor, M. (2014). Taking control over intracellular fatty acid levels is essential for the analysis of thermogenic function in cultured primary brown and brite/beige adipocytes. EMBO Rep 15, 1069-1076.

Lichtenbelt, W.D.v.M. (2011). Human brown fat and obesity: methodological aspects. Front Endocrinol (Lausanne) 2, 52.

Lichtenbelt, W.D.v.M., Vanhommerig, J.W., Smulders, N.M., Drossaerts, J.M.A.F.L., Kemerink, G.J., Bouvy, N.D., Schrauwen, P., and Teule, G.J.J. (2009). Cold-Activated Brown Adipose Tissue in Healthy Men. N Engl J Med 360, 1500-1508.

Lidell, M.E., Betz, M.J., Dahlqvist Leinhard, O., Heglind, M., Elander, L., Slawik, M., Mussack, T., Nilsson, D., Romu, T., Nuutila, P., et al. (2013). Evidence for two types of brown adipose tissue in humans. Nat Med 19, 631-634.

Lin, C.S., and Klingenberg, M. (1980). Isolation of the uncoupling protein from brown adipose tissue mitochondria. FEBS Lett 113, 299-303.

Lindholm, E., Klannemark, M., Agardh, E., Groop, L., and Agardh, C.D. (2004). Putative role of polymorphisms in UCP1-3 genes for diabetic nephropathy. J Diabetes Complications 18, 103-107.

Liu, J., Fox, C.S., Hickson, D., Sarpong, D., Ekunwe, L., May, W.D., Hundley, G.W., Carr, J.J., and Taylor, H.A. (2010). Pericardial adipose tissue, atherosclerosis, and cardiovascular disease risk factors: the Jackson heart study. Diabetes Care 33, 1635-1639.

Liu, X., Post, W.S., McLenithan, J., Terrin, M., Magder, L., Zeb, I., Budoff, M., and Mitchell, B.D. (2014). Determinants of intrathoracic adipose tissue volume and associations with cardiovascular disease risk factors in Amish. Nutr Metab Cardiovasc Dis 24, 286-293.

Lomax, M.A., Sadiq, F., Karamanlidis, G., Karamitri, A., Trayhurn, P., and Hazlerigg, D.G. (2007). Ontogenic loss of brown adipose tissue sensitivity to beta-adrenergic stimulation in the ovine. Endocrinology 148, 461-468.

Long, J.Z., Svensson, K.J., Tsai, L., Zeng, X., Roh, H.C., Kong, X., Rao, R.R., Lou, J., Lokurkar, I., Baur, W., et al. (2014). A smooth muscle-like origin for beige adipocytes. Cell Metab 19, 810-820.

Lu, M.T., Park, J., Ghemigian, K., Mayrhofer, T., Puchner, S.B., Liu, T., Fleg, J.L., Udelson, J.E., Truong, Q.A., Ferencik, M., et al. (2016). Epicardial and paracardial adipose tissue volume and attenuation - Association with high-risk coronary plaque on computed tomographic angiography in the ROMICAT II trial. Atherosclerosis 251, 47-54.

Ludwig, J., Viggiano, T.R., McGill, D.B., and Oh, B.J. (1980). Nonalcoholic steatohepatitis: Mayo Clinic experiences with a hitherto unnamed disease. Mayo Clin Proc 55, 434-438.

Lusis, A.J., Seldin, M.M., Allayee, H., Bennett, B.J., Civelek, M., Davis, R.C., Eskin, E., Farber, C.R., Hui, S., Mehrabian, M., et al. (2016). The Hybrid Mouse Diversity Panel: a resource for systems genetics analyses of metabolic and cardiovascular traits. J Lipid Res 57, 925-942.

Maack, T., Suzuki, M., Almeida, F.A., Nussenzveig, D., Scarborough, R.M., McEnroe, G.A., and Lewicki, J.A. (1987). Physiological role of silent receptors of atrial natriuretic factor. Science 238, 675-678.

MacDougald, O.A., Hwang, C.S., Fan, H., and Lane, M.D. (1995). Regulated expression of the obese gene product (leptin) in white adipose tissue and 3T3-L1 adipocytes. Proc Natl Acad Sci U S A 92, 9034-9037.

Magkos, F., Fraterrigo, G., Yoshino, J., Luecking, C., Kirbach, K., Kelly, S.C., de Las Fuentes, L., He, S., Okunade, A.L., Patterson, B.W., et al. (2016). Effects of Moderate and Subsequent Progressive Weight Loss on Metabolic Function and Adipose Tissue Biology in Humans with Obesity. Cell Metab 23, 591-601.

Mahabadi, A.A., Massaro, J.M., Rosito, G.A., Levy, D., Murabito, J.M., Wolf, P.A., O'Donnell, C.J., Fox, C.S., and Hoffmann, U. (2009). Association of pericardial fat, intrathoracic fat, and visceral abdominal fat with cardiovascular disease burden: the Framingham Heart Study. Eur Heart J 30, 850-856.

Maloney, S.K., Fuller, A., Mitchell, D., Gordon, C., and Overton, J.M. (2014). Translating animal model research: does it matter that our rodents are cold? Physiology (Bethesda) 29, 413-420.

Mant, A., Williams, S., and O'Kelly, I. (2013). Acid sensitive background potassium channels K2P3.1 and K2P9.1 undergo rapid dynamin-dependent endocytosis. Channels (Austin) 7, 288-302.

Marchington, J.M., Mattacks, C.A., and Pond, C.M. (1989). Adipose tissue in the mammalian heart and pericardium: structure, foetal development and biochemical properties. Comp Biochem Physiol B 94, 225-232.

Marchington, J.M., and Pond, C.M. (1990). Site-specific properties of pericardial and epicardial adipose tissue: the effects of insulin and high-fat feeding on lipogenesis and the incorporation of fatty acids in vitro. Int J Obes 14, 1013-1022.

Markan, K.R., Naber, M.C., Ameka, M.K., Anderegg, M.D., Mangelsdorf, D.J., Kliewer, S.A., Mohammadi, M., and Potthoff, M.J. (2014). Circulating FGF21 is liver derived and enhances glucose uptake during refeeding and overfeeding. Diabetes 63, 4057-4063.

Mazurek, T., Zhang, L., Zalewski, A., Mannion, J.D., Diehl, J.T., Arafat, H., Sarov-Blat, L., O'Brien, S., Keiper, E.A., Johnson, A.G., et al. (2003). Human epicardial adipose tissue is a source of inflammatory mediators. Circulation 108, 2460-2466.

McKenney, M.L., Schultz, K.A., Boyd, J.H., Byrd, J.P., Alloosh, M., Teague, S.D., Arce-Esquivel, A.A., Fain, J.N., Laughlin, M.H., Sacks, H.S., et al. (2014). Epicardial adipose excision slows the progression of porcine coronary atherosclerosis. Journal of Cardiothoracic Surgery 9.

McLaughlin, T., Lamendola, C., Liu, A., and Abbasi, F. (2011). Preferential fat deposition in subcutaneous versus visceral depots is associated with insulin sensitivity. J Clin Endocrinol Metab 96, E1756-1760.

Miroux, B., Frossard, V., Raimbault, S., Ricquier, D., and Bouillaud, F. (1993). The topology of the brown adipose tissue mitochondrial uncoupling protein determined with

antibodies against its antigenic sites revealed by a library of fusion proteins. EMBO J 12, 3739-3745.

Mishra, R.K., Beatty, A.L., Jaganath, R., Regan, M., Wu, A.H., and Whooley, M.A. (2014). B-type natriuretic peptides for the prediction of cardiovascular events in patients with stable coronary heart disease: the Heart and Soul Study. J Am Heart Assoc 3.

Mitschke, M.M., Hoffmann, L.S., Gnad, T., Scholz, D., Kruithoff, K., Mayer, P., Haas, B., Sassmann, A., Pfeifer, A., and Kilic, A. (2013). Increased cGMP promotes healthy expansion and browning of white adipose tissue. FASEB J 27, 1621-1630.

Mittelman, S.D., Van Citters, G.W., Kim, S.P., Davis, D.A., Dea, M.K., Hamilton-Wessler, M., and Bergman, R.N. (2000). Longitudinal compensation for fat-induced insulin resistance includes reduced insulin clearance and enhanced beta-cell response. Diabetes 49, 2116-2125.

Miyoshi, H., Souza, S.C., Zhang, H.H., Strissel, K.J., Christoffolete, M.A., Kovsan, J., Rudich, A., Kraemer, F.B., Bianco, A.C., Obin, M.S., et al. (2006). Perilipin promotes hormone-sensitive lipase-mediated adipocyte lipolysis via phosphorylation-dependent and -independent mechanisms. J Biol Chem 281, 15837-15844.

Mondal, S., Raja, K., Schweizer, U., and Mugesh, G. (2016). Chemistry and Biology in the Biosynthesis and Action of Thyroid Hormones. Angew Chem Int Ed Engl 55, 7606-7630.

Moreno-Santos, I., Perez-Belmonte, L.M., Macias-Gonzalez, M., Mataro, M.J., Castellano, D., Lopez-Garrido, M., Porras-Martin, C., Sanchez-Fernandez, P.L., Gomez-Doblas, J.J., Cardona, F., et al. (2016). Type 2 diabetes is associated with decreased PGC1alpha expression in epicardial adipose tissue of patients with coronary artery disease. J Transl Med 14, 243.

Mossenbock, K., Vegiopoulos, A., Rose, A.J., Sijmonsma, T.P., Herzig, S., and Schafmeier, T. (2014). Browning of white adipose tissue uncouples glucose uptake from insulin signaling. PLoS One 9, e110428.

Mostyn, A., Attig, L., Larcher, T., Dou, S., Chavatte-Palmer, P., Boukthir, M., Gertler, A., Djiane, J., M, E.S., and Abdennebi-Najar, L. (2014). UCP1 is present in porcine adipose tissue and is responsive to postnatal leptin. J Endocrinol 223, M31-38.

Moulin, K., Truel, N., Andre, M., Arnauld, E., Nibbelink, M., Cousin, B., Dani, C., Penicaud, L., and Casteilla, L. (2001). Emergence during development of the white-adipocyte cell phenotype is independent of the brown-adipocyte cell phenotype. Biochemical Journal 356, 659-664.

Mukoyama, M., Nakao, K., Hosoda, K., Suga, S., Saito, Y., Ogawa, Y., Shirakami, G., Jougasaki, M., Obata, K., Yasue, H., et al. (1991). Brain natriuretic peptide as a novel cardiac hormone in humans. Evidence for an exquisite dual natriuretic peptide system, atrial natriuretic peptide and brain natriuretic peptide. J Clin Invest 87, 1402-1412.

Muppidi, J., Porter, M., and Siegel, R.M. (2004). Measurement of apoptosis and other forms of cell death. Curr Protoc Immunol Chapter 3, Unit 3 17.

Nagano, G., Ohno, H., Oki, K., Kobuke, K., Shiwa, T., Yoneda, M., and Kohno, N. (2015). Activation of classical brown adipocytes in the adult human perirenal depot is highly correlated with PRDM16-EHMT1 complex expression. PLoS One 10, e0122584.

NCD-RisC (2016). Worldwide trends in diabetes since 1980: a pooled analysis of 751 population-based studies with 4.4 million participants. Lancet 387, 1513-1530.

Nedergaard, J., Golozoubova, V., Matthias, A., Asadi, A., Jacobsson, A., and Cannon, B. (2001). UCP1: the only protein able to mediate adaptive non-shivering thermogenesis and metabolic inefficiency. Biochim Biophys Acta-Bioenerg 1504, 82-106.

Nicholls, D.G., and Locke, R.M. (1984). Thermogenic mechanisms in brown fat. Physiol Rev 64, 1-64.

Nicol, F., Lefranc, H., Arthur, J.R., and Trayhurn, P. (1994). Characterization and postnatal development of 5'-deiodinase activity in goat perirenal fat. Am J Physiol 267, R144-149.

Noble, J.E., and Bailey, M.J. (2009). Quantitation of protein. Methods Enzymol 463, 73-95.

Oelkrug, R., Goetze, N., Exner, C., Lee, Y., Ganjam, G.K., Kutschke, M., Muller, S., Stohr, S., Tschop, M.H., Crichton, P.G., et al. (2013). Brown fat in a protoendothermic mammal fuels eutherian evolution. Nat Commun 4, 2140.

Ogawa, Y., Kurosu, H., Yamamoto, M., Nandi, A., Rosenblatt, K.P., Goetz, R., Eliseenkova, A.V., Mohammadi, M., and Kuro-o, M. (2007). BetaKlotho is required for metabolic activity of fibroblast growth factor 21. Proc Natl Acad Sci U S A 104, 7432-7437.

Oishi, P., Sharma, S., Grobe, A., Azakie, A., Harmon, C., Johengen, M.J., Hsu, J.H., Fratz, S., Black, S.M., and Fineman, J.R. (2007). Alterations in cGMP, soluble guanylate cyclase, phosphodiesterase 5, and B-type natriuretic peptide induced by chronic increased pulmonary blood flow in lambs. Pediatr Pulmonol 42, 1057-1071.

Ojha, S., Fainberg, H.P., Wilson, V., Pelella, G., Castellanos, M., May, S.T., Lotto, A.A., Sacks, H., Symonds, M.E., and Budge, H. (2016). Gene pathway development in human epicardial adipose tissue during early life. JCI Insight 1.

Ojha, S., Robinson, L., Yazdani, M., Symonds, M.E., and Budge, H. (2013). Brown adipose tissue genes in pericardial adipose tissue of newborn sheep are downregulated by maternal nutrient restriction in late gestation. Pediatr Res 74, 246-251.

Oka, T., Hikoso, S., Yamaguchi, O., Taneike, M., Takeda, T., Tamai, T., Oyabu, J., Murakawa, T., Nakayama, H., Nishida, K., et al. (2012). Mitochondrial DNA that escapes from autophagy causes inflammation and heart failure. Nature 485, 251-255.

Opie, L.H., and Walfish, P.G. (1963). Plasma free fatty acid concentrations in obesity. N Engl J Med 268, 757-760.

Organization, W.H. (2006). Global Database on Body Mass Index.

Ouellet, V., Labbe, S.M., Blondin, D.P., Phoenix, S., Guerin, B., Haman, F., Turcotte, E.E., Richard, D., and Carpentier, A.C. (2012). Brown adipose tissue oxidative metabolism contributes to energy expenditure during acute cold exposure in humans. J Clin Invest 122, 545-552.

Ouellet, V., Routhier-Labadie, A., Bellemare, W., Lakhal-Chaieb, L., Turcotte, E., Carpentier, A.C., and Richard, D. (2011). Outdoor temperature, age, sex, body mass index, and diabetic status determine the prevalence, mass, and glucose-uptake activity of 18F-FDG-detected BAT in humans. J Clin Endocrinol Metab 96, 192-199.

Owens, K.M., Kulawiec, M., Desouki, M.M., Vanniarajan, A., and Singh, K.K. (2011). Impaired OXPHOS complex III in breast cancer. PLoS One 6, e23846.

Pacak, K., and Del Rivero, J. (2000). Pheochromocytoma. In Endotext, L.J. De Groot, P. Beck-Peccoz, G. Chrousos, K. Dungan, A. Grossman, J.M. Hershman, C. Koch, R. McLachlan, M. New, R. Rebar, et al., eds. (South Dartmouth MA: MDText.com, Inc.).

Packer, L. (1960). Metabolic and structural states of mitochondria. I. Regulation by adenosine diphosphate. J Biol Chem 235, 242-249.

Pagnon, J., Matzaris, M., Stark, R., Meex, R.C., Macaulay, S.L., Brown, W., O'Brien, P.E., Tiganis, T., and Watt, M.J. (2012). Identification and functional characterization of protein kinase A phosphorylation sites in the major lipolytic protein, adipose triglyceride lipase. Endocrinology 153, 4278-4289.

Palou, A., Pico, C., Bonet, M.L., and Oliver, P. (1998). The uncoupling protein, thermogenin. Int J Biochem Cell Biol 30, 7-11.

Pan, C.S., Zhang, J., Yu, F., Teng, X., Cao, C.Q., Wu, W., Tang, C.S., and Qi, Y.F. (2010). Adrenomedullin ameliorates the development of atherosclerosis in apoE-/- mice. Peptides 31, 1150-1158.

Park, J., Byun, B.H., Jung, C.W., Moon, H., Chang, K.J., Lim, I., Kim, B.I., Choi, C.W., and Lim, S.M. (2014). Perirenal (18)F-FDG Uptake in a Patient with a Pheochromocytoma. Nucl Med Mol Imaging 48, 233-236.

Patsouris, D., Qi, P., Abdullahi, A., Stanojcic, M., Chen, P., Parousis, A., Amini-Nik, S., and Jeschke, M.G. (2015). Burn Induces Browning of the Subcutaneous White Adipose Tissue in Mice and Humans. Cell Rep 13, 1538-1544.

Paz-Filho, G., Wong, M.L., and Licinio, J. (2011). Ten years of leptin replacement therapy. Obesity Reviews 12, e315-e323.

Peirce, V., Carobbio, S., and Vidal-Puig, A. (2014). The different shades of fat. Nature 510, 76-83.

Pelleymounter, M.A., Cullen, M.J., Baker, M.B., Hecht, R., Winters, D., Boone, T., and Collins, F. (1995). Effects of the obese gene-product on body-weight regulation in ob/ob mice Science 269, 540-543.

Petrovic, N., Walden, T.B., Shabalina, I.G., Timmons, J.A., Cannon, B., and Nedergaard, J. (2010). Chronic peroxisome proliferator-activated receptor gamma (PPARgamma) activation of epididymally derived white adipocyte cultures reveals a population of thermogenically competent, UCP1-containing adipocytes molecularly distinct from classic brown adipocytes. J Biol Chem 285, 7153-7164.

Petruzzelli, M., Schweiger, M., Schreiber, R., Campos-Olivas, R., Tsoli, M., Allen, J., Swarbrick, M., Rose-John, S., Rincon, M., Robertson, G., et al. (2014). A switch from white to brown fat increases energy expenditure in cancer-associated cachexia. Cell Metab 20, 433-447.

Picciotto, M.R., and Wickman, K. (1998). Using knockout and transgenic mice to study neurophysiology and behavior. Physiol Rev 78(4):1131-63.

Plaisier, C.L., Bennett, B.J., He, A., Guan, B., Lusis, A.J., Reue, K., and Vergnes, L. (2012). Zbtb16 has a role in brown adipocyte bioenergetics. Nutr Diabetes 2, e46.

Poher, A.L., Veyrat-Durebex, C., Altirriba, J., Montet, X., Colin, D.J., Caillon, A., Lyautey, J., and Rohner-Jeanrenaud, F. (2015). Ectopic UCP1 Overexpression in White Adipose Tissue Improves Insulin Sensitivity in Lou/C Rats, a Model of Obesity Resistance. Diabetes 64, 3700-3712.

Ponchel, F., Dorak, M.T. (Ed.) (2006). Real-time PCR (London & New York: Taylor & Francis), pp. 146.

Pope, M., Budge, H., and Symonds, M.E. (2014). The developmental transition of ovine adipose tissue through early life. Acta Physiol 210, 20-30.

Poulos, S.P., Hausman, D.B., and Hausman, G.J. (2010). The development and endocrine functions of adipose tissue. Molecular and Cellular Endocrinology 323, 20-34.

Powelka, A.M., Seth, A., Virbasius, J.V., Kiskinis, E., Nicoloro, S.M., Guilherme, A., Tang, X., Straubhaar, J., Cherniack, A.D., Parker, M.G., et al. (2006). Suppression of oxidative metabolism and mitochondrial biogenesis by the transcriptional corepressor RIP140 in mouse adipocytes. J Clin Invest 116, 125-136.

Power, C., Lake, J.K., and Cole, T.J. (1997). Measurement and long-term health risks of child and adolescent fatness. Int J Obes Relat Metab Disord 21, 507-526.

Pradidarcheep, W., Stallen, J., Labruyere, W.T., Dabhoiwala, N.F., Michel, M.C., and Lamers, W.H. (2009). Lack of specificity of commercially available antisera against muscarinergic and adrenergic receptors. Naunyn Schmiedebergs Arch Pharmacol 379, 397-402.

Prentice, A.M. (2006). The emerging epidemic of obesity in developing countries. Int J Epidemiol 35, 93-99.

Puar, T., van Berkel, A., Gotthardt, M., Havekes, B., Hermus, A.R., Lenders, J.W., van Marken Lichtenbelt, W.D., Xu, Y., Brans, B., and Timmers, H.J. (2016). Genotype-Dependent Brown Adipose Tissue Activation in Patients With Pheochromocytoma and Paraganglioma. J Clin Endocrinol Metab 101, 224-232.

Puigserver, P., Wu, Z., Park, C.W., Graves, R., Wright, M., and Spiegelman, B.M. (1998). A cold-inducible coactivator of nuclear receptors linked to adaptive thermogenesis. Cell 92, 829-839.

Rabelo, R., Schifman, A., Rubio, A., Sheng, X., and Silva, J.E. (1995). Delineation of thyroid hormone-responsive sequences within a critical enhancer in the rat uncoupling protein gene. Endocrinology 136, 1003-1013.

Radonic, A., Thulke, S., Mackay, I.M., Landt, O., Siegert, W., and Nitsche, A. (2004). Guideline to reference gene selection for quantitative real-time PCR. Biochem Biophys Res Commun 313, 856-862.

Randle, P.J., Garland, P.B., Hales, C.N., and Newsholme, E.A. (1963). The glucose fatty-acid cycle. Its role in insulin sensitivity and the metabolic disturbances of diabetes mellitus. Lancet 1, 785-789.

Rao, R.R., Long, J.Z., White, J.P., Svensson, K.J., Lou, J., Lokurkar, I., Jedrychowski, M.P., Ruas, J.L., Wrann, C.D., Lo, J.C., et al. (2014). Meteorin-like is a hormone that regulates immune-adipose interactions to increase beige fat thermogenesis. Cell 157, 1279-1291.

Renehan, A.G., Tyson, M., Egger, M., Heller, R.F., and Zwahlen, M. (2008). Body-mass index and incidence of cancer: a systematic review and meta-analysis of prospective observational studies. Lancet 371, 569-578.

Reynisdottir, S., Dauzats, M., Thorne, A., and Langin, D. (1997). Comparison of hormone-sensitive lipase activity in visceral and subcutaneous human adipose tissue. J Clin Endocrinol Metab 82, 4162-4166.

Ribeiro, M.O., Bianco, S.D., Kaneshige, M., Schultz, J.J., Cheng, S.Y., Bianco, A.C., and Brent, G.A. (2010). Expression of uncoupling protein 1 in mouse brown adipose tissue is thyroid hormone receptor-beta isoform specific and required for adaptive thermogenesis. Endocrinology 151, 432-440.

Ricci, R., and Bevilacqua, F. (2012). The potential role of leptin and adiponectin in obesity: A comparative review. Vet J 191, 292-298.

Ricquier, D., Nechad, M., and Mory, G. (1982). Ultrastructural and biochemical characterization of human brown adipose tissue in pheochromocytoma. J Clin Endocrinol Metab 54, 803-807.

Robb, L., Mifsud, L., Hartley, L., Biben, C., Copeland, N.G., Gilbert, D.J., Jenkins, N.A., and Harvey, R.P. (1998). epicardin: A novel basic helix-loop-helix transcription factor gene expressed in epicardium, branchial arch myoblasts, and mesenchyme of developing lung, gut, kidney, and gonads. Dev Dyn 213, 105-113.

Robinson, T.L., Sutherland, I.A., and Sutherland, J. (2007). Validation of candidate bovine reference genes for use with real-time PCR. Vet Immunol Immunopathol 115, 160-165.

Rogers, G.W., Brand, M.D., Petrosyan, S., Ashok, D., Elorza, A.A., Ferrick, D.A., and Murphy, A.N. (2011). High throughput microplate respiratory measurements using minimal quantities of isolated mitochondria. PLoS One 6, e21746.

Rong, J.X., Qiu, Y., Hansen, M.K., Zhu, L., Zhang, V., Xie, M., Okamoto, Y., Mattie, M.D., Higashiyama, H., Asano, S., et al. (2007). Adipose mitochondrial biogenesis is suppressed in db/db and high-fat diet-fed mice and improved by rosiglitazone. Diabetes 56, 1751-1760.

Rosell, M., Kaforou, M., Frontini, A., Okolo, A., Chan, Y.W., Nikolopoulou, E., Millership, S., Fenech, M.E., MacIntyre, D., Turner, J.O., et al. (2014). Brown and white adipose tissues: intrinsic differences in gene expression and response to cold exposure in mice. Am J Physiol Endocrinol Metab 306, E945-964.

Rosenwald, M., Perdikari, A., Rulicke, T., and Wolfrum, C. (2013). Bi-directional interconversion of brite and white adipocytes. Nat Cell Biol 15, 659-667.

Rosito, G.A., Massaro, J.M., Hoffmann, U., Ruberg, F.L., Mahabadi, A.A., Vasan, R.S., O'Donnell, C.J., and Fox, C.S. (2008). Pericardial fat, visceral abdominal fat, cardiovascular disease risk factors, and vascular calcification in a community-based sample: the Framingham Heart Study. Circulation 117, 605-613.

Rothwell, N.J., and Stock, M.J. (1989). Surgical removal of brown fat results in rapid and complete compensation by other depots. Am J Physiol 257, R253-258.

Rousseau, C., Bourbouloux, E., Campion, L., Fleury, N., Bridji, B., Chatal, J.F., Resche, I., and Campone, M. (2006). Brown fat in breast cancer patients: analysis of serial (18)F-FDG PET/CT scans. Eur J Nucl Med Mol Imaging 33, 785-791.

Rytka, J.M., Wueest, S., Schoenle, E.J., and Konrad, D. (2011). The portal theory supported by venous drainage-selective fat transplantation. Diabetes 60, 56-63.

Sacks, H.S., and Fain, J.N. (2007). Human epicardial adipose tissue: a review. Am Heart J 153, 907-917.

Sacks, H.S., and Fain, J.N. (2011). Human epicardial fat: what is new and what is missing? Clinical and Experimental Pharmacology and Physiology 38, 879-887.

Sacks, H.S., Fain, J.N., Bahouth, S.W., Ojha, S., Frontini, A., Budge, H., Cinti, S., and Symonds, M.E. (2013). Adult Epicardial Fat Exhibits Beige Features. Journal of Clinical Endocrinology & Metabolism 98, E1448-E1455.

Sacks, H.S., Fain, J.N., Holman, B., Cheema, P., Chary, A., Parks, F., Karas, J., Optican, R., Bahouth, S.W., Garrett, E., et al. (2009). Uncoupling Protein-1 and Related Messenger Ribonucleic Acids in Human Epicardial and Other Adipose Tissues: Epicardial Fat Functioning as Brown Fat. Journal of Clinical Endocrinology & Metabolism 94, 3611-3615.

Sadoul, J.L., Peyron, J.F., Ballotti, R., Debant, A., Fehlmann, M., and Van Obberghen, E. (1985). Identification of a cellular 110 000-Da protein substrate for the insulin-receptor kinase. Biochem J 227, 887-892.

Saito, M., Okamatsu-Ogura, Y., Matsushita, M., Watanabe, K., Yoneshiro, T., Nio-Kobayashi, J., Iwanaga, T., Miyagawa, M., Kameya, T., Nakada, K., et al. (2009). High incidence of metabolically active brown adipose tissue in healthy adult humans: effects of cold exposure and adiposity. Diabetes 58, 1526-1531.

Saito, Y., Nakao, K., Itoh, H., Yamada, T., Mukoyama, M., Arai, H., Hosoda, K., Shirakami, G., Suga, S., Minamino, N., et al. (1989). Brain natriuretic peptide is a novel cardiac hormone. Biochem Biophys Res Commun 158, 360-368.

Sanchez-Gurmaches, J., and Guertin, D.A. (2013). Adipocyte lineages: Tracing back the origins of fat. Biochim Biophys Acta.

Sarzani, R., Dessi-Fulgheri, P., Paci, V.M., Espinosa, E., and Rappelli, A. (1996). Expression of natriuretic peptide receptors in human adipose and other tissues. J Endocrinol Invest 19, 581-585.

Schermer, S.J., Bird, J.A., Lomax, M.A., Shepherd, D.A., and Symonds, M.E. (1996). Effect of fetal thyroidectomy on brown adipose tissue and thermoregulation in newborn lambs. Reprod Fertil Dev 8, 995-1002.

Schiebinger, R.J., Baker, M.Z., and Linden, J. (1987). Effect of adrenergic and muscarinic cholinergic agonists on atrial natriuretic peptide secretion by isolated rat atria. Potential role of the autonomic nervous system in modulating atrial natriuretic peptide secretion. J Clin Invest 80, 1687-1691.

Schimmel, R.J., Buhlinger, C.A., and Serio, R. (1980). Activation of adenosine 3',5'-monophosphate-dependent protein kinase and its relationship to cyclic AMP and lipolysis in hamster adipose tissue. J Lipid Res 21, 250-256.

Schlein, C., Talukdar, S., Heine, M., Fischer, A.W., Krott, L.M., Nilsson, S.K., Brenner, M.B., Heeren, J., and Scheja, L. (2016). FGF21 Lowers Plasma Triglycerides by Accelerating Lipoprotein Catabolism in White and Brown Adipose Tissues. Cell Metab 23, 441-453.

Schweiger, M., Eichmann, T.O., Taschler, U., Zimmermann, R., Zechner, R., and Lass, A. (2014). Measurement of Lipolysis. Methods Enzymol 538, 171-193.

Seale, P., Bjork, B., Yang, W., Kajimura, S., Chin, S., Kuang, S., Scime, A., Devarakonda, S., Conroe, H.M., Erdjument-Bromage, H., et al. (2008). PRDM16 controls a brown fat/skeletal muscle switch. Nature 454, 961-967.

Seale, P., Conroe, H.M., Estall, J., Kajimura, S., Frontini, A., Ishibashi, J., Cohen, P., Cinti, S., and Spiegelman, B.M. (2011). Prdm16 determines the thermogenic program of subcutaneous white adipose tissue in mice. J Clin Invest 121, 96-105.

Sell, H., Deshaies, Y., and Richard, D. (2004). The brown adipocyte: update on its metabolic role. International Journal of Biochemistry & Cell Biology 36, 2098-2104.

Semenov, A.G., Tamm, N.N., Seferian, K.R., Postnikov, A.B., Karpova, N.S., Serebryanaya, D.V., Koshkina, E.V., Krasnoselsky, M.I., and Katrukha, A.G. (2010). Processing of pro-B-type natriuretic peptide: furin and corin as candidate convertases. Clin Chem 56, 1166-1176.

Sengenes, C., Zakaroff-Girard, A., Moulin, A., Berlan, M., Bouloumie, A., Lafontan, M., and Galitzky, J. (2002). Natriuretic peptide-dependent lipolysis in fat cells is a primate specificity. Am J Physiol Regul Integr Comp Physiol 283, R257-265.

Sengul, C., Cevik, C., Ozveren, O., Oduncu, V., Sunbul, A., Akgun, T., Can, M.M., Semiz, E., and Dindar, I. (2011). Echocardiographic epicardial fat thickness is associated with carotid intima-media thickness in patients with metabolic syndrome. Echocardiography 28, 853-858.

Shabalina, I.G., Petrovic, N., de Jong, J.M., Kalinovich, A.V., Cannon, B., and Nedergaard, J. (2013). UCP1 in brite/beige adipose tissue mitochondria is functionally thermogenic. Cell Rep 5, 1196-1203.

Sharma, A., Markey, M., Torres-Munoz, K., Varia, S., Kadakia, M., Bubulya, A., and Bubulya, P.A. (2011). Son maintains accurate splicing for a subset of human pre-mRNAs. J Cell Sci 124, 4286-4298.

Sharp, L.Z., Shinoda, K., Ohno, H., Scheel, D.W., Tomoda, E., Ruiz, L., Hu, H., Wang, L., Pavlova, Z., Gilsanz, V., et al. (2012). Human BAT possesses molecular signatures that resemble beige/brite cells. PLoS One 7, e49452.

Shinoda, K., Luijten, I.H., Hasegawa, Y., Hong, H., Sonne, S.B., Kim, M., Xue, R., Chondronikola, M., Cypess, A.M., Tseng, Y.H., et al. (2015). Genetic and functional characterization of clonally derived adult human brown adipocytes. Nat Med 21, 389-394.

Sidossis, L.S., Porter, C., Saraf, M.K., Borsheim, E., Radhakrishnan, R.S., Chao, T., Ali, A., Chondronikola, M., Mlcak, R., Finnerty, C.C., et al. (2015). Browning of Subcutaneous White Adipose Tissue in Humans after Severe Adrenergic Stress. Cell Metab 22, 219-227.

Silva, J.E., and Larsen, P.R. (1983). Adrenergic activation of triiodothyronine production in brown adipose tissue. Nature 305, 712-713.

Silva, J.E., and Larsen, P.R. (1985). Potential of brown adipose tissue type II thyroxine 5'-deiodinase as a local and systemic source of triiodothyronine in rats. J Clin Invest 76, 2296-2305.

Sjoholm, K., Palming, J., Olofsson, L.E., Gummesson, A., Svensson, P.A., Lystig, T.C., Jennische, E., Brandberg, J., Torgerson, J.S., Carlsson, B., et al. (2005). A Microarray search for genes predominantly expressed in human omental adipocytes: Adipose tissue as a major production site of serum amyloid A. Journal of Clinical Endocrinology & Metabolism 90, 2233-2239.

Skulachev, V.P. (1991). Fatty acid circuit as a physiological mechanism of uncoupling of oxidative phosphorylation. FEBS Lett 294, 158-162.

Smorlesi, A., Frontini, A., Giordano, A., and Cinti, S. (2012). The adipose organ: white-brown adipocyte plasticity and metabolic inflammation. Obesity Reviews 13, 83-96.

Sondergaard, E., Gormsen, L.C., Christensen, M.H., Pedersen, S.B., Christiansen, P., Nielsen, S., Poulsen, P.L., and Jessen, N. (2015). Chronic adrenergic stimulation induces brown adipose tissue differentiation in visceral adipose tissue. Diabet Med 32, e4-8.

Soppela, P., Sormunen, R., Saarela, S., Huttunen, P., and Nieminen, M. (1992). Localization, cellular morphology and respiratory capacity of "brown" adipose tissue in newborn reindeer. Comp Biochem Physiol Comp Physiol 101, 281-293.

Soukas, A., Socci, N.D., Saatkamp, B.D., Novelli, S., and Friedman, J.M. (2001). Distinct transcriptional profiles of adipogenesis in vivo and in vitro. J Biol Chem 276, 34167-34174.

Souza, S.C., Christoffolete, M.A., Ribeiro, M.O., Miyoshi, H., Strissel, K.J., Stancheva, Z.S., Rogers, N.H., D'Eon, T.M., Perfield, J.W., 2nd, Imachi, H., et al. (2007). Perilipin regulates the thermogenic actions of norepinephrine in brown adipose tissue. J Lipid Res 48, 1273-1279.

Sparks, L.M., Moro, C., Ukropcova, B., Bajpeyi, S., Civitarese, A.E., Hulver, M.W., Thoresen, G.H., Rustan, A.C., and Smith, S.R. (2011). Remodeling lipid metabolism and improving insulin responsiveness in human primary myotubes. PLoS One 6, e21068.

Speake, P.F., Pirie, S.C., Kibble, J.D., Muneer, A., Taylor, D., Birring, S., and Green, R. (1993). Dose-response effects of adrenergic and cholinergic stimulation on atrial natriuretic peptide secretion from beating isolated guinea-pig atria. Clin Sci (Lond) 85, 5-12.

Speakman, J.R., and Keijer, J. (2012). Not so hot: Optimal housing temperatures for mice to mimic the thermal environment of humans. Mol Metab 2, 5-9.

Stackley, K.D., Beeson, C.C., Rahn, J.J., and Chan, S.S. (2011). Bioenergetic profiling of zebrafish embryonic development. PLoS One 6, e25652.

Stanford, K.I., Middelbeek, R.J., Townsend, K.L., An, D., Nygaard, E.B., Hitchcox, K.M., Markan, K.R., Nakano, K., Hirshman, M.F., Tseng, Y.H., et al. (2013). Brown adipose tissue regulates glucose homeostasis and insulin sensitivity. J Clin Invest 123, 215-223.

Stier, A., Bize, P., Habold, C., Bouillaud, F., Massemin, S., and Criscuolo, F. (2014). Mitochondrial uncoupling prevents cold-induced oxidative stress: a case study using UCP1 knockout mice. J Exp Biol 217, 624-630.

Stine, R.R., Shapira, S.N., Lim, H.W., Ishibashi, J., Harms, M., Won, K.J., and Seale, P. (2016). EBF2 promotes the recruitment of beige adipocytes in white adipose tissue. Mol Metab 5, 57-65.

Suga, S., Nakao, K., Hosoda, K., Mukoyama, M., Ogawa, Y., Shirakami, G., Arai, H., Saito, Y., Kambayashi, Y., Inouye, K., et al. (1992). Receptor selectivity of natriuretic peptide family, atrial natriuretic peptide, brain natriuretic peptide, and C-type natriuretic peptide. Endocrinology 130, 229-239.

Svensson, P.A., Jernas, M., Sjoholm, K., Hoffmann, J.M., Nilsson, B.E., Hansson, M., and Carlsson, L.M. (2011). Gene expression in human brown adipose tissue. International journal of molecular medicine 27, 227-232.

Symonds, M.E., Andrews, D.C., Buss, D.S., Clarke, L., Darby, C.J., and Lomax, M.A. (1996). Effect of rearing temperature on perirenal adipose tissue development and thermoregulation following methimazole treatment of postnatal lambs. Exp Physiol 81, 995-1006.

Symonds, M.E., Bird, J.A., Clarke, L., Gate, J.J., and Lomax, M.A. (1995). Nutrition, temperature and homeostasis during perinatal development. Exp Physiol 80, 907-940.

Symonds, M.E., Bird, J.A., Sullivan, C., Wilson, V., Clarke, L., and Stephenson, T. (2000). Effect of delivery temperature on endocrine stimulation of thermoregulation in lambs born by cesarean section. J Appl Physiol (1985) 88, 47-53.

Tack, C.J., Stienstra, R., Joosten, L.A.B., and Netea, M.G. (2012). Inflammation links excess fat to insulin resistance: the role of the interleukin-1 family. Immunological Reviews 249, 239-252.

Tanindi, A., Erkan, A.F., and Ekici, B. (2015). Epicardial adipose tissue thickness can be used to predict major adverse cardiac events. Coronary Artery Disease 26, 686-691.

Tchernof, A., Belanger, C., Morisset, A.S., Richard, C., Mailloux, J., Laberge, P., and Dupont, P. (2006). Regional differences in adipose tissue metabolism in women: minor effect of obesity and body fat distribution. Diabetes 55, 1353-1360.

Tews, D., and Wabitsch, M. (2011). Renaissance of Brown Adipose Tissue. Hormone Research in Paediatrics 75, 231-239.

Thomas, S.A., and Palmiter, R.D. (1997). Thermoregulatory and metabolic phenotypes of mice lacking noradrenaline and adrenaline. Nature 387, 94-97.

Tong, C., Li, P., Wu, N.L., Yan, Y., and Ying, Q.L. (2010) Production of p53 gene knockout rats by homologous recombination in embryonic stem cells. Nature 467(7312):211-3.

Tong, M., and Sadoshima, J. (2016). Mitochondrial autophagy in cardiomyopathy. Curr Opin Genet Dev 38, 8-15.

Trayhurn, P. (2007). Adipocyte biology. Obesity Reviews 8, 41-44.

Trayhurn, P., Temple, N.J., and Van Aerde, J. (1989). Evidence from immunoblotting studies on uncoupling protein that brown adipose tissue is not present in the domestic pig. Can J Physiol Pharmacol 67, 1480-1485.

Tremblay, A., Despres, J.P., Theriault, G., Fournier, G., and Bouchard, C. (1992). Overfeeding and energy expenditure in humans. Am J Clin Nutr 56, 857-862.

Uldry, M., Yang, W., St-Pierre, J., Lin, J., Seale, P., and Spiegelman, B.M. (2006). Complementary action of the PGC-1 coactivators in mitochondrial biogenesis and brown fat differentiation. Cell Metab 3, 333-341.

Untergasser, A., Cutcutache, I., Koressaar, T., Ye, J., Faircloth, B.C., Remm, M., and Rozen, S.G. (2012). Primer3--new capabilities and interfaces. Nucleic Acids Res 40, e115.

Ussar, S., Lee, K.Y., Dankel, S.N., Boucher, J., Haering, M.F., Kleinridders, A., Thomou, T., Xue, R., Macotela, Y., Cypess, A.M., et al. (2014). ASC-1, PAT2, and P2RX5 are cell surface markers for white, beige, and brown adipocytes. Sci Transl Med 6, 247ra103.

Valle, A., Santandreu, F.M., Garcia-Palmer, F.J., Roca, P., and Oliver, J. (2008). The serum levels of 17beta-estradiol, progesterone and triiodothyronine correlate with brown adipose tissue thermogenic parameters during aging. Cell Physiol Biochem 22, 337-346.

van der Lans, A.A., Hoeks, J., Brans, B., Vijgen, G.H., Visser, M.G., Vosselman, M.J., Hansen, J., Jorgensen, J.A., Wu, J., Mottaghy, F.M., et al. (2013). Cold acclimation recruits human brown fat and increases nonshivering thermogenesis. J Clin Invest 123, 3395-3403.

van Marken Lichtenbelt, W.D., Vanhommerig, J.W., Smulders, N.M., Drossaerts, J.M., Kemerink, G.J., Bouvy, N.D., Schrauwen, P., and Teule, G.J. (2009). Cold-activated brown adipose tissue in healthy men. N Engl J Med 360, 1500-1508.

Vandesompele, J., De Preter, K., Pattyn, F., Poppe, B., Van Roy, N., De Paepe, A., and Speleman, F. (2002). Accurate normalization of real-time quantitative RT-PCR data by geometric averaging of multiple internal control genes. Genome biology 3, RESEARCH0034.

Vegiopoulos, A., Muller-Decker, K., Strzoda, D., Schmitt, I., Chichelnitskiy, E., Ostertag, A., Berriel Diaz, M., Rozman, J., Hrabe de Angelis, M., Nusing, R.M., et al. (2010). Cyclooxygenase-2 controls energy homeostasis in mice by de novo recruitment of brown adipocytes. Science 328, 1158-1161.

Vijgen, G.H., Bouvy, N.D., Teule, G.J., Brans, B., Schrauwen, P., and van Marken Lichtenbelt, W.D. (2011). Brown adipose tissue in morbidly obese subjects. PLoS One 6, e17247.

Vijgen, G.H.E.J., Bouvy, N.D., Teule, G.J.J., Brans, B., Hoeks, J., Schrauwen, P., and Lichtenbelt, W.D.v.M. (2012). Increase in Brown Adipose Tissue Activity after Weight Loss in Morbidly Obese Subjects. Journal of Clinical Endocrinology & Metabolism 97, E1229-E1233.

Virtanen, K.A., Lidell, M.E., Orava, J., Heglind, M., Westergren, R., Niemi, T., Taittonen, M., Laine, J., Savisto, N.J., Enerback, S., et al. (2009). Functional brown adipose tissue in healthy adults. N Engl J Med 360, 1518-1525.

Vitali, A., Murano, I., Zingaretti, M.C., Frontini, A., Ricquier, D., and Cinti, S. (2012). The adipose organ of obesity-prone C57BL/6J mice is composed of mixed white and brown adipocytes. J Lipid Res 53, 619-629.

Vollmer, R.R., Baruchin, A., Kolibal-Pegher, S.S., Corey, S.P., Stricker, E.M., and Kaplan, B.B. (1992). Selective activation of norepinephrine- and epinephrine-secreting chromaffin cells in rat adrenal medulla. Am J Physiol 263, R716-721.

Walden, T.B., Hansen, I.R., Timmons, J.A., Cannon, B., and Nedergaard, J. (2012). Recruited vs. nonrecruited molecular signatures of brown, "brite," and white adipose tissues. American Journal of Physiology-Endocrinology and Metabolism 302, E19-E31.

Walker, G.E., Verti, B., Marzullo, P., Savia, G., Mencarelli, M., Zurleni, F., Liuzzi, A., and Di Blasio, A.M. (2007). Deep subcutaneous adipose tissue: a distinct abdominal adipose depot. Obesity (Silver Spring) 15, 1933-1943.

Walker, J.M. (1994). The bicinchoninic acid (BCA) assay for protein quantitation. Methods Mol Biol 32, 5-8.

Wang, Q., Zhang, M., Ning, G., Gu, W., Su, T., Xu, M., Li, B., and Wang, W. (2011). Brown adipose tissue in humans is activated by elevated plasma catecholamines levels and is inversely related to central obesity. PLoS One 6, e21006.

Wang, S., Wang, X., Ye, Z., Xu, C., Zhang, M., Ruan, B., Wei, M., Jiang, Y., Zhang, Y., Wang, L., et al. (2015). Curcumin promotes browning of white adipose tissue in a norepinephrine-dependent way. Biochem Biophys Res Commun 466, 247-253.

Wei, H., Chiba, S., Moriwaki, C., Kitamura, H., Ina, K., Aosa, T., Tomonari, K., Gotoh, K., Masaki, T., Katsuragi, I., et al. (2015). A clinical approach to brown adipose tissue in the para-aortic area of the human thorax. PLoS One 10, e0122594.

Weidmann, P., Hasler, L., Gnadinger, M.P., Lang, R.E., Uehlinger, D.E., Shaw, S., Rascher, W., and Reubi, F.C. (1986). Blood levels and renal effects of atrial natriuretic peptide in normal man. J Clin Invest 77, 734-742.

Wertheimer, E., and Shapiro, B. (1948). The physiology of adipose tissue. Physiol Rev 28, 451-464.

Wheeler, G.L., Shi, R., Beck, S.R., Langefeld, C.D., Lenchik, L., Wagenknecht, L.E., Freedman, B.I., Rich, S.S., Bowden, D.W., Chen, M.Y., et al. (2005). Pericardial and visceral adipose tissues measured volumetrically with computed tomography are highly associated in type 2 diabetic families. Invest Radiol 40, 97-101.

Wikstrom, J.D., Mahdaviani, K., Liesa, M., Sereda, S.B., Si, Y., Las, G., Twig, G., Petrovic, N., Zingaretti, C., Graham, A., et al. (2014). Hormone-induced mitochondrial fission is utilized by brown adipocytes as an amplification pathway for energy expenditure. EMBO J 33, 418-436.

Winkler, E., and Klingenberg, M. (1994). Effect of fatty acids on H+ transport activity of the reconstituted uncoupling protein. J Biol Chem 269, 2508-2515.

World Health Organization (2014). Obesity and overweight fact sheet.

Wu, J., Bostrom, P., Sparks, L.M., Ye, L., Choi, J.H., Giang, A.H., Khandekar, M., Virtanen, K.A., Nuutila, P., Schaart, G., et al. (2012). Beige adipocytes are a distinct type of thermogenic fat cell in mouse and human. Cell 150, 366-376.

Wu, M., Wei, C., Lian, Z., Liu, R., Zhu, C., Wang, H., Cao, J., Shen, Y., Zhao, F., Zhang, L., et al. (2016). Rosa26-targeted sheep gene knock-in via CRISPR-Cas9 system. Sci Rep 6, 24360.

Wyllie, A.H. (1980). Glucocorticoid-induced thymocyte apoptosis is associated with endogenous endonuclease activation. Nature 284, 555-556.

Xue, B., Rim, J.S., Hogan, J.C., Coulter, A.A., Koza, R.A., and Kozak, L.P. (2007). Genetic variability affects the development of brown adipocytes in white fat but not in interscapular brown fat. J Lipid Res 48, 41-51.

Yang, H., Wang, H., Jaenisch, R. (2014). Generating genetically modified mice using CRISPR/Cas-mediated genome engineering Nat Protoc 9(8):1956-68.

Ye, L., Wu, J., Cohen, P., Kazak, L., Khandekar, M.J., Jedrychowski, M.P., Zeng, X., Gygi, S.P., and Spiegelman, B.M. (2013). Fat cells directly sense temperature to activate thermogenesis. Proc Natl Acad Sci U S A 110, 12480-12485.

Yeo, G.S.H., and Heisler, L.K. (2012). Unraveling the brain regulation of appetite: lessons from genetics. Nature Neuroscience 15, 1343-1349.

Yoneshiro, T., Aita, S., Matsushita, M., Okamatsu-Ogura, Y., Kameya, T., Kawai, Y., Miyagawa, M., Tsujisaki, M., and Saito, M. (2011). Age-related decrease in cold-activated brown adipose tissue and accumulation of body fat in healthy humans. Obesity (Silver Spring) 19, 1755-1760.

Young, J.B., Saville, E., Rothwell, N.J., Stock, M.J., and Landsberg, L. (1982). Effect of diet and cold exposure on norepinephrine turnover in brown adipose tissue of the rat. J Clin Invest 69, 1061-1071.

Yu, C., Chen, Y., Cline, G.W., Zhang, D., Zong, H., Wang, Y., Bergeron, R., Kim, J.K., Cushman, S.W., Cooney, G.J., et al. (2002). Mechanism by which fatty acids inhibit insulin activation of insulin receptor substrate-1 (IRS-1)-associated phosphatidylinositol 3-kinase activity in muscle. J Biol Chem 277, 50230-50236.

Zhang, Y.Y., Proenca, R., Maffei, M., Barone, M., Leopold, L., and Friedman, J.M. (1994). Positional cloning of the mouse obese gene and its human homolog. Nature 372, 425-432.

Zhang, Z., Zhang, H., Li, B., Meng, X., Wang, J., Zhang, Y., Yao, S., Ma, Q., Jin, L., Yang, J., et al. (2014). Berberine activates thermogenesis in white and brown adipose tissue. Nat Commun 5, 5493.

Zimmermann, R., Strauss, J.G., Haemmerle, G., Schoiswohl, G., Birner-Gruenberger, R., Riederer, M., Lass, A., Neuberger, G., Eisenhaber, F., Hermetter, A., et al. (2004). Fat mobilization in adipose tissue is promoted by adipose triglyceride lipase. Science 306, 1383-1386.

Zuber, S.M., Kantorovich, V., and Pacak, K. (2011). Hypertension in pheochromocytoma: characteristics and treatment. Endocrinol Metab Clin North Am 40, 295-311, vii.

Appendices

Publications

Vergnes, L.*, **Davies, G.R.***, Lin, J., Yeh, M., Livhits, M., Harari, A., Symonds, M.E., Sacks, H.S and Reue, K. (2016) Adipocyte browning and higher mitochondrial function in peri-adrenal but not subcutaneous fat in pheochromocytoma. Journal of Clinical Endocrinology and Metabolism (In Press)

*Contributed equally

Oral presentations

Davies, G.R., Vergnes, L., Yeh, M., Livhits, M., Harari, A., Symonds, M.E., Sacks, H.S and Reue, K. (2016) Augmented Adipocyte Browning and Mitochondrial Function in Periadrenal Fat but not Subcutaneous Fat in Pheochromocytoma Patients, *Experimental Biology 2016, San Diego, CA, USA.* Awarded a travel grant to attend the conference from the Biochemical Society.

Davies, G.R., Vergnes, L., Yeh, M., Livhits, M., Harari, A., Symonds, M.E., Sacks, H.S and Reue, K. (2015) Differences in the browning capacity of white adipose tissue depots in patients with pheochromocytoma, *The Rank Prize Funds Mini-Symposium on Nutrition and Obesity, Grasmere, UK.*

Davies, G.R., Birtwistle, M., Pope, M., Perry, V., Sacks, H.S., Budge, H., Symonds M.E. (2014) The developmental transition of epicardial, paracardial and omental adipose tissue during early life in the sheep, *Experimental Biology 2014, San*

Diego, CA, USA. Awarded a travel grant to attend the conference from the Graduate School, University of Nottingham.

Poster presentations

Davies, G.R., Birtwistle, M., Pope, M., Perry, V., Sacks, H.S., Budge, H., Symonds M.E. (2015) Differences in natriuretic peptide receptor expression between adipose tissue depots in the sheep, *Keystone Symposium on Brown and Beige Fat, Snowbird, UT, USA*

Davies, G.R., Birtwistle, M., Pope, M., Perry, V., Sacks, H.S., Budge, H., Symonds M.E. (2013) The developmental transition of epicardial, paracardial and omental adipose tissue during early life in the sheep, *BHF Centre of Research Excellence Adipose Tissue Workshop, Edinburgh, UK*.

Davies, G.R., Birtwistle, M., Pope, M., Perry, V., Sacks, H.S., Budge, H., Symonds M.E (2013) The developmental transition of ovine epicardial, paracardial and omental adipose tissue during early life, *International Congress of Physiological Sciences (IUPS), Birmingham, UK*.

Subject characteristics

Subject number	Study group	Reason for adrenalectomy	Age	BMI	Co-morbidities	Regular Medications
1	Control	Hyperaldosteronism	37	34.7	Hypertension	Aldactone, amlodipine
2	Control	Non-functioning	59	22.7	Hypertension	ACE inhibitor
3	Control	Cushings	39	35.5	Asthma	
4	Control	Hyperaldosteronism	50	42.5	Hypertension	Amlodipine, metoprolol,
5	Control	Cushings	57	35.4	Hyperlipidemia, diabetes, hypertension	ACE inhibitor, insulin
6	Control	Hyperaldosteronism	54	26.4	Dyslipidemia, hypertension	Amlodipine, angiotensin II receptor blocker
7	Control	Hyperaldosteronism	40	20.8	Hypertension	Eplerenone, Labetalol, , KCl
8	Control	Non-functioning	62	31.2	Diabetes, hypertension	ACE inhibitor, atorvastatin, insulin, metformin
9	Control	Non-functioning	45	37.6		Premarin
10	Control	Hyperaldosteronism	56	32.5	Hypertension	Aldactone, atorvastatin
11	Control	Non-functioning	57	30.7		Lansoprazole
12	Control	Hyperaldosteronism	37	26.1	Hypertension	
13	Control	Hyperaldosteronism	62	34.9	Diabetes, hypertension	ACE inhibitor, hydrochlorothiazide, metformin, metoprolol, triamterene
14	Control	Hyperaldosteronism	63	27.6	Hypertension	ACE inhibitor, hydrochlorothiazide, KCl
15	Control	Hyperaldosteronism	67	26.6	Hypertension	ACE inhibitor, Amlodipine
16	Control	Hyperaldosteronism	51	24.1	Hypertension	Atorvastatin, eplerenone, KCl,

Subject number	Study group	Reason for adrenalectomy	Age	BMI	Co-morbidities	Regular Medications
17	Control	Non-functioning	59	19.8		Atorvastatin
18	Control	Hyperaldosteronism	50	31.9	Hypertension	
19	Control	Non-functioning	47	26.2	Hypertension	Metoprolol
20	Control	Non-functioning	53	49.1	Diabetes, hypertension	Angiotensin II receptor blocker, diltiazem, insulin
21	Pheo Unilocular	Pheochromoctoma	46	22.8		Metoprolol, phenoxybenzamine
22	Pheo Unilocular	Pheochromoctoma	50	41.6	Hypogonadism	Amlodipin, phenoxybenzamine, metoprolol,
23	Pheo Unilocular	Pheochromoctoma	69	26.3	Hypertension	Amlodipin, atorvastatin, metoprolol, losartan, phenoxybenzamine
24	Pheo Unilocular	Pheochromoctoma	57	21.9		Atorvastatin, carvedilol, phenoxybenzamine, topiramate,
25	Pheo Unilocular	Pheochromoctoma	20	23.8		Nifedipine, phenoxybenzamine,
26	Pheo Unilocular	Pheochromoctoma	55	30.1		Phenoxybenzamine
27	Pheo Multilocular	Pheochromoctoma	51	26.5	Hyperlipidemia	Metoprolol, phenoxybenzamine, propranalol, , simvastatin, terazosin
28	Pheo Multilocular	Pheochromoctoma	51	31.4	Hyperlipidemia	Phenoxybenzamine
29	Pheo Multilocular	Pheochromoctoma	53	29.4	Hypercholesterolemia	Phenoxybenzamine
31	Pheo Multilocular	Pheochromoctoma	52	23		Diovan, hydrochlorothiazide, phenoxybenzamine

Subject number	Study group	Reason for adrenalectomy	Age	BMI	Co-morbidities	Regular Medications
31	Pheo Multilocular	Pheochromoctoma	52	23		Diovan, hydrochlorothiazide phenoxybenzamine,
32	Pheo Multilocular	Pheochromoctoma	53	28.5		Phenoxybenzamine
33	Pheo Multilocular	Pheochromoctoma	66	21.1	Iron overload	Atrovastatin, phenoxybenzamine,